



Universiteit
Leiden
The Netherlands

Oxidation, aggregation and immunogenicity of therapeutic proteins

Torosantucci, R.

Citation

Torosantucci, R. (2013, September 17). *Oxidation, aggregation and immunogenicity of therapeutic proteins*. Retrieved from <https://hdl.handle.net/1887/21762>

Version: Corrected Publisher's Version

License: [Licence agreement concerning inclusion of doctoral thesis in the Institutional Repository of the University of Leiden](#)

Downloaded from: <https://hdl.handle.net/1887/21762>

Note: To cite this publication please use the final published version (if applicable).

Cover Page



Universiteit Leiden



The handle <http://hdl.handle.net/1887/21762> holds various files of this Leiden University dissertation.

Author: Torosantucci, Riccardo

Title: Oxidation, aggregation and immunogenicity of therapeutic proteins

Issue Date: 2013-09-17

Oxidation, aggregation and immunogenicity of therapeutic proteins

Riccardo Torosantucci

The research described in this thesis was performed at:

- The Division of Drug Delivery Technology at the Leiden Academic Centre for Drug Research (LACDR), Leiden University, Leiden, The Netherlands.
- The Department of Pharmaceutics, Utrecht Institute for Pharmaceutical Sciences (UIPS), Utrecht University, Utrecht, the Netherlands.
- The Department of Pharmaceutical Chemistry of Kansas University, Lawrence, Kansas, USA.

This research was financially supported by Organon NV, part of Merck Sharp & Dohme and Schering-Plough.

The cover of this thesis was design by Ernesto Venanzi, Rome: human insulin aggregates detected by light microscopy, surrounded by oxidized amino acids and the chemical structure of 2-amino-3-(3,4-dioxocyclohexa-1,5-dien-1-yl) propanoic acid (DOCH), measured in oxidized and aggregated therapeutic proteins.

Printed by Gildeprint, Enschede, The Netherlands.

Copyright: © 2013 Riccardo Torosantucci. All rights reserved. No part of this thesis may be reproduced or transmitted in any form or by any means without written permission of the author.

ISBN: 978-94-6108-483-5

Oxidation, aggregation and immunogenicity of therapeutic proteins

Oxidatie, aggregatie en immunogeniciteit van therapeutische eiwitten
(met een samenvatting in het Nederlands)

Proefschrift

ter verkrijging van
de graad van Doctor aan de Universiteit Leiden,
op gezag van Rector Magnificus prof. mr. C.J.J.M. Stolker,
volgens besluit van het College voor Promoties
te verdedigen op dinsdag 17 september 2013 des middags te 15:00 uur

door

Riccardo Torosantucci

Geboren op 22 september 1980 te Rome, Italië

Promotiecommissie

Promotoren: Prof. dr. W. Jiskoot
Prof. dr. H. Schellekens

Co-promotor: Dr. V. Brinks

Overige leden: Prof. dr. M. Danhof, Universiteit Leiden
Prof. dr. H. W. Frijlink, Universiteit Groningen
Dr. M. van de Weert, Universiteit Kopenhagen
Prof. dr. ir. W.E. Hennink, Universiteit Utrecht

“Memento audere semper”

Gabriele D'Annunzio

Ad Alberto, Antonella, Gaetana ed Olga Ekin

Table of contents

Chapter 1	11
General introduction	
Chapter 2	19
Oxidation of therapeutic proteins and peptides: structural and biological consequences	
Chapter 3	49
Plain and mono-PEGylated recombinant human insulin exhibit similar stress-induced aggregation profiles	
Chapter 4	75
Chemical modifications in aggregates of recombinant human insulin induced by metal-catalyzed oxidation: covalent cross-linking via Michael addition to tyrosine oxidation products	
Chapter 5	115
Triethylenetetramine prevents insulin aggregation and fragmentation during copper catalyzed oxidation	
Chapter 6	143
Identification of oxidation sites and covalent cross- links in metal catalyzed oxidized interferon beta-1a: potential implications for protein aggregation and immunogenicity	
Chapter 7	179
Immune mechanisms underlying immunogenicity of aggregated recombinant human interferon alpha-2a in immune tolerant mice	

Chapter 8	203
Development of a transgenic mouse model to study the immunogenicity of recombinant human insulin	
Chapter 9	227
Summary and perspectives	
Appendix 1	237
Nederlandse samenvatting (Dutch summary)	
Appendix 2	245
Abbreviations	
Appendix 3	249
List of publications	
Appendix 4	253
Curriculum Vitae	
Appendix 5	257
Acknowledgements	

Chapter 1

General introduction

Introduction

Recombinant human therapeutic proteins are macromolecules widely used to treat a broad number of diseases for which often no other class of drugs is effective [1].

Administration of highly purified recombinant human therapeutic proteins, however, despite their similarity to their endogenous counterparts, frequently induces the production of anti-drug antibodies (ADAs) [2]. ADAs can be divided into binding antibodies (BABs), which bind to protein regions not relevant for the biological activity, and neutralizing antibodies (NABs) recognizing the active site of the protein. BABs can affect the clearance of the protein and thereby indirectly change its therapeutic efficacy, while NABs directly neutralize the protein's biological activity [3]. These adverse pharmacological consequences resulting from the immunogenicity of therapeutic proteins are a major obstacle during their development.

Factors influencing immunogenicity

Several factors affect the immunogenicity of therapeutic proteins, including structural aspects (e.g., primary structure, higher-order structures, glycosylation, PEGylation), formulation, treatment regimen, route of administration, co-medication and genetic background of the patient [2].

In addition, the absence of standardized assays for measuring ADAs makes it extremely difficult to compare results between laboratories and between published studies.

Among the product-related factors, structural modifications like aggregation, chemical degradation (particularly oxidation) and combinations thereof are important risk factors for immunogenicity and are therefore discussed in more detail below.

Aggregation

Aggregation concerns processes by which the smallest naturally occurring monomeric subunit forms larger assemblies, which can be as small as a dimer and as large as a visible precipitate [4]. Such assemblies, hereafter referred to as protein aggregates, can be formed during production, transportation,

storage and administration, and are often accompanied by other physical and chemical degradation processes [4].

Several non-clinical and clinical studies have related therapeutic protein aggregates to immunogenicity [2-3, 5-6]. For instance, the effect of different recombinant human interferon alfa (rhIFN α) aggregates on the immunogenicity has been studied in immune tolerant mouse models. Braun et al. [7] upon i.p. injection of different aggregated rhIFN α -2a formulations, found that all the aggregates tested were highly immunogenic in transgenic immune tolerant Balb/C mice. Similarly, various aggregates of rhIFN α -2b induced ADAs in transgenic immune tolerant mice [8]. Also recombinant human interferon beta (rhIFN β) aggregation has been correlated with enhanced immunogenicity. Furthermore, it has been demonstrated that the removal of protein aggregates from rhIFN β formulations reduces the immunogenicity of rhIFN β [9-11]. In addition to that, rhIFN β -1b (Betaferon[®]), which contains more aggregates than rhIFN β -1a products (Avonex[®], Rebif[®]), has been found to be the most immunogenic product in several preclinical and clinical studies [12].

Chemical degradation

Oxidation and deamidation are major chemical degradation processes in proteins. One of the impurities found in rhIFN α -2a formulations because of improper storage was an oxidized form [13]. Although the oxidation sites were not determined, in a clinical trial it emerged that the oxidized and aggregated form was more immunogenic when compared with the native counterpart [13].

Particularly interesting are observations that several protein aggregates induced via metal catalyzed oxidation are immunogenic in preclinical models. For instance, Hermeling et al. showed that upon oxidative stress induced by Cu²⁺/ascorbate catalyzed oxidation, rhIFN α -2b formed aggregates that were more immunogenic than other types of rhIFN α -2b aggregates [8, 14]. Similarly, rhIFN β -1a aggregates [15] and monoclonal antibody aggregates [16] (IgG1), both produced via the same oxidative system, were shown to be highly immunogenic in transgenic immune tolerant mouse models. In addition, immunization of H^{2k} mice with oxidized insulin B chain yielded a higher immune response when compared with the non oxidized form [17].

Deamidation, which mainly occurs at asparagine residues, could elicit immune responses as a result of generation of newly exposed antigenic

determinants [18]. Deamidated serum albumin is immunogenic and potentially could induce autoimmune reactions [19]. Furthermore, deamidation of glutamine residues in gliadin peptides is critical for the creation of epitopes involved in coeliac autoimmune disease [20].

Mouse models to predict the immunogenicity of protein therapeutics and to investigate underlying immune mechanisms

Nearly all protein therapeutics are immunogenic. Immunogenicity prediction and prevention is an important issue to consider when developing novel therapeutic products.

To this end, animal models are increasingly used to study immunogenicity of therapeutic proteins. The employment of classical non transgenic animal models is not suitable for immunological studies of non conserved proteins, which being foreign for the animal will induce a classical immune reaction [21].

Using transgenic immune tolerant mouse models overcome this problem, since these mice express the human endogenous counterpart of the therapeutic protein under investigation. Such models have been used mainly to investigate product-related factors, especially the presence of various structurally different protein aggregates, involved in immunogenicity [5, 15].

The use of animals rather than in vitro models has the advantage that the immune mechanisms underlying immunogenicity of therapeutic proteins can be studied in an organism with intact immune system and responses.

Aim and outline of the thesis

The aim of the research described in this thesis is to study the chemical mechanisms responsible for protein aggregation induced by metal catalyzed oxidation and to investigate the relationship between protein oxidation, aggregation and immunogenicity. To this end, recombinant human insulin (further referred to as insulin), rhIFN β -1a and rhIFN α -2a are used in conjunction with transgenic mice immune tolerant for the respective human endogenous counterparts.

The impact of PEGylation on aggregate formation and excipients to prevent metal catalyzed oxidation are also evaluated.

Chapter 2 reviews the structural and biological consequences of oxidation of protein and peptide therapeutics.

Chapter 3 evaluates the susceptibility of PEGylated insulin on aggregation upon chemical and physical stress. Insulin is conjugated on lysine B29 with 5-kDa PEG. Next, insulin and PEG-insulin are subjected to heating, metal-catalyzed oxidation, and glutaraldehyde mediated cross-linking. Finally, the products are characterized physicochemically by complementary analytical methods.

Chapter 4 investigates the chemical mechanism responsible for insulin aggregation during metal-catalyzed oxidation. Bivalent copper and ascorbate are used as oxidative system and liquid chromatography electrospray ionization tandem mass spectrometry (ESI-LC-MS/MS) is employed for identifying the target of oxidation and cross-links mediating insulin aggregation.

Chapter 5 describes the antioxidant properties of several excipients, which are evaluated by quantifying aggregate content and chemical degradation in several insulin formulations exposed to bivalent copper and ascorbate.

Chapter 6 aims to study the chemical changes in aggregated and oxidized rhIFN β -1a, generated by metal catalyzed oxidation, and the correlation between the structural changes in the aggregated protein and its immunogenicity, previously evaluated in transgenic mice immune tolerant for rhIFN β .

Chapter 7 sheds light on the immune mechanism responsible for the immunogenicity of oxidized and aggregated rhIFN α -2a and studies if the presence of aggregated rhIFN β increases rhIFN α 's immunogenicity, using transgenic mice immune tolerant for the human protein. The presence of immunological memory is evaluated after rechallenge with aggregated or native rhIFN α and depletion from CD4⁺ T-cells is used to test for CD4⁺ T-cell involvement in immunogenicity.

Chapter 8 describes the development and the application of a transgenic mouse model for studying the immunogenicity of insulin. The immunogenicity of aggregated and oxidized insulin, non-aggregated oxidized insulin and several commercial insulin formulations is evaluated.

Chapter 9 summarizes the findings and conclusions of this thesis and discusses the perspectives for further research on strategies to prevent protein degradation and analytical tools for protein characterization.

References

- [1] T. Dingermann. Recombinant therapeutic proteins: production platforms and challenges. *Biotechnol. J.* **2008**, *3*, 90-97.
- [2] H. Schellekens. Bioequivalence and the immunogenicity of biopharmaceuticals. *Nat. Rev. Drug. Discov.* **2002**, *1*, 457-462.
- [3] A. S. Rosenberg. Effects of protein aggregates: an immunologic perspective. *AAPS J.* **2006**, *8*, E501-507.
- [4] M. E. Cromwell, E. Hilario, F. Jacobson. Protein aggregation and bioprocessing. *AAPS J.* **2006**, *8*, E572-579.
- [5] S. Hermeling, D. J. Crommelin, H. Schellekens, W. Jiskoot. Structure-immunogenicity relationships of therapeutic proteins. *Pharm. Res.* **2004**, *21*, 897-903.
- [6] H. Schellekens. The immunogenicity of therapeutic proteins. *Discov. Med.* **2010**, *9*, 560-564.
- [7] A. Braun, L. Kwee, M. A. Labow, J. Alsenz. Protein aggregates seem to play a key role among the parameters influencing the antigenicity of interferon alpha (IFN-alpha) in normal and transgenic mice. *Pharm. Res.* **1997**, *14*, 1472-1478.
- [8] S. Hermeling, L. Aranha, J. M. A. Damen, M. Slijper, H. Schellekens, D. J. A. Crommelin, W. Jiskoot. Structural characterization and immunogenicity in wild-type and immune tolerant mice of degraded recombinant human interferon alpha2b. *Pharm. Res.* **2005**, *22*, 1997-2006.
- [9] M. M. van Beers, M. Sauerborn, F. Gilli, V. Brinks, H. Schellekens, W. Jiskoot. Aggregated recombinant human interferon Beta induces antibodies but no memory in immune-tolerant transgenic mice. *Pharm. Res.* **2010**, *27*, 1812-1824.
- [10] R. A. Rifkin, E. T. Maggio, S. Dike, D. A. Kerr, M. Levy. n-Dodecyl-beta-d-Maltoside Inhibits Aggregation of Human Interferon-beta-1b and Reduces Its Immunogenicity. *J. Neuroimmune Pharmacol.* **2011**, *6*, 158-162.
- [11] M. B. Seefeldt, M. S. Rosendahl, J. L. Cleland, L. K. Hesterberg. Application of high hydrostatic pressure to dissociate aggregates and refold proteins. *Curr. Pharm. Biotechnol.* **2009**, *10*, 447-455.

- [12] M. M. C. van Beers, W. Jiskoot, H. Schellekens. On the Role of Aggregates in the Immunogenicity of Recombinant Human Interferon Beta in Patients with Multiple Sclerosis. *J. Interferon Cytokine Res.* **2010**, *30*, 767-775.
- [13] E. Hochuli. Interferon immunogenicity: technical evaluation of interferon-alpha 2a. *J Interferon Cytokine Res* **1997**, *17 Suppl 1*, S15-21.
- [14] S. Hermeling, H. Schellekens, C. Maas, M. F. Gebbink, D. J. Crommelin, W. Jiskoot. Antibody response to aggregated human interferon alpha2b in wild-type and transgenic immune tolerant mice depends on type and level of aggregation. *J. Pharm. Sci.* **2006**, *95*, 1084-1096.
- [15] M. M. van Beers, M. Sauerborn, F. Gilli, V. Brinks, H. Schellekens, W. Jiskoot. Oxidized and aggregated recombinant human interferon beta is immunogenic in human interferon beta transgenic mice. *Pharm. Res.* **2011**, *28*, 2393-2402.
- [16] V. Filipe, W. Jiskoot, A. H. Basmeleh, A. Halim, H. Schellekens. Immunogenicity of different stressed IgG monoclonal antibody formulations in immune tolerant transgenic mice. *MAbs* **2012**, *4*, 740-752.
- [17] P. E. Jensen. Immunogenicity of B chain in insulin responder and nonresponder mice. *Cell. Immunol.* **1990**, *130*, 129-138.
- [18] F. C. Westall. Released myelin basic protein: the immunogenic factor? *Immunochemistry* **1974**, *11*, 513-515.
- [19] P. N. Lukash Al, Tibulsky IE. Autoantigenic properties of deamidated serum albumin. *Immunologiya* **1987**, *68*.
- [20] H. Sjostrom, K. E. Lundin, O. Molberg, R. Korner, S. N. McAdam, D. Anthonsen, H. Quarsten, O. Noren, P. Roepstorff, E. Thorsby, L. M. Sollid. Identification of a gliadin T-cell epitope in coeliac disease: general importance of gliadin deamidation for intestinal T-cell recognition. *Scand. J. Immunol.* **1998**, *48*, 111-115.
- [21] V. Brinks, W. Jiskoot, H. Schellekens. Immunogenicity of Therapeutic Proteins: The Use of Animal Models. *Pharm. Res.* **2011**, *28*, 2379-2385.

Chapter 2

Oxidation of therapeutic proteins and peptides: structural and biological consequences

Riccardo Torosantucci¹, Christian Schöneich², Wim Jiskoot¹

¹Division of Drug Delivery Technology, Leiden Academic Centre for Drug Research (LACDR), Leiden University, Leiden, the Netherlands.

²Department of Pharmaceutical Chemistry of Kansas University, Lawrence, Kansas, USA.

Submitted for publication

Abstract

Oxidation is a common degradation pathway that affects therapeutic proteins and peptides during production, purification, formulation, transportation, storage and handling of solid and liquid preparations. In the present work we review the scientific literature about structural and biological consequences of protein/peptide oxidation. Representative examples are discussed of specific products whose oxidation has been recently studied, including monoclonal antibodies, calcitonin, granulocyte colony-stimulating factor, growth hormone, insulin, interferon alpha and beta, oxytocin and parathyroid hormone. These examples illustrate that oxidation often leads to modifications of higher-order structures, including aggregate induction, and can generate products that are pharmacokinetically different, biologically less active and/or potentially more immunogenic than their native counterpart. It is therefore crucially important during the pharmaceutical development of therapeutic proteins and peptides to comprehensively characterize oxidation products and evaluate the impact of oxidation-induced structural modifications on the biological properties of the drug.

Introduction

In the last thirty years proteins and peptides have gained importance in the treatment of a broad number of diseases for which no other therapy is available [1]. Instability, however, represents a serious problem in the development of therapeutic proteins and peptides [2].

In particular oxidation, which has been reported to occur during production [3], purification [4], formulation [5] and storage [6], is a major concern [7], as it can extensively modify the primary structure of proteins and peptides, by which changes in secondary, tertiary and quaternary structure may arise [8-10]. Whereas there are several excellent reviews describing oxidation mechanisms [11], products of amino acid oxidation [12-16], the biochemical basis of protein oxidation [17-18] and strategies to prevent oxidation [2, 11-12, 17], to the best of our knowledge, only one review, published twenty years ago, described the pharmaceutical consequences of protein oxidation [19]. At that time, however, experimental data about biological consequences of oxidation were scarce.

Here we aim to give an update on the current knowledge about the consequences of oxidative modification for amino acid residues (i.e. primary structure), higher-order structures (i.e. secondary, tertiary and quaternary structure), biological activity, half-life and immunogenicity of several protein and peptide therapeutics.

After briefly introducing the potential causes of oxidation during production, purification, formulation and storage, we will discuss the consequences of oxidation for: monoclonal antibodies (mAbs), calcitonin (CT), granulocyte colony-stimulating factor (G-CSF), growth hormone (GH), insulin, recombinant human interferon alpha-2a (IFN α -2a) interferon alpha-2b (IFN α -2b) and interferon beta-1a (IFN β -1a), oxytocin and parathyroid hormone (PTH).

Oxidation of proteins and peptides

Most biopharmaceuticals are produced by recombinant DNA technologies, usually by employing microbial hosts like *E. coli* [20] or mammalian cells like Chinese hamster ovary (CHO) cells [21]. Already during the production steps, the concentration of dissolved oxygen (DO) can influence the oxidative state of therapeutic proteins, as demonstrated for the production in *E. coli* of recombinant human IFN γ , where an increase in carbonyl groups [18] (a general

marker of oxidative modification) correlated with a relatively high DO concentration (i.e. 60% DO), suggesting that the aerobic environment should be scrupulously monitored [3]. However, also low oxygen concentration (a condition known as hypoxia) may induce oxidative stress through the production of reactive oxygen species in mammalian host cells, likely generated by electrons leaking from the mitochondrial electron transport chain [22-25]. In support of this, oxidation-induced fragmentation of recombinant human IgG1 produced in CHO cells was observed in the purified material and, interestingly, the same degradation was reproduced by *in vitro* incubation of the protein with hydrogen peroxide [26].

Besides oxidation that may arise during the production in cell culture, oxidation can occur in the subsequent downstream processes. For instance, purification of lactate dehydrogenase, using metal affinity chromatography, yielded an oxidized product [4].

During formulation and storage several excipients and impurities can directly or indirectly favor oxidation. For instance, hydrogen peroxide has been encountered as an impurity in polymeric excipients such as polyethylene glycol (PEG) or polysorbate [5, 27]. Additionally, these polymeric excipients can spontaneously oxidize in aerobic environment, without the aid of a catalyst (auto-oxidation) [28-29], generating several peroxides. Among the impurities which might favor oxidation, transition metals represent a common threat, as they can catalyze oxidation reactions [14] already at submicromolar concentration [30]. Furthermore, transition metals being air pollutants [31-32] may contaminate buffers [33] and excipients such as sugars, surfactants and amino acids [34]. Also, they can be released from containers [11], making it difficult to fully avoid their presence in formulations.

Chemical modifications in amino acids induced by oxidation

Potentially all 20 natural amino acids can be oxidized [16], however, cysteine (Cys), histidine (His), methionine (Met), phenylalanine (Phe), tryptophan (Trp) and tyrosine (Tyr) are generally most prone to oxidation, due to the high reactivity of sulfur atoms and aromatic rings towards various reactive oxygen species [12]. Table I provides a comprehensive summary of reported cases of protein/peptide oxidation, including the chemical changes in primary and higher-order structures, as well as observed biological consequences.

Table 1. Summary of reported structural and biological consequences of oxidation of protein and peptide therapeutics.

Protein ^a	Oxidative stress ^b	Chemical changes in primary structure ^c	Changes in higher-order structure	Biological consequences	Ref.
IgG1 (humanized monoclonal)	H ₂ O ₂	M252 (HC ^d)	Reduced melting temperature (T _m) of CH2 domain	Decreased binding to FcRn	49
		M428 (HC)			
		M358 (HC)			
IgG1 Fc (human, E. coli derived)	H ₂ O ₂	M252 (HC)	Subtle conformational changes	Reduction of serum half-life	50, 52
		M428 (HC)			
		M33 (HC)			
IgG1 (not specified)	H ₂ O ₂	M209 (HC)	Altered secondary and tertiary structure	n.i.	51
		M33 (HC)			
IgG1 (human monoclonal)	TBHP	M34 (HC)	Large structural change in the region of heavy chain residues 247-253	Decreased binding affinity for protein A, protein G and FcRn	48, 38
		M83 (HC)			
		M253 (HC)			
		M429 (HC)			
		M4 (LC)			

IgG1 (HER2)	Aggregation and fragmentation	n.i.	59
	TBHP, H ₂ O ₂ and storage	M83 (HC) M253 (HC) W32 (LC)	
IgG1 (humanized MEDI-493)	ultraviolet (UV) light irradiation	W105 (HC)	60
	production in CHO cell culture, H ₂ O ₂	M C H	26
IgG1 (fully human)			
	Cu ²⁺ /ascorbate	n.i.	56
IgG2	Cu ²⁺ /ascorbate	M34 (HC) M82 (HC) M246 (HC) M352 (HC) M391 (HC) M422 (HC) H304 (HC) H427 (HC) W156 (HC)	57, 58
	H ₂ O ₂	M34 (HC), M246 (HC), M352 (HC), M391 (HC)	57, 58

sCT	Thermal stress	M34 (HC) M246 (HC) M422 (HC)	Changes in secondary and tertiary structure Aggregation	n.i.	57, 58
	Mechanical stress	M34 (HC) M82 (HC) M246 (HC) M352 (HC) M391 (HC) M422 (HC) W36 (LC) W47 (HC) W98 (LC) W156 (HC) W271 (HC)	Changes in secondary and tertiary structure Aggregation	n.i.	57, 58
	H ₂ O ₂	n.i.	Formation of fibrillar aggregates	n.i.	66
	Storage	C	Dimerization involving Cys residues and trisulfide variants	n.d.	67
	Fe ²⁺ /ascorbate/light	n.i.	Changes in secondary structure Formation of fibrillar aggregates	n.i.	61
	H ₂ O ₂	M1, M122, M127, M138	Conformational changes	Altered biological activity and serum half life	68, 69
G-CSF					

GH	TBHP	M1	Conformational changes	Altered biological activity and serum half life	69
		M122			
		M127			
		M138			
	H ₂ O ₂	M14	Subtle conformational changes	Minor effect on receptor binding and <i>in vitro</i> biological potency	73
		M125			
	H ₂ O ₂	M14	Subtle conformational changes	Decreased thermal stability	74
		M125			
	Cu ²⁺ /ascorbate	H18	Subtle conformational changes	n.i.	80
		H21	Formation of dimers		
AAPH	M14	Aggregation	n.i.	78	
	M125				
	M170				
	L101 Y103				
Insulin	Storage	C	Aggregation	n.i.	83
	Cu ²⁺ /ascorbate	H (B5, B10)	Changes in secondary and tertiary structure	Immunogenic in transgenic immune tolerant mice	9, 10
		F (B1, B24, B25) Y (A14, A19, B16, B26)	Aggregation		

	Cu ²⁺ /H ₂ O ₂ And in vitro incubation with plasma from diabetic patients	F and Y oxidation products	n.i.	Decreased hypoglycemic activity	96
	Cu ²⁺ /H ₂ O ₂	F and Y oxidation products	Aggregation	Decrease in the insulin-dependent glucose utilization by human adipose tissue	97
IFN alpha-2a	H ₂ O ₂	n.i.	n.i.	Reduced biological activity	99
	Storage	n.i.	n.i.	Enhanced immunogenicity	100, 101
	Cu ²⁺ /ascorbate	n.i.	Changes in secondary structure Aggregation	Immunogenic in transgenic immune tolerant mice	(e)
IFN alpha-2b	Cu ²⁺ /ascorbate	M16 M21 M148	Changes in secondary structure Aggregation	Immunogenic in transgenic immune tolerant mice	105
	Storage	M111	Changes in secondary structure	n.d.	104

IFN beta-1a	Storage	C	Disulfide linked aggregates	n.i.	107
	Cu ²⁺ /ascorbate	n.i.	Structural changes Aggregation	n.i.	109
Oxytocin	Storage at different pH and temperature	C Y	Tri- and tetra sulfide derivatives Dityrosine linked dimers	n.i.	112
PTH	Storage	n.i.	Changes in secondary structure Aggregation	n.i.	116
	H ₂ O ₂	M8 M18	Changes in secondary structure	n.i.	118
	H ₂ O ₂	M8 M18	n.i.	Reduced biological activity	119
bPTH	H ₂ O ₂	M8	n.i.	Reduced biological activity	121
pPTH	H ₂ O ₂	M8	n.i.	Reduced biological activity	122

a: sCT: salmon calcitonin; G-CSF: granulocyte colony-stimulating factor; GH: growth hormone; PTH: parathyroid hormone.

b: TBPH: tert-butylhydroperoxide; AAPH: 2,2'-azobis(2-methylpropanamide).

c: Amino acid residues in one letter code: C: cysteine; F: phenylalanine; H: histidine; M: methionine; W: tryptophan; Y: tyrosine.

d: Abbreviations: A and B: insulin chain A and chain B, respectively; HC and LC: IgG heavy chain and light chain, respectively; n.d.: not detected; n.i.: not investigated.

e: unpublished data by Sauerborn et al.

As oxidative modifications at the amino acid level have been extensively reviewed elsewhere [12-13, 16], we focus the discussion below on the higher-order structural consequences and the biological consequences observed for several representative protein and peptide drugs.

Consequences of protein and peptide oxidation

Monoclonal antibodies

All human IgGs feature a characteristic “Y” shape [35]: the lower part contains a single crystallizable region (Fc) critical for effector functions and half-life [36]. The upper part consists of two identical regions (Fab) that contain the complementarity determining regions (CDRs) responsible for antigen binding [37]. Most mAbs belong to the IgG1 and IgG2 subclasses, which share 97% of sequence homology [38]. The Fc region can contain up to four Met residues: Met residues at positions 252 and 428 (based on the Eu numbering system [39]) are conserved in all IgGs [40], the presence of Met 358 in IgG1 is dependent on the allele of the gene [41], while Met 397 is only present in IgG2 and IgG3 [42]. Modification of any of these Met residues may adversely affect the Fc-dependent effector function of mAbs [42].

Several authors investigated the susceptibility to oxidation of Met residues under different stress or storage conditions [43-47]. However, few studies reported the consequences of such modifications on protein structure and pharmacokinetics.

Oxidation of Met 252 and Met 428 reduced the binding with Protein A [48] (a protein often used in affinity chromatography) and the neonatal Fc receptor (FcRn) [38, 49]. This can reduce the biological half-life of the antibody, as shown by Wang et al. [50], who demonstrated that a mAb containing 80% of oxidized Met 252 features more than 4-fold reduction in the half-life in transgenic mice with human FcRn. When the percentage of Met oxidation was lower, i.e. 40%, the measured half-life was comparable to that of the native mAb.

Liu et al. [51] noticed that hydrogen peroxide-induced oxidation of Met residues in *E. coli*-expressed Fc, resulted in alteration of secondary and tertiary structure, evaluated by circular dichroism spectroscopy, and in a reduced melting temperature of the CH2 domain (note that Liu et al. referred to Met 33 and Met 209, which correspond to Met 252 and Met 428 on the

intact heavy chain sequence). It must be mentioned that the Fc used was produced in *E. coli* and thus lacks glycosylation, which is important for protein stability: Met oxidation in a glycosylated IgG1 led to similar changes in the thermal stability but conformational changes of the antibody with oligosaccharides were minor, indicating a partial protective effect of the sugar moiety [52-53]. Interestingly, also the deamidation rate of Asn 67 and Asn 96 increased, likely as a result of Met oxidation-mediated conformational changes [51]. Destabilization of the α -helix of the residues 247-253 of the Fc region of IgG1 was also observed upon hydrogen peroxide treatment [54-55]. These findings suggest that oxidation of Met residues can result in conformational changes of mAbs.

Metal catalyzed oxidation (MCO) of a monoclonal human IgG, induced by Cu^{2+} /ascorbate, generated mainly micron-sized aggregates with secondary and tertiary structure alterations that were immunogenic in a transgenic, immune-tolerant mouse model [56]. A monoclonal IgG2 was evaluated under similar stress conditions and the authors observed severe changes in secondary and tertiary structure, associated with the site specific oxidation of His 304 and His 427, besides oxidation of several Met residues and of Trp 156 [57-58]. Also particles in the size range between 0.2-10 μm were detected.

Similarly, oxidation of IgG2 with hydrogen peroxide modified the higher order structural properties of the protein and induced the formation of polydisperse aggregates. In addition to Met oxidation, Trp oxidation was observed but not the oxidation of His [57-58].

Hensel et al. suggested that the oxidation of Trp 32 (in the CDR region of the light chain) was mainly responsible for the progressive loss of target binding and biological activity [59]. Similarly, the oxidation of Trp 105, a residue in the CDR3 of the heavy chain of a humanized mAb against respiratory syncytial virus, was considered responsible for the activity loss [60]. Altogether, these results demonstrate that Met is only one of the potential targets of oxidation and oxidation frequently compromises the conformation and biological functions of monoclonal IgGs.

Calcitonin

CT is a polypeptide hormone of 32 amino acids which, in aqueous solution, assumes an unstructured conformation [61]. Mainly human and salmon

calcitonin (hCT and sCT, respectively) are used for therapeutic purposes. The two polypeptides share only 50% sequence homology, nonetheless higher order structural features are similar between the two hormones [61]. In aqueous solution, hCT tends to aggregate faster than sCT, causing the formation of fibrillar precipitates [61].

Aggregated and oxidized forms of hCT were observed *in vivo* in plasma under non-pathological conditions [62], justifying studies on the consequences of CT oxidation. Although CT contains Met, His, Phe and Tyr residues, all of which are potential oxidation targets, oxidation (during storage or forced oxidative stress) of this polypeptide hormone appears to affect mainly Met 8, the only Met residue available. Reduction of bioactivity was observed upon oxidation of Met 8 [63-64]; however, more recently it was found that the aggregation rate of Met oxidized hCT decreased [65], illustrating that oxidation not necessarily accelerates aggregation.

Aggregation of sCT accompanied by alteration of secondary structure was observed upon hydrogen peroxide treatment [66]: this suggests that mild oxidative conditions are capable of inducing structural changes in sCT.

Dimers involving Cys residues as well as a trisulfide derivative were measured in a different study investigating the stability of the hormone in aqueous solutions [67]. These findings suggest that aggregation involving disulfide scrambling of the thiol groups can be involved in sCT aggregation.

When testing the effect of hydroxyl radicals generated via a modified Fenton reaction (60-W tungsten lamp in combination with ferrous sulfate and ascorbic acid), sCT amyloid aggregates were detected. Interestingly, they were structurally similar to what was observed *in vivo* for hCT, in carcinoma medullary plaques [61].

In conclusion, *in vitro* oxidation of CT might produce fibrillar aggregates similar in structure as those observed *in vivo*. Met and Cys residues seem to be responsible for the observed structural changes. However, it is still poorly investigated if oxidation of His and Tyr, both present in hCT as well as sCT, can occur and contributes to aggregation or structural changes of this polypeptide.

Granulocyte colony-stimulating factor

Recombinant human G-CSF contains 175 amino acid residues, several of which are susceptible to oxidation [68].

Simultaneous oxidation of all four Met residues (in position 1, 122, 127 and 138) resulted in a dramatic decrease of the biological activity to 3% [69]. The biological activity of the HPLC fraction containing G-CSF with only Met 1 oxidized, was largely retained (i.e. 80% relative to G-CSF prior to oxidation), indicating that this residue is less important for the activity. In addition, engineered variants of G-CSF, where either Met 127 or Met 138 was replaced by leucine (Leu), were still sensitive to oxidation-induced inactivation. However, the variant with Leu replacement at both sites was more stable and retained *in vitro* biological activity following oxidative stress. All these experiments suggest that oxidation of Met 127 and Met 138 accounted for most of the activity loss [69].

Besides oxidation of Met residues in G-CSF, Cys oxidation is a point of concern. Under physiological conditions (37 °C, pH 7.0), G-CSF showed a significant propensity to aggregate. Several studies demonstrated that the free Cys in position 17, upon oxidation, forms a new disulfide bridge that is responsible for G-CSF aggregation [68, 70-71].

Growth hormone

Oxidative modifications of recombinant human growth hormone (hGH) have been widely described (Table I), mainly with respect to Met oxidation.

Relatively mild oxidative conditions, attained during exposure to hydrogen peroxide, have been reported to lead to selective generation of Met sulfoxides from the two most accessible Met residues in hGH (Met 14 and Met 125). Although this does not seem to induce gross conformational changes [72-73], the thermal stability of the protein dropped [74]. This may be due to the generation of Met 14 and Met 125 sulfoxides, which increases the polarity and the size of these amino acids; furthermore the new hydrogen bond networks that the protein can establish, may contribute to the observed decrease in thermal stability [74].

Cunningham et al. showed that Met 14 contributes only slightly to the binding of the hormone to its receptor [75]. In agreement with this study, the oxidation of Met 14 and Met 125 was reported to have little effect on hGH's receptor affinity and potency [73].

In contrast, Met 170 is located within the core of the native protein [76]. Nevertheless, the mass spectrometric analysis of a marketed hGH product

(Genotropin®, expressed in *E. coli* K12) revealed that 2% of the expressed protein contains several chemical modifications, including Met 170 sulfoxide [77]. This residue is located on the alpha helix IV of hGH, which is involved in one of the two receptor binding sites [76].

Steinmann et al. detected the oxidation of Met 170 (together with that of Met 14 and Met 125) during the exposure of hGH to peroxy radicals generated from 2,2'-azobis(2-methylpropionamidine) (AAPH) [78]. In addition, the authors detected di-tyrosine, Leu 101 hydroperoxide and several oxidation products of Tyr 103. These oxidation conditions led to the formation of dimers (21%) and trimers (13%).

Light exposure resulted in the selective oxidation of His 21 [79]. Furthermore, MCO, induced by exposure to Cu²⁺/ascorbate, specifically modified His 18 and His 21, which are both located on helix I and are critical for the integrity of the metal binding site of this hormone [80-81].

Insulin

One of the first reported experiments involving insulin oxidation dates back to 1948 when Frederick Sanger employed a mixture of hydrogen peroxide and formic acid, which generates performic acid, to fractionate insulin's A and B chains. Previously reduced Cys residues were oxidized to cysteic acid and also Tyr oxidation products were observed [82]. Since then, insulin oxidation has been extensively investigated.

Covalent aggregation of lyophilized insulin was observed upon storage at different temperatures and moisture contents [83]. Reduction of the native disulfide bridge followed by re-oxidation was responsible for new intermolecular disulfide bridges that mediate aggregate formation. Furthermore, aggregation involving Cys residues does not necessarily require the presence of this amino acid in its reduced form (i.e. free thiol groups) [83].

Therapeutic formulations of insulin, in solution or in suspension, analyzed after long term stability studies contained dimers and oligomers resulting from reduction-oxidation of Cys residues [83]. Formation of insulin aggregates with altered 3D structure was observed upon MCO using Cu²⁺/ascorbate. In particular, the Tyr oxidation products 3,4-dihydroxyphenylalanine (DOPA) and 2-amino-3-(3,4-dioxocyclohexa-1,5-dien-1-yl) propanoic acid (DOCH) were observed [9]. The latter, being an electrophile, was shown to be involved

in covalent cross-links with several amino groups of the insulin molecule, which led to new intra- and intermolecular cross-links. This oxidized and aggregated insulin induced anti-insulin antibodies when injected in transgenic mice immune tolerant for human insulin (unpublished data). MCO also led to the oxidation of His B5 and B10, which are important binding sites for zinc ions that play a central role in the formation of insulin's quaternary structure [84-85].

In the presence of zinc ions, insulin exists as hexamers [86], which are the main components in several long-acting therapeutic insulin formulations [87]. Oxidative stress that targets insulin's His residues involved in zinc ion binding can therefore result in unexpected pharmacokinetics.

Several studies have investigated the oxidative modifications that insulin can undergo in diabetic patients. Subjects affected by diabetes have generally high glucose plasma concentrations (hyperglycemia) and display oxidative stress associated with a decrease in the concentration of biological antioxidants such as reduced glutathione (GSH) [88]. The former event is responsible for glycation of insulin, i.e. the formation of a covalent adduct between insulin and glucose, where insulin is oxidized (loss of hydrogen atoms from amino groups).

Glycated insulin has been measured *in vivo* and its biological activity was decreased [89]. Another important consequence of hyperglycemia is the generation of α -oxoaldehydes like glyoxal, methylglyoxal and 3-deoxyglucosone [90], which can react with insulin generating aggregates of oxidized insulin [91].

Furthermore oxidative stress is responsible for lipid peroxidation of n-3 and n-6 polyunsaturated fatty acids, which eventually generates reactive aldehydes such as 4-hydroxy-2-hexenal and 4-hydroxy-2-nonenal [92]. The reaction between insulin and these reactive aldehydes (α , β unsaturated carbonyl compounds) occurs through Michael addition and introduces new carbonyl groups in the insulin molecule [92]. Glucose uptake as well as the hypoglycemic effect in mice was significantly reduced after treatment with insulin oxidized with reactive aldehydes, compared to treatment with native insulin [92].

More recently, based on the hypothesis that the plasma copper ion concentration is higher in diabetic patients than in normal subjects, Cheng et

al. studied the copper induced catalyzed oxidation of glycated insulin, which yielded aggregates, fragments and oxidation products [93].

Similarly, Guedes et al. investigated MCO of glycated insulin using the Fenton reaction, which induced aggregation and fragmentation of oxidized glycated insulin [94]. It is noteworthy that besides oxidation, insulin was found to be glycated on several sites including the N-terminal Gly A1, which is important for the biological activity [94-95].

Montes-Cortes et al. [96] discovered that the incubation of insulin with plasma from diabetic patients resulted in Tyr oxidation products, increased carbonyl content and decreased biological activity, similar to what observed upon Fenton oxidation of insulin [96-97]. These results suggest that a correlation between *in vivo* and *in vitro* oxidation may exist and that oxidative modifications on the insulin molecule can decrease the biological activity of this polypeptide hormone.

Interferon alpha

During storage, particularly at neutral and acidic conditions, IFN α -2a is known to undergo oxidation of Met residues [98].

Hydrogen peroxide-induced oxidation generated an IFN α -2a variant that featured reduced specific biological activity [99], but the sites of oxidation were not determined.

Immunogenicity of oxidized and aggregated IFN α -2a, formulated as lyophilized powder and stored at ambient temperature, was evaluated in patients: the oxidized form was more immunogenic than several other formulations of non-oxidized rhIFN α -2a [100-101]. Recently IFN α -2a oxidized by Cu²⁺/ascorbate was found to undergo structural modifications and aggregation; this product was immunogenic in a transgenic mouse model immune-tolerant for human IFN α -2a (unpublished results).

In IFN α -2b, all of the 5 Met residues are sensitive to oxidation in solution under different tested storage conditions [102]. Here, Met 111 oxidizes very easily and IFN α -2b containing oxidized Met 111 has been detected in a cream for topical use [103]. The alpha-helical content of the protein containing oxidized Met 111 was slightly decreased parallel to an increase in the beta-sheet contribution; however, the biological activity was not affected [104].

MCO of IFN α -2b, where Met 16, Met 21 and Met 148 were converted into the sulfoxide derivatives, generated aggregates that were immunogenic in the transgenic immune tolerant mouse model mentioned above [105].

Interferon beta

Under mild oxidative conditions, achieved with hydrogen peroxide, Orru et al. [106] observed the oxidation of the surface exposed Met 117 in IFN β -1a, which was the most reactive Met residue, followed by the oxidation of Met 36 and Met 1. Cys residues and the carbohydrate moiety were not modified and the biological activity of the protein was fully retained, pointing to minor consequences of Met oxidation for the activity of this cytokine [106].

Free Cys 17 in IFN β -1a can be involved in redox chemistry as demonstrated by the detection of 2% of disulfide linked aggregates after prolonged storage [107].

Furthermore, deglycosylated IFN β -1a was more sensitive to formation of insoluble, disulfide-linked aggregates with diminished biological activity, indicating a protective role of the carbohydrate moiety [108].

The oxidation of IFN β -1a with Cu²⁺/ascorbate generated covalent aggregates that contained native-like epitopes, had an average diameter of 1.6 μ m and were immunogenic in transgenic mice immune tolerant for human IFN β [109]. These aggregates were shown to be cross-linked through 1,4 and 1,6-type addition at Tyr oxidation products [110]. Oxidation mediated by hydrogen peroxide of IFN β -1a also yielded immunogenic IFN β -1a aggregates, but the percentage of monomeric IFN β -1a was higher compared to the MCO protein [109].

Oxytocin

Oxytocin is a small peptide which contains a six-amino acid ring (Cys1, Tyr2, Ile3, Gln4, Asn5, Cys6) and a tail of three amino acids (Pro7, Leu8, Gly9-NH2) [111]. As for CT, oxytocin formed tri- and tetrasulfide derivatives (introduction of one and two sulfur atoms, respectively, into its chemical structure) under accelerated degradation conditions at different pH and temperature [112].

Besides degradation involving sulfur atoms, heat stressed oxytocin formulations at pH 4.5, 7.0 and 9.0, generated also di-tyrosine-linked dimers, albeit at low percentages [112].

Rosei et al. showed that Tyr 2 in the oxytocin molecule, even though it is located internally in the primary sequence, functions better as hydrogen donor than free Tyr [113]. Hence, Tyr radicals, which are precursors in the generation of di-tyrosines [114], can be easily formed in the oxytocin molecule.

Parathyroid hormone

Synthetic parathyroid hormone contains two Met, three His, one Trp and one Phe, residues which are particularly oxidation-sensitive under several applied experimental conditions [34].

Oxidation of this hormone has been detected in blood from patients with renal disease [115]. During long term storage of hPTH (1-34) up to 24 weeks at room temperature, oxidation-induced aggregation and loss of secondary structure were observed. Although the oxidation sites were not determined, it was found that sucrose substantially reduced hPTH (1-34) oxidation. This protective effect was due to a more compact conformation that the hormone assumed in presence of the sugar, where amino acid residues sensitive to oxidation are more buried [116].

hPTH (1-34) features minimal tertiary structure [117], but the secondary structure is well defined and consists of approximately 33% alpha-helical content and 32% β -sheet [118]. Circular dichroism spectroscopic studies indicated that most of the secondary structure resides in the N-terminal region of this hormone, in agreement with the findings that oxidation of Met 8, close to the N-terminal region, produces substantial changes, while oxidation of Met 18 has a small impact on the secondary structure [118]. This finding correlated well with the observed alteration in biological activity: oxidation of Met 8, caused a remarkably larger suppression of the activity when compared to that of Met 18 [119].

More recently it was discovered that oxidation of Met 8 (into a sulfide radical cation during Fenton oxidation) results in the specific hydrolysis of the peptide bond between Met 8 and His 9, suggesting that also fragmentation of PTH (1-34) can occur during oxidation catalyzed by iron (II) [120].

A similar decreased activity by oxidation was observed for bovine [121] and porcine PTH, which both share Met 8 (but not Met 18) with the human counterpart [122]. Thus, the region around Met 8 is important for the activity. Nonetheless Met 18 in human PTH is another receptor recognition site [123], which would explain why the activity further decreased when both Met 8 and Met 18 are oxidized [119]. Based on these results the native secondary structure seems to be essential for receptor binding, as it is strongly perturbed upon oxidation of Met residues [118]. Additional studies indicated that Met 18 oxidizes more easily than Met 8, probably because PTH assumes a secondary structure that protects Met 8 against oxidation. Indeed, unfolding of the protein with 3 M guanidinium hydrochloride eliminated this difference, as it generates similarly surface-exposed Met residues [124].

Conclusion

The structural and biological consequences of several therapeutic proteins and peptides were reviewed. Redox chemistry of Cys residues is widely involved in the generation of new intra- and intermolecular covalent bonds, as observed for IFN β -1a, insulin, calcitonin and oxytocin.

Met oxidation usually involves solvent-exposed residues and often results in altered protein conformation and biological activity, even when the aggregation state of the protein is not affected.

His oxidation is generally catalyzed by trace metals that induce site-specific oxidation and can have drastic consequences on the pharmacokinetics or the activity of the protein, as observed for insulin and GH.

Phe and Tyr oxidation can yield Tyr oxidation products, which are electrophiles prone to 1,4- and 1,6-type addition: such modifications mediated aggregates formation in insulin and IFN β -1a. Oxidation-induced aggregation of a monoclonal IgG, IFN α -2a, IFN α -2b and IFN β -1a probably occurred via the same mechanism. All these oxidized and aggregated products were found to be more immunogenic than their native counterparts in mouse models, and for IFN α -2a also in human patients.

Trp oxidation, although occurring in the minority of the studied proteins, can also be responsible for bio-activity loss, as observed in some mAbs.

In conclusion, oxidation of peptides and proteins is an important degradation pathway. From the case studies discussed in this review, it is

clear that oxidation not only leads to changes in the primary structure, but also can perturb higher-order structures and induce aggregation, which in turn can have important biological consequences, such as altered pharmacokinetics, loss of function and enhanced immunogenicity. Therefore, it cannot be emphasized enough that control of oxidation during production, purification, formulation, transportation, storage and use of therapeutic proteins and peptides is of utmost importance for their quality, safety and efficacy.

References

- [1] B. Leader, Q. J. Baca, D. E. Golan. Protein therapeutics: a summary and pharmacological classification. *Nat. Rev. Drug. Discov.* **2008**, *7*, 21-39.
- [2] W. Wang. Instability, stabilization, and formulation of liquid protein pharmaceuticals. *Int. J. Pharm.* **1999**, *185*, 129-188.
- [3] J. Mohammadian-Mosaabadi, H. Naderi-Manesh, N. Maghsoudi, R. Khalilzadeh, S. A. Shojaosadati, M. Ebrahimi. Effect of oxidative stress on the production of recombinant human interferon-gamma in *Escherichia coli*. *Biotechnol. Appl. Biochem.* **2005**, *41*, 37-42.
- [4] R. Krishnamurthy, R. D. Madurawe, K. D. Bush, J. A. Lumpkin. Conditions Promoting Metal-Catalyzed Oxidations during Immobilized Cu-Iminodiacetic Acid Metal Affinity-Chromatography. *Biotechnol. Prog.* **1995**, *11*, 643-650.
- [5] B. A. Kerwin. Polysorbates 20 and 80 used in the formulation of protein biotherapeutics: Structure and degradation pathways. *J. Pharm. Sci.* **2008**, *97*, 2924-2935.
- [6] T. Takenawa, A. Yokota, M. Oda, H. Takahashi, M. Iwakura. Protein oxidation during long storage: identification of the oxidation sites in dihydrofolate reductase from *Escherichia coli* through LC-MS and fragment studies. *J. Biochem.* **2009**, *145*, 517-523.
- [7] C. Schöneich, L. B. Barrón. Posttranslational Oxidative Modifications of Proteins. *Encyclopedia of Analytical Chemistry.* **2006**.
- [8] B. A. Kerwin, R. L. Remmele, Jr. Protect from light: photodegradation and protein biologics. *J. Pharm. Sci.* **2007**, *96*, 1468-1479.
- [9] R. Torosantucci, O. Mozziconacci, V. Sharov, C. Schöneich, W. Jiskoot. Chemical modifications in aggregates of recombinant human insulin induced by metal-catalyzed oxidation: covalent cross-linking via michael addition to tyrosine oxidation products. *Pharm. Res.* **2012**, *29*, 2276-2293.
- [10] R. Torosantucci, B. Kükroer, A. Mero, M. Van Winsen, R. Tantipolphan, W. Jiskoot. Plain and mono-pegylated recombinant human insulin exhibit similar stress-induced aggregation profiles. *J. Pharm. Sci.* **2011**, *100*, 2574-2585.

- [11] K. C. Waterman, R. C. Adami, K. M. Alsante, J. Hong, M. S. Landis, F. Lombardo, C. J. Roberts. Stabilization of pharmaceuticals to oxidative degradation. *Pharm. Dev. Technol.* **2002**, *7*, 1-32.
- [12] S. Li, C. Schöneich, R. T. Borchardt. Chemical instability of protein pharmaceuticals: Mechanisms of oxidation and strategies for stabilization. *Biotechnol. Bioeng.* **1995**, *48*, 490-500.
- [13] E. R. Stadtman, B. S. Berlett. Fenton chemistry. Amino acid oxidation. *J. Biol. Chem.* **1991**, *266*, 17201-17211.
- [14] E. R. Stadtman. Metal ion-catalyzed oxidation of proteins: biochemical mechanism and biological consequences. *Free Radic. Biol. Med.* **1990**, *9*, 315-325.
- [15] E. R. Stadtman. Oxidation of free amino acids and amino acid residues in proteins by radiolysis and by metal-catalyzed reactions. *Annu. Rev. Biochem.* **1993**, *62*, 797-821.
- [16] M. J. Davies. The oxidative environment and protein damage. *Biochim. Biophys. Acta* **2005**, *1703*, 93-109.
- [17] S. Barelli, G. Canellini, L. Thadikaran, D. Crettaz, M. Quadroni, J. S. Rossier, J. D. Tissot, N. Lion. Oxidation of proteins: Basic principles and perspectives for blood proteomics. *Proteomics Clin. Appl.* **2008**, *2*, 142-157.
- [18] E. Shacter. Quantification and significance of protein oxidation in biological samples. *Drug Metab. Rev.* **2000**, *32*, 307-326.
- [19] J. L. Cleland, M. F. Powell, S. J. Shire. The Development of Stable Protein Formulations - a Close Look at Protein Aggregation, Deamidation, and Oxidation. *Crit. Rev. Ther. Drug* **1993**, *10*, 307-377.
- [20] M. Kamionka. Engineering of therapeutic proteins production in Escherichia coli. *Curr. Pharm. Biotechnol.* **2011**, *12*, 268-274.
- [21] K. R. Jayapal, K. F. Wlaschin, W. S. Hu, M. G. S. Yap. Recombinant protein therapeutics from CHO cells - 20 years and counting. *Chem. Eng. Prog.* **2007**, *103*, 40-47.
- [22] T. Miyata, S. Takizawa, C. van Ypersele de Strihou. Hypoxia. 1. Intracellular sensors for oxygen and oxidative stress: novel therapeutic targets. *Am. J. Physiol. Cell. Physiol.* **2011**, *300*, C226-231.
- [23] B. W. Row, R. G. Liu, W. Xu, L. Kheirandish, D. Gozal. Intermittent hypoxia is associated with oxidative stress and spatial learning deficits in the rat. *Am. J. Resp. Crit. Med.* **2003**, *167*, 1548-1553.
- [24] V. Pialoux, R. Mounier. Hypoxia-induced oxidative stress in health disorders. *Oxid. Med. Cell. Longev.* **2012**, 940121.
- [25] A. A. Lin, W. M. Miller. CHO cell responses to low oxygen: regulation of oxygen consumption and sensitization to oxidative stress. *Biotechnol. Bioeng.* **1992**, *40*, 505-516.
- [26] B. X. Yan, Z. Yates, A. Balland, G. R. Kleemann. Human IgG1 Hinge Fragmentation as the Result of H2O2-mediated Radical Cleavage. *J. Biol. Chem.* **2009**, *284*, 35390-35402.

- [27] Y. Wu, J. Levons, A. S. Narang, K. Raghavan, V. M. Rao. Reactive impurities in excipients: profiling, identification and mitigation of drug-excipient incompatibility. *AAPS Pharm. Sci. Tech.* **2011**, *12*, 1248-1263.
- [28] E. T. Maggio. Polysorbates, peroxides, protein aggregation, and immunogenicity: a growing concern. *J. Excip. Food Chem.* **2012**, *Vol 3*.
- [29] D. M. Miller, G. R. Buettner, S. D. Aust. Transition-Metals as Catalysts of Autoxidation Reactions. *Free Radic. Biol. Med.* **1990**, *8*, 95-108.
- [30] X. Huang, C. S. Atwood, R. D. Moir, M. A. Hartshorn, R. E. Tanzi, A. I. Bush. Trace metal contamination initiates the apparent auto-aggregation, amyloidosis, and oligomerization of Alzheimer's A β peptides. *J. Biol. Inorg. Chem.* **2004**, *9*, 954-960.
- [31] M. Lodovici, E. Bigagli. Oxidative stress and air pollution exposure. *J. Toxicol.*, **2011**, 487074.
- [32] I. Romieu, F. Castro-Giner, N. Kunzli, J. Sunyer. Air pollution, oxidative stress and dietary supplementation: a review. *Eur. Respir. J.* **2008**, *31*, 179-197.
- [33] G. R. Buettner, B. A. Jurkiewicz. Catalytic metals, ascorbate and free radicals: combinations to avoid. *Radiat. Res.* **1996**, *145*, 532-541.
- [34] J. A. Ji, B. Y. Zhang, W. Cheng, Y. J. Wang. Methionine, Tryptophan, and Histidine Oxidation in a Model Protein, PTH: Mechanisms and Stabilization. *J. Pharm. Sci.* **2009**, *98*, 4485-4500.
- [35] R. Rojas, G. Apodaca. Immunoglobulin transport across polarized epithelial cells. *Nat. Rev. Mol. Cell. Biol.* **2002**, *3*, 944-955.
- [36] Z. An, G. Forrest, R. Moore, M. Cukan, P. Haytko, L. Huang, S. Vitelli, J. Z. Zhao, P. Lu, J. Hua, C. R. Gibson, B. R. Harvey, D. Montgomery, D. Zaller, F. Wang, W. Strohl. IgG2m4, an engineered antibody isotype with reduced Fc function. *MAbs* **2009**, *1*, 572-579.
- [37] B. Al-Lazikani, A. M. Lesk, C. Chothia. Standard conformations for the canonical structures of immunoglobulins. *J. Mol. Biol.* **1997**, *273*, 927-948.
- [38] H. Pan, K. Chen, L. Chu, F. Kinderman, I. Apostol, G. Huang. Methionine oxidation in human IgG2 Fc decreases binding affinities to protein A and FcRn. *Protein Sci.* **2009**, *18*, 424-433.
- [39] G. M. Edelman, B. A. Cunningham, W. E. Gall, P. D. Gottlieb, U. Rutishauser, M. J. Waxdal. The covalent structure of an entire gammaG immunoglobulin molecule. *Proc. Natl. Acad. Sci. U. S. A.* **1969**, *63*, 78-85.
- [40] U. Rutishauser, B. A. Cunningham, C. Bennett, W. H. Konigsberg, G. M. Edelman. Amino acid sequence of the Fc region of a human gamma G-immunoglobulin. *Proc. Natl. Acad. Sci. U. S. A.* **1968**, *61*, 1414-1421.
- [41] E. van Loghem. Allotypic markers. *Monogr. Allergy.* **1986**, *19*, 40-51.
- [42] H. K. Khor, M. E. Jacoby, T. C. Squier, G. C. Chu, D. Chelius. Identification of methionine sulfoxide diastereomers in immunoglobulin gamma antibodies using methionine sulfoxide reductase enzymes. *MAbs* **2010**, *2*, 299-308.

- [43] R. G. Keck. The use of t-butyl hydroperoxide as a probe for methionine oxidation in proteins. *Anal. Biochem.* **1996**, *236*, 56-62.
- [44] P. Qi, D. B. Volkin, H. Zhao, M. L. Nedved, R. Hughes, R. Bass, S. C. Yi, M. E. Panek, D. Wang, P. Dalmonte, M. D. Bond. Characterization of the photodegradation of a human IgG1 monoclonal antibody formulated as a high-concentration liquid dosage form. *J. Pharm. Sci.* **2009**, *98*, 3117-3130.
- [45] H. Liu, G. Gaza-Bulseco, L. Zhou. Mass spectrometry analysis of photo-induced methionine oxidation of a recombinant human monoclonal antibody. *J. Am. Soc. Mass. Spectrom.* **2009**, *20*, 525-528.
- [46] P. E. Rao, D. J. Kroon. Orthoclone OKT3. Chemical mechanisms and functional effects of degradation of a therapeutic monoclonal antibody. *Pharm. Biotechnol.* **1993**, *5*, 135-158.
- [47] X. M. Lam, J. Y. Yang, J. L. Cleland. Antioxidants for prevention of methionine oxidation in recombinant monoclonal antibody HER2. *J. Pharm. Sci.* **1997**, *86*, 1250-1255.
- [48] G. Gaza-Bulseco, S. Faldu, K. Hurkmans, C. Chumsae, H. Liu. Effect of methionine oxidation of a recombinant monoclonal antibody on the binding affinity to protein A and protein G. *J. Chromatogr. B. Analyt. Technol. Biomed. Life Sci.* **2008**, *870*, 55-62.
- [49] A. Bertolotti-Ciarlet, W. R. Wang, R. Lownes, P. Pristatsky, Y. L. Fang, T. McKelvey, Y. Z. Li, Y. S. Li, J. Drummond, T. Prueksaritanont, J. Vlasak. Impact of methionine oxidation on the binding of human IgG1 to FcRn and Fc gamma receptors. *Mol. Immunol.* **2009**, *46*, 1878-1882.
- [50] W. Wang, J. Vlasak, Y. Li, P. Pristatsky, Y. Fang, T. Pittman, J. Roman, Y. Wang, T. Prueksaritanont, R. Ionescu. Impact of methionine oxidation in human IgG1 Fc on serum half-life of monoclonal antibodies. *Mol. Immunol.* **2011**, *48*, 860-866.
- [51] D. Liu, D. Ren, H. Huang, J. Dankberg, R. Rosenfeld, M. J. Cocco, L. Li, D. N. Brems, R. L. Remmele. Structure and stability changes of human IgG1 Fc as a consequence of methionine oxidation. *Biochemistry* **2008**, *47*, 5088-5100.
- [52] S. Wang, R. Ionescu, N. Peekhaus, J. Y. Leung, S. Ha, J. Vlasak. Separation of post-translational modifications in monoclonal antibodies by exploiting subtle conformational changes under mildly acidic conditions. *J. Chromatogr. A.* **2010**, *1217*, 6496-6502.
- [53] H. Liu, G. Gaza-Bulseco, T. Xiang, C. Chumsae. Structural effect of deglycosylation and methionine oxidation on a recombinant monoclonal antibody. *Mol. Immunol.* **2008**, *45*, 701-708.
- [54] W. Burkitt, P. Domann, G. O'Connor. Conformational changes in oxidatively stressed monoclonal antibodies studied by hydrogen exchange mass spectrometry. *Protein. Sci.* **2010**, *19*, 826-835.
- [55] D. Houde, Y. Peng, S. A. Berkowitz, J. R. Engen. Post-translational modifications differentially affect IgG1 conformation and receptor binding. *Mol. Cell. Proteomics* **2010**, *9*, 1716-1728.

- [56] V. Filipe, W. Jiskoot, A. H. Basmeh, A. Halim, H. Schellekens. Immunogenicity of different stressed IgG monoclonal antibody formulations in immune tolerant transgenic mice. *MAbs* **2012**, *4*, 740-752 .
- [57] Q. Luo, M. K. Joubert, R. Stevenson, R. R. Ketchem, L. O. Narhi, J. Wypych. Chemical modifications in therapeutic protein aggregates generated under different stress conditions. *J. Biol. Chem.* **2011**, *286*, 25134-25144.
- [58] M. K. Joubert, Q. Luo, Y. Nashed-Samuel, J. Wypych, L. O. Narhi. Classification and characterization of therapeutic antibody aggregates. *J. Biol. Chem.* **2011**, *286*, 25118-25133.
- [59] M. Hensel, R. Steurer, J. Fichtl, C. Elger, F. Wedekind, A. Petzold, T. Schlothauer, M. Molhoj, D. Reusch, P. Bulau. Identification of potential sites for tryptophan oxidation in recombinant antibodies using tert-butylhydroperoxide and quantitative LC-MS. *PLoS One* **2011**, *6*, e17708.
- [60] Z. P. Wei, J. H. Feng, H. Y. Lin, S. Mullapudi, E. Bishop, G. I. Tous, J. Casas-Finet, F. Hakki, R. Strouse, M. A. Schenerman. Identification of a single tryptophan residue as critical for binding activity in a humanized monoclonal antibody against respiratory syncytial virus. *Anal. Chem.* **2007**, *79*, 2797-2805.
- [61] M. C. Gaudiano, M. Diociaiuti, P. Bertocchi, L. Valvo. Effects induced by hydroxyl radicals on salmon calcitonin: a RP-HPLC, CD and TEM study. *Biochim. Biophys. Acta.* **2003**, *1623*, 33-40.
- [62] P. H. Tobler, F. A. Tschopp, M. A. Dambacher, W. Born, J. A. Fischer. Identification and characterization of calcitonin forms in plasma and urine of normal subjects and medullary carcinoma patients. *J. Clin. Endocrinol. Metab.* **1983**, *57*, 749-754.
- [63] R. Neher, B. Riniker, R. Maier, P. G. Byfield, T. V. Gudmundsson, I. MacIntyre. Human calcitonin. *Nature* **1968**, *220*, 984-986.
- [64] B. Riniker, R. Neher, R. Maier, F. W. Kahnt, P. G. Byfield, T. V. Gudmundsson, L. Galante, I. MacIntyre. Human calcitonin. I. Isolation and characterization. *Helv. Chim. Acta.* **1968**, *51*, 1738-1742.
- [65] F. Mulinacci, E. Poirier, M. A. Capelle, R. Gurny, T. Arvinte. Enhanced physical stability of human calcitonin after methionine oxidation. *Eur. J. Pharm. Biopharm.* **2011**, *78*, 229-238.
- [66] M. C. Gaudiano, M. Colone, C. Bombelli, P. Chistolini, L. Valvo, M. Diociaiuti. Early stages of salmon calcitonin aggregation: Effect induced by ageing and oxidation processes in water and in the presence of model membranes. *Biochim. Biophys. Acta* **2005**, *1750*, 134-145.
- [67] V. Windisch, F. DeLuccia, L. Duhau, F. Herman, J. J. Mencil, S. Y. Tang, M. Vuilhorgne. Degradation pathways of salmon calcitonin in aqueous solution. *J. Pharm. Sci.* **1997**, *86*, 359-364.

- [68] J. L. Reubsæet, J. H. Beijnen, A. Bult, E. Hop, S. D. Scholten, J. Teeuwssen, W. J. Underberg. Oxidation of recombinant methionyl human granulocyte colony stimulating factor. *J. Pharm. Biomed. Anal.* **1998**, *17*, 283-289.
- [69] H. S. Lu, P. R. Fausset, L. O. Narhi, T. Horan, K. Shinagawa, G. Shimamoto, T. C. Boone. Chemical modification and site-directed mutagenesis of methionine residues in recombinant human granulocyte colony-stimulating factor: Effect on stability and biological activity. *Arch. Biochem. Biophys.* **1999**, *362*, 1-11.
- [70] T. Arakawa, S. J. Prestrelski, L. O. Narhi, T. C. Boone, W. C. Kenney. Cysteine 17 of recombinant human granulocyte-colony stimulating factor is partially solvent-exposed. *J. Protein. Chem.* **1993**, *12*, 525-531.
- [71] S. W. Raso, J. Abel, J. M. Barnes, K. M. Maloney, G. Pipes, M. J. Treuheit, J. King, D. N. Brems. Aggregation of granulocyte-colony stimulating factor in vitro involves a conformationally altered monomeric state. *Protein. Sci.* **2005**, *14*, 2246-2257.
- [72] F. Mulinacci, S. E. J. Bell, M. A. H. Capelle, R. Gurny, T. Arvinte. Oxidized Recombinant Human Growth Hormone That Maintains Conformational Integrity. *J. Pharm. Sci.* **2011**, *100*, 110-122.
- [73] L. C. Teh, L. J. Murphy, N. L. Huq, A. S. Surus, H. G. Friesen, L. Lazarus, G. E. Chapman. Methionine oxidation in human growth hormone and human chorionic somatomammotropin. Effects on receptor binding and biological activities. *J. Biol. Chem.* **1987**, *262*, 6472-6477.
- [74] F. Mulinacci, M. A. Capelle, R. Gurny, A. F. Drake, T. Arvinte. Stability of human growth hormone: influence of methionine oxidation on thermal folding. *J. Pharm. Sci.* **2011**, *100*, 451-463.
- [75] B. C. Cunningham, J. A. Wells. Comparison of a structural and a functional epitope. *J. Mol. Biol.* **1993**, *234*, 554-563.
- [76] A. M. de Vos, M. Ultsch, A. A. Kossiakoff. Human growth hormone and extracellular domain of its receptor: crystal structure of the complex. *Science* **1992**, *255*, 306-312.
- [77] F. Hepner, E. Czeszar, E. Roitinger, G. Lubec. Mass spectrometrical analysis of recombinant human growth hormone (Genotropin(R)) reveals amino acid substitutions in 2% of the expressed protein. *Proteome Sci.* **2005**, *3*, 1.
- [78] D. Steinmann, J. A. Ji, Y. J. Wang, C. Schöneich. Oxidation of human growth hormone by oxygen-centered radicals: formation of Leu-101 hydroperoxide and Tyr-103 oxidation products. *Mol. Pharm.* **2012**, *9*, 803-814.
- [79] S. H. Chang, G. M. Teshima, T. Milby, B. GilleceCastro, E. CanovaDavis. Metal-catalyzed photooxidation of histidine in human growth hormone. *Anal. Biochem.* **1997**, *244*, 221-227.
- [80] S. W. Hovorka, J. Hong, J. L. Cleland, C. Schöneich. Metal-catalyzed oxidation of human growth hormone: modulation by solvent-induced changes of protein conformation. *J. Pharm. Sci.* **2001**, *90*, 58-69.

- [81] F. Zhao, E. Ghezzi-Schöneich, G. I. Aced, J. Hong, T. Milby, C. Schöneich. Metal-catalyzed oxidation of histidine in human growth hormone. Mechanism, isotope effects, and inhibition by a mild denaturing alcohol. *J. Biol. Chem.* **1997**, *272*, 9019-9029.
- [82] F. Sanger. Fractionation of oxidized insulin. *Biochem. J.* **1949**, *44*, 126-128.
- [83] H. R. Costantino, R. Langer, A. M. Klivanov. Moisture-Induced Aggregation of Lyophilized Insulin. *Pharm. Res.* **1994**, *11*, 21-29.
- [84] S. W. Hovorka, H. Biesiada, T. D. Williams, A. Huhmer, C. Schöneich. High sensitivity of Zn²⁺ insulin to metal-catalyzed oxidation: detection of 2-oxo-histidine by tandem mass spectrometry. *Pharm. Res.* **2002**, *19*, 530-537.
- [85] V. Sadineni, C. Schöneich. Selective oxidation of Zn²⁺ Insulin catalyzed by Cu²⁺. *J. Pharm. Sci.* **2007**, *96*, 1844-1847.
- [86] R. Tantipolphan, S. Romeijn, J. den Engelsman, R. Torosantucci, T. Rasmussen, W. Jiskoot. Elution behavior of insulin on high-performance size exclusion chromatography at neutral pH. *J. Pharm. Biomed. Anal.* **2010**, *52*, 195-202.
- [87] I. Jonassen, S. Havelund, T. Hoeg-Jensen, D. B. Steensgaard, P. O. Wahlund, U. Ribel. Design of the novel protraction mechanism of insulin degludec, an ultra-long-acting basal insulin. *Pharm. Res.* **2012**, *29*, 2104-2114.
- [88] A. C. Maritim, R. A. Sanders, J. B. Watkins, 3rd. Diabetes, oxidative stress, and antioxidants: a review. *J. Biochem. Mol. Toxicol.* **2003**, *17*, 24-38.
- [89] S. J. Hunter, A. C. Boyd, F. P. O'Harte, A. M. McKillop, M. I. Wiggam, M. H. Mooney, J. T. McCluskey, J. R. Lindsay, C. N. Ennis, R. Gamble, B. Sheridan, C. R. Barnett, H. McNulty, P. M. Bell, P. R. Flatt. Demonstration of glycated insulin in human diabetic plasma and decreased biological activity assessed by euglycemic-hyperinsulinemic clamp technique in humans. *Diabetes* **2003**, *52*, 492-498.
- [90] P. J. Thornalley, A. Langborg, H. S. Minhas. Formation of glyoxal, methylglyoxal and 3-deoxyglucosone in the glycation of proteins by glucose. *Biochem. J.* **1999**, *344 Pt 1*, 109-116.
- [91] X. Jia, D. J. Olson, A. R. Ross, L. Wu. Structural and functional changes in human insulin induced by methylglyoxal. *FASEB J.* **2006**, *20*, 1555-1557.
- [92] N. J. Pillon, R. E. Vella, L. Souleere, M. Becchi, M. Lagarde, C. O. Soulage. Structural and functional changes in human insulin induced by the lipid peroxidation byproducts 4-hydroxy-2-nonenal and 4-hydroxy-2-hexenal. *Chem. Res. Toxicol.* **2011**, *24*, 752-762.
- [93] R. Z. Cheng, S. Kawakishi. Site-specific oxidation of histidine residues in glycated insulin mediated by Cu²⁺. *Eur. J. Biochem.* **1994**, *223*, 759-764.
- [94] S. Guedes, R. Vitorino, M. R. M. Domingues, F. Amado, P. Domingues. Oxidative modifications in glycated insulin. *Anal. Bioanal. Chem.* **2010**, *397*, 1985-1995.
- [95] J. Gliemann, S. Gammeltoft. The biological activity and the binding affinity of modified insulins determined on isolated rat fat cells. *Diabetologia* **1974**, *10*, 105-113.
- [96] D. H. Montes-Cortes, J. J. Hicks, G. M. Ceballos-Reyes, J. R. Garcia-Sanchez, R. Medina-Navarro, I. M. Olivares-Corichi. Chemical and functional changes of human insulin by in

- vitro incubation with blood from diabetic patients in oxidative stress. *Metabolism* **2010**, *59*, 935-942.
- [97] I. M. Olivares-Corichi, G. Ceballos, R. Medina-Santillan, R. Medina-Navarro, A. M. Guzman-Grenfell, J. J. Hicks. Oxidation by reactive oxygen species (ROS) alters the structure of human insulin and decreases the insulin-dependent D-glucose-C14 utilization by human adipose tissue. *Front. Biosci.* **2005**, *10*, 3127-3131.
- [98] V. K. Sharma, D. S. Kalonia. Polyethylene glycol-induced precipitation of interferon alpha-2a followed by vacuum drying: development of a novel process for obtaining a dry, stable powder. *AAPS Pharm. Sci.* **2004**, *6*, E4.
- [99] L. Larocque, A. Bliu, R. Xu, A. Diress, J. Wang, R. Lin, R. He, M. Girard, X. Li. Bioactivity determination of native and variant forms of therapeutic interferons. *J. Biomed. Biotechnol.* **2011**, *2011*, 174615.
- [100] J. C. Ryff. Clinical investigation of the immunogenicity of interferon-alpha 2a. *J. Interferon Cytokine Res.* **1997**, *17 Suppl 1*, S29-33.
- [101] E. Hochuli. Interferon immunogenicity: technical evaluation of interferon-alpha 2a. *J. Interferon Cytokine Res.* **1997**, *17 Suppl 1*, S15-21.
- [102] M. Cindric, N. Galic, M. Vuletic, M. Klaric, V. Drevenkar. Evaluation of recombinant human interferon alpha-2b structure and stability by in-gel tryptic digestion, H/D exchange and mass spectrometry. *J. Pharm. Biomed. Anal.* **2006**, *40*, 781-787.
- [103] G. L. Praveen Kumar RB, Jinghui Shen, Kim Gaspar, John Docherty, Marianna Foldvari. Stabilization of Interferon alpha-2b in a Topical Cream. *Pharmaceutical Technology* **2009**, *33*, 80-86.
- [104] G. Gitlin, A. Tsarbopoulos, S. T. Patel, W. Sydor, B. N. Pramanik, S. Jacobs, L. Westreich, S. Mittelman, J. N. Bausch. Isolation and characterization of a monomethioninesulfoxide variant of interferon alpha-2b. *Pharm. Res.* **1996**, *13*, 762-769.
- [105] S. Hermeling, L. Aranha, J. M. A. Damen, M. Slijper, H. Schellekens, D. J. A. Crommelin, W. Jiskoot. Structural characterization and immunogenicity in wild-type and immune tolerant mice of degraded recombinant human interferon alpha2b. *Pharm. Res.* **2005**, *22*, 1997-2006.
- [106] S. Orru, A. Amoresano, R. Siciliano, R. Napoleoni, O. Finocchiaro, A. Datola, E. De Luca, A. Sirna, P. Pucci. Structural analysis of modified forms of recombinant IFN-beta produced under stress-simulating conditions. *Biol. Chem.* **2000**, *381*, 7-17.
- [107] M. Karpusas, M. Nolte, C. B. Benton, W. Meier, W. N. Lipscomb, S. Goelz. The crystal structure of human interferon beta at 2.2-angstrom resolution. *Proc. Natl. Acad. Sci. U. S. A.* **1997**, *94*, 11813-11818.
- [108] L. Runkel, W. Meier, R. B. Pepinsky, M. Karpusas, A. Whitty, K. Kimball, M. Brickelmaier, C. Muldowney, W. Jones, S. E. Goelz. Structural and functional differences between glycosylated and non-glycosylated forms of human interferon-beta (IFN-beta). *Pharm. Res.* **1998**, *15*, 641-649.

- [109] M. M. van Beers, M. Sauerborn, F. Gilli, V. Brinks, H. Schellekens, W. Jiskoot. Oxidized and aggregated recombinant human interferon beta is immunogenic in human interferon beta transgenic mice. *Pharm. Res.* **2011**, *28*, 2393-2402.
- [110] R. Torosantucci, V. S. Sharov, M. van Beers, V. Brinks, C. Schöneich, W. Jiskoot. Identification of Oxidation Sites and Covalent Cross-Links in Metal Catalyzed Oxidized Interferon Beta-1a: Potential Implications for Protein Aggregation and Immunogenicity. *Mol. Pharm.* **2013**, *10*, 2311-2322.
- [111] C. Avanti, J. P. Amorij, D. Setyaningsih, A. Hawe, W. Jiskoot, J. Visser, A. Kedrov, A. J. M. Driessen, W. L. J. Hinrichs, H. W. Frijlink. A New Strategy to Stabilize Oxytocin in Aqueous Solutions: I. The Effects of Divalent Metal Ions and Citrate Buffer. *Aaps Journal* **2011**, *13*, 284-290.
- [112] A. Hawe, R. Poole, S. Romeijn, P. Kasper, R. van der Heijden, W. Jiskoot. Towards heat-stable oxytocin formulations: analysis of degradation kinetics and identification of degradation products. *Pharm. Res.* **2009**, *26*, 1679-1688.
- [113] R. C. M. A. Rosei, C. Blarzino, C. Foppoli, L. Mosca. The oxidation of oxytocin and vasopressin by peroxidase/H₂O₂ system. *Amino Acids* **1995**, *8*, 385-391.
- [114] Y. Kato, N. Kitamoto, Y. Kawai, T. Osawa. The hydrogen peroxide/copper ion system, but not other metal-catalyzed oxidation systems, produces protein-bound dityrosine. *Free Radic. Biol. Med.* **2001**, *31*, 624-632.
- [115] B. Hocher, F. P. Armbruster, S. Stoeva, C. Reichetzeder, H. J. Gron, I. Lieker, D. Khadzhynov, T. Slowinski, H. J. Roth. Measuring parathyroid hormone (PTH) in patients with oxidative stress--do we need a fourth generation parathyroid hormone assay? *PLoS One* **2012**, *7*, e40242.
- [116] M. Kamberi, Y. J. Kim, B. Jun, C. M. Riley. The effects of sucrose on stability of human brain natriuretic peptide [hBNP (1-32)] and human parathyroid hormone [hPTH (1-34)]. *J. Pept. Res.* **2005**, *66*, 348-356.
- [117] J. A. Barden, B. E. Kemp. NMR solution structure of human parathyroid hormone(1-34). *Biochemistry* **1993**, *32*, 7126-7132.
- [118] J. E. Zull, S. K. Smith, R. Wiltshire. Effect of methionine oxidation and deletion of amino-terminal residues on the conformation of parathyroid hormone. Circular dichroism studies. *J. Biol. Chem.* **1990**, *265*, 5671-5676.
- [119] Y. Nabuchi, E. Fujiwara, K. Ueno, H. Kuboniwa, Y. Asoh, H. Ushio. Oxidation of recombinant human parathyroid hormone: Effect of oxidized position on the biological activity. *Pharm. Res.* **1995**, *12*, 2049-2052.
- [120] O. Mozziconacci, J. A. Ji, Y. J. Wang, C. Schöneich. Metal-catalyzed oxidation of protein methionine residues in human parathyroid hormone (1-34): formation of homocysteine and a novel methionine-dependent hydrolysis reaction. *Mol. Pharm.* **2013**, *10*, 739-755.

- [121] A. L. Frelinger, 3rd, J. E. Zull. Oxidized forms of parathyroid hormone with biological activity. Separation and characterization of hormone forms oxidized at methionine 8 and methionine 18. *J. Biol. Chem.* **1984**, *259*, 5507-5513.
- [122] J. S. Woodhead, J. L. O'Riordan, H. T. Keutmann, M. L. Stoltz, B. F. Dawson, H. D. Niall, C. J. Robinson, J. T. Potts, Jr. Isolation and chemical properties of porcine parathyroid hormone. *Biochemistry* **1971**, *10*, 2787-2792.
- [123] M. P. Caulfield, R. L. McKee, M. E. Goldman, L. T. Duong, J. E. Fisher, C. T. Gay, P. A. DeHaven, J. J. Levy, E. Roubini, R. F. Nutt, et al. The bovine renal parathyroid hormone (PTH) receptor has equal affinity for two different amino acid sequences: the receptor binding domains of PTH and PTH-related protein are located within the 14-34 region. *Endocrinology* **1990**, *127*, 83-87.
- [124] A. L. Frelinger, 3rd, J. E. Zull. The role of the methionine residues in the structure and function of parathyroid hormone. *Arch. Biochem. Biophys.* **1986**, *244*, 641-649.

Chapter 3

Plain and mono-PEGylated recombinant human insulin exhibit similar stress-induced aggregation profiles

Riccardo Torosantucci¹, Başak Kükrer¹, Anna Mero², Margot Van Winsen¹, Ruedeeporn Tantipolphan¹, Wim Jiskoot¹

¹Division of Drug Delivery Technology, Leiden Academic Centre for Drug Research (LACDR), Leiden University, Leiden, The Netherlands.

²Department of Pharmaceutical Sciences, University of Padova, Padova, Italy.

Journal of Pharmaceutical Sciences **2011**, *100*, 2574-2585.

Abstract

PEGylation has been suggested to improve the stability of insulin, but evidence for that is scarce. Here we compared the forced aggregation behavior of insulin and mono-PEGylated insulin (PEG-insulin). Therefore, recombinant human insulin was conjugated on Lys B29 with 5 kDa PEG. PEG-insulin was purified by size exclusion chromatography (SEC) and characterized by mass spectrometry. Next, insulin and PEG-insulin were subjected to heating at 75 °C, metal-catalyzed oxidation and glutaraldehyde cross-linking. The products were characterized physicochemically by complementary analytical methods. Mono-PEGylation of insulin was confirmed by SEC and mass spectrometry. Under each of the applied stress conditions, insulin and PEG-insulin showed comparable degradation profiles. All the stressed samples showed submicron aggregates in the size range between 50-500 nm. Covalent aggregates and conformational changes were found for both oxidized products. Insulin and its PEGylated counterpart also exhibited similar characteristics when exposed to heat stress, i.e. slightly changed secondary and tertiary structures, covalent aggregates with partially intact epitopes and separation of chain A from chain B. Glutaraldehyde-treated insulin and PEG-insulin both contained covalent and noncovalent aggregates with intact epitopes, showed partially perturbed secondary structure and substantial loss of tertiary structure. From these results we conclude that PEGylation does not protect insulin against forced aggregation.

Introduction

Throughout almost one century, different production platforms, purification protocols and formulations have been investigated in order to produce highly purified insulin with high physico-chemical stability [1]. Still, none of the current insulin formulations is capable of fully protecting this small polypeptide hormone against degradation. In particular, insulin aggregation is hard to avoid and the presence of covalent aggregates in insulin products has been associated with the induction of anti-insulin antibodies from which systemic hypersensitivity and insulin resistance may arise [2-4].

With the progress made in organic and amino acid chemistry, the chemical modification of proteins has become one of the methods to improve the half-life of a therapeutic protein. In particular, PEGylation has been widely used to achieve this aim and PEGylation has been proposed also as a way to increase the stability of biopharmaceutical products [5-6]. A great number of procedures and chemicals have been developed to achieve site-specific modifications [7].

The influence of PEG conjugation to insulin on its stability with respect to the formation of fibrils has been investigated by several authors [8-10]. Briefly, it was found that PEGylation on lysine (Lys) B29 or phenylalanine (Phe) B1 improved insulin's long-term physical stability, as evaluated by a shaking testing done at 100 strokes/min and 37 °C, parallel to an enhancement of its plasma half-life. The higher the molecular weight of PEG (ranging between 750 Da and 2 kDa), the more stable the conjugated protein was found to be. However, when conjugating 5 kDa PEG on Phe B1, a slight decrease in the biological activity has been found [6]. A similar decrease in the activity of the hormone was observed when two 600 Da or 2 kDa PEG chains were covalently bound to the protein [6]. However, no literature is available concerning the behavior of PEGylated-insulin when exposed to other stress factors.

The aim of this work was to investigate the effect of three different stress methods on the stability of PEGylated-insulin in comparison to unmodified insulin, with a special emphasis on the formation of amorphous, non-fibrillar aggregates. To this end, mono-PEGylated insulin (PEG-insulin) was prepared by site-specific linkage of 5 kDa PEG onto Lys B29 of recombinant human insulin. Both proteins, insulin and PEG-insulin, were exposed to three stress conditions, i.e. thermal stress, oxidation by Cu²⁺/ascorbate, and cross-linking with glutaraldehyde. By using complementary physicochemical analytical

methods, we show that the sensitivity of PEG-insulin to these stress factors is comparable to that of its unmodified counterpart.

Materials and Methods

Materials

Recombinant human insulin containing 0.4% (w/w) zinc ions was provided by Schering Plough, Oss, The Netherlands. Glutaraldehyde, sodium borohydride, L-ascorbic acid, copper (II) chloride, arginine, disodium hydrogen phosphate, boric acid and ammonium bicarbonate were purchased from Sigma-Aldrich, Germany. Alpha-methoxy omega-carboxylic acid succinimidyl ester poly(ethylene glycol) (MeO-PEG-NHS, 5 kDa) was purchased from Iris Biotech GmbH, Germany. Glacial acetic acid and acetonitrile were purchased from Boom, The Netherlands. 2,5-dihydroxybenzoic acid (DHB) and sinapinic acid (SA) peptide/protein calibrations standards for MALDI-TOF MS were purchased from Bruker Daltonik GmbH, Bremen, Germany. Deionized water for MS measurements was obtained from a Milli-Q water purification system (Millipore, USA). All chemicals were of analytical grade and used without further purification.

Synthesis and purification of PEG-insulin

Ten mg of insulin were dissolved in 0.1 M hydrochloric acid and brought to a final volume of 1 mL with 60% acetonitrile/40% H_3BO_3 0.1 M, pH 10. Under these alkaline conditions the nucleophilicity of the ϵ -amino group of the Lys B29 is higher than that of the α -amino groups of Gly A1 and Phe B1, so the conjugation should preferentially occur in position B29 [9].

A 3-fold molar excess of MEO-PEG-NHS, 5 kDa, was added in three times, 1 equivalent every 15 minutes, to the insulin solution. After 45 minutes the reaction mixture was purified by SEC, using an Insulin HMWP Column, 7.8 x 300 mm (Waters) and an Agilent 1200 HPLC system (Agilent Technologies, Palo Alto, CA, USA) coupled to a UV detector set at 276 nm. The mobile phase was composed of a mixture of 1 g/L L-arginine aqueous solution:acetonitrile:glacial acetic acid 65:20:15 (v/v/v) as reported in the United States and European pharmacopeias [11-12]. The elution buffer was freshly prepared, filtered and degassed prior to use.

After purification, PEG-insulin was concentrated to about 0.5 mg/mL using centrifugal filter units (Ultra 15 mL, 10 kDa, Amicon, Millipore, USA) and dialyzed against 10 mM sodium phosphate, pH 7.4 (PB), using Slide-A-Lyzer dialysis cassettes with 10 kDa cut-off (Biorad, The Netherlands).

Reduction and alkylation of PEG-insulin

To confirm that PEG was conjugated to chain B, first sodium phosphate buffer was exchanged with 0.1 M ammonium bicarbonate (ABI), pH 8, using centrifugal filter units. Next PEG-insulin was reduced by a 50-fold excess of DTT and alkylated by a 100-fold excess of iodoacetamide with respect to the moles of disulfides contained in the insulin molecule, as reported by Tuesca et al [13].

Digestion of PEG-insulin and insulin

To confirm the site of conjugation, 0.5 mg/mL of PEG-insulin and insulin in 0.1 M ABI, pH 8, were treated with a 0.25 mL of gel immobilized trypsin (Pierce Chemical Company, Rockville, IL). The mixture was incubated overnight at 37 °C. The sample was shaken for ten seconds at 300 rpm every five minute using a Thermomixer (Eppendorf, USA). The immobilized trypsin was then removed from the solution by centrifugation and the supernatant was recovered, concentrated with centrifugal filter units (Amicon, Ultra 15 mL, 3 kDa) and kept at 4 °C until analysis. MS results were eventually compared.

Forced degradation of insulin and PEG-insulin

All the formulations and the dilutions were made in PB. PEG-insulin was obtained as described above. Insulin (not PEGylated) was first dissolved in 0.1 M hydrochloric acid and diluted in PB. The pH was adjusted to 7.4 using 0.1 M sodium hydroxide and the insulin concentration was determined by UV spectroscopy, using a molecular weight of 5.8 kDa and an extinction coefficient of $6200 \text{ M}^{-1} \text{ cm}^{-1}$ at 276 nm [14]. Further dilution in PB was done to obtain a final insulin concentration of 0.5 mg/mL.

Heat treatment was done by heating solutions of 0.5 mg/mL insulin and PEG-insulin, 1 mL in 1.5-mL safe-lock eppendorf tubes, at 75 °C for 1 hour using a water bath [15].

Metal-catalyzed oxidation was performed by adding to solutions of 0.5 mg/mL insulin and PEG-insulin, 2.5 mL in 5-mL glass light-resistant vials, 0.4 mM CuCl₂ in PB, to a final concentration of 40 μM. The reaction was allowed to proceed for 10 minutes and subsequently 40 mM L-ascorbic acid in PB was added to a final concentration of 4 mM. After three hours of incubation at room temperature the reaction was quenched by adding 100 mM EDTA in PB, to a final concentration of 1 mM [16]. The oxidized samples were dialyzed at 4 °C against PB for 24 hours.

Cross-linking with glutaraldehyde was achieved by incubating for 2 minutes 2.5 mL (in 5-mL glass light-resistant vials) of 0.5 mg/mL insulin and PEG-insulin solutions, with glutaraldehyde (final concentration of 4.23 mM). After 2 minutes, 11 μL of 12% (w/w) NaBH₄ in 14 M NaOH, diluted 30 times in water, was added to a final concentration of 646 μM and the mixtures were left in the dark at room temperature for 20 hours [17]. Next, the solutions were dialyzed at 4 °C against PB for 24 hours.

UV spectroscopy

UV/VIS measurements were performed with an Agilent 8453 UV/VIS spectrophotometer (Waldbronn, Germany), which included a Peltier element for temperature control. Quartz cells with a path length of 1 cm were used for all measurements. Scans were taken from 200-900 nm with 1 nm intervals at 25 °C.

Near-UV and far-UV circular dichroism (CD) spectroscopy

Near-UV CD and far-UV CD spectra were recorded from 250 to 320 nm and 190 to 250 nm, respectively, using a Jasco J-815 CD spectrometer (Jasco International, Tokyo, Japan). Analyses were performed in a 1-cm (near-UV CD) and a 1-mm (far-UV CD) path length quartz cuvette at 20 °C using a scan rate of 100 nm/min, a response time of 2 s, and a bandwidth of 1 nm. Each spectrum was the result of an averaging of 6 repeated scans and background

corrected with the corresponding buffer spectrum. The CD signals were converted to molar ellipticity per amino acid residue.

Nanoparticle tracking analysis (NTA)

NTA measurements were performed at room temperature with a NanoSight LM20 (NanoSight, Amesbury, United Kingdom), equipped with a sample chamber with a 640-nm laser and a Viton fluoroelastomer O-ring, as described previously by Filipe et al ^[18]. Briefly, the samples were injected in the sample chamber with sterile syringes (BD Discardit II, New Jersey, USA) until the liquid reached the tip of the nozzle. The software used for capturing and analyzing the data was the NTA 2.0 Build 127. The samples were measured for 60 s with manual shutter and gain adjustments. The “single shutter and gain mode” was used to capture the protein aggregates. The mean size was calculated by using the NTA software.

Light obscuration analysis

Light obscuration analysis was performed using a PAMAS SVSS-C (PAMAS GmbH, Bad Salzuflen, Germany). The pre-run volume was 0.3 mL and for each sample, 3 measurements were done, using a volume of 0.2 mL. Between each measurement, the instrument was washed with Milli-Q water, followed by 30% (v) ethanol in water if necessary. After cleaning, water was measured to confirm that the instrument was cleaned (max. 50 particles/mL, 1 μ m). For the measurement the samples were diluted 100-fold in PB and the blank was subtracted.

Intrinsic and extrinsic steady state fluorescence spectroscopy

Intrinsic fluorescence was measured in 96-well plates using the plate reader unit of the FS920 fluorescence spectrometer (Edinburgh Instruments). For the measurement, all the formulations were diluted to a concentration of 0.1 mg/mL to avoid inner filter effects. Tyrosine was selectively excited at 275 nm. The emission spectra were recorded from 290 to 400 nm using a step size of 2 nm, gain of 145, Z-position of 20 mm, number of flashes 50 with a frequency of 400 Hz. The extrinsic fluorescent dyes 4,4'-dianilino-1,1'-

binaphthyl-5,5'-disulfonic acid (Bis-ANS) and thioflavin T (ThT) were employed to characterize the aggregates [19].

For measurements of Bis-ANS fluorescence, 10 μL of an aqueous solution of 42 μM Bis-ANS were added to 200 μL of 0.1 mg/mL (PEGylated) insulin sample. The concentration of the stock solution was determined by using an extinction coefficient of 16760 $\text{M}^{-1} \text{cm}^{-1}$ in water at 385 nm. Each sample was excited at 385 nm and the emission spectra were recorded between 400 and 550 nm, using a step size of 2 nm, gain of 150, Z-position of 20 mm, number of flashes 50 with a frequency of 400 Hz.

For measurements of ThT fluorescence, 10 μL of a 210 μM aqueous solution of ThT were added to 200 μL of 0.1 mg/mL (PEGylated) insulin sample. The determination of the concentration of the stock solution was done using an extinction coefficient of 36000 $\text{M}^{-1} \text{cm}^{-1}$ in water at 412 nm. Each sample was excited at 450 nm and the emission spectra were recorded between 465 and 600 nm, using a step size of 2 nm, gain of 130, Z-position of 20 mm, number of flashes 50 with a frequency of 400 Hz.

Sodium dodecyl sulfate polyacrylamide gel electrophoresis (SDS-PAGE)

Acrylamide gradient gels (10-20% tris-tricine) were purchased from Bio-Rad and run under reducing (sample buffer containing 5% (v/v) β -mercaptoethanol) and nonreducing (sample buffer without β -mercaptoethanol) conditions at 100 V at room temperature. The cathode electrophoresis buffer was 0.1 M tris(hydroxymethyl) aminomethane, 0.1 M tricine, and 3 mM SDS, pH 8.3. The anode electrophoresis buffer was 0.1 M Tris pH 8.9. Gel electrophoresis was performed with a Biorad Protean III system (Biorad, Veenendaal, The Netherlands). Samples were boiled at 95 $^{\circ}\text{C}$ for 2 minutes and then centrifuged for 1 minute at 13000 rpm, before application to the gel. A polypeptide marker solution (Biorad, The Netherlands) was included on the gel for apparent molecular weight determination.

Western blotting

Proteins run on SDS-PAGE gels were blotted onto a polyvinylidene difluoride (PVDF) immuno blotting membrane, overnight at 4 $^{\circ}\text{C}$ using a mini trans-blot

system with a voltage applied of 30 V (Biorad, The Netherlands). Blots were blocked for 2 hours at room temperature with 0.1% (w/v) nonfat milk powder in 0.1% (v/v) Tween 20 in phosphate-buffered saline (PBS) with constant orbital shaking. After washing with 0.1% (v/v) Tween 20 in PBS and with water, the blots were incubated with polyclonal guinea pig anti-human insulin antibody (Abcam) in 0.1% (w/v) nonfat milk powder in 0.1% (v/v) Tween 20 in PBS overnight at 4 °C with constant orbital shaking. Blots were washed with 0.1% (v/v) Tween 20 in PBS and with water. Blots were incubated with peroxidase labeled goat polyclonal anti-guinea pig IgG (Abcam) in 0.1% (w/v) nonfat milk powder in 0.1% (v/v) Tween 20 in PBS overnight at 4 °C with constant orbital shaking. Blots were washed with 0.1% (v/v) Tween 20 in PBS and with water and incubated in a solution of 4-chloro-1-naphthol (Sigma-Aldrich) in methanol (20% (v/v)), water, and H₂O₂ (0.015% (v/v)). After color development the blots were stored in water overnight in the dark to increase the intensity of the bands.

Mass spectrometry

Matrix-assisted laser desorption/ionization time-of-flight mass spectrometry (MALDI-TOF MS) was performed on BIFLEX MALDI-TOF MS (Bruker Daltonics, Bremen, Germany). Specifically, 1 µL of sample solution and 1 µL of matrix solution were mixed in an Eppendorf tube and applied onto the MALDI sample plate and let to dry at room temperature. Saturated DHB was prepared in a mixture of 50% acetonitrile, 50% deionized water, and 0.1% trifluoroacetic acid as matrix solutions. Analysis was performed in the linear positive mode with delayed extraction of 200 ns. The samples were irradiated by a 337 nm pulsed nitrogen laser. The laser intensity was optimized to give the best signal-to-noise ratio for each sample. The acceleration voltage was 19 kV. Each mass spectrum was generated by averaging ~300 laser shots. MALDI-TOF MS evaluation was performed with FlexAnalysis Software (Bruker Daltonics) by a centroid peak detection algorithm with a signal-to-noise threshold of 3, a peak width of 1 m/z, a height of 80%. External calibration was performed by using a solution of peptide and protein calibration standards from Bruker Daltonics.

Results and Discussion

For the preparation of PEG-insulin we used PEG with a chain length of 5 kDa, because shorter PEGs are likely less stabilizing [10] and PEG with a longer chain length would compromise insulin's specific activity [8]. In this section are reported the results related with the synthesis, purification and characterization of PEG-insulin, followed by the characterization of the aggregates. SEC, NTA, light obscuration and SDS-PAGE were used for investigating the size and (non)covalent nature of the aggregates; UV, CD, and fluorescence spectroscopy for obtaining information about protein conformation and Western blotting for studying the integrity of epitopes.

Synthesis and purification of mono-PEGylated insulin

As can be seen from Figure 1, the yield of PEG-insulin, as determined by SEC and based on integrated peak area, progressively increased with the addition of MeO-PEG-NHS, while the percentage of unmodified insulin decreased. Beyond the addition of 3 equivalents of PEG, only a substantial increase of bi-PEGylated insulin, but not PEG-insulin, was achieved (results not shown).

The crude reaction mixture was purified by collecting the SEC fraction eluting between 15 and 17 minutes. The same SEC procedure was used for preparative and quantitative purposes. By re-analyzing the purified fraction on SEC, the final percentage of PEG-insulin was found to be $99.0 \pm 0.4\%$ (Figure 1, Table I).

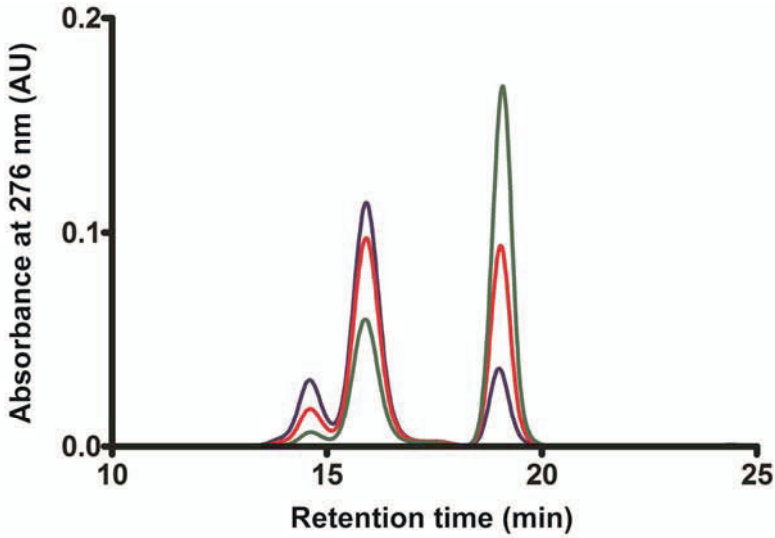


Figure 1. Synthesis of PEG-insulin as monitored by SEC: chromatograms of the reaction mixture after adding 1 eq. (green), 2 eq. (red), 3 eq. (blue) of PEG 5 kDa. After adding each equivalent, the reaction mixture was allowed to equilibrate for 15 minutes.

Table I. Summary of SEC analysis of unstressed insulin and PEG-insulin* (in %).

Sample	Monomer	Dimer	Trimer	Larger aggregates	Fragments	Insoluble
Insulin	99.3 ± 0.1	0.7 ± 0.1	nd	nd	nd	nd
PEG-insulin	99.0 ± 0.4	0.8 ± 0.3	nd	nd	0.2 ± 0.0	nd
HI	89.5 ± 0.3	5.1 ± 0.2	nd	nd	2.6 ± 0.1	2.9 ± 0.3
HPI	85.4 ± 2.5	2.6 ± 0.4	nd	nd	5.3 ± 0.8	6.7 ± 2.1
MI	73.6 ± 0.2	20.3 ± 0.2	6.1 ± 0.3	nd	nd	nd
MPI	64.2 ± 10.3	13.3 ± 1.5	nd	nd	22.5 ± 11.7	nd
CRI**	70.7 ± 0.3	28.2 ± 0.5	29.1 ± 0.1	51.4 ± 1.8	2.5 ± 0.0	nd
CRPI**	133.3 ± 4.8	16.3 ± 1.1	nd	nd	1.7 ± 1.0	nd

* Percentages are based on the AUC of the peaks. Errors are the deviation from the average between two batches. nd = not detectable.

** For glutaraldehyde-treated samples, the total AUC was higher when compared with the native protein, probably due to changes in the molar extinction coefficient or extensive light scattering.

Mass spectrometric analysis of mono-PEGylated insulin

MALDI-TOF MS analysis revealed the presence of mono-PEGylated insulin, showing a peak centered at $m/z \sim 10600$ (Figure 2, red spectrum). The typical distribution of peaks 44 Da apart from each other is related to the polydispersity of the PEG, i.e. the varying number of ethylene oxide monomer units in the polymer chain.

Confirmation of the site of conjugation was achieved in two steps. First, PEG-insulin was reduced, alkylated, purified by SEC and analyzed with MALDI-TOF MS to prove that PEG is indeed bound to chain B but not chain A. The charge distribution centered at $m/z \sim 8400$ matches well the calculated mass centered around 8359 Da for a fully alkylated insulin B chain conjugated with PEG 5 kDa (Figure 2, black spectrum).

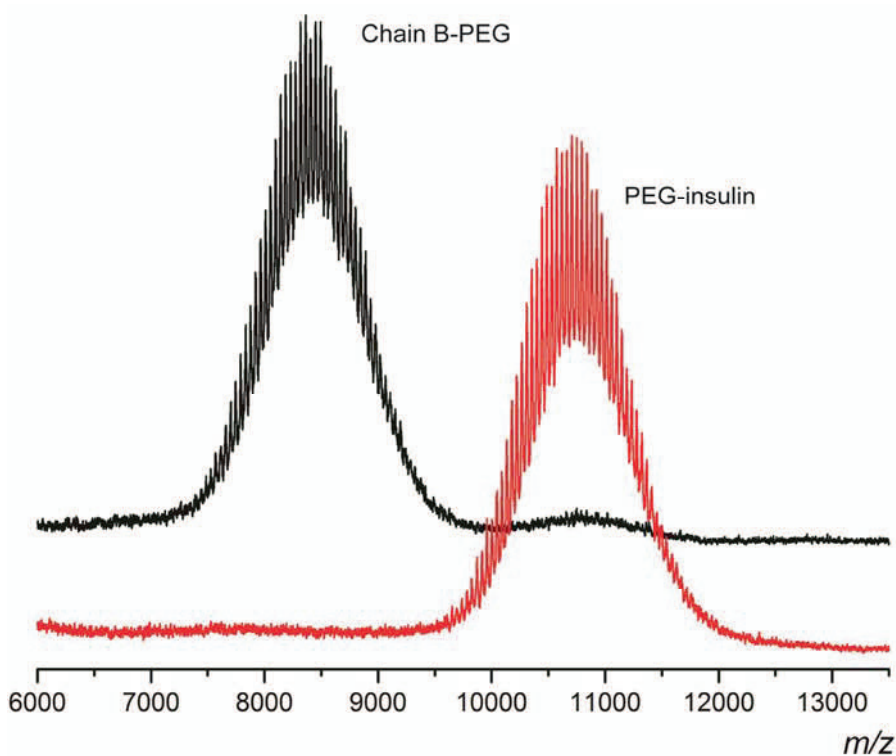


Figure 2. Matrix-assisted laser desorption/ionization time of flight mass spectrometry spectra of PEG-insulin (red) and chain B of reduced/alkylated PEG-insulin purified by size-exclusion chromatography (black).

There was no evidence of any PEG conjugated to chain A (results not shown).

Second, plain insulin as well as the conjugate was subjected to trypsin digestion to confirm that PEGylation had occurred at the C-terminal end of the B-chain, more precisely on Lys B-29. Trypsin is a common enzyme used for the selective cleavage of peptides/proteins at the carboxyl side of the amino acid residues Lys (K) and arginine (R). As can be seen in Figure 3, only chain B of insulin has two sites that can readily be cleaved by trypsin.

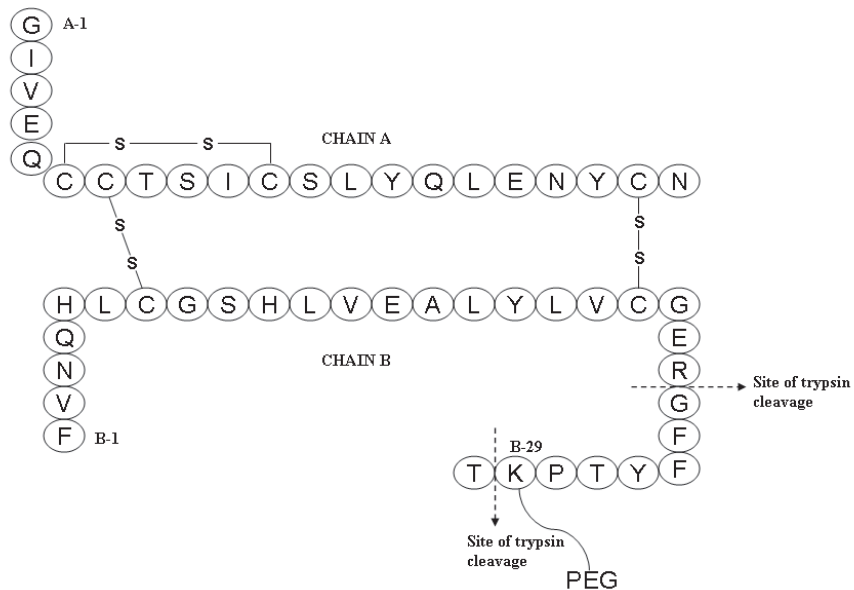


Figure 3. Primary structure of human insulin, including the theoretical cleavage sites of trypsin and the site of PEG conjugation.

The site of the conjugation could be confirmed indirectly by detecting the peptidic fragment (A₁-A₂₁)-(B₁-B₂₂) for both the unmodified insulin (Figure 4, panel A) and PEG-insulin (Figure 4, panel B).

For unmodified insulin, the peak at 4869.4 Da depicted in Figure 4, panel A, corresponds well to the calculated molecular weight of 4866.2 Da for chain A-(B₁-B₂₂) fragment. The peaks at 5710.5 Da and 5812.1 Da correspond to chain A-(B₁-B₂₉) and undigested insulin, respectively. In the spectrum of plain insulin also masses of 959.4 Da and 858.4 Da corresponding to B₂₃-B₃₀ and B₂₃-B₂₉, respectively, could be discerned (data not shown). The spectrum of

digested PEG-insulin (without reduction/alkylation) showed a main peak at 4869.7 Da (Figure 4, panel B) belonging to chain A-(B₁-B₂₂), indicating that the PEG conjugation was definitely not on chain A. Moreover, beneath the main peak a low-signal peak distribution with the PEG profile (44-Da spacing) can be seen, most likely corresponding to the peptide fragments (B₂₃-B₃₀)-PEG and (B₂₃-B₂₉)-PEG. For comparison, the reduced and alkylated PEG-insulin was also digested by trypsin under the same conditions.

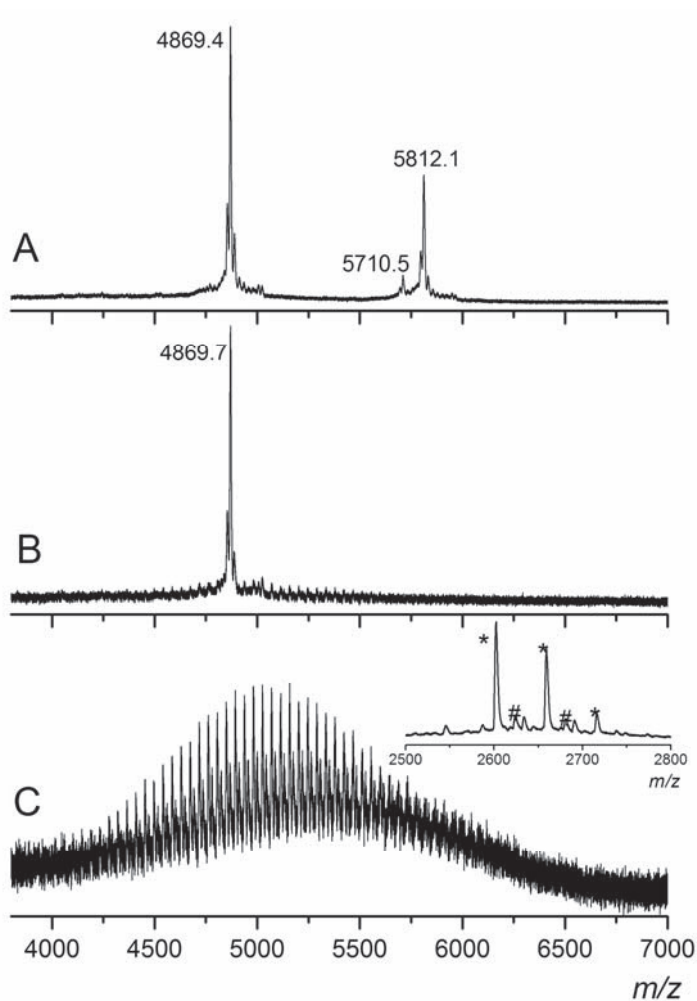


Figure 4. Comparison of MALDI-TOF MS spectra of A) digested insulin, B) digested PEG-insulin and C) digested PEG-insulin after reduction/alkylation. The inset in panel C shows the fully and over-alkylated chain B₁-B₂₂ (*) and chain A (#) peaks.

As can be seen in Figure 4, panel C, the intense 4869 Da peak belonging to chain A-(B₁-B₂₂) had disappeared. Instead, a series of overlaying Gaussian peak distributions were detected. In Figure 4, panel C, the overlapping charge distributions can be attributed to the (B₂₃-B₃₀)-PEG and (B₂₃-B₂₉)-PEG fragments and free PEG, with theoretical masses centered around 5777 Da, 5676 and 4933 Da, respectively. The inset in panel C of Figure 4, indicates that there is no PEG attached to chain (B₁-B₂₂) (*) and chain A (#) fragments.

Altogether, these results show that we successfully synthesized insulin that is mono-PEGylated at Lys (B₂₉).

Characterization of insulin and PEG-insulin

SEC of native insulin and PEG-insulin showed a main peak of monomeric protein which in both cases represented more than 99% of the protein (Table I and Figure 5, panel A).

SDS-PAGE under nonreducing conditions showed a monomer band with an apparent molecular weight of approximately 6 kDa and 12.5 kDa for plain and PEGylated insulin, respectively (Figure 5, panel B, left). The broad band for PEG-insulin can be ascribed to the heterogeneous molecular weight of the PEG (cf. the MS results, Figure 2). The higher apparent molecular weight for the PEGylated insulin in SDS-PAGE as compared to the MS data is due to the fact that PEG hardly interacts with SDS, resulting in a lower electrophoretic mobility of PEG-insulin as compared to a non-PEGylated protein with the same molecular weight. Western blotting showed that both plain and PEG-insulin reacted with polyclonal anti-human insulin antibody (Figure 5, panel B, right).

NTA is an emerging technique which is particularly suitable to determine the particle size in polydisperse samples [18]. Since insulin monomers and small oligomers do not scatter enough light to be detected by this method, only larger nano-sized aggregates are selectively detected. For the native proteins, relatively low counts between 0.5-1.0*10⁸ particles per mL, with a size distribution centered at ~100 nm, were detected (Figure 5, panel C, Table II).

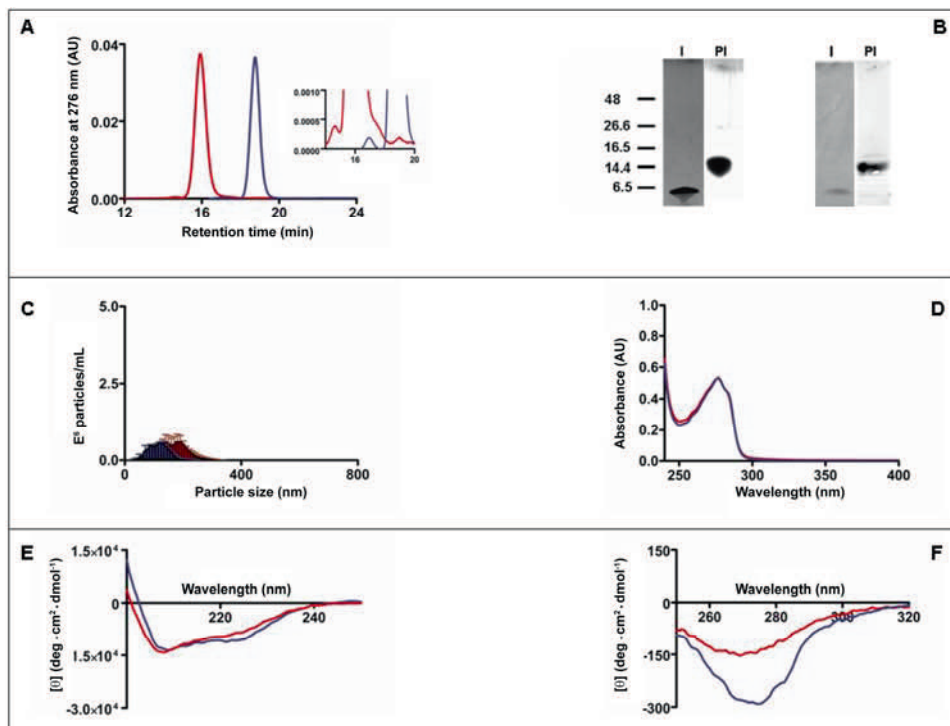


Figure 5. Main characteristics of insulin (I) (blue color) and PEG-insulin (PI) (red color) samples: (A) SEC (the inset shows the zoom in of insulin and PEG-insulin for a better correlation with the % reported in table I), (B, left side) nonreducing SDS-PAGE (numbers indicate M.W. in kDa) and (B, right side) corresponding Western blot, (C) NTA, (D) UV, (E) far-UV CD, (F) near-UV CD.

Subvisible particles in the range between 1 and 200 μm were analyzed by light obscuration. For both insulin and PEG-insulin, approximately $100\text{--}200 \times 10^3$ particles per mL were found (Table II), mainly in the size range 1-3 μm .

The UV spectra of proteins can give important information regarding the presence of aggregates in the solution. The decrease in A_{280}/A_{260} ratio in particular indicates the presence of aggregates [20]. The ratio found for insulin and PEG-insulin obtained from the UV spectra (Figure 5, panel D) was similar (Table III).

Far-UV CD was employed to investigate the secondary structure. PEG-insulin showed a slightly higher $\theta_{208\text{nm}}/\theta_{223\text{nm}}$ ratio (Figure 5, panel E and Table III) as compared to plain insulin. This change has been observed by other authors

and has been assigned to a slight increase in antiparallel β -structure content [9, 21],

Table II. Concentration and mean size of the particles detected with NTA and light obscuration*.

Sample	Nanoparticle Tracking Analysis		Light Obscuration (10 ³ /mL)		
	10 ⁸ /mL	Mean size (nm)	1-10 μ m	10-25 μ m	> 25 μ m
Insulin	0.52 \pm 0.04	116.5 \pm 5.5	155 \pm 38	3.35 \pm 1.66	0.83 \pm 0.83
PEG-insulin	0.78 \pm 0.26	168.0 \pm 3.0	286 \pm 35	-	0.41 \pm 0.41
HI	1.14 \pm 0.12	197.5 \pm 22.5	172 \pm 37	-	-
HPI	1.96 \pm 0.5	242.5 \pm 48.5	215 \pm 19	0.41 \pm 0.41	-
MI	1.05 \pm 0.1	193.0 \pm 1.0	138 \pm 3	2.50 \pm 0.83	2.91 \pm 1.25
MPI	4.65 \pm 1.39	160.0 \pm 20.0	381 \pm 68	0.42 \pm 0.41	-
CRI	7.00 \pm 1.92	248.0 \pm 10.0	415 \pm 95	4.58 \pm 0.41	3.74 \pm 0.41
CRPI	5.50 \pm 0.50	185.5 \pm 18.5	403 \pm 3	2.92 \pm 2.08	0.41 \pm 0.41

* Concentration obtained by NTA is cumulative and is reported as 10⁸ (E⁸ instead of E⁶ used in Figures 5-8, panel C). Errors are the deviation from the average between two batches. - = no particles detected.

Additional information concerning insulin's structure was obtained by analyzing its near-UV CD spectrum in the region 260–320 nm.

The signal in this region is due to the absorbance of insulin's tyrosine, phenylalanine and disulfides, and is substantially affected by its self association state [22-23]. In particular, reduction of the 273 nm CD-band is observed when insulin is dissociated [24-25]. Plain insulin presented a higher negative molar ellipticity band when compared with PEG-insulin, which can be explained by the association state of plain insulin differing from that of PEG-insulin, since in the free protein hexamer prevails [26] (Figure 5, panel F and Table III), whereas the conjugated protein appeared to be in the dimeric state, as reported by Hinds et al [9].

Intrinsic tyrosine fluorescence spectroscopy was used to further analyze the tertiary structure of the proteins. Upon excitation at 275 nm, native insulin showed an emission maximum at 299 \pm 1 nm. PEG-insulin showed a similar spectrum concerning the position of the emission maximum and the intensity (Table III).

These results indicate that both plain insulin and PEG-insulin have structural properties that are consistent with earlier reports, PEG-insulin exhibiting a lower association state than plain insulin.

Table III. Summary of spectroscopic measurements of unstressed and stressed insulin and PEG-insulin*.

Sample	UV	Circular Dichroism			Intrinsic Fluorescence	Bis-ANS Fluorescence
	A 280/260	[θ]208/223	% alpha helix	[θ]273	Intensity (a.u.)	Intensity (a.u.)
Insulin	1.56 ± 0.00	1.23 ± 0.00	39.2 ± 3.7	-314.7 ± 29.4	12.7 ± 0.3	2.25 ± 0.05
PEG- insulin	1.52 ± 0.06	1.57 ± 0.05	33.5 ± 1.5	-148.3 ± 2.9	12.9 ± 0.5	3.97 ± 0.92
HI	1.42 ± 0.01	1.31 ± 0.02	33.7 ± 0.3	-250.6 ± 0.4	10.9 ± 0.0	15.76 ± 1.48
HPI	1.45 ± 0.02	1.63 ± 0.02	30.9 ± 1.9	-122.4 ± 8.4	12.7 ± 1.9	6.85 ± 1.49
MI	1.43 ± 0.01	1.37 ± 0.04	26.8 ± 3.2	-113.4 ± 10.4	7.4 ± 1.0	5.91 ± 0.04
MPI	1.26 ± 0.00	1.87 ± 0.10	10.2 ± 0.0	-55.5 ± 19.8	6.3 ± 1.9	5.88 ± 0.06
CRI	1.03 ± 0.00	1.54 ± 0.01	31.6 ± 0.9	15.5 ± 7.4	7.3 ± 0.4	5.76 ± 0.31
CRPI	1.08 ± 0.00	1.58 ± 0.07	30.7 ± 0.5	50.2 ± 11.3	12.2 ± 0.0	5.58 ± 0.62

* Molar ellipticity in (deg* cm²* dmol⁻¹), % of alpha helix calculated as reported by Pocker et al [21]. Errors are the deviation from the average between two batches.

Characterization of heat-stressed insulin and PEG-insulin

Analysis by SEC showed that heat-stressed insulin (HI) and PEG-insulin (HPI) samples contained small amounts of dimers (Figure 6, panel A, Table I). Whereas the dimer content was slightly higher for heated insulin, heated PEG-insulin showed a larger fraction of unrecovered material (Table I), likely insoluble aggregates. Moreover, in both samples a fragment eluting at ~21 min was observed (Figure 6, panel A), which was identified as chain A by MALDI-TOF MS (not shown).

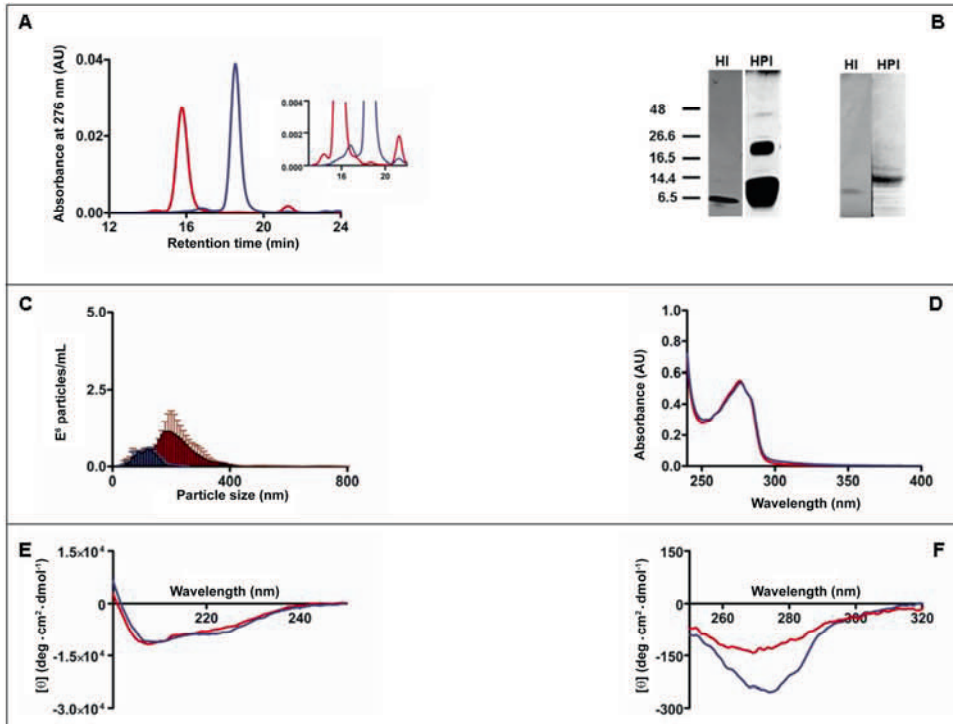


Figure 6. Main characteristics of heated insulin (HI) (blue color) and heated PEG-insulin (HPI) (red color) samples: (A) SEC (the inset shows the zoom in of insulin and PEG-insulin for a better correlation with the % reported in table I), (B, left side) nonreducing SDS-PAGE (numbers indicate M.W. in kDa) and (B, right side) corresponding Western blot, (C) NTA, (D) UV, (E) far-UV CD, (F) near-UV CD.

SDS-PAGE of HI showed a clear monomer band under nonreducing conditions, indicating the absence of covalent aggregates. For HPI, besides the monomer, a band with an apparent molecular weight of approximately 25 kDa and less intense bands with higher molecular weight were detected (Figure 6, panel B, left), indicating the presence of covalent aggregates. In Western blotting analysis only the monomer was detected, both for HI and HPI (Figure 6, panel B, right).

In NTA both HI and HPI showed an increase in particle concentration compared to the proteins before heat treatment (Table II). The size distribution of HPI was centered at about 200 nm, slightly larger than for HI (Figure 6, panel C). Light obscuration did not present major differences in subvisible particle counts with respect to the native proteins (Table II).

The UV spectra practically overlapped with those of the native proteins, although a small decrease in A280/A260 ratio was observed (Figure 6, panel D and Table III), consistent with the presence of small amount of aggregates in both HI and HPI.

Far-UV CD spectra of HI and HPI (Figure 6, panel E) were characterized by a slight increase in the 208/223 nm ratio, a slightly reduced intensity and consequently a decrease in the calculated alpha helix (Table III). The CD signals in the near-UV region (Figure 6, panel F) also were slightly reduced (Table III), indicating that HI and HPI also underwent small changes in the tertiary and quaternary structures.

The fluorescence emission spectrum was not shifted, but the intensity of HI (but not HPI) had slightly decreased (Table III).

Bis-ANS fluorescence was measured as a sensitive probe for the formation of new hydrophobic pockets in heat-stressed proteins [19, 27]. For HI and HPI Bis-ANS fluorescence was increased by approximately 5 and 2 fold, respectively (Table III), indicating a moderate increase in hydrophobicity after heating.

Thioflavin T fluorescence of the stressed samples was as low as that of native insulin and PEG-insulin (data not shown), indicating that the samples were free from fibrils.

In conclusion, the heated samples, insulin and PEG-insulin, showed similar degradation profiles.

Characterization of oxidized insulin and PEG-insulin

Metal catalyzed oxidized insulin (MI) and PEG-insulin (MPI) showed similar loss of monomer, as analyzed by SEC (Figure 7, panel A, Table I). Both MI and MPI contained substantial amounts of oligomers, mainly dimers. Besides, MPI but not MI, showed considerable fragmentation, which is likely related with the ability of radical oxidants to cleave the C-C bond of PEG [24]. Insoluble aggregates, based on the AUC of the peaks, were not found.

Nonreducing SDS-PAGE showed that both MI and MPI contained various covalent aggregates (Figure 7, panel B, left). Whereas the multimeric species present in MI reacted with the antiserum in Western blotting, the blot of MPI did not show any stained bands. This can be due to an extensive loss of the native epitopes and/or less efficient transfer to the PVDF membrane of the oligomeric PEGylated species (Figure 7, panel B, right).

Both stressed samples showed elevated levels of submicron aggregates when analyzed with NTA, mainly in the range size between 150-250 nm (Figure 7, panel C and Table II). This effect was most pronounced for MPI. Subvisible particle counts by light obscuration were similar to those for the unstressed proteins (Table II).

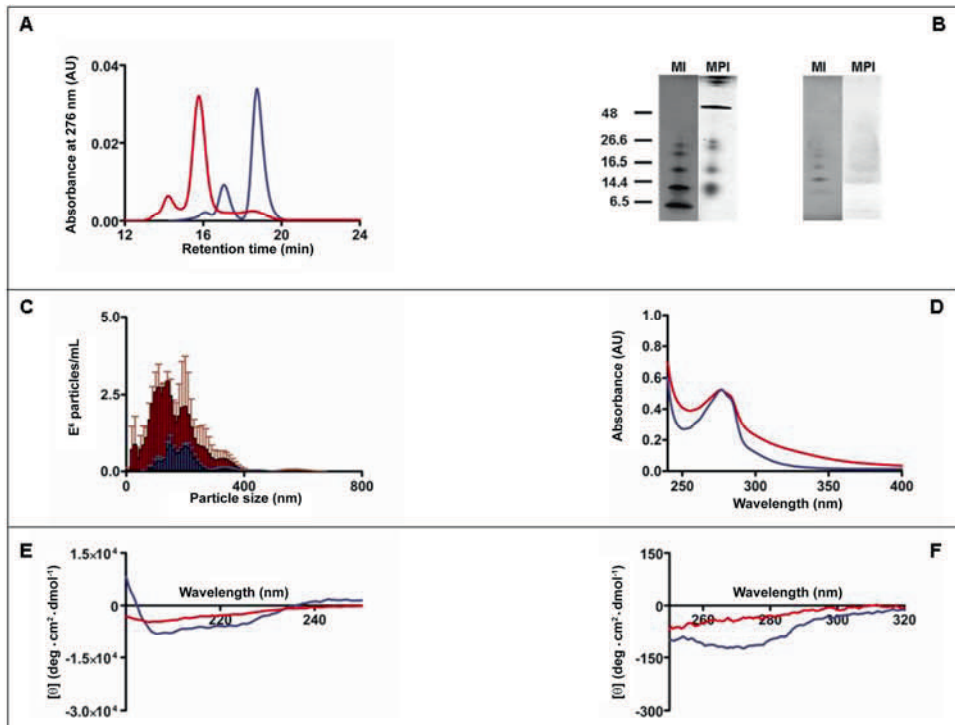


Figure 7. Main characteristics of oxidized insulin (MI) (blue color) and oxidized PEG-insulin (MPI) (red color) samples: (A) SEC, (B, left side) nonreducing SDS-PAGE (numbers indicate M.W. in kDa) and (B, right side) corresponding Western blot, (C) NTA, (D) UV, (E) far-UV CD, (F) near-UV CD.

The UV spectra of MI and MPI in Figure 7, panel D showed an increase in light scattering, indicating the presence of particles. This is clearly reflected in the reduced A280/A260 ratio compared to the unstressed compounds (Table III).

The far-UV CD spectrum of MI showed a reduction of the intensity of the entire spectrum with an increase in the 208/223 nm ratio (Figure 7, E), indicating a substantial decrease in alpha-helical content (Table III). MPI

showed an even more extensive reduction in the alpha helix content. Also the near-UV CD signals of MI and MPI were much smaller as compared to the unstressed proteins, providing evidence that both proteins had undergone considerable loss of tertiary and quaternary structure.

Bis-ANS fluorescence (Table III) was approximately 2 fold higher than for the native proteins, indicating a moderate increase in hydrophobicity. Thioflavin T fluorescence of the stressed samples was as low as that of native insulin and PEG-insulin (data not shown), indicating that the samples were free from fibrils.

Concluding, when oxidation mediated by radicals occurs, PEG might promote rather than prevent aggregation and loss of insulin's structural features.

Characterization of glutaraldehyde-treated insulin and PEG-insulin

According to SEC, glutaraldehyde-treated insulin (CRI) showed an increase in dimer, trimer and some bigger oligomers, whereas glutaraldehyde-treated PEG-insulin (CRPI) showed a small decrease in the monomer content, parallel to the formation of dimer, (Figure 8, panel A, Table I). PEG only partially prevented the formation of bigger oligomers. Insoluble aggregates, based on the AUC of the peaks, were not found.

Nonreducing SDS-PAGE confirmed the formation of covalent oligomeric species in both CRI and CRPI (Figure 8, panel B, left). Reducing SDS-PAGE confirmed the presence of nonreducible species, in contrast with the non-stressed, heat-stressed and oxidized products (results not shown).

Western blotting revealed that most of the multimeric species in CRPI and CRI contained native epitopes (Figure 8, panel B, right), whereas the monomers in both cases react only weakly with the antiserum.

NTA showed that both CRI and CRPI contained elevated levels of submicron particles, with sizes up to ~700 nm (Figure 8, panel C, Table II). Only a minimal increase in the concentration of subvisible particle content, but not size, was observed by light obscuration analysis (Table II).

The UV spectra (Figure 8, panel D) showed a substantial reduction of the A280/A260 ratio for both CRI and CRPI (Table III), which is consistent with extensive aggregation observed with other methods.

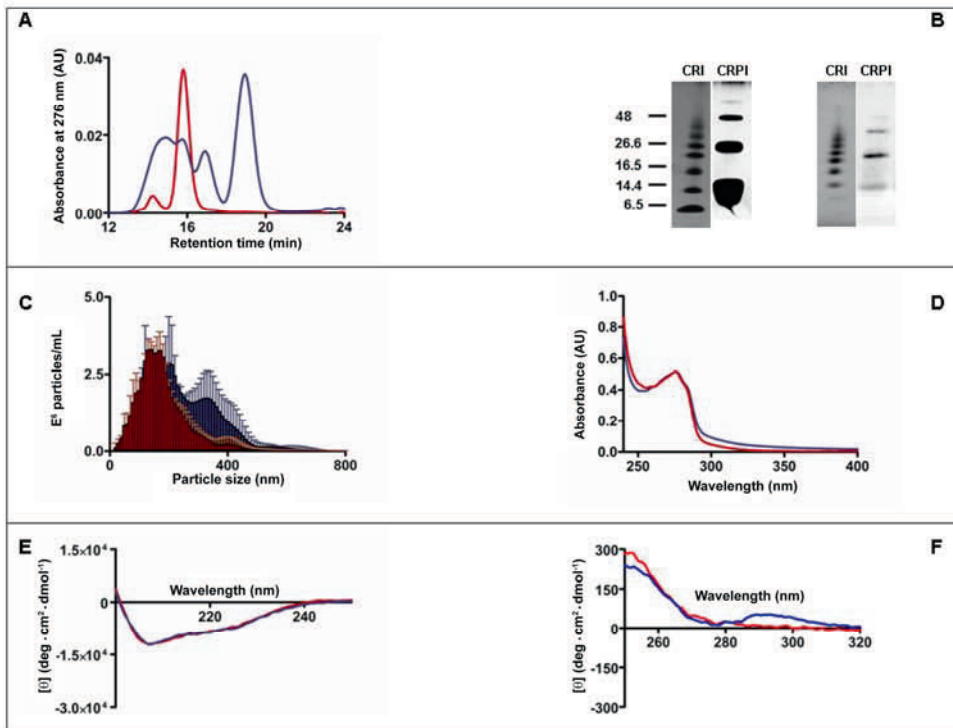


Figure 8. Main characteristics of cross-linked insulin (CRI) (blue color) and cross-linked PEG-insulin (CRPI) (red color) samples: (A) SEC, (B, left side) nonreducing SDS-PAGE (numbers indicate M.W. in kDa) and (B, right side) corresponding Western blot, (C) NTA, (D) UV, (E) far-UV CD, (F) near-UV CD.

Far-UV CD (Figure 8, panel E, Table III) indicated a loss of alpha helix content for both CRI and CRPI. The near-UV region of the spectrum showed major changes (Figure 8, panel F), indicating major perturbations of the tertiary/quaternary structures.

The extrinsic fluorescence measured with Bis-ANS (Table III) indicates that new hydrophobic surfaces were created in the cross-linked samples.

Thioflavin T fluorescence was not enhanced (not shown), indicating the absence of fibrillar species.

In conclusion, PEG is not capable to preserve insulin's structural features when the protein is treated with cross-linking agent as glutaraldehyde.

Conclusion

With this study, we demonstrated that exposure of insulin and PEG-insulin to three different stress factors, i.e. short heat exposure, metal catalyzed oxidation and cross-linking with glutaraldehyde, results in afibrillar aggregates with characteristics that strongly depend on the stress factor. In contrast, the quality of the aggregates, as shown by SEC, SDS-PAGE, Western blotting and NTA, and the altered structural properties of the proteins, as observed by CD and extrinsic fluorescence, were remarkably similar for insulin and PEGylated insulin, indicating that PEGylation neither positively nor negatively affects the sensitivity of insulin to the stress factors applied.

Acknowledgements

The authors thank Schering-Plough for financial support and providing insulin for this project, and Iris Van Laar for her valuable help in analyzing the samples.

References

- [1] T. Rasmussen, R. Tantipolphan, M. van de Weert, W. Jiskoot. The molecular chaperone alpha-crystallin as an excipient in an insulin formulation. *Pharm. Res.* **2010**, *27*, 1337-1347.
- [2] M. A. Ganz, T. Unterman, M. Roberts, R. Uy, S. Sahgal, M. Samter, L. C. Grammer. Resistance and allergy to recombinant human insulin. *J. Allergy Clin. Immunol.* **1990**, *86*, 45-51.
- [3] J. R. Greenfield, A. Tuthill, M. A. Soos, R. K. Semple, D. J. Halsall, A. Chaudhry, S. O'Rahilly. Severe insulin resistance due to anti-insulin antibodies: response to plasma exchange and immunosuppressive therapy. *Diabet. Med.* **2009**, *26*, 79-82.
- [4] R. Koyama, K. Nakanishi, M. Kato, S. Yamashita, H. Kuwahara, H. Katori. Hypoglycemia and hyperglycemia due to insulin antibodies against therapeutic human insulin: Treatment with double filtration plasmapheresis and prednisolone. *Am. J. Med. Sci.* **2005**, *329*, 259-264.
- [5] F. M. Veronese. Peptide and protein PEGylation: a review of problems and solutions. *Biomaterials* **2001**, *22*, 405-417.
- [6] F. M. Veronese, A. Mero. The impact of PEGylation on biological therapies. *BioDrugs* **2008**, *22*, 315-329.
- [7] G. E. Means, R. E. Feeney. Chemical modifications of proteins: history and applications. *Bioconjug. Chem.* **1990**, *1*, 2-12.

- [8] T. Uchio, M. Baudys, F. Liu, S. C. Song, S. W. Kim. Site-specific insulin conjugates with enhanced stability and extended action profile. *Adv. Drug Deliv. Rev.* **1999**, *35*, 289-306.
- [9] K. Hinds, J. J. Koh, L. Joss, F. Liu, M. Baudys, S. W. Kim. Synthesis and characterization of poly(ethylene glycol)-insulin conjugates. *Bioconjug. Chem.* **2000**, *11*, 195-201.
- [10] K. D. Hinds, S. W. Kim. Effects of PEG conjugation on insulin properties. *Adv. Drug Deliv. Rev.* **2002**, *54*, 505-530.
- [11] Insulin, The United States Pharmacopeia Convention, Inc., Rockville, MD, **2002**.
- [12] Insulin, Human, European Directorate for the Quality of Medicines (EDQM), **2001**.
- [13] A. D. Tuesca, C. Reiff, J. I. Joseph, A. M. Lowman. Synthesis, characterization and in vivo efficacy of PEGylated insulin for oral delivery with complexation hydrogels. *Pharm. Res.* **2009**, *26*, 727-739.
- [14] J. Brange, L. Langkjaer, S. Havelund, A. Volund. Chemical stability of insulin. 1. Hydrolytic degradation during storage of pharmaceutical preparations. *Pharm. Res.* **1992**, *9*, 715-726.
- [15] K. Huus, S. Havelund, H. B. Olsen, M. van de Weert, S. Frokjaer. Thermal dissociation and unfolding of insulin. *Biochemistry* **2005**, *44*, 11171-11177.
- [16] S. Li, T. H. Nguyen, C. Schöneich, R. T. Borchardt. Aggregation and precipitation of human relaxin induced by metal-catalyzed oxidation. *Biochemistry* **1995**, *34*, 5762-5772.
- [17] D. A. McCarthy, M. Field, P. Mumford, B. K. Pell, E. J. Holborow, R. N. Maini. The production of small IgG aggregates by glutaraldehyde cross-linking. *J. Immunol. Methods* **1985**, *82*, 349-358.
- [18] V. Filipe, A. Hawe, W. Jiskoot. Critical evaluation of Nanoparticle Tracking Analysis (NTA) by NanoSight for the measurement of nanoparticles and protein aggregates. *Pharm. Res.* **2010**, *27*, 796-810.
- [19] A. Hawe, M. Sutter, W. Jiskoot. Extrinsic fluorescent dyes as tools for protein characterization. *Pharm. Res.* **2008**, *25*, 1487-1499.
- [20] L. A. Kuelzto and C. R. Middaugh. Ultraviolet absorption spectroscopy. In W. Jiskoot and D. J. A. Crommelin (eds.), M. f. S. A. o. P. Pharmaceuticals, B. P. A. A. P. (Vol. 3, Arlington, **2005**, pp. 1Y25).
- [21] Y. Pocker, S. B. Biswas. Conformational dynamics of insulin in solution. Circular dichroic studies. *Biochemistry* **1980**, *19*, 5043-5049.
- [22] S. M. Kelly, T. J. Jess, N. C. Price. How to study proteins by circular dichroism. *Biochim. Biophys. Acta* **2005**, *1751*, 119-139.
- [23] J. Goldman, Carpenete.Fh. Zinc Binding, Circular-Dichroism, and Equilibrium Sedimentation Studies on Insulin (Bovine) and Several of Its Derivatives. *Biochemistry* **1974**, *13*, 4566-4574.
- [24] F. Kawai. Microbial degradation of polyethers. *Appl. Microbiol. Biotechnol.* **2002**, *58*, 30-38.

- [25] R. Tantipolphan, S. Romeijn, J. den Engelsman, R. Torosantucci, T. Rasmussen, W. Jiskoot. Elution behavior of insulin on high-performance size exclusion chromatography at neutral pH. *J. Pharm. Biomed. Anal.* **2010**, *52*, 195-202.
- [26] J. F. Hansen. The Self-Association of Zinc-Free Human Insulin and Insulin Analog B13-Glutamine. *Biophys. Chem.* **1991**, *39*, 107-110.
- [27] A. Hawe, J. C. Kasper, W. Friess, W. Jiskoot. Structural properties of monoclonal antibody aggregates induced by freeze-thawing and thermal stress. *Eur. J. Pharm. Sci.* **2009**, *38*, 79-87.

Chapter 4

Chemical modifications in aggregates of recombinant human insulin induced by metal-catalyzed oxidation: covalent cross-linking via Michael addition to tyrosine oxidation products

Riccardo Torosantucci^{1,2}, Olivier Mozziconacci², Victor Sharov², Christian Schöneich² and Wim Jiskoot¹

¹Division of Drug Delivery Technology, Leiden Academic Centre for Drug Research (LACDR), Leiden University, Leiden, the Netherlands.

²Department of Pharmaceutical Chemistry of Kansas University, Lawrence, Kansas, USA.

Pharmaceutical Research **2012**, 29, 2276-2293.

Abstract

Purpose. To elucidate the chemical modifications in covalent aggregates of recombinant human insulin induced by metal catalyzed oxidation (MCO).

Methods. Insulin was exposed for 3 hours at room temperature to the oxidative system copper(II)/ascorbate. Chemical derivatization with 4-(aminomethyl) benzenesulfonic acid (ABS) was performed to detect 3,4-dihydroxyphenylalanine (DOPA) formation. Electrospray ionization-mass spectrometry (ESI-MS) was employed to localize the amino acids targeted by oxidation and the cross-links involved in insulin aggregation. Oxidation at different pH and temperature was monitored with size exclusion chromatography (SEC) and ESI-MS analysis to further investigate the chemical mechanism(s), to estimate the aggregates content and to quantify DOPA in aggregated insulin.

Results. The results implicate the formation of DOPA and 2-amino-3-(3,4-dioxocyclohexa-1,5-dien-1-yl) propanoic acid (DOCH), followed by Michael addition, as responsible for new cross-links resulting in covalent aggregation of insulin during MCO. Michael addition products were detected between DOCH at positions B16, B26, A14, and A19, and free amino groups of the N-terminal amino acids Phe B1 and Gly A1, and side chains of Lys B29, His B5 and His B10. Fragments originating from peptide bond hydrolysis were also detected.

Conclusion. MCO of insulin leads to covalent aggregation through cross-linking via Michael addition to tyrosine oxidation products.

Introduction

During pharmaceutical production and storage, therapeutic proteins can be exposed to components that are able to induce metal-catalyzed oxidation (MCO) [1], i.e. redox active transition metals, peroxides and reductants [2-3]. MCO of therapeutic proteins [4] such as recombinant human interferon alfa and recombinant human interferon beta has been reported to form highly immunogenic aggregates [5-7], providing evidence that protein oxidation can potentially lead to severe side reactions and loss of therapeutic effect.

Furthermore, it has been shown that in diabetic complications [8], copper ion concentrations are higher than in normal subjects [9]. Therefore, MCO is a potential cause of insulin degradation *in vivo* as well, when the production of reactive oxygen species (ROS) exceeds the endogenous antioxidant defense.

Montes-Cortes et al. [10] showed that the carbonyl content of human insulin and the hydroxylation of phenylalanine, based on the formazan assay [11], is increased after exposure of insulin to the plasma of diabetic patients, which can contain high concentrations of oxidants [12].

Moreover, in a recent paper we showed that MCO induces significant covalent aggregation of insulin *in vitro* [13]. However, the underlying mechanisms of insulin aggregation through MCO are still unknown. Previous reports on the MCO of human insulin and glycated insulin indicate that both histidine residues are easily oxidized to 2-oxo histidine [2, 9].

Here we provide a more detailed analysis of the chemical modifications that occur during the MCO of recombinant human insulin, induced by Cu^{2+} and L-ascorbic acid as a representative electron donor [14-16], focusing on the amino acids that are modified and on the chemical mechanisms that lead to cross-linked insulin, as a consequence of the modifications in the primary structure.

Since previous studies have demonstrated the presence of DOPA in proteins like cataractous lens proteins [17] and in atherosclerotic lesions [18], emphasis was placed on the detection of oxidation products arising from the four Tyr and the three Phe contained in insulin and, especially, on the formation of 2-amino-3-(3,4-dioxocyclohexa-1,5-dien-1-yl) propanoic acid (DOCH), which constitutes a Michael acceptor for nucleophilic addition. Figure 1, panel A, displays the primary structure of insulin, the Glu-C digestion sites, the amino acids (in blue) with nucleophilic function, and the amino acids (in red) that can be oxidized to 3,4-dihydroxyphenylalanine (DOPA) and DOCH.

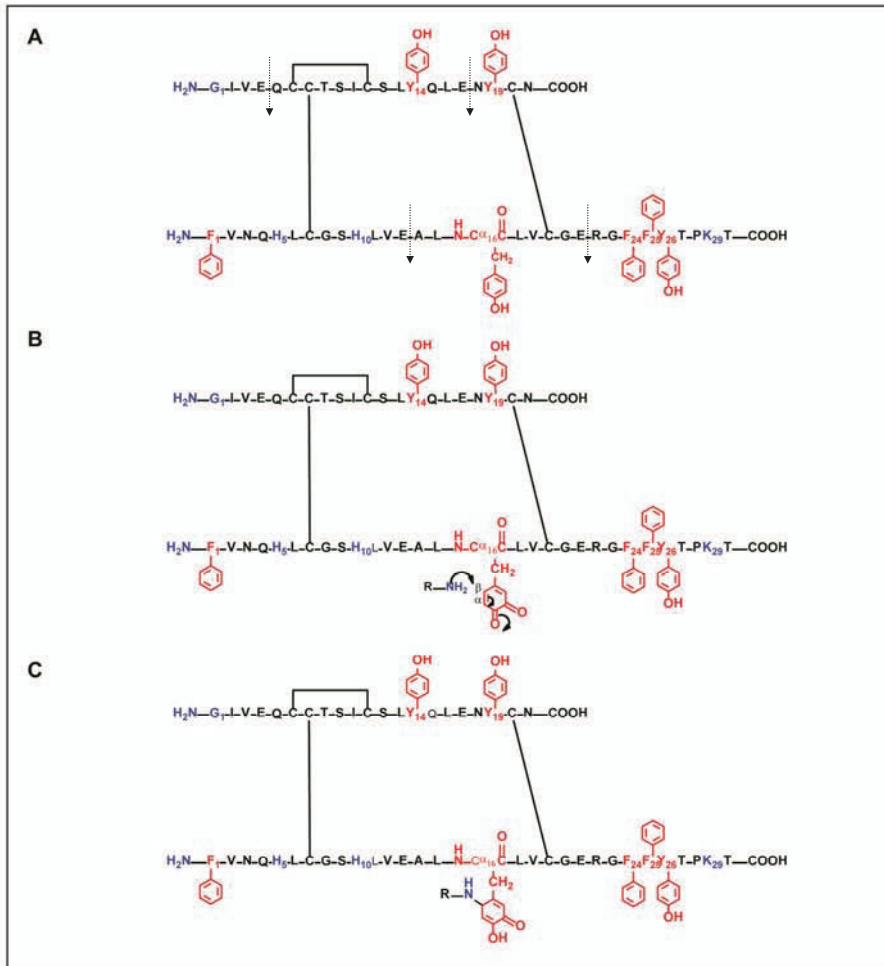
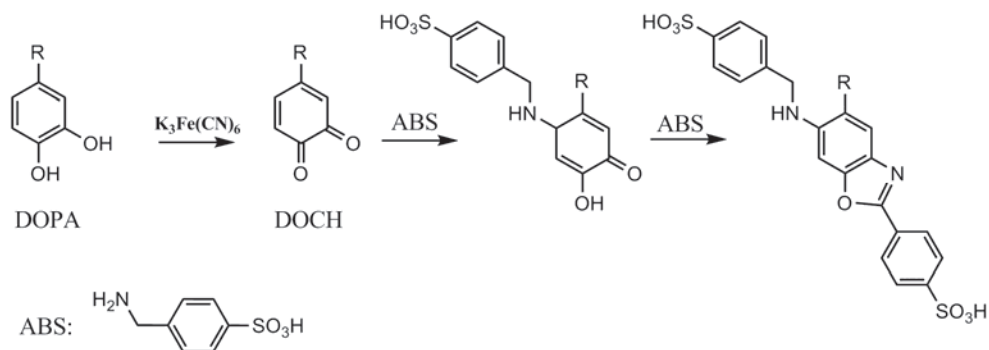


Figure 1. (A) primary structure of human insulin with the Glu-C endoproteinase digestion sites (dashed arrows). In blue are shown the nucleophilic amino acids which can be involved in Michael addition. In red the amino acids that can be oxidized to DOPA and DOCH. (B) Michael addition on oxidized human insulin. The amino group that initiates a nucleophilic reaction with the α,β unsaturated carbonyl compound (DOCH), represents one of the nucleophilic amino acids of human insulin (in blue). (C) Product of Michael addition on oxidized insulin (note that the hydrogen on the alpha carbon at position 16 was omitted for graphic requirements).

In the same Figure, panel B representatively illustrates the Michael addition on DOCH at position B16, and panel C shows the product of Michael addition on oxidized insulin (note that the hydrogen on the alpha carbon at position 16 was omitted for graphic requirements). Complementary detection of DOPA

and DOCH was achieved using mass spectrometry and fluorogenic tagging with 4 (aminomethyl)benzene sulfonic acid (ABS) (Scheme 1), according to the method reported recently by Sharov et al [19-20].



Scheme 1. Chemical derivatization of DOPA and DOCH with ABS.

Our results indicate that all aromatic amino acids of insulin, i.e. His, Tyr and Phe, are subject to MCO, predominantly yielding mono- and/or dihydroxylation products (or their respective oxidation products, i.e. DOCH from DOPA). Important for the mechanistic analysis of covalent protein aggregation, we detected cross-links between DOCH at positions B16, B26, A14, and A19 and free amino groups of the N-terminal amino acids Phe B1 and Gly A1, and the side chains of Lys B29, His B5 and His B10.

Materials and Methods

Materials

Recombinant human insulin containing 0.4% (w/w) zinc was provided by Merck (Oss, The Netherlands). L-ascorbic acid, ethylenediaminetetraacetic acid sodium salt (EDTA), copper dichloride, arginine, monobasic and dibasic sodium hydrogen phosphate, ammonium bicarbonate (ABI), sodium citrate and citric acid, dithiothreitol (DTT), iodoacetamide (IAM) and the solvents glacial acetic acid and acetonitrile were purchased from Sigma-Aldrich (St.Louis, MO, USA). Millipore Q water was used for the preparation of all the formulations and solutions. All chemicals were of analytical grade and used without further purification. ABS was synthesized according to a published

procedure [21]. Glu-C endoproteinase used in this study was purchased from Promega (Madison, WI, USA). Centrifugal filter units with a volume capacity of 4 mL and a molecular weight cut-off of 3 kDa were purchased from Millipore (Billerica, MA, USA). Cassette dialysis slides with a 2 kDa cut-off were purchased from Thermo Scientific (Asheville, NC, USA).

Metal-catalyzed oxidation of insulin

Insulin oxidation was performed at three pH values: pH 7.4 in 50 mM sodium phosphate buffer (PB), pH 3.0 in 50 mM sodium citrate buffer (CB) and at pH 8.0 in 250 mM ammonium bicarbonate (ABI). For all the oxidation reactions, insulin was first dissolved in 0.1 M hydrochloric acid and then diluted into the corresponding buffer. Depending on the desired pH, 0.1 M sodium hydroxide was used. When CB was used, the final pH of 3 was achieved without further addition of base. Insulin concentration was measured by UV spectroscopy using a molecular weight of 5.8 kDa and an extinction coefficient of $6200 \text{ M}^{-1} \text{ cm}^{-1}$ at 276 nm [22]. Further dilutions in PB, ABI or CB were performed to obtain a final insulin concentration of 1 mg/mL. Controls included 1 mg/mL of insulin in 50 mM PB, pH 7.4; in 50 mM CB, pH 3.0; and in 250 mM ABI, pH 8.0. MCO was performed by addition to 1 mL of 1 mg/mL insulin, 100 μL of 0.4 mM CuCl_2 in 50 mM PB, pH 7.4, or in 50 mM CB, pH 3, or in 250 mM ABI, pH 8, depending on the desired pH, to a final concentration of 40 μM CuCl_2 . The reaction was performed in 2-mL Eppendorf tubes covered with aluminum foil to protect the reaction mixture from light. After 10 minutes of incubation of insulin with Cu^{2+} , to allow copper to bind to insulin, the oxidation reaction was started by the addition of 110 μL of 40 mM L-ascorbic acid in 50 mM PB, pH 7.4, or in 50 mM CB, pH 3, or in 250 mM ABI, pH 8, depending on the desired pH, to a final concentration of 4 mM. The reaction was quenched after 3 hours of incubation at room temperature by adding 12.1 μL of a 100 mM EDTA in 50 mM PB, pH 7.4, or in 50 mM CB, pH 3, or in 250 mM ABI, pH 8, depending on the desired pH, to a final concentration of 1 mM [15]. To monitor the presence of protein fragments, the oxidation was also performed (in PB with the same amount of copper and L-ascorbic acid) at room temperature and at 37 °C for 24 hours before quenching. The oxidized samples were extensively dialyzed at 4 °C against 50 mM ammonium bicarbonate (ABI) buffer, pH 8.0, for 24 h. In another experiment, the oxidized

sample in 50 mM sodium citrate buffer pH 3, was extensively dialyzed at 4 °C in 50 mM sodium phosphate buffer, pH 7.4, using centrifugal filter units. After that the sample was left to equilibrate for 12 hours at room temperature.

ABS-derivatization of undigested samples

Solutions of native insulin and insulin oxidized at pH 3.0 (in CB) and pH 7.4 (in PB), dialyzed into 50 mM ABI, were treated with 0.1 M sodium hydroxide to a final pH of 9.0. Subsequently, to 100 μ L of these solutions, 11 μ L of a solution of 100 mM ABS dissolved in water were added to a final concentration of 10 mM. Next, 1.1 μ L of 50 mM $K_3Fe(CN)_6$ dissolved in water was added to a final concentration of 0.5 mM. The reaction was conducted for 1 hour at room temperature before performing SEC analysis. Controls for non-specific fluorescence included derivatization reagents (without protein) incubated under the same conditions and non-derivatized protein.

Reduction, alkylation and ABS-derivatization of insulin

Solutions of native insulin and oxidized insulin, dialyzed into 50 mM ABI, pH 8.0, were reduced using 50 mM dithiothreitol (DTT), freshly prepared in 50 mM ABI, pH 8.0, added to a final concentration of 5 mM. The samples were incubated for 45 minutes at 45 °C using a thermo heating bath (Thermo Scientific, Asheville, NC, USA). Subsequently, 200 mM iodoacetamide (IAM), freshly prepared in 50 mM ABI, pH 8.0, was added to a final concentration of 20 mM. The pH of 100 μ L of dialyzed, reduced and alkylated insulin samples was adjusted to 9.0 with 0.1 M sodium hydroxide. Then, 11 μ L of a solution of 100 mM ABS dissolved in water were added to a final concentration of 10 mM. Subsequently, 1.11 μ L of 50 mM $K_3Fe(CN)_6$ dissolved in water was added to a final concentration of 0.5 mM. The reaction was conducted for 1 hour at room temperature before performing digestion with Glu-C.

Glu-C digestion

The proteolytic digestion was performed after reduction, alkylation and ABS-derivatization of insulin, by incubating the samples with Glu-C endoproteinase in a ratio insulin: Glu-C endoproteinase 10:1 (w/w), overnight at 37 °C.

Size-exclusion chromatography

An Insulin HMWP column (7.8 × 300 mm, Waters, Milford, MA, USA) was connected to a Shimadzu HPLC system (UFLC Shimadzu Instrument equipped with two LC-20AT pumps, Columbia, MD) coupled to a photo-diode array detector (Shimadzu, SPD-M20A) and a fluorescence detector (Shimadzu, RF-20A). The photo diode array detector allowed for the recording of the UV spectrum in the region between 200-800 nm. Undigested insulin samples, without ABS treatment, were injected to calculate the percentages of the aggregates and to measure tyrosine fluorescence. Moreover, undigested insulin samples that were treated with ABS were injected to measure the benzoxazole fluorescence, which can be formed only in presence of DOPA and/or DOCH. The percentage of aggregates was calculated based on peak areas of the UV peaks at 276 nm (chromatograms not shown), as reported by Hermeling et al [5-6]. The fluorescence detector was set at various different excitation (Ex) and emission (Em) wavelengths, depending on the type of analysis: Ex 275 nm/Em 302 nm was used for monitoring Tyr fluorescence and Ex 360/Em 490 nm was used for the detection of the benzoxazole fluorescence of the ABS-derivatized samples. The mobile phase was composed of a mixture of 1 g/L L-arginine in water/acetonitrile/glacial acetic acid 65:20:15 (v/v/v) as reported in the United States and European pharmacopeias [23-24]. The elution buffer was freshly prepared, filtered using a regenerated cellulose filter (Sartorius Stedim Biotech, Arvada, CO) and degassed prior to use.

Steady-state fluorescence spectroscopy

The benzoxazole fluorescence of the ABS-derivatized samples was measured upon excitation at 360 nm. The emission spectra were recorded from 490 nm to 600 nm with a 5-nm bandwidth on a Shimadzu RF-5000U spectrofluorometer. To monitor the presence of dityrosine, the non-derivatized, oxidized samples were analyzed after dialysis in 50 mM ABI, pH 8.0, using an excitation wavelength of 315 nm and detection at 420 nm [25]. After ABS-derivatization and dialysis, sample volumes were diluted with 50 mM ABI to 0.5 mL. Spectra were recorded in 0.5 mL 1-cm path length fluorescence cuvettes (Hellma, Plainview, NY, USA). Controls for non-specific

fluorescence included samples without a substrate or reagents incubated under the same conditions.

Mass spectrometry

Digested and non digested peptides were analyzed by means of an LTQ-FT hybrid linear quadrupole ion trap Fourier transform ion cyclotron resonance (FT-ICR) mass spectrometer (Thermo-Finnigan, Bremen, Germany) and a SYNAPT-G2 (Waters Corporation, Milford, MA), both located in the Mass Spectrometry Laboratory of the University of Kansas, under the conditions as described by Ikehata et al [26]. In short, peptides were separated on a reversed-phase LC Packings PepMap C18 column (0.300 × 150 mm) at a flow rate 10 μ L/min with a linear gradient from 0 to 65% acetonitrile in 0.06% aqueous formic acid over a period of 55 min using LC Packing Ultimate Chromatograph (Dionex). LC-MS experiments were performed in a data-dependent acquisition manner using Xcalibur 2.0 software (Thermo Scientific). Five most intensive precursor ions in a survey MS1 mass spectrum acquired over a mass range of 300–2000 m/z were selected and fragmented in the linear ion trap by collision-induced dissociation. The ion selection threshold was 500 counts. The MS/MS spectra obtained were analyzed with the software MassMatrix [27–30]. MassMatrix was used to generate the theoretical fragment tables of the b and y ions of the different oxidized and cross-linked products. The theoretical fragments were compared to the experimental MS/MS spectra to validate the structures, which were taken into consideration only if the difference between the theoretical and the experimental m/z of the parent ion (and the fragment ions) was strictly below 0.1 Da. The SYNAPT-G2 instrument was operated for maximum resolution with all lenses optimized on the $[M + 2H]^{2+}$ ion from the [Glu]¹-fibrinopeptide B. The cone voltage was 30 V and Ar was admitted to the collision cell. The spectra were acquired using a mass range of 50–2000 m/z. The data were accumulated for 0.7 sec per cycle. The CID data, at the MS² level, acquired with the FT-ICR instrument were obtained after an attenuation of the parent ion of 35%. The mass window to collect the parent ion was fixed to 0.1 Da. Deconvolution of the electrospray ionization data of the undigested insulin was obtained using the maximum entropy distribution algorithm implemented in the Masslynx MaxEnt software (Waters Corporation, Milford, MA) using an adduct of 1 proton. Assuming a normal statistical distribution of

the noise, a uniform Gaussian with a width at half height of 0.5 Da was used. A number of fifty iterations and a range between 0-36000 Da were used to build the most probable mass spectrum of the parent ions.

Results

To guide the reader through the results, these will be presented in three sections: 1) Aggregation profile of oxidized insulin and elucidation of aggregation mechanism, 2) MS analysis of undigested insulin samples, and 3) identification of chemical modifications by MS/MS analysis of reduced, alkylated, ABS-derivatized and digested samples.

Aggregation profile of oxidized insulin and elucidation of aggregation mechanism

Investigation of the chemical mechanisms, as well as the aggregation profile, was achieved with SEC. This technique was employed for several purposes: to detect and quantify the percentage of monomer loss, and the formation of covalent dimers and high-molecular-weight oligomers (HMWO) during MCO, by using UV detection at 276 nm (note that the composition of the mobile phase does not allow us to estimate the amount of non-covalent aggregates since these will be dissociated because of the organic solvent and the low pH of the eluent ^[31]); to monitor Tyr fluorescence in oxidized insulin, by using an excitation wavelength of 275 nm with emission set at 302 nm, and to detect the development of DOPA and DOCH through derivatization with ABS.

Furthermore, we used SEC to monitor the presence of fragments after prolonged oxidation. The percentages found (Table I) are in agreement with our previous results ^[13]. MCO under our applied standard conditions leads to a loss of 25.6% of monomer and the formation of 18.8% of dimer and 6.8% of HMWO (Figure 2, panel A). The derivatization with ABS, followed by SEC analysis, allowed the detection of DOPA and DOCH, in the monomer, as well as in the aggregates (Figure 2, panel B).

The overall results point to the presence of Tyr and Phe oxidation products in all insulin species formed during MCO. A much weaker overall fluorescent signal was detected for the derivatized non-oxidized insulin (Figure 2, panel B), suggesting that a low percentage of DOPA was already present in the

starting material, which could have been oxidized during production, storage and handling.

The fluorescence spectra of the ABS derivatized samples (data not shown) were in agreement with the fluorescence detection performed with SEC: a low but measurable fluorescence emission was found for the native insulin derivatized with ABS and a 6-fold higher fluorescence signal was obtained for the oxidized insulin derivatized with ABS.

Aggregated insulin was almost completely absent when MCO was performed at pH 3.0 (panel C of Figure 2). This result suggests that the aggregation process, which appears to be mediated by nucleophilic reactions with DOCH, is inhibited at lower pH, likely due to protonation of free amino groups and His residues.

Nevertheless, DOPA and DOCH were detected after derivatization with ABS (Figure 2, panel D), indicating that the lower pH did not inhibit insulin oxidation. Hence, it may be possible that insulin oxidized at pH 3.0 would still aggregate if the pH is increased after oxidation. To test this hypothesis, the buffer of the insulin sample oxidized at pH 3.0 was subsequently exchanged with 50 mM sodium phosphate buffer, pH 7.4, using centrifugal filter units. The sample was left to equilibrate for 12 hours at room temperature before SEC analysis.

Figure 2, panel E and Table I represent the chromatograms and the percentages of aggregates for this experiment, displaying an increased amount of insulin dimer and trimer after the buffer change.

Altogether these results indicate that Michael addition, the addition of a nucleophile to an α,β -unsaturated carbonyl compound ^[32], may be the main mechanism of covalent insulin aggregation during MCO. Moreover, this experiment disproves a major role of S-S scrambling in insulin aggregation during MCO. However, the occurrence of non-covalent (besides covalent) aggregation cannot be fully excluded.

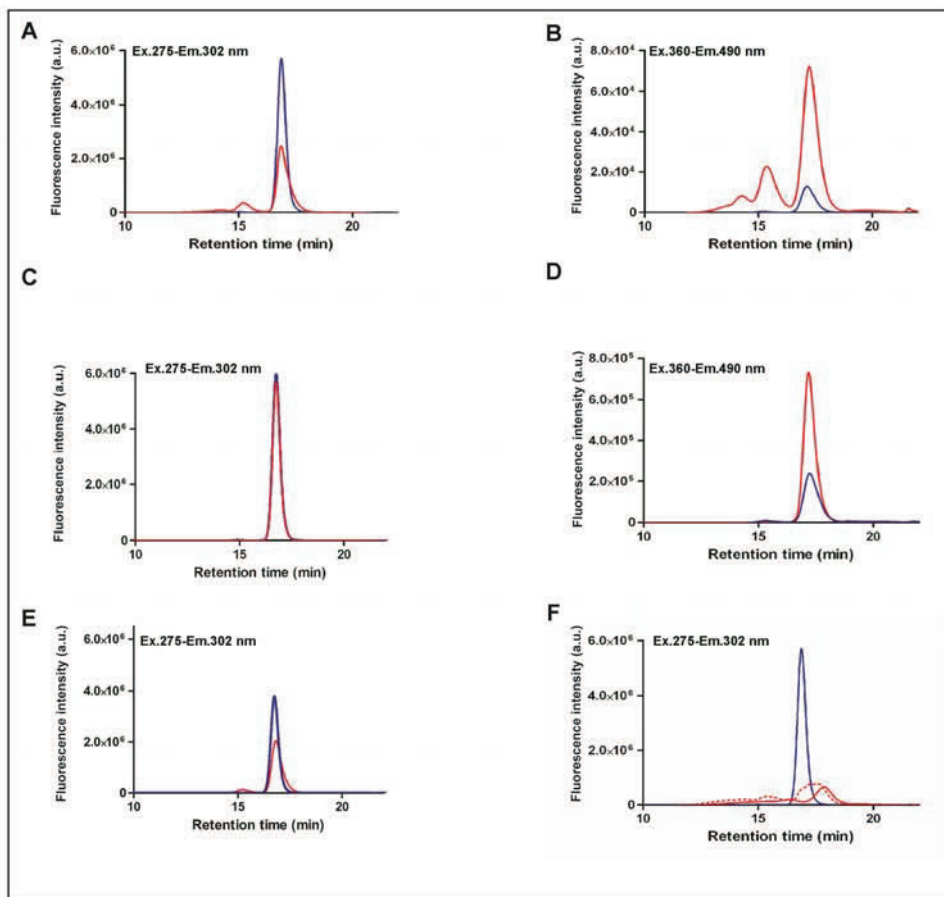


Figure 2. SEC with intrinsic tyrosine fluorescence detection (panels A, C, E, F; Ex 275 nm-Em 302 nm) and ABS fluorescence detection (panels B, D): (A) insulin oxidized in PB 50 mM, pH 7.4, for 3 hours at room temperature (in red) and its control, untreated insulin (in blue); (B) oxidized insulin (pH 7.4), derivatized with ABS (in red) and its control, untreated insulin derivatized with ABS (in blue); (C) insulin oxidized in 50 mM sodium citrate, pH 3.0, for 3 hours at room temperature (in red) and its control, untreated insulin (in blue); (D) oxidized insulin (pH 3.0), derivatized with ABS (in red) and its control, untreated insulin derivatized with ABS (in blue); (E) insulin oxidized in 50 mM sodium citrate, pH 3.0, for 3 hours at room temperature, exchanged in 50 mM PB, pH 7.4, for 12 hours at room temperature (in red) and its control, oxidized insulin (pH 3) (in blue); (F) insulin oxidized in 50 mM PB, pH 7.4, for 24 hours, at room temperature (dotted red line) and at 37 °C (solid red line), untreated insulin (blue line).

Table I. Percentages of monomer, dimer and high-molecular-weight oligomers (HMWO) for the insulin oxidized under different conditions and native insulin.[§]

Sample	%Monomer	%Dimer	%HMWO
Oxidized insulin in PB, pH 7.4	74.4 ± 0.9	18.8 ± 1.4	6.8 ± 1.2
Oxidized insulin in ABI, pH 8.0	96.1 ± 0.7	3.9 ± 0.7	ND [#]
Oxidized insulin in sodium citrate, pH 3	99.2 ± 0.3	0.8 ± 0.3	ND
Oxidized insulin in sodium citrate, pH 3.0, spiked into PB, pH 7.4	88.8 ± 1.3	9.3 ± 1.1	1.9 ± 0.1
Native insulin in PB, pH 7.4	99.4 ± 0.2	0.6 ± 0.2	ND

[§] Based on SEC analysis with UV detection at 276 nm; data represent mean ± standard deviation of 3 individual batches

[#] ND = not detected

Additional evidence for Michael addition was provided in an experiment in which we performed the oxidation of insulin at pH 8.0, in the presence of a relatively high concentration (0.25 M) of ammonium bicarbonate. Under these conditions ammonia competes with nucleophilic functional groups of insulin (i.e. the N-terminus of Gly A1 and Phe B1, and the side chains of His B5, B10 and Lys B29) for the addition to DOCH, thereby inhibiting aggregate formation, as shown in Figure 3, panel A and indicated by the low percentages of covalent aggregates measured (Table I). This was confirmed with FT-ICR MS analysis, performed on oxidized insulin in ABI, after reduction, alkylation and Glu-C digestion. As can be seen in the chemical structure representatively depicted in panel B of Figure 3, two amino groups (highlighted in blue) are covalently bound to the first Phe residue and one amino group is covalently bound to the second Phe residue, indicating that Michael addition occurred between both oxidized Phe residues and ammonia originating from the buffer.

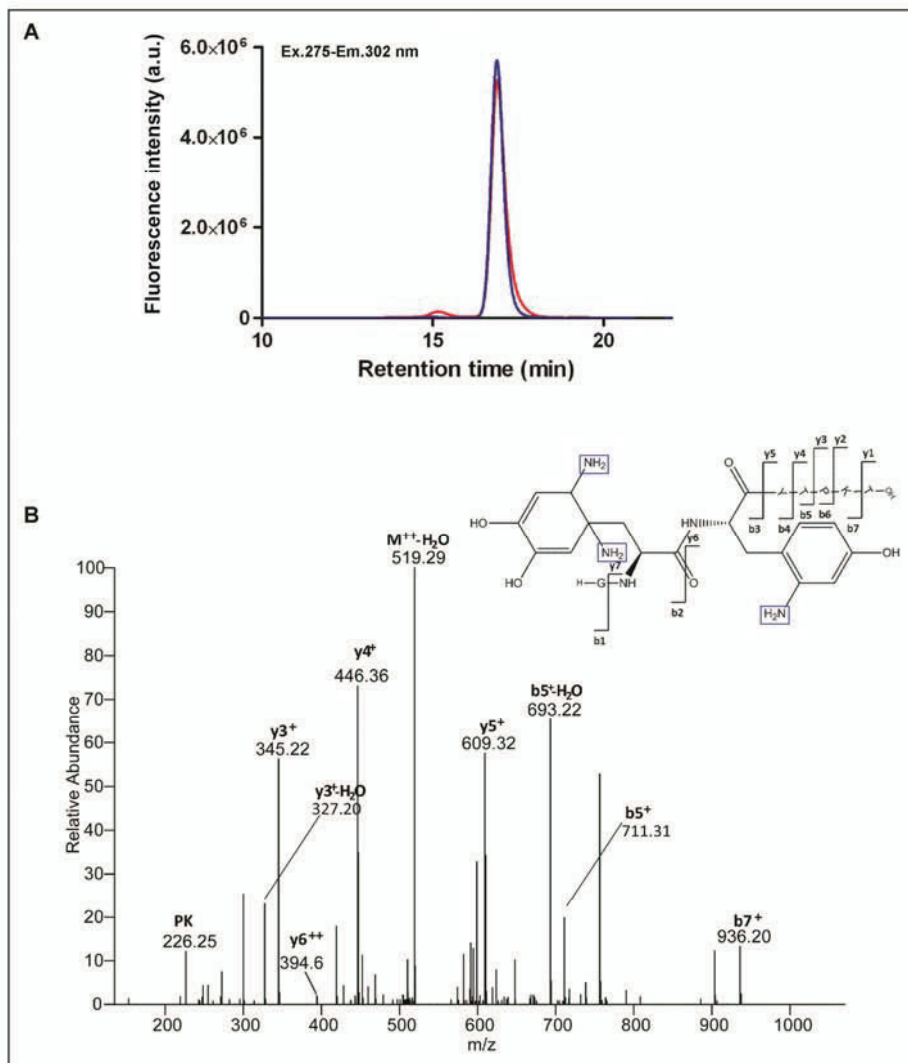


Figure 3. (A) SEC with intrinsic tyrosine fluorescence detection (Ex 275 nm-Em 302 nm) of insulin oxidized for 3 hours at room temperature in ABI 0.25 M (in red) and its control (in blue). (B) MS/MS of peptidic fragment obtained from oxidized insulin in ABI 0.25 M, reduced (DTT), alkylated (IAM), and digested with Glu-C. The amino groups added through Michael addition to the oxidized phenylalanine are highlighted in blue.

These Michael addition products are generated by addition of the nucleophiles to the two β -type carbon atoms in the oxidation product DOCH, and are consistent with the mass increases of the respective original Phe

residues; however, due to the low abundance of sample we did not confirm the regiochemistry of nucleophile addition by NMR. The most relevant ions in the MS/MS spectra, which allow to confirm the addition of ammonia to DOCH, are $b5^+$, $y6^{++}$ and $y5^+$. The first, with m/z 711.31 of a singly charged ion, shows the sequence $G_{B23}FFYT_{B27}$ plus the additional molecular weight of three oxygen atoms and three ammonia molecules. These data suggest that the sequence PKT is neither oxidized, nor derivatized with amino groups. The doubly charged ion $y6^{++}$, with m/z 394.6, related to the sequence $F_{B25}YTPKT_{B30}$, shows that one oxygen and one ammonia molecule are incorporated into this sequence. Of course the Tyr residue could be the target for this incorporation; however, the ion $y5^+$ argues against this hypothesis where the singly charged ion with m/z 609.32 represents the unmodified sequence $Y_{B26}TPKT_{B30}$.

To evaluate the potential of MCO to induce fragmentation, already reported by other authors for the MCO of glycated insulin [9, 33], and by our group for the MCO of PEGylated insulin [13], human insulin was oxidized in 50 mM PB, pH 7.4, for 24 hours at room temperature and 37 °C. Figure 2, panel F clearly shows the elution of species after the monomer peak, which indicates the formation of lower molecular weight species.

MS analysis of undigested insulin samples

The FT-ICR MS analysis presented in this section was performed on oxidized insulin and native insulin (our control), prior to reduction, alkylation, ABS-derivatization and digestion with Glu-C. This analysis was executed to monitor the formation of oxidized monomers and to confirm the MCO-induced fragmentation, as well as to quantify these species relative to native insulin.

Oxidation

Human insulin contains three Phe and four Tyr residues. Oxidation of Phe to DOPA would require the incorporation of two oxygen atoms. Instead, oxidation of Tyr to DOPA would be represented by the incorporation of one oxygen atom. Hence, it should be possible to detect mass increases corresponding to ten atoms of oxygen per monomer, considering DOPA as oxidation product of Phe and Tyr. Based on this number, after deconvoluting each MS spectrum by using the maximum entropy distribution algorithm

(Figure 4), we added up the intensities observed for all monomers containing additional oxygen atoms ($n=0-10$) (i.e., for the masses $5804.63+16$, $5804.63+32+\dots+5804.63+160$ Da).

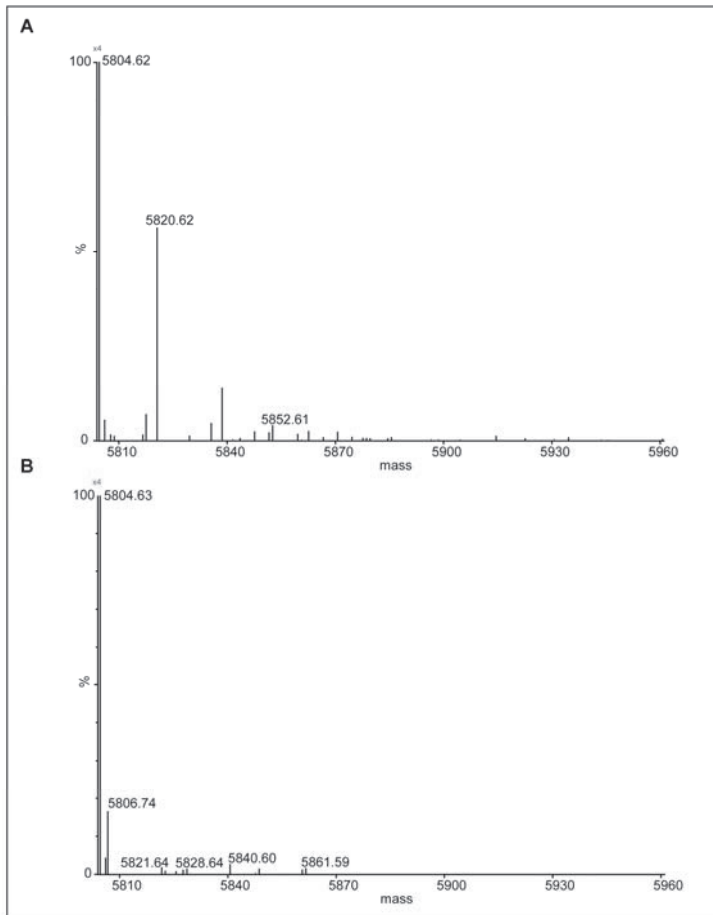


Figure 4. Mass spectrum (MS) of undigested insulin and undigested insulin oxidized for 3 hours at room temperature in 50 mM PB, pH 7.4. Spectra are shown for oxidized insulin (A) and native insulin (B) in the m/z range 5805-5961 to show the oxidized monomer. Spectra were obtained using the maximum entropy distribution algorithm implemented in the Masslynx MaxEnt software (Waters Corporation, Milford, MA) using an adduct of 1 proton. (Please note that 5804.63 represents the molecular mass of unprotonated insulin).

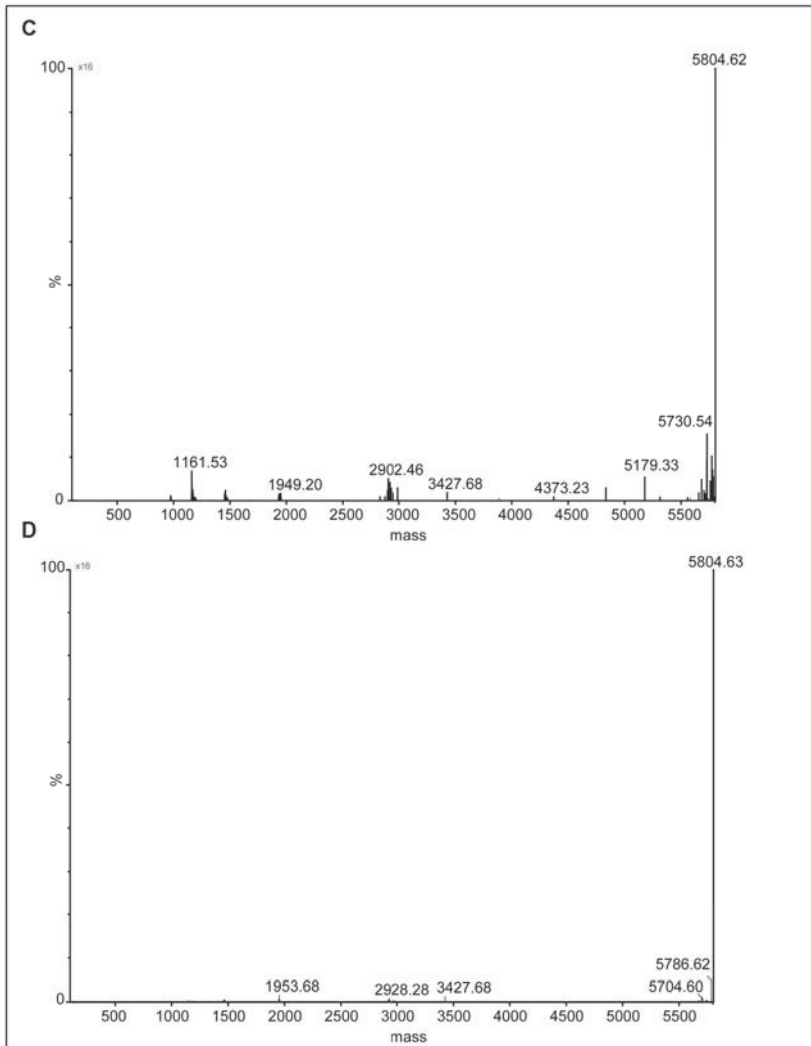


Figure 4. Mass spectrum (MS) of undigested insulin and undigested insulin oxidized for 3 hours at room temperature in 50 mM PB, pH 7.4. Spectra are shown for oxidized insulin (C) and native insulin (D) in the m/z range 100-5805 to show insulin fragments. Spectra were obtained using the maximum entropy distribution algorithm implemented in the Masslynx MaxEnt software (Waters Corporation, Milford, MA) using an adduct of 1 proton. (Please note that 5804.63 represents the molecular mass of unprotonated insulin).

The resulting intensity of oxidized monomer in insulin exposed to MCO was found to be ~ 300 fold higher than that in non-oxidized insulin (Figure 5), suggesting that the amount of insulin monomer containing oxygen had increased dramatically after MCO. These calculations are possible because after deconvolution of the mass-to-charge ratios, the absolute intensity of each ion is conserved. For better clarity, the oxidized monomer in insulin exposed to MCO and that of the non-oxidized insulin are presented in the mass range 5805-5961 (Figure 4, panel A and B). Figure 4, panel A shows that the intensity of the mass signal at 5820.62 Da (indicating incorporation of one oxygen atom) and the intensity of the mass signal at 5852.61 Da (indicating incorporation of three oxygen atoms) are much more intense after oxidation. Note that signals indicating incorporation of several other numbers of oxygen atoms were detected too, although with lower intensity. Although MS analysis cannot detail which amino acid is exactly oxidized, our calculation provides a first estimation for the extent of MCO in the insulin monomer.

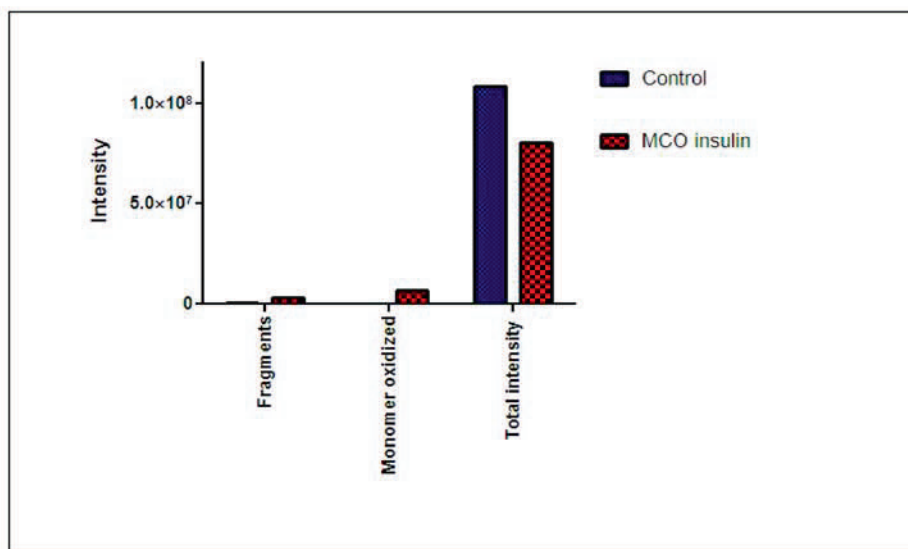


Figure 5. Plot representing the intensity of fragments and oxidized monomer relative to the total intensity of all detected peaks for native insulin (control, in blue) and insulin oxidized for 3 hours at room temperature in 50 mM PB, pH 7.4 (in red). Data are derived from the spectra reported in Figure 4.

Fragmentation

In order to detect and quantify the yield of insulin fragments relative to native insulin and to understand if fragmentation, measured by SEC, occurred during sample preparation for analysis (reduction, alkylation, ABS-derivatization and digestion) or prior to sample preparation, i.e. during the exposure of insulin to Cu^{2+} and ascorbate, MS analysis of native and oxidized insulin was performed prior to and after reduction, alkylation, ABS-derivatization and digestion. Panel C and D of Figure 4, represent a zoom (16X) into the mass region between 100 and 5805 Da: clearly the oxidized insulin contains new peptides of a lower molecular weight compared to insulin. We processed the MS spectra of oxidized and non-oxidized insulin as follows: 1) deconvolution using the maximum entropy distribution algorithm; 2) sum of the intensities of all the fragments with a molecular weight between that of glycine (the smallest amino acid in insulin) and the molecular weight measured for insulin (i.e. 5804.6 Da) minus the molecular weight of glycine, after hydrolysis. The procedure that was employed is summarized in formula 1:

$$I_{\text{total}} = \sum_{i=j}^k [\text{Fragment}]_i \left\{ \begin{array}{l} j = \text{Mw}(\text{Gly}) = 75.03 \\ k = \text{Mw}(\text{Insulin} - \text{Gly} + \text{H}_2\text{O}) \\ k = 5804.63 - 75.03 + 18 \\ [\text{Fragment}]_i = \text{Mw of the } i^{\text{th}} \text{ fragment} \end{array} \right. \quad (1)$$

The MS spectra of the oxidized and native insulin that were used for this calculation are displayed in Figure 4, panel C and D, respectively. Figure 5 represents the histograms plotted using the intensity values of the same spectra. The total intensity of the control (i.e. native insulin), was calculated between masses of 0 Da and 36000 Da, i.e. until just beyond the theoretical molecular weight of the insulin hexamer. Based on this calculation, the total yield of fragments in the non-oxidized control was 0.3% compared to 3.1% in insulin exposed to Cu^{2+} and ascorbate (percentages have been calculated dividing the total intensity of the fragments over the total intensity of the native insulin used as a control). For a better view of the fragments, we provide a zoom of the range between 100-5805 Da of native insulin and oxidized insulin (Figure 4, panel C and D). Altogether these results suggest that MCO induces peptidic fragmentation. We did not explore in more detail

the mechanism(s) by which such fragmentation occurs, nor did we search for all the possible cross-links in which the new N-termini could be involved. However, we did note the generation of new cross-links between insulin and such fragments (see below), which contain new N-termini and C-terminal amino acids not generated by Glu-C digestion.

Identification of chemical modifications by MS/MS analysis of reduced, alkylated, ABS-derivatized and digested samples

The FT-ICR MS analysis of oxidized and native insulin (control) was performed after reduction, alkylation, ABS-derivatization and digestion with Glu-C, by injecting the samples into the mass spectrometer by liquid chromatography. The aim of this analysis was to map the chemical modifications in the primary structure of insulin, to identify the nonreducible cross-links involved in insulin aggregation and to identify the fragments.

Because different kind of oxidized, ABS-derivatized, and non-oxidized fragments were found, we hereafter define “fragments” as peptides resulting from at least one cleavage site that differs from the one expected from proteolytic digestion by Glu-C (i.e. after glutamic acid; Glu; E) and we define “Glu-C fragments” as peptides originating from the expected proteolytic cleavage sites of Glu-C.

Table II lists all the detected “Glu-C fragments” (oxidized and ABS-derivatized) and “fragments” (oxidized, ABS-derivatized and non-oxidized). Non-oxidized Glu-C fragments were measured for both oxidized and native insulin but are not listed in Table II, since their presence was expected and represents the majority of Glu-C fragments. MS/MS spectra of all fragments is available in the supplementary material, online on <http://link.springer.com/article/10.1007%2Fs11095-012-0755-z>).

Non-oxidized fragments are only briefly discussed in this manuscript, because the main focus of our work was to elucidate the chemical mechanisms of insulin aggregation during MCO. As displayed in Table II, the following section is divided into the following subsections: oxidized Glu-C fragments, ABS-derivatized Glu-C fragments, oxidized fragments, ABS-derivatized fragments, non-oxidized fragments. Regarding the description of these fragments, the prefixes and subscripts A and B refer to sequences from the A

and B chain, respectively, while b and y refer to the cleavage sites according to the nomenclature introduced by Roepstorff [34].

Table II. Fragments identified in reduced, alkylated, ABSderivatized and digested (Glu-C) insulin and oxidized insulin, as determined by mass spectrometry.[§]

Samples	Glu-C fragments oxidized	Glu-C fragments ABS-derivatized	Fragments oxidized	Fragments ABS-derivatized	Fragments Non-oxidized
Oxidized insulin	R ₂₂₂ GFF ^Y *TPKT ₁₀₀ Fig. S1 A, B, C	R ₂₂₂ GFF ^Y *TPKT ₁₀₀ Fig. S5	F ⁿ ₁₀ VNQHLCG ₉₉ Fig. S7	A ₁₁₄ L ^Y *LVG ₉₇ Fig. S10	L ₄₁₃ YQLE ₁₇ Fig. S13
	A ₁₀ L ^Y *LYCGE ₁₀₂ Fig. S2	R ₂₂₂ GFF ^Y *TPKT ₁₀₀ Fig. S6	E ₂₂₂ RGF ^{**} *FTTPKT ₁₀₀ Fig. S8	S ₁₁₂ L ^Y *QLE ₁₇ Fig. S11	I ₄₁₀ CSLY ₁₄ Fig. S14
	F ⁿ ₁₀ VNQHLCGSHLVE ₁₁₃ Fig. S3		F ⁿ ₁₀ VNQHLCGSHLVEAL ₁₁₅ Fig. S9	S ₁₂₃ L ^Y *QLE ₁₇ Fig. S12	S ₁₂₃ L ^Y *QLE ₁₇ Fig. S15
	F ⁿ ₁₀ VNQHLCGSHLVEALYLVCGE ₁₂₁ Fig. S4		H ₁₀₅ LCGSH [*] LVEAL ₁₁₅ MS/MS not shown		S ₁₁₂ L ^Y *QLE ₁₇ Fig. S16
			F ₁₀ VNQH [*] LCCG ₉₉ MS/MS not shown		Y ₄₁₄ QLE ₁₇ Fig. S17
			F ₁₀ VNQH [*] LCCGSH ₁₀₁ MS/MS not shown		G ₁₀₅ SHLV ₁₀₃ Fig. S18
			F ₁₀ VNQH [*] LCCGSHL ₁₀₁ MS/MS not shown		H ₁₀₅ LVEAL ₁₁₅ Fig. S19
					F ₁₀ VNQHLCGSH ₉₉ Fig. S20
					Y ₄₁₄ LVG ₉₇ Fig. S21
					G ₁₀₅ ERGF ^Y ₁₀₂ Fig. S22
					G ₁₁₁ VEQC ₁₀₄ Fig. S23
					A ₁₁₄ L ^Y LVCG ₁₀₀ Fig. S24
					Q ₁₁₅ LENYCN ₁₂₁ Fig. S25
					L ₄₁₀ CGSHLV ₁₀₃ Fig. S26
Insulin	R ₂₂₂ GFF ^Y *TPKT ₁₀₀ Fig. S1 A, B, C				G ₁₀₅ FTTPKT ₁₀₀ Fig. S27
					L ₄₁₃ YQLE ₁₇ Fig. S13

[§] oxidation of insulin was performed by MCO for 3 hours at room temperature in 50 mM PB, pH 7.4.

* incorporation of one oxygen atom; ** incorporation of two oxygen atoms.

incorporation of one ABS molecule; ## incorporation of two ABS molecules.

Oxidized Glu-C fragments*R_{B22}GFF*Y*TPKT_{B30}*

The C-terminal region of chain B contains two Phe and one Tyr in positions B24, B25 and B26, respectively. DOPA and DOCH can arise from the oxidation of all these residues. Thus it becomes of primary importance to identify the ions, which allows us to discriminate between different oxidation products. The MS/MS spectra reported in supplementary Figure S1A provides evidence for the oxidation of Phe B25 to Tyr where * indicates the incorporation of one oxygen atom. The ion b_3^+ , despite its low intensity, indicates that Phe B24 is present in the native, non-oxidized state, where m/z 361.2 corresponds to the singly charged ion of the sequence RGF. Instead, the ion b_4^+ provides evidence for oxidation of Phe B25. A careful analysis of the spectra (Figures S1B) reveals the contemporary presence of two different y_5^+ ions, indicated as (*F4*) y_5^+ with m/z 625.5 (which corresponds to a structure containing Tyr B26 oxidized) and, (*HO-F4*) y_5^+ with m/z 609.4 (which corresponds to a structure containing Phe B25 oxidized). Panel C shows the b_4^+ ions for these two coexisting structures, again representing oxidation of Phe B25 or Tyr B26, respectively. Hence, both Phe B25 and Tyr B26 are targets for the incorporation of one oxygen atom.

*A_{B14}LY*LVCGE_{B21}*

Supplementary Figure S2 displays the MS/MS data for the peptide ALY*LVCGE, which contains an expected Glu-C cleavage site, where Y* represents the incorporation of one oxygen into Tyr, i.e. the formation of DOPA (the Cys residue is alkylated with IAM). This product is confirmed through the presence of the ions b_3^+ - b_5^+ (although b_3^+ and b_4^+ show low intensities) and y_5^+ . The singly charged ions b_3^+ , b_4^+ and b_5^+ indicate that the oxygen is in one of the following sequences: ALY, ALYL, or ALYLV. The singly charged ion y_5^+ indicates that the sequence LVCGE is not oxidized. Therefore, oxygen incorporation must have occurred on one of the first three amino acids, ALY, where Tyr represents the most oxidation-sensitive target amino acid. Further evidence for Tyr B16 oxidation through ABS derivatization is given below.

*F*_{B1}VNQHLCGSHLVE_{B13}*

The N-terminus of chain B, Phe B1, displays a mass increase consistent with the oxidation of Phe B1 to cyclohexadienone. The MS/MS analysis (Figure S3) of the sequence F*VNQHLCGSHLVE indicates the formal addition of one oxygen atom and loss of 2 hydrogens from Phe B1, i.e. a mass increase of 14 Da through the appearance of the following ions: $y9^+$, which suggests that the sequence HLCGSHLVE is not oxidized, and $b6^+$, indicating the oxidation of the sequence FVNQHL. In this sequence, HL can be excluded as an oxidation target because of the nature of $y9^+$. Since in the sequence FVNQ, F is most sensitive to oxidation we conclude that oxidation targets Phe B1.

*F**_{B1}VNQHLCGSHLVEALYLVCGE_{B21}*

Phe B1 can be further oxidized to DOCH (Figure S4). The observed masses of the ions $y17^{++}-H_2O$ and $y17^+$ exclude any oxidation of other amino acids sensitive to oxidation in F**_{B1}VNQHLCGSHLVEALYLVCGE_{B21}. The ion $y17^+$ with m/z 1899.82 shows an intensity which is about 80% of that of $b16^+$ with m/z 1898.75; thus, it should not be considered the first isotope peak of $b16^+$, which would be expected at m/z 1899.75.

ABS-derivatized Glu-C fragments*R_{B22}GFFY#TPKT_{B30} and R_{B22}GFFY##TPKT_{B30}*

Supplementary Figure S5 shows that Tyr B26 is converted to DOPA and/or DOCH, indicated by derivatization with one molecule of ABS (designated with the symbol #). The ions with m/z 361.28 and m/z 508.26, corresponding to $b3^+$ and $b4^+$, respectively, suggest that both Phe B24 and Phe B25 are not oxidized in this sequence. If for instance, Phe B24 (in the sequence RGF_{B24}FYTPKT) had been oxidized, the $b3^+$ ion would have been expected with m/z 377.28 (i.e. 361.28+16 Da). Instead, the ions $b5^+$ and $b6^+$ provide evidence that Tyr B26 is the target of oxidation. For additional evidence, supplementary Figure S6 displays the MS/MS spectrum of RGFFY##TPKT, derivatized with two molecules of ABS, as shown in the displayed structure. Here, the ions $b3^+$ and $b4^+$ are identical to the ones reported in Figure S5, although more intense. The ion with m/z 1037.29 corresponding to $b5^+$ and the ion $y5^+$, reported in the inset of Figure S6, confirm that the original Tyr

contains two ABS molecules. We had realized in the past [19-20], that derivatization with ABS can lead to the incorporation of one or two molecules of ABS into the final benzoxazole product (see scheme 1), depending on the availability of ammonia, resulting in competition of ammonia and ABS for the position in 6 of the benzoxazole. In addition to that, it seems that the competition between ammonia and ABS depends on the steric hindrance of the peptide which is derivatized: i.e., derivatization with two ABS molecules of sterically less accessible DOPA and DOCH can be kinetically less favorable than that of more exposed residues. It must be noticed that the sequence $R_{B22}GFFYTPKT_{B30}$, depicted in Figures S5 and S6, does not necessarily belong to the same B chain: in other words, the sequence derivatized with one ABS molecule could be involved in the formation of HMWO, while the doubly ABS-derivatized sequence can actually be present in the monomer as well, although oxidized, and subsequently be derivatized with two ABS molecules.

Oxidized fragments

*F*_{B1}VNQHLCG_{B8}*

Phe B1 is oxidized to hydroxylated Phe, indicated through the MS/MS data displayed in Figure S7: the ion $y7^+$ shows that none of the amino acids in the sequence C-terminal to Phe B1, VNQHLCG, is oxidized. Therefore, the ion $b5^+$ confirms oxidation of Phe B1. In fact, Phe hydroxylation can occur in positions ortho, meta and para; however, only the latter would lead to Tyr.

*E_{B21}RGF**FYTPKT_{B30}*

The MS/MS data displayed in Figure S8 are consistent with the oxidation of Phe B24 to DOCH. The ions $b4^+$ and $y6^+$ are fundamental to confirm the oxidation of Phe B24 since the first indicates the presence of the sequence ERGF**, and the second, suggests that the sequence FYTPKT is not oxidized. Further confirmation of the chemical structure in which Phe B24 is doubly oxidized arises from the detection of the internal fragment GF**FY with m/z 545.39, which can be produced during the analysis via specific pathways consistent with the mobile proton model [35].

*F*_{B1}VNQHLCGSHLVEAL_{B15}*

Phe B1 oxidation is also evident in the sequence F*VNQHLCGSHLVEAL, indicated by the MS/MS data displayed in Figure S9. Here it is sufficient to consider the ions y13⁺ and b14⁺⁺. The ion y13⁺ indicates that the sequence NQHLCGSHLVEAL is not modified. On the other hand b14⁺⁺ indicates oxidation in the sequence FVNQHLCGSHLVEA. By exclusion, this limits oxidation to the N-terminal subsequence FV, where F represents the most oxidation-sensitive amino acid.

ABS-derivatized fragments*A_{B14}LY#LVC_{B19}*

We further corroborated the formation of DOPA through derivatization of the oxidized peptide ALY*LVC with ABS (Figure S10). The only possible site for derivatization in this peptide is an oxidized Tyr residue, since ABS derivatization requires the presence of DOPA (which during the derivatization is oxidized with K₃Fe(CN)₆ to DOCH).

S_{A12}LY#QLE_{A17} and S_{A12}LY##QLE_{A17}

The MS spectra presented in Figures S11 and S12 provide evidence for the ABS derivatization of Tyr A14 within the sequence SLYQLE. Successful derivatization with one and two molecules of ABS indicates oxidation of Tyr A14 to either DOPA or DOCH. In both Figures the ions b3⁺ with m/z 560.11 and 730.07, respectively and, the ion y4⁺ with m/z 748.39 and 918.15, respectively, indicate derivatization of the original Tyr residue with one and two ABS molecules.

Non-oxidized fragments

Two types of non-oxidized fragments were detected in the control (Table II). They are likely generated during production or storage as a consequence of low traces of transition metals. Instead, 14 non-oxidized fragments were detected as a result of MCO, summarized in the last column of Table II. The MS/MS data of all these fragments are reported in the Supplementary Material (Figures S13-S27, available online).

Covalent cross-links

This section focuses on the identification of covalent cross-links by MS/MS analysis. Figure 6 summarizes all the covalent cross-links detected as a result of the MCO of insulin.

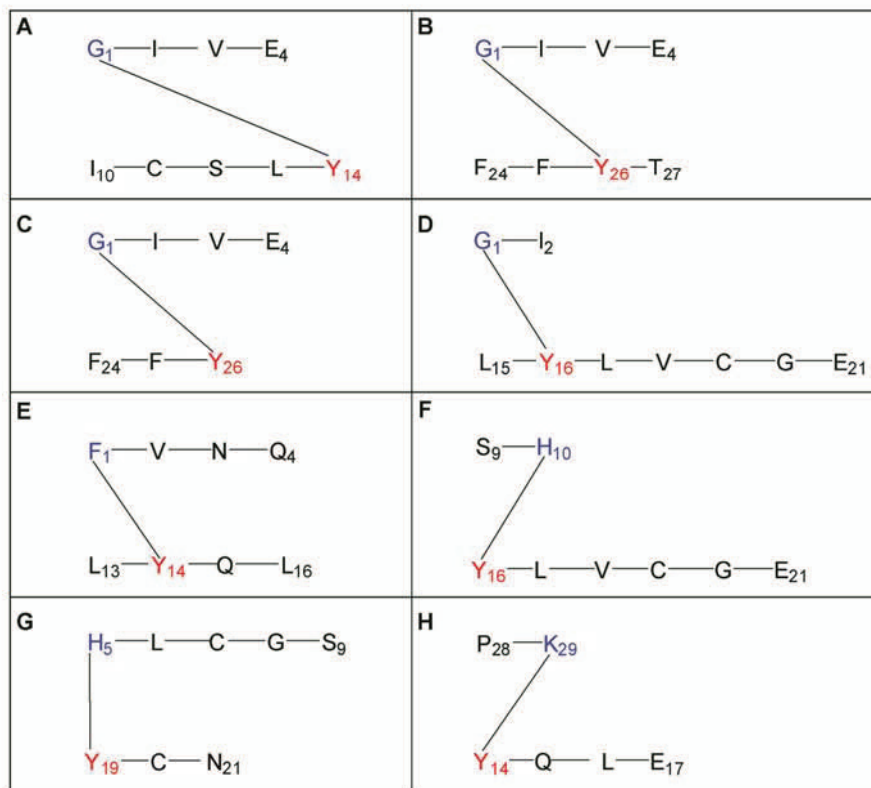


Figure 6. Identified inter-/intra-molecular cross-links measured after MCO of insulin, between (A) Gly A1-Tyr A14, (B and C) Gly A1-Tyr B26, (D) Gly A1-Tyr B16, (E) Phe B1-Tyr A14, (F) His B10-Tyr B16, (G) His B5-Tyr A19, (H) Lys B29-Tyr A14. In blue are shown the amino acids with nucleophilic properties and in red the amino acids oxidized to DOCH, which are Michael acceptor for nucleophilic addition. Further details are given in Figure 7 and in the main text in the section “*Covalent cross-links*”.

Gly A1 – Tyr A14 cross-link

Figure 7 panel A displays the MS/MS data consistent with a cross-link between Gly A1 and Tyr A14. The ions $Bb1^+$, $By3^+$ and $Ab3^+$ are the most relevant ones to confirm the cross-link between Gly A1 and Tyr A14.

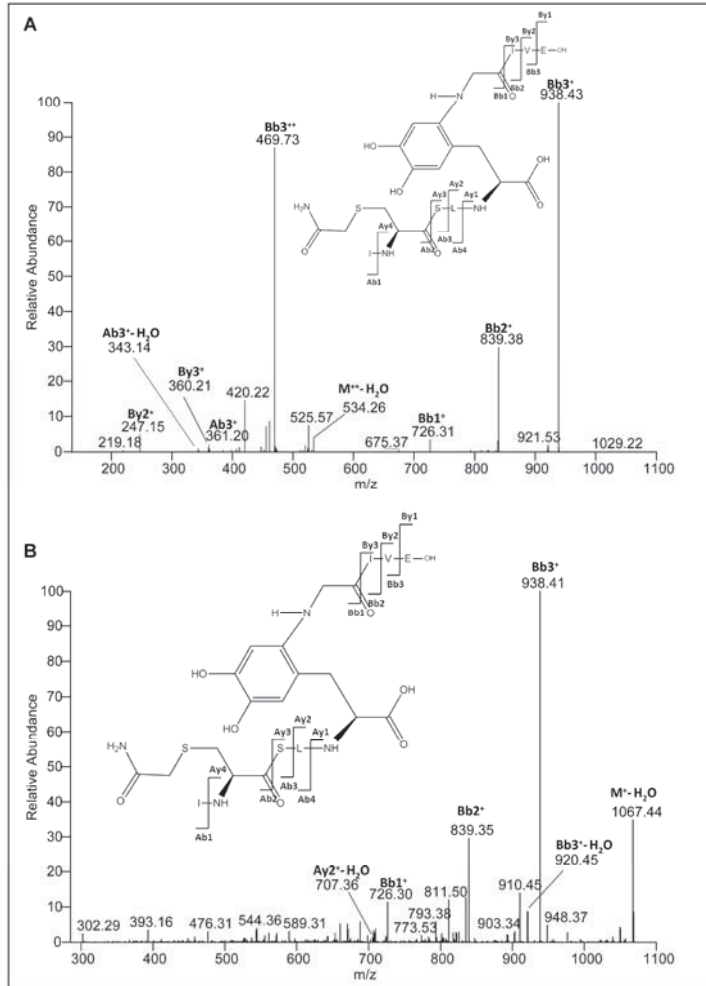


Figure 7. MS/MS of (A and B) sequence GIVE cross-linked through the glycine A1 to the sequence ICSLY. The fragments have been obtained after reduction (DTT), alkylation (IAM), ABS-derivatization and digestion (Glu-C) of oxidized insulin. Further explanation can be found in the text.

In particular Bb1⁺ shows that the sequence ICSLY is covalently attached to Gly. The ion By3⁺ indicates that the sequence IVE is not involved in the cross-link and, therefore, can be dissociated during the MS/MS analysis since it is connected to Gly A1 only through a peptide bond. Finally, the ion Ab3⁺ provides evidence that ICS is not involved in the cross-link. In the structure provided in Figure 7, panel A, the covalent attachment of Gly A1 to Tyr A14 is representatively shown for the position in 6 of the original DOPA (or DOCH) product. While, in principle, Michael addition is possible also at positions 1 and 2, position 6 is sterically less hindered, and that is why we selected to represent the adduct formation at position 6. However, we have currently no evidence for this regioselectivity. Further confirmation of the structure reported in Figure 7, panel A was obtained through the spectrum displayed in Figure 7, panel B, where the ion M⁺-H₂O was detected.

Gly A1 – Tyr B 26 cross-link

Figure 7, panel C represents the cross-link of Gly A1 of the sequence GIVE to Tyr B26. The mass spectra displayed in Figures 7, panel C, represents sodium adducts of the respective peptide fragment(s), likely due to incomplete removal of buffer during dialysis. Therefore, all the m/z of the ions presented in Figure 7, panel C and D, have an increased mass of 23 Da. The ion [By2+Na]⁺, representing the singly charged sequence VE, suggests that the amino acids Val and Glu are not involved in the new covalent bond. If this sequence had been involved in the new covalent bond with Tyr, it would not have been possible to detect the ion [By2+Na]⁺, since only dissociation of peptide bonds occurs during the low energy collision with the inert gas. [Bb2+Na]⁺ indicates that the sequence GI is covalently bound to the sequence FFY. We excluded the possibility of DOPA as the product of one of the Phe residues, since in such case the ion [Bb2+Na]⁺ would have a mass increase (relative to the expected mass of the fragment of unmodified insulin) larger than 16 Da (the oxidation of Phe to DOPA and DOCH requires two oxygen atoms); if one of the Phe residues were exclusively oxidized to Tyr, the ion [Bb2+Na]⁺ would feature the same molecular weight as the one detected in this MS/MS spectrum. In such case, however, it would not be possible to observe Michael addition, since the new Tyr residue (generated from the

mono-oxidation of Phe) is not a Michael acceptor unless it is further oxidized to a quinone.

In panel D of Figure 7 the original sequence FFY shows additional oxidation of both Phe residues (in contrast to panel C, which shows the native Phe residues in FFY): one of them to DOPA and the second one to a 6-amino substituted DOPA, likely originating from Michael addition of ammonia to a DOPA oxidation product.

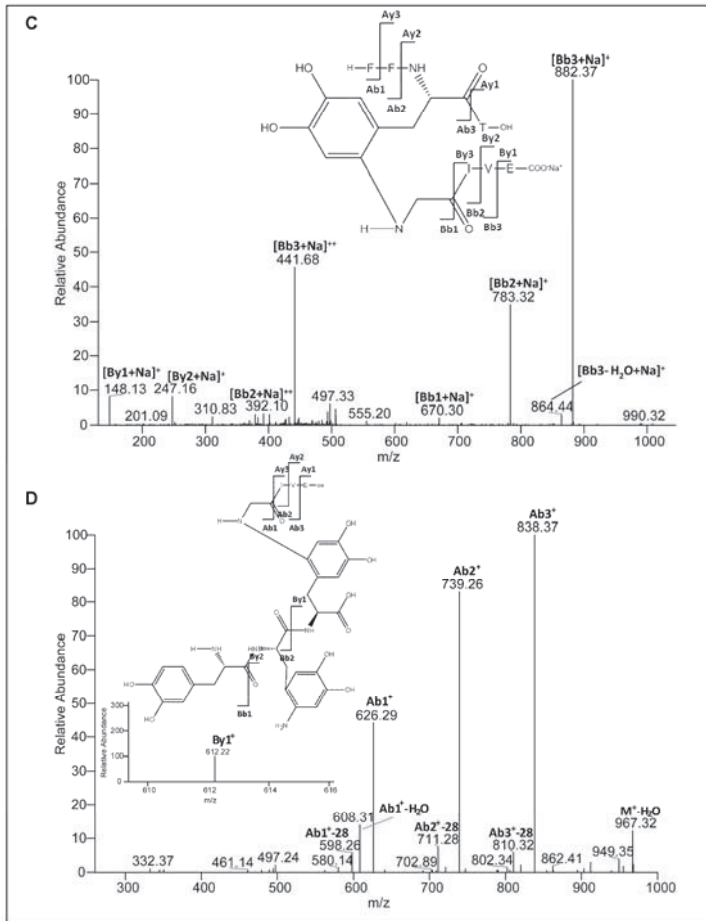


Figure 7. MS/MS of (C) sequence GIVE cross-linked through the glycine A1 to the sequence FFYT, (D) sequence GIVE cross-linked through the glycine A1 to the sequence FFY. The fragments have been obtained after reduction (DTT), alkylation (IAM), ABS-derivatization and digestion (Glu-C) of oxidized insulin. Further explanation can be found in the text.

The ions $By1^+$, with m/z 612.22, displayed in the inset, and $Ab1^+$, with m/z 626.29, unequivocally indicate that the covalent bond is between Gly and Tyr: $By1^+$ represents the singly charged sequence Y-GIVE and $Ab1^+$ corresponds to the singly charged sequence FFY-G. The combination of both demonstrates that the new covalent bond, not dissociable during MS/MS analysis, is located between Tyr and Gly. Importantly, our results show that predominantly Tyr oxidation products serve as Michael acceptors for cross-link formation during the MCO of insulin (see also below). There are several possible rationales for this behavior, including protein conformation and the respective yields of Tyr and Phe oxidation products: the oxidation of Phe to DOCH requires one additional oxidation step compared with that of Tyr to DOCH, suggesting that DOCH formation from Tyr is kinetically favorable.

Gly A1 - Tyr B16 cross-link

Figure 7 panel E displays MS/MS data consistent with a covalent cross-link between Gly A1 and Tyr B16. The most relevant ion in this figure is $Ab2^+$ with m/z 479.27, which demonstrates that the sequence GI is covalently bound to LY. Since Ile and Leu do not contain functional groups amenable to Michael addition, we conclude that the covalent bond is formed between Gly and Tyr.

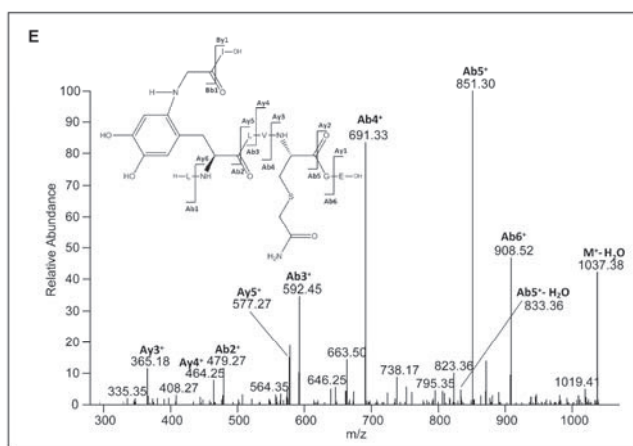


Figure 7. MS/MS of (E) sequence GI cross-linked through the glycine A1 to the sequence LYLVCGE. The fragments have been obtained after reduction (DTT), alkylation (IAM), ABS-derivatization and digestion (Glu-C) of oxidized insulin. Further explanation can be found in the text.

Phe B1 – Tyr A14 cross-link

Phe B1 is not only a possible target for oxidation; the free N-terminal amino group can react via Michael addition with DOCH. The spectrum depicted in panel F of Figure 7 shows the relevant ions consistent with a cross-link between Phe B1 and Tyr A14: Ab1⁺ with m/z 697.36 shows the existence of a peptide containing the following amino acids: Phe, Tyr, Gln and two Leu, plus the molecular weight of one oxygen atom. However considering only the ion Ab1⁺, it is not possible to localize the oxygen addition and to characterize the nature of the cross-link. The ion Bb2⁺, with m/z 797.36, indicates that the sequence FVNQ is connected to the sequence LY. The ion Ay3⁺ -NH₃, with m/z 343.16, excludes any covalent cross-link of the sequence VNQ. In the sequence LY only Tyr oxidation can lead to a Michael acceptor for the amino terminal of Phe B1, which suggests a cross-link such as depicted in Figure 7, panel F.

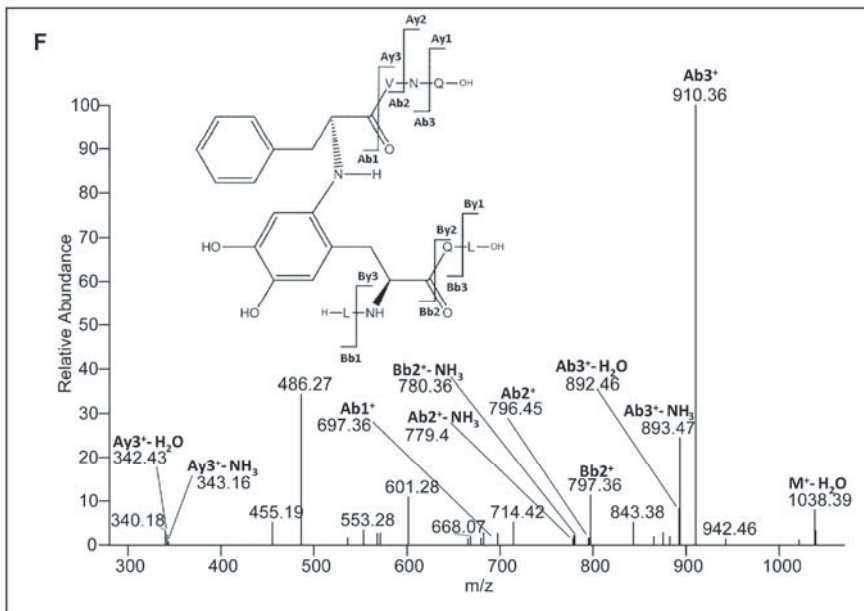


Figure 7. MS/MS of (F) sequence FVNQ cross-linked through the phenylalanine B1 to the sequence LYQL. The fragments have been obtained after reduction (DTT), alkylation (IAM), ABS-derivatization and digestion (Glu-C) of oxidized insulin. Further explanation can be found in the text.

His B10 – Tyr B16 cross-link

Figure 7, panel G displays a cross-link between His B10 of the sequence SH and Tyr B16 of the sequence YLVCG. The relevant ions in this spectrum are $Ab1^+$ and $Ay4^+$. Ion $Ab1^+$, with m/z 420.14, suggests that the sequence SH is covalently bound to the original Tyr residue (after oxidation of Tyr to DOCH). The deprotonated imidazole nitrogen of His is an appropriate nucleophile for Michael addition, demonstrated for example for His addition to dehydroalanine [36].

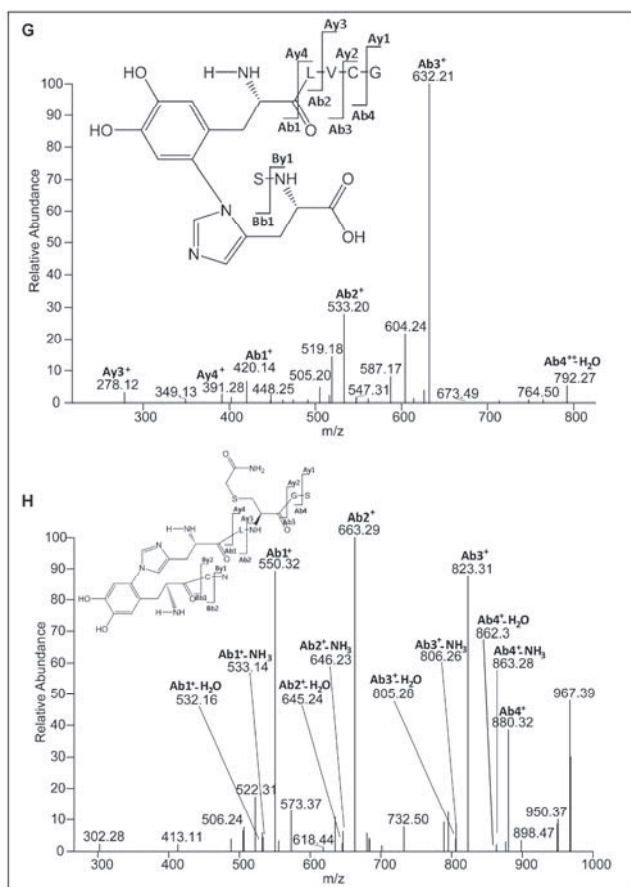


Figure 7

Figure 7. MS/MS of (G) sequence SH cross-linked through the histidine B10 to the sequence YLVCG, (H) sequence HLCGS cross-linked through the histidine B5 to the sequence YCN. The fragments have been obtained after reduction (DTT), alkylation (IAM), ABS-derivatization and digestion (Glu-C) of oxidized insulin. Further explanation can be found in the text.

His B5 – Tyr A19 cross-link

Panel H of Figure 7 displays a cross-link between His B5 of the sequence HLCGS and Tyr A19 of the sequence YCN and the MS/MS data supporting this assignment. We note that the ion $Ab1^+-NH_3$ shows an intensity which is about 80% of that of $Ab1^+-H_2O$. Thus, the ion with m/z 533.14 should not be considered the second isotope of $Ab1^+-H_2O$, suggesting that the N-terminal amino group of the His is free and not involved in the new covalent bond.

Lys B29 – Tyr A14 cross-link

Figure 7, panel I represents the cross-link between Lys B29 and Tyr A14. The relevant ion in the spectra is $Ab1^+$, since it localizes the cross-link to Tyr and the amino acids Pro and Lys in the sequence PK. Because the MS/MS data in panel I shows no b ions, we cannot conclude whether the cross-link involves the side chain amino group of Lys or the amino group of Pro. The latter would require that non-oxidative fragmentation between Thr B27 and Pro B28 occurs prior to cross-linking; the side chain amino group of Lys B29 represents a good nucleophile and it can therefore be assumed that at least some of the cross-links are formed through the reaction of Tyr A14 with Lys B29.

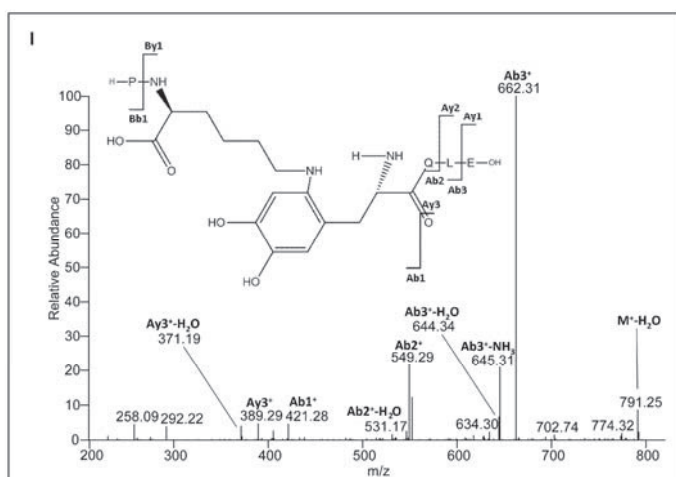


Figure 7. MS/MS of (I) sequence PK cross-linked through the lysine B29 to the sequence YQLE. The fragments have been obtained after reduction (DTT), alkylation (IAM), ABS-derivatization and digestion (Glu-C) of oxidized insulin. Further explanation can be found in the text.

Discussion

We performed a detailed mass spectrometric analysis of insulin in order to elucidate the mechanisms and amino acid residues involved in MCO and MCO-mediated aggregation. The oxidation of Phe and Tyr leads to the formation of catechol structures that can be further oxidized to DOCH. These oxidation products serve as Michael acceptors for cross-links with several nucleophiles present in the insulin sequence.

Formation of dityrosine, as a potential structure involved in the cross-linking of insulin, was not detected, neither with fluorescence measurement (see material and methods), nor with the help of MassMatrix software. This is not surprising since it has been reported that only the hydrogen peroxide/copper system is capable of inducing dityrosine formation [37].

Schiff base formation could potentially be in competition with Michael addition, nonetheless such cross-links can be reversed relatively easily and based on our results does not appear to be the main mechanism of insulin aggregation.

Changes in the primary structure, as reported in this paper, may alter the biological activity of insulin with severe consequences on the glycemic control.

Furthermore, changes in the secondary, tertiary and quaternary structure as a consequence of oxidation, as reported by us before [13], may generate new repetitive epitopes or open the access to hidden epitopes that could contribute to the formation of immunogenic products.

In addition to the characterization and localization of oxidation products, we provided quantitative data on the amount of fragments and oxidized monomers. An important feature of insulin exposed to MCO is the appearance of fragments, which increases the number of polypeptide nucleophiles available for Michael addition. At this point, we do not know whether the observed insulin fragmentation precedes or follows cross-link formation.

Furthermore, it is unknown whether Glu-C might have a different specificity towards oxidized protein. The actual mechanism of cleavage is currently unknown, but we can exclude the classical oxidative cleavage [38] since we did not detect the α,β -dicarbonyl products expected for such a mechanism. Instead, all non-specific cleavages appear to involve a hydrolytic cleavage of the respective peptide bonds. It may be possible that the addition of Cu^{2+} and

ascorbate promote the formation of peptide-metal complexes with hydrolytic activity, such as described for the cleavage of amides through Cu^{2+} [39].

Surprisingly, most of the non-specific peptide fragments we detected were already reported by other authors, e.g. after the oxidation of glycosylated insulin by Fenton chemistry [9, 33]; however, Guedes et al. [33] interpreted the cleavage mechanism as oxidative cleavage, which is *inconsistent* with the intact C- and N-termini of the detected peptide fragments.

Through MCO experiments at various pH, and in the presence of ammonia, we are able to confirm that Michael addition between insulin chains causes covalent aggregation. In the presence of ammonia, which competes for Michael addition to DOCH, aggregation was almost completely inhibited. Although such experimental conditions allow to prevent aggregation, we noted the introduction of an amino group on oxidized Tyr or Phe which might still have consequences for the immunogenicity of this small polypeptide hormone.

Several proteins have been shown to form aggregates after exposure to Cu^{2+} /ascorbate, such as recombinant SHa(29–231) prion protein [40], superoxide dismutase [41], monoclonal IgG2 [42], interferon alpha-2b [5-6] and interferon beta-1a [7]. The results presented in this paper may serve as a model to rationalize the chemical mechanisms of aggregation during MCO of proteins in general. Although insulin lacks Trp and Met, which are also prone to oxidation [43-44] and are present in most other proteins, DOPA and DOCH should not be formed from oxidation of Trp or Met, thus they cannot act as electron acceptor for Michael addition.

Since MCO was performed at pH 7.4, where insulin is present mainly in the hexameric state [45], the cross-links we measured are likely to be *intermolecular* cross-links, i.e. formed between different insulin molecules. As an example we calculated the distance of Gly A1 and Tyr A14 and Gly A1 and Tyr A19 within the same A-chain (using Swiss pdb viewer [46-47] and T6 human insulin at 1.0 Å resolution, 1MSO pdb file). An average of 18.5 Å was measured for a theoretical covalent bond between the amino group of Gly A1 and the carbon in ortho of the aromatic ring of Tyr A14, and an average of 8.3 Å for the amino group of Gly A1 and the carbon in ortho of the aromatic ring of Tyr A19, which seems to be too far for an *intramolecular* reaction (e.g., the length of the peptidic bond between Gly A1 and Ile A2 is 1.3 Å).

We also noticed that Phe residues, oxidized to DOCH, were not involved in cross-links, nor were they derivatized with ABS. In both cases this could be due to low accessibility of Phe residues which might belong to chains B involved in the formation of HMWO, in which only DOCH originated from Tyr is accessible for ABS derivatization. Moreover, in the case of cross-links it could be speculated that the oxidation of Tyr to DOCH (which requires the addition of only one oxygen atom), is kinetically favorable over the oxidation of Phe to DOCH (which requires two oxidation steps). This can potentially lead to a depletion of the nucleophiles available in the insulin molecule.

Conclusion

Oxidation is one important degradation process that proteins can undergo. In this work we highlighted the potential consequences of DOPA and DOCH formation and also illustrated how the knowledge of oxidation mechanisms can be utilized to investigate the mechanism of covalent aggregation. To this end, recombinant human insulin was used as a model: oxidation of aromatic amino acids residues, besides others, leads to α,β unsaturated carbonyl compounds, which are electron acceptors for Michael addition. These reactive groups, resulting from oxidation, not only can lead to covalent protein aggregation, as shown for insulin in this paper, but also may lead to cross-links between protein molecules and amino acids, which are typically present during cell culture and are often used as formulation excipients. This must be taken into consideration during production and formulation development of therapeutic proteins.

Acknowledgements

The authors thank Dr. Nadya Galeva for performing MS measurements, Merck (Oss, The Netherlands) and The University of Kansas and the National Institutes of Health (PO1AG12993) for financial support, and Merck for providing insulin for this project, Leiden University Fund/Slingelands (LUF, 1111/19-4-11\0, SI) and Nederlandse Stichting voor Farmacologische Wetenschappen (NSFW) for the travel grants to Riccardo Torosantucci.

References

- [1] E. R. Stadtman, C. N. Oliver. Metal-catalyzed oxidation of proteins. Physiological consequences. *J. Biol. Chem.* **1991**, *266*, 2005-2008.
- [2] V. Sadineni, C. Schöneich. Selective oxidation of Zn²⁺ - Insulin catalyzed by Cu²⁺. *J. Pharm. Sci.* **2007**, *96*, 1844-1847.
- [3] F. Zhao, E. Ghezzi-Schöneich, G. I. Aced, J. Hong, T. Milby, C. Schöneich. Metal-catalyzed oxidation of histidine in human growth hormone. Mechanism, isotope effects, and inhibition by a mild denaturing alcohol. *J. Biol. Chem.* **1997**, *272*, 9019-9029.
- [4] N. Jenkins. Modifications of therapeutic proteins: challenges and prospects. *Cytotechnology* **2007**, *53*, 121-125.
- [5] S. Hermeling, H. Schellekens, C. Maas, M. F. Gebbink, D. J. Crommelin, W. Jiskoot. Antibody response to aggregated human interferon alpha2b in wild-type and transgenic immune tolerant mice depends on type and level of aggregation. *J. Pharm. Sci.* **2006**, *95*, 1084-1096.
- [6] S. Hermeling, L. Aranha, J. M. A. Damen, M. Slijper, H. Schellekens, D. J. A. Crommelin, W. Jiskoot. Structural characterization and immunogenicity in wild-type and immune tolerant mice of degraded recombinant human interferon alpha2b. *Pharm. Res.* **2005**, *22*, 1997-2006.
- [7] M. M. van Beers, M. Sauerborn, F. Gilli, V. Brinks, H. Schellekens, W. Jiskoot. Oxidized and aggregated recombinant human interferon beta is immunogenic in human interferon beta transgenic mice. *Pharm. Res.* **2011**, *28*, 2393-2402.
- [8] M. Brownlee. The pathobiology of diabetic complications: a unifying mechanism. *Diabetes* **2005**, *54*, 1615-1625.
- [9] R. Z. Cheng, S. Kawakishi. Site-Specific Oxidation of Histidine-Residues in Glycated Insulin-Mediated by Cu²⁺. *Eur. J. Biochem.* **1994**, *223*, 759-764.
- [10] D. H. Montes-Cortes, J. J. Hicks, G. M. Ceballos-Reyes, J. R. Garcia-Sanchez, R. Medina-Navarro, I. M. Olivares-Corichi. Chemical and functional changes of human insulin by in vitro incubation with blood from diabetic patients in oxidative stress. *Metabolism* **2010**, *59*, 935-942.
- [11] S. P. Gieseg, J. A. Simpson, T. S. Charlton, M. W. Duncan, R. T. Dean. Protein-bound 3,4-dihydroxyphenylalanine is a major reductant formed during hydroxyl radical damage to proteins. *Biochemistry* **1993**, *32*, 4780-4786.
- [12] E. Wright, Jr., J. L. Scism-Bacon, L. C. Glass. Oxidative stress in type 2 diabetes: the role of fasting and postprandial glycaemia. *Int. J. Clin. Pract.* **2006**, *60*, 308-314.
- [13] R. Torosantucci, B. Kukrer, A. Mero, M. Van Winsen, R. Tantipolphan, W. Jiskoot. Plain and mono-pegylated recombinant human insulin exhibit similar stress-induced aggregation profiles. *J. Pharm. Sci.* **2011**, *100*, 2574-2585.

- [14] R. A. Lovstad. Copper catalyzed oxidation of ascorbate (vitamin C). Inhibitory effect of catalase, superoxide dismutase, serum proteins (ceruloplasmin, albumin, apotransferrin) and amino acids. *Int. J. Biochem.* **1987**, *19*, 309-313.
- [15] S. Li, T. H. Nguyen, C. Schöneich, R. T. Borchardt. Aggregation and precipitation of human relaxin induced by metal-catalyzed oxidation. *Biochemistry* **1995**, *34*, 5762-5772.
- [16] E. R. Stadtman. Oxidation of free amino acids and amino acid residues in proteins by radiolysis and by metal-catalyzed reactions. *Annu. Rev. Biochem.* **1993**, *62*, 797-821.
- [17] S. Fu, R. Dean, M. Southan, R. Truscott. The hydroxyl radical in lens nuclear cataractogenesis. *J. Biol. Chem.* **1998**, *273*, 28603-28609.
- [18] S. Fu, M. J. Davies, R. Stocker, R. T. Dean. Evidence for roles of radicals in protein oxidation in advanced human atherosclerotic plaque. *Biochem. J.* **1998**, *333 (Pt 3)*, 519-525.
- [19] V. S. Sharov, E. S. Dremina, N. A. Galeva, G. S. Gerstenecker, X. Li, R. T. Dobrowsky, J. F. Stobaugh, C. Schöneich. Fluorogenic Tagging of Peptide and Protein 3-Nitrotyrosine with 4-(Aminomethyl)-benzenesulfonic Acid for Quantitative Analysis of Protein Tyrosine Nitration. *Chromatographia* **2010**, *71*, 37-53.
- [20] V. S. Sharov, E. S. Dremina, J. Pennington, J. Killmer, C. Asmus, M. Thorson, S. J. Hong, X. Li, J. F. Stobaugh, C. Schöneich. Selective fluorogenic derivatization of 3-nitrotyrosine and 3,4-dihydroxyphenylalanine in peptides: a method designed for quantitative proteomic analysis. *Methods. Enzymol.* **2008**, *441*, 19-32.
- [21] C. Gallo-Rodriguez, X. D. Ji, N. Melman, B. D. Siegman, L. H. Sanders, J. Orlina, B. Fischer, Q. Pu, M. E. Olah, P. J. van Galen, et al. Structure-activity relationships of N6-benzyladenosine-5'-uronamides as A3-selective adenosine agonists. *J. Med. Chem.* **1994**, *37*, 636-646.
- [22] J. Brange, L. Langkjaer, S. Havelund, A. Volund. Chemical stability of insulin. 1. Hydrolytic degradation during storage of pharmaceutical preparations. *Pharm. Res.* **1992**, *9*, 715-726.
- [23] Insulin, Human, European Directorate for the Quality of Medicines (EDQM), **2001**.
- [24] Insulin, The United States Pharmacopeia Convention, Inc., Rockville, MD, **2002**.
- [25] C. Giulivi, K. J. Davies. Dityrosine: a marker for oxidatively modified proteins and selective proteolysis. *Methods. Enzymol.* **1994**, *233*, 363-371.
- [26] K. Ikehata, T. G. Duzhak, N. A. Galeva, T. Ji, Y. M. Koen, R. P. Hanzlik. Protein targets of reactive metabolites of thiobenzamide in rat liver in vivo. *Chem. Res. Toxicol.* **2008**, *21*, 1432-1442.
- [27] H. Xu, M. A. Freitas. A mass accuracy sensitive probability based scoring algorithm for database searching of tandem mass spectrometry data. *BMC Bioinformatics* **2007**, *8*, 133.

- [28] H. Xu, M. A. Freitas. MassMatrix: a database search program for rapid characterization of proteins and peptides from tandem mass spectrometry data. *Proteomics* **2009**, *9*, 1548-1555.
- [29] H. Xu, L. Yang, M. A. Freitas. A robust linear regression based algorithm for automated evaluation of peptide identifications from shotgun proteomics by use of reversed-phase liquid chromatography retention time. *BMC Bioinformatics* **2008**, *9*, 347.
- [30] H. Xu, L. Zhang, M. A. Freitas. Identification and characterization of disulfide bonds in proteins and peptides from tandem MS data by use of the MassMatrix MS/MS search engine. *J. Proteome Res.* **2008**, *7*, 138-144.
- [31] R. Tantipolphan, S. Romeijn, J. den Engelsman, R. Torosantucci, T. Rasmussen, W. Jiskoot. Elution behavior of insulin on high-performance size exclusion chromatography at neutral pH. *J. Pharm. Biomed. Anal.* **2010**, *52*, 195-202.
- [32] T. Tokoroyama. Discovery of the Michael Reaction. *Eur. J. Org. Chem.* **2010**, *2010* 2009-2016. .
- [33] S. Guedes, R. Vitorino, M. R. M. Domingues, F. Amado, P. Domingues. Oxidative modifications in glycated insulin. *Anal. Bioanal. Chem.* **2010**, *397*, 1985-1995.
- [34] P. Roepstorff, J. Fohlman. Proposal for a common nomenclature for sequence ions in mass spectra of peptides. *Biomed. Mass. Spectrom.* **1984**, *11*, 601.
- [35] B. Paizs, S. Suhai. Fragmentation pathways of protonated peptides. *Mass. Spectrom. Rev.* **2005**, *24*, 508-548.
- [36] W. W. Carol M. Taylor. Histidinoalanine: a crosslinking amino acid. *Tetrahedron* **2007**, *63*, 9033-9047
- [37] Y. Kato, N. Kitamoto, Y. Kawai, T. Osawa. The hydrogen peroxide/copper ion system, but not other metal-catalyzed oxidation systems, produces protein-bound dityrosine. *Free. Radic. Biol. Med.* **2001**, *31*, 624-632.
- [38] C. L. Hawkins, M. J. Davies. Generation and propagation of radical reactions on proteins. *Biochim. Biophys. Acta* **2001**, *1504*, 196-219.
- [39] C. J. Developing artificial hydrolytic metalloenzymes by a unified mechanistic approach. *Accounts Chem. Res.* **1991**, *24*, 145-152.
- [40] J. R. Requena, D. Groth, G. Legname, E. R. Stadtman, S. B. Prusiner, R. L. Levine. Copper-catalyzed oxidation of the recombinant SHa(29-231) prion protein. *Proc. Nat. Acad. Sci. USA* **2001**, *98*, 7170-7175.
- [41] R. Rakhit, P. Cunningham, A. Furtos-Matei, S. Dahan, X. F. Qi, J. P. Crow, N. R. Cashman, L. H. Kondejewski, A. Chakrabarty. Oxidation-induced misfolding and aggregation of superoxide dismutase and its implications for amyotrophic lateral sclerosis. *J. Biol. Chem.* **2002**, *277*, 47551-47556.
- [42] Q. Z. Luo, M. K. Joubert, R. Stevenson, R. R. Ketchem, L. O. Narhi, J. Wypych. Chemical Modifications in Therapeutic Protein Aggregates Generated under Different Stress Conditions. *J. Biol. Chem.* **2011**, *286*, 25134-25144.

- [43] S. W. Taylor, E. Fahy, J. Murray, R. A. Capaldi, S. S. Ghosh. Oxidative post-translational modification of tryptophan residues in cardiac mitochondrial proteins. *J. Biol. Chem.* **2003**, *278*, 19587-19590.
- [44] Y. H. Kim, A. H. Berry, D. S. Spencer, W. E. Stites. Comparing the effect on protein stability of methionine oxidation versus mutagenesis: steps toward engineering oxidative resistance in proteins. *Protein. Eng.* **2001**, *14*, 343-347.
- [45] J. Brange, L. Langkjoer. Insulin structure and stability. *Pharm. Biotechnol.* **1993**, *5*, 315-350.
- [46] N. Guex, M. C. Peitsch. SWISS-MODEL and the Swiss-PdbViewer: an environment for comparative protein modeling. *Electrophoresis* **1997**, *18*, 2714-2723.
- [47] N. Guex, A. Diemand, M. C. Peitsch. Protein modelling for all. *Trends. Biochem. Sci.* **1999**, *24*, 364-367.

Chapter 5

Triethylenetetramine prevents insulin aggregation and fragmentation during copper catalyzed oxidation

Riccardo Torosantucci¹, Daniel Weinbuch¹, Robin Klem¹ and Wim Jiskoot¹

¹Division of Drug Delivery Technology, Leiden Academic Centre for Drug Research (LACDR), Leiden University, Leiden, the Netherlands.

European Journal of Pharmaceutics and Biopharmaceutics **2013**, *84*, 464-471.

Abstract

Metal catalyzed oxidation via the oxidative system Cu^{2+} /ascorbate is known to induce aggregation of therapeutic proteins, resulting in enhanced immunogenicity. Hence, inclusion of anti-oxidants in protein formulations is of great interest. In this study, using recombinant human insulin (insulin) as a model, we investigated the ability of several excipients, in particular triethylenetetramine (TETA), reduced glutathione (GSH) and ethylenediamine tetraacetic acid (EDTA), for their ability to prevent protein oxidation, aggregation and fragmentation. Insulin (1 mg/ml) was oxidized with $40 \mu\text{M}$ Cu^{2+} and 4 mM ascorbate in absence or presence of excipients. Among the excipients studied, 1 mM of TETA, EDTA or GSH prevented insulin aggregation upon metal catalyzed oxidation (MCO) for 3 hours at room temperature, based on size exclusion chromatography (SEC). At lower concentration ($100 \mu\text{M}$), for 72 hours at 4°C , TETA was the only one to inhibit almost completely oxidation-induced insulin aggregation, fragmentation and structural changes, as indicated by SEC, nanoparticle tracking analysis, light obscuration particle counting, intrinsic/extrinsic fluorescence, circular dichroism and chemical derivatization. In contrast, GSH had a slight pro-oxidant effect, as demonstrated by the higher percentage of aggregates and a more severe structural damage, whereas EDTA offered substantially less protection. TETA also protected a monoclonal IgG1 against MCO-induced aggregation, suggesting its general applicability. In conclusion, TETA is a potential candidate excipient for inclusion in formulations of oxidation-sensitive proteins.

Introduction

Protein oxidation in liquid and solid formulations is a major concern in biotherapeutics development, as it can modify protein's structure, function and safety [1-2].

Bivalent copper ion (Cu^{2+}) in particular is an atmospheric pollutant that easily contaminates surfaces and experimental buffers and at sub-micromolar concentration ($\leq 0.8 \mu\text{M}$) initiates the auto-aggregation and oligomerization of Alzheimer's $A\beta$ peptides [3].

Further, metal catalyzed oxidation (MCO) via the oxidative system Cu^{2+} /ascorbate [4] induces aggregation and alterations in protein structure [2, 5-6], and has been shown in preclinical models to increase the immunogenicity of therapeutic proteins [7-10].

Additionally, we recently showed that human insulin, exposed to the same oxidative system, forms irreversible covalent aggregates via Michael addition to 2-amino-3-(3,4-dioxocyclohexa-1,5-dien-1-yl) propanoic acid (DOCH), formed as a consequence of phenylalanine and tyrosine oxidation [11]. Hence, molecules able to inhibit the dramatic effect of copper ions and its catalyzed oxidation of protein are of great importance in protein formulation. Since the year 2000, 48 parenteral drugs containing EDTA in various salt forms have been approved [12]. Although several classes of compounds including polyphenols [13], sugars [14], amino acids [15], thiols [16-17] and chelating agents [18] have been reported to have antioxidant properties, an effective anti-oxidant protecting proteins against copper mediated MCO has not yet been identified.

The aim of this work was to protect insulin from aggregation, fragmentation and oxidative modification upon oxidation induced via Cu^{2+} /ascorbate. With the use of complementary analytical techniques, including size exclusion chromatography (SEC), nanoparticle tracking analysis (NTA), light obscuration particle counting (LOPC), chemical derivatization with benzylamine and 2,4-dinitrophenylhydrazine (DNPH), circular dichroism, and intrinsic and extrinsic fluorescence, we show that $100 \mu\text{M}$ triethylenetetramine (TETA) [19], unlike reduced glutathione (GSH) [16-17] and ethylenediamine tetraacetic acid (EDTA) [20], is capable of inhibiting aggregation and oxidation of recombinant human insulin formulated in 50 mM phosphate buffer, pH 7.4. Moreover, we show that the anti-oxidant properties

of TETA are applicable to a monoclonal IgG1 as well. Based on our results, we believe that this chelating agent, already approved in 1985 by FDA for the treatment of Wilson's disease [21] and extensively investigated for inhibiting the oxidative stress in diabetic patients [22-32], is an excellent candidate for oxidation-sensitive protein formulations.

Materials and Methods

Materials

Recombinant human insulin (further referred to as insulin) containing 0.4% (w/w) zinc ions was provided by Merck, Oss, the Netherlands. A human monoclonal antibody of the IgG1 subclass (further referred to as IgG) was kindly provided by Dr. Vasco Filipe and described in earlier studies [33]. Disodium hydrogen phosphate, sodium sulfate, trisodium citrate, sodium azide, sucrose, DNPH, benzylamine, potassium ferricyanide ($K_3Fe(CN)_6$), TETA, EDTA, GSH, chlorogenic acid, DL-methionine, melatonin, L-histidine, (\pm)- α -tocopherol, L-tyrosine, L-carnosine, L-carnitine hydrochloride, copper (I) chloride, copper (II) chloride, ascorbic acid were purchased in the highest purity available from Sigma-Aldrich, Schnellendorf, Germany. Dialysis cassettes (Slide-A-Lyzer 0.5 to 3 mL, 2 kDa cutoff) and 3,3',5,5'-tetramethylbenzidine (TMB) were obtained from Thermo Fisher Scientific, Breda, The Netherlands. Deionized water was purified through a Purelab Ultra System (ELGA LabWater Global Operations, Marlow, UK) prior to use.

Insulin formulations

Insulin formulations were prepared using a stock solution of 1.14 mg/mL insulin (concentration determined by UV spectroscopy [34], prepared by dissolving 11.4 mg insulin in 0.5 mL 0.1 M HCl, followed by addition of 9.5 mL 50 mM sodium phosphate buffer, pH 7.4 (PB). All the formulations contained a final concentration of 1 mg/mL insulin in PB and, when required, 40 μ M Cu^{2+} and 4 mM ascorbate (positive control, excipient free MCO insulin) and 100 μ M excipients (MCO insulin containing excipients).

The negative control was prepared by adding 120 μ L PB to 880 μ L insulin stock solution. The positive control was obtained by adding to 880 μ L insulin stock solution, 10 μ L PB, followed by 100 μ L $CuCl_2$ solution (10x stock in PB)

and, after 10 minutes, 10 μ L ascorbate solution (100x stock in PB). The same procedure was followed to prepare MCO insulin containing excipients, by adding instead of PB, 10 μ L excipient solution (TETA or GSH or EDTA, 100x stock in PB).

Metal catalyzed oxidation

Insulin samples (1 mg/mL) were oxidized for 24, 48 and 72 hours at 4 °C. Pilot studies conducted with several excipients (Table I) were performed using a final excipient concentration of 1 mM (previously prepared as 10 mM stock solutions in PB). MCO was performed for 3 hours at room temperature, using the same Cu²⁺ and ascorbate concentrations as indicated above. Note that the pH of L-tyrosine stock solution was adjusted to about 10 to increase its solubility, however this did not affect the pH of the final insulin formulation. Vitamin E was prepared by previous dissolution of the oil (4.0 μ L, equivalent to 4.3 mg) in 10 μ L of analytical grade acetone, followed by dissolution in 990 μ L PB, to obtain a stock solution of 10 mM, which was then further diluted 10 fold in the final insulin formulation. All the other excipients tested were soluble at 10 mM concentration in PB.

SEC was performed right after the desired time of incubation, without dialysis of the samples. For all other analyses described in this work (see below), samples were analyzed after 72 hours of MCO at 4 °C and extensive dialysis against PB.

The antioxidant properties of TETA were further studied with IgG, prepared at a concentration of 0.5 mg/mL in 10 mM sodium citrate buffer, 5% (w/v) sucrose, pH 6.0 (CSB). MCO was performed with Cu²⁺ and ascorbate (prepared as 10x and 100x concentrated stock solution in CSB), and used at a final concentration of 40 μ M and 4 mM, respectively. TETA was prepared as 10 mM stock in the same buffer and used at a final concentration of 100 μ M. MCO was conducted for 3 hours at room temperature. SEC was performed immediately after MCO without dialysis of the samples and Bis-ANS extrinsic fluorescence measurements were performed after extensive dialysis against CSB, as described below.

Size Exclusion Chromatography

Insulin and IgG were analyzed by SEC as previously reported [5, 10]. Briefly an Insulin HMWP Column, 7.8 × 300 mm (Waters, Milford, MA, US) and an Agilent 1200 high-performance liquid chromatography system (Agilent Technologies, Palo Alto, California, US) coupled to an ultraviolet (UV) detector set at 276 nm was employed for insulin. The mobile phase was composed of a mixture of 1 g/L L arginine aqueous solution/acetonitrile/glacial acetic acid 65:20:15 (v/v/v). A TSK Gel 4000 SW_{XL} column (300 mm × 7.8 mm) with a TSK Gel 4000 SW_{XL} pre-column (Tosoh Bioscience, Montgomeryville, PA, USA) was used for IgG, employing the same system and UV detector, set at 280 nm. The mobile phase was composed of 100 mM sodium phosphate, 100 mM sodium sulfate, 0.05 % (w/v) sodium azide, pH 7.1. A flow rate of 0.5 ml/min was applied for both analyses.

Nanoparticle tracking analysis

Nanoparticle tracking analysis (NTA) measurements were performed at room temperature with a NanoSight LM20 (NanoSight Ltd., Minton Park, Amesbury, Wiltshire, UK), equipped with a sample chamber with a 640 nm laser. Sample, at a concentration of approximately 0.5 mg/mL, were injected into the chamber automatically using sterile syringes (BD Discardit II, New Jersey) connected to an automatic pump (NanoSight Ltd., Minton Park, Amesbury, Wiltshire, UK). The software used for capturing and analyzing the data was the NTA 2.0 Build 127 (NanoSight Ltd., Minton Park, Amesbury, Wiltshire, UK). Samples were measured for 90 s with manual shutter and gain adjustments. The “single shutter and gain mode” was used to capture the protein aggregates. The mean arithmetic size was calculated by using the NTA software. Each sample was measured in duplicate. Placebo formulations showed a particle concentration that was too low to allow accurate measurements, hence subtraction of the buffer solution counts from the sample counts was not performed.

Light obscuration particle counting

Light obscuration analysis was performed using a PAMAS SVSS-C (PAMAS GmbH, Bad Salzufen, Germany). The pre-run volume was 0.3 mL and for each

sample, three measurements were performed using a volume of 0.2 mL per measurement. Between each measurement, the instrument was washed with Millipore Q water, followed by 30% (v/v) ethanol in water, if necessary, until the background signal was less than 10 particles/mL. Placebo formulation signals were subtracted from the corresponding protein sample signals.

Intrinsic and Bis-ANS extrinsic steady state fluorescence spectroscopy

To measure the intrinsic tyrosine fluorescence, dialyzed insulin samples were diluted in PB to 0.1 mg/mL. Duplicates of 200 μ L of each sample, pipette into wells of a flat black 96 well plate (Greiner Bio-One B.V., Alphen a/d Rijn, NL) were measured with a Tecan infinite M1000 fluorometer (Tecan group Ltd., Männedorf, Switzerland). The excitation wavelength was set at 275 nm and the emission spectrum was recorded between 290-400 nm.

Extrinsic Bis-ANS fluorescence was used to monitor the formation of exposed hydrophobic regions. To 198 μ L (n=2) of 0.1 mg/mL dialyzed insulin or IgG sample, 2 μ L Bis-ANS (stock 100 μ M in water), was added to a final concentration of 1 μ M. Samples were excited at 385 nm using the instrument described above and the emission spectra were recorded from 400 nm to 600 nm. A step size of 2 nm, 50 flashes with a frequency of 400 Hz, a gain of 189 for IgG and 150 for insulin and, a Z-position of 21.5 mm for IgG and 20.0 mm for insulin, were used.

Benzylamine derivatization

Benzylamine derivatization was performed to determine the relative amount of DOPA (3,4-dihydroxyphenylalanine) and DOCH (2-amino-3-(3,4-dioxocyclohexa-1,5-dien-1-yl) propanoic acid) in each insulin sample [35]. The dialyzed samples in 50 mM ammonium bicarbonate (ABI) pH 9.0 were diluted with the same buffer to 0.1 mg/mL. To 500 μ L of these solutions, 1 μ L of pure benzylamine was added to a final concentration of 20 mM. Next, 5 μ L of 50 mM $K_3Fe(CN)_6$ dissolved in ABI pH 9.0, were added to a final concentration of 0.5 mM. The reaction was conducted for 2h at room temperature before performing a fluorescence emission scan with an excitation wavelength of 360 nm and an emission range of 400-550 nm. Controls for non-specific

fluorescence included derivatization reagents (without protein) and non-derivatized protein incubated under the same conditions.

Carbonyl analysis with DNPH

Free carbonyl groups, which can arise from oxidation of lysine, proline and isoleucine, were measured using a sensitive ELISA method described by Buss et al. [36], which requires less protein than the conventional colorimetric carbonyl assay [37], besides being more accurate [38]. Briefly, 45 μL of dialyzed sample in PB were mixed with 45 μL 10 mM DNPH in 2 M HCl to allow DNPH to react (via Schiff base formation) with potential carbonyl groups generated on the insulin molecule during MCO. After 45 min. of incubation at room temperature, 10 μL of this solution were added to 1 mL PB. Next, 200 μL aliquots were added in triplicate into wells of a Greiner Microlon 96 well ELISA plate and incubated overnight. Subsequently the wells were washed 5 times with 300 μL washing buffer (PB with 0.05 % (w/v) Tween 20) and blocked for 2 hours at room temperature with 300 μL blocking buffer (0.1% w/v BSA, 0.1% Tween 20 in PB). Next, plates were washed three times with washing buffer and 200 μL of antibody solution (anti-DNP-antibody 1:1000, 0.1% BSA, 0.1% Tween 20 in PB) were added to the wells for 1 h at 37 °C. After a final washing step, the ELISA was developed by the addition of 100 μL TMB. Plates were incubated until a blue color became clearly visible (~10 min) and the colorimetric reaction was then stopped by the addition of 100 μL 0.18 M sulfuric acid. Absorbance at 450 nm was measured using Tecan's infinite M1000 plate reader controlled by the i-control 1.5 software (Tecan group Ltd., Männedorf, Switzerland). In order to roughly estimate the nmol of carbonyl groups formed per mg of insulin, MCO insulin excipients free and non oxidized insulin, were analyzed via the classical colorimetric assay, as previously described [37].

Circular dichroism spectroscopy

Near- and far-UV circular dichroism (CD) measurements were performed on a J 815 CD spectrometer (Jasco International, Tokyo, Japan) connected to a Jasco PTC 423S temperature controller set to 25 °C. For near-UV CD analysis, 800 μL sample diluted to 0.8 mg/mL in PB was measured in a 1-cm path

length quartz cuvette while for far-UV CD, 300 μ L sample diluted to a concentration of 0.2 mg/mL in PB was measured in a 1-mm path length quartz cuvette. Spectra were recorded from 250-320 nm and 190-250 nm for near- and far-UV CD measurements, respectively, at a scan rate of 100 nm/min, a bandwidth of 1 nm and a response time of 2 s. CD spectra of six sequential measurements were averaged and corrected for the blank (PB). The CD signals were converted to molar ellipticity per amino acid residue ($[\theta]$). Alpha helix content was estimated based on $[\theta]$ at 223 nm ($[\theta]_{223}$), according to Pocker et al [39].

Results

Aggregate and particle content: SEC, NTA, LOPC

At the beginning of this work, extensive pilot studies were conducted to test the potential antioxidant activity of several excipients at 1 mM concentration: L-carnitine, L-carnosine, chlorogenic acid, ethylenediaminetetraacetic acid (EDTA), melatonin, DL-methionine, reduced L-glutathione (GSH), triethylenetetramine (TETA), histidine, (\pm)- α -tocopherol (vitamin E) and L-tyrosine. After confirming via SEC that none of the excipient employed affected insulin's aggregation state after 3 hours of incubation at room temperature (data not shown), oxidative studies were performed as previously reported [5]. Results (Table I) indicate that insulin oxidized in presence of 1 mM of one of the excipients reported above, shows similar or even higher amounts of aggregates compared with insulin oxidized in absence of excipients, except for TETA, GSH and EDTA, where no differences with the negative control were detected (Table I). Based on the results of the initial screening, TETA, GSH and EDTA were selected to be studied in more detail for their putative protective action against MCO of insulin.

Table I. Aggregate content in MCO insulin samples from a screening study.

MCO ^a	Excipient (1 mM)	Aggregate content (%) ^b
No	None (negative control)	0.5 ± 0.2
Yes	None (positive control)	21.5 ± 4.2
Yes	L-carnitine	24.2 ± 5.4
Yes	L-carnosine	22.7 ± 0.2
Yes	Chlorogenic acid	39.3 ± 1.2
Yes	Melatonin	24.1 ± 6.9
Yes	DL-methionine	41.6 ± 7.1
Yes	L-histidine	29.2 ± 6.1
Yes	(±)- α -Tocopherol (vitamin E)	32.9 ± 4.0
Yes	L-tyrosine	25.8 ± 1.3
Yes	TETA	0.7 ± 0.2
Yes	GSH	0.8 ± 0.2
Yes	EDTA	0.6 ± 0.1

^a MCO was performed by incubation with 40 μ M Cu²⁺ and 4 mM ascorbate for 3 hours at room temperature.

^b Calculated from SEC data as previously reported [8].

The experimental procedure to test TETA, GSH and EDTA, was established based on the typical storage temperature of liquid protein formulations and on using a minimal required amount of excipients based on previous work on the anti-oxidant activity of EDTA [20]. Additionally, at 1 mM concentration, GSH still presents some reducing activity with respect to insulin disulfide bridges, while EDTA and, to a lower extent TETA, appear to sequester zinc ions, as indicated by near-UV CD which showed a decrease in $[\theta]$ at 273 nm ($[\theta]_{273}$; data not shown). MCO studies were therefore conducted with 100 μ M excipient, at 4 °C for 72 hours.

SEC was used to demonstrate that none of the excipients used affected insulin's aggregation state during the applied incubation time (data not shown). Following MCO, the chromatographic behavior of each sample was investigated (Figure 1A). Native insulin shows a single peak with a retention time of 17.3 minutes, representing monomeric insulin. Note that the mobile phase employed contains acetonitrile and acetic acid, which dissociate native non-covalent oligomeric insulin species (i.e. dimer, tetramer, hexamer) normally present in PB at pH 7.4 in presence of zinc ions ^[44], while it does not dissociate the covalent aggregates obtained by MCO ^[11]. The elution behavior of MCO insulin, formulated without excipients, presents several peaks eluted earlier than 17.3 minutes as well as a broad main peak eluting at a slightly longer retention time. This indicates that MCO induced extensive aggregation and fragmentation. The amount of insulin aggregates was calculated as previously reported ^[5], using the area under the curve (AUC) obtained by SEC (i.e. $AUC_{\text{aggregate peak}}/AUC_{\text{total native}} \times 100\%$) (Figure 1A).

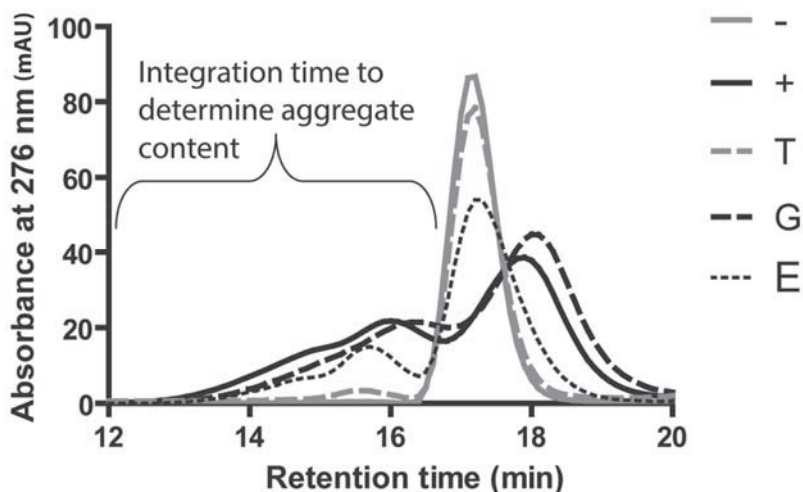


Figure 1A. SEC profiles of insulin samples incubated for 72 h. Brackets delineate the time region for AUC integration used for calculation of the aggregate content. Negative control (-) was insulin incubated in PB, other samples were incubated with 40 μM Cu^{2+} and 4 mM ascorbate in absence (+, positive control) or presence of (TETA (T), GSH (G), EDTA (E)) 100 μM excipients as indicated in the graph.

The chromatogram of MCO insulin formulated with 100 μM TETA almost completely overlapped with that of native insulin, suggesting TETA's protective effect towards aggregation and fragmentation. GSH (100 μM) formulated MCO insulin showed a similar behavior as excipient free MCO insulin, indicating absence of any beneficial activity of GSH at this concentration. Finally, in EDTA (100 μM) formulated MCO insulin high amounts of aggregates were measured, but fragmentation seemed to be partially inhibited, as indicated by the absence of species eluting after the monomeric peak. Figure 1B illustrates the strong time-dependent increase in aggregate content of MCO insulin formulated without excipients or with GSH or EDTA. In contrast, after 24 and 48 hours the aggregate content of MCO insulin formulated with TETA was almost as low as that in unmodified insulin (negative control), and only after 72 hours the amount of aggregates calculated had increased to a few percent. In conclusion, 100 μM TETA is highly effective in preventing MCO induced insulin aggregation and fragmentation while the other two candidates had hardly any protective effect under our experimental conditions.

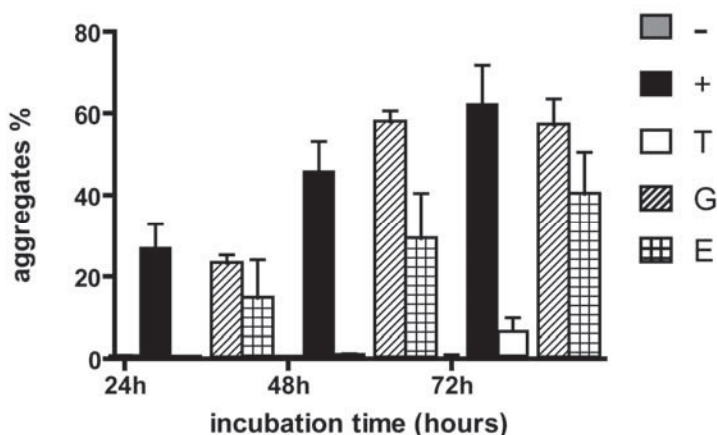


Figure 1B. Percentages of aggregated insulin calculated from SEC profiles after 24 h, 48 h and 72 h of incubation time at 4 °C. Negative control (-) was insulin incubated in PB, other samples were incubated with 40 μM Cu^{2+} and 4 mM ascorbate in absence (+, positive control) or presence of (TETA (T), GSH (G), EDTA (E)) 100 μM excipients as indicated in the graph. Error bars represent the deviation from the average of two batches.

Interestingly, the same concentration of TETA appeared to be a valuable antioxidant also in presence of monovalent copper ions ($40 \mu\text{M Cu}^+$) as indicated by the absence of aggregates (based on SEC, data not shown) during MCO performed for 3 hours at room temperature using the oxidative system Cu^+ /ascorbate.

NTA was used to monitor the formation of submicron-sized particles during MCO and the results are presented in Figure 2 and Table II. For native insulin relatively low particle counts were obtained. For the positive control, an approximately seven fold higher particle concentration was measured. MCO insulin formulated with TETA showed low particle counts comparable to those in the negative control, demonstrating a protective effect of TETA, whereas samples containing GSH or EDTA contained substantially higher particle concentrations.

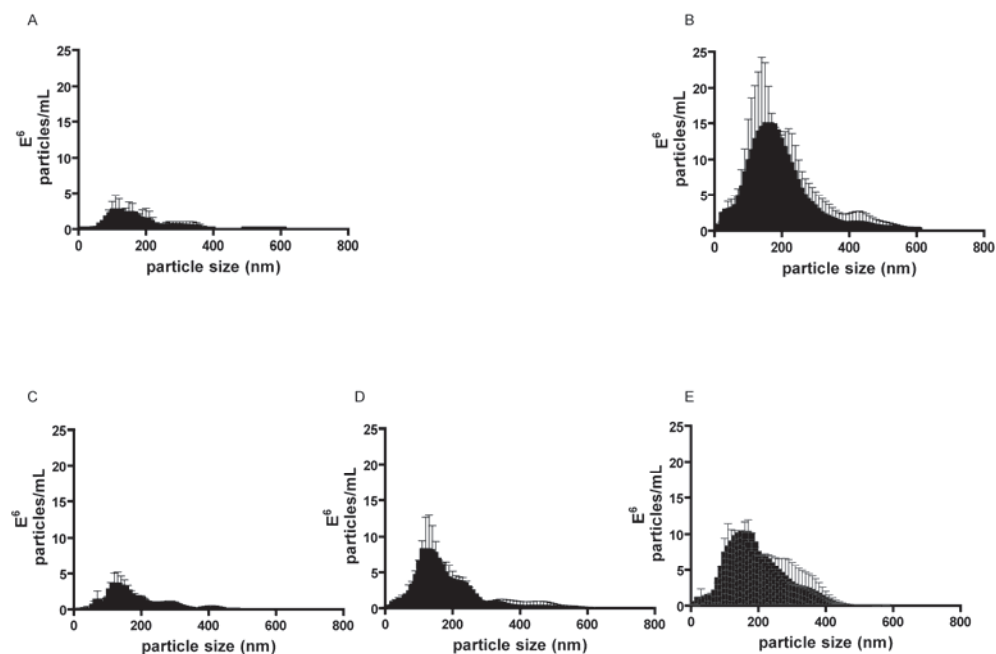


Figure 2. NTA analysis of insulin samples incubated for 72 h: Negative control (insulin incubated in PB) (A), other samples were incubated with $40 \mu\text{M Cu}^{2+}$ and 4 mM ascorbate in absence of excipient (B) (positive control) or in presence of $100 \mu\text{M TETA}$ (C), GSH (D), or EDTA (E). Error bars represent the deviation from the average of two batches.

LOPC was employed to estimate micron-sized aggregates. Non oxidized insulin contained a low background of $0.79 \pm 0.27 \cdot 10^3$ particles/mL. In the positive control, the particle concentration in the range 1-10 μm was about ten fold higher than in the negative control (see Table II). MCO of insulin formulated with GSH presented a two fold increase in particle concentration when compared with native insulin, while the TETA- and EDTA-containing formulations showed an approximately three fold increase in particle concentration (in the range 1-10 μm), suggesting a similar inhibiting effect of the excipients on micron-sized particle formation. Micron particles in the larger size range (>10 μm) were barely detected in most of the samples, although the level for the EDTA-containing sample was slightly elevated (Table II).

Table II. Particles concentration and spectroscopic features of insulin samples formulated with and without excipients.

Sample ^a	NTA ^b		LOPC particles concentration (10 ³ /mL) ^c			CD % alpha helix ^d	Benzoxazole fluorescence Intensity (a.u.) ^e
	Mean size (nm)	Particles concentration (10 ⁸ /mL)	1-10 μm	10-25 μm	>25 μm		
-	193.7 ± 3.8	0.38 ± 0.01	0.79 ± 0.27	0.06 ± 0.05	0.02 ± 0.02	44.9 ± 1.9	5.2 ± 0.3
+	216.9 ± 27.7	2.60 ± 0.05	7.65 ± 3.31	0.08 ± 0.05	0.02 ± 0.01	34.3 ± 2.9	16.5 ± 0.7
T	182.1 ± 12.2	0.69 ± 0.10	2.44 ± 0.40	0.05 ± 0.01	0.02 ± 0.007	39.6 ± 0.9	6.3 ± 0.4
G	193.2 ± 20.4	1.14 ± 0.04	1.71 ± 0.21	0.02 ± 0.02	0.01 ± 0.005	26.9 ± 0.5	15.8 ± 2.5
E	200.1 ± 22.4	1.80 ± 0.25	2.85 ± 0.92	0.2 ± 0.1	0.1 ± 0.09	38.5 ± 0.7	15.0 ± 1.7

^a Negative control (-), positive control (excipient free MCO insulin,+), MCO insulin formulated with 100 μM TETA (T), GSH (G), and EDTA (E).

^b Placebo formulations showed negligible particle counts in NTA.

^c For LOPC analysis, particle counts of placebo formulations were subtracted from the corresponding protein sample. Typically, the particle concentration of placebo formulations was between 0.19-0.40*10³ particles/mL, between 0.01*-0.05*10³ particles/mL and negligible in the size ranges 1-10 μm, 10-25 μm and >25 μm, respectively.

^d Calculated according to Pocker et al [39].

^e Calculated based on the fluorescence at the emission maximum (460 nm).

Chemical modifications: DOPA, DOCH and carbonyl content

As previously reported by Sharov et al. [40-41], benzylamine and its derivatives can selectively form a benzoxazole with characteristic fluorescence, after reaction with phenylalanine and tyrosine oxidation products like DOPA (3,4-dihydroxyphenylalanine) and DOCH (2-amino-3-(3,4-dioxocyclohexa-1,5-dien-1-yl) propanoic acid), providing a useful qualitative tool to identify the presence of specific oxidative chemical modifications. Results (Table II) clearly indicate that oxidized phenylalanine and tyrosine are barely detectable in non oxidized insulin, while in the positive control (excipient free MCO insulin), a three fold higher fluorescence was measured, indicating chemical modification of these aromatic amino acid residues. TETA formulated MCO insulin appeared not to contain these oxidized species, as revealed by its benzoxazole fluorescence spectrum, the intensity of which was comparable to that of plain (non oxidized) insulin treated with benzylamine. By contrast, oxidized insulin formulated with GSH and EDTA showed increased benzoxazole fluorescence intensity comparable to that of the positive control, pointing to the generation of DOPA and DOCH during MCO (Table II).

Other widely used markers of oxidative stress are carbonyl groups, which can be formed during reaction of lysine, proline and isoleucine with reactive oxygen species [42-43]. Figure 3A shows results of the carbonyl content measured for all samples via a sensitive ELISA method. Native insulin gave an OD 450 nm signal comparable to that of the blank (reagent incubated in buffer). The positive control, presented a much higher absorbance, caused by the hydrazone formed between DNPH and new carbonyl groups on the insulin molecule. According to a direct spectroscopic measurement of DNPH-modified MCO insulin, the carbonyl content in the positive control was estimated to be 24.8 ± 7.9 nmol/mg of insulin, which is in the same order of magnitude as the value reported by Montes-Cortes et al. for insulin exposed to plasma from diabetic patient containing reactive oxygen species (ROS), for 4 hours at 37 °C [42]. The relatively small increase in the carbonyl content observed for TETA-containing insulin formulation exposed to MCO, relative to that of the positive control, suggests that TETA almost totally inhibits MCO induced insulin oxidation. In contrast, GSH and EDTA did not have any protecting effect (Figure 3A).

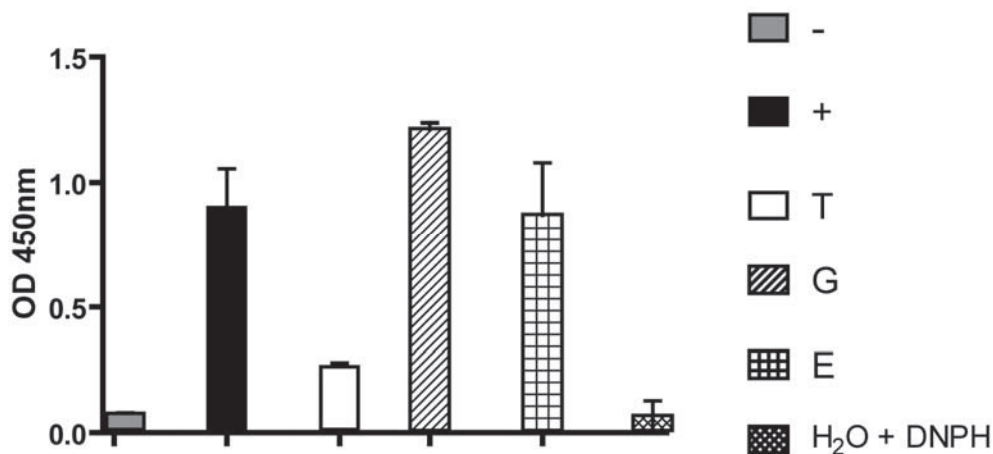


Figure 3A. Carbonyl content of insulin samples incubated for 72 h at 4 °C. Negative control (-) was insulin incubated in PB, other samples were incubated with 40 μM Cu^{2+} and 4 mM ascorbate in absence (+, positive control) or presence of 100 μM TETA (T), GSH (G), or EDTA (E), as indicated in the graph. Error bars represent the deviation from the average of two batches.

Secondary and tertiary structure: far-UV CD, intrinsic and extrinsic steady state fluorescence

Spectroscopic techniques can provide useful information about the higher order structural features of a protein. To investigate whether the excipients used would disturb insulin's quaternary structure, near-UV CD measurements were performed after incubating the formulations for 72 hours at 4 °C (without MCO). The negative magnitude of the near-UV CD signal at 273 nm ($[\theta]_{273}$) is directly proportional to the native noncovalent association state of insulin (i.e. monomer < dimer < hexamer) [44]. Our results suggest that with 100 μM of excipient, insulin remained in its tetrameric-hexameric state when formulated with TETA or GSH in PB ($[\theta]_{273}$ 289.4 \pm 0.2 and 312.5 \pm 1.5 deg cm² dmol⁻¹, respectively). However, in the EDTA-containing formulation insulin's quaternary structure was partially dissociated towards a dimeric-tetrameric equilibrium, as indicated by a reduced $[\theta]_{273}$ (227.1 \pm 3 deg cm² dmol⁻¹). This was expected because EDTA in this concentration is known to deplete zinc from insulin, resulting in a drop of the negative CD signal [44]. Therefore, near-UV CD was not further performed in the following studies on the antioxidant activity of each excipient.

For insulin, far-UV CD has been widely used to estimate the alpha helix content [39, 45-46]. Table II shows that the content in alpha helix in the negative control is about 45%, which is in line with the literature [39]. MCO of excipient free insulin induced approximately 10% loss in alpha helix content as expected based on our previous studies [39]. TETA insulin showed a minimal loss of 5%, when compared to negative control, while insulin's secondary structure in MCO insulin formulated with GSH, appeared to be seriously perturbed, leading to approximately 20% loss in alpha helix. This is likely due a pro-oxidant activity of the excipient, which in fact can reduce Cu^{2+} into Cu^+ , which eventually generates hydroxyl radical species in aerobic environment [4]. EDTA formulated MCO insulin showed a slight decrease in alpha helix content roughly comparable to that of TETA formulated MCO insulin.

Fluorescence spectroscopy performed with an excitation wavelength of 275 nm gives information about the environment of the four tyrosine residues in insulin at positions A14, A19, B16 and B26. Non oxidized insulin showed an emission maximum at 299 ± 1 nm (Figure 3B). MCO insulin showed a substantial decrease in the fluorescence intensity but no shift in the emission maximum, suggesting a change in tertiary structure and/or chemical modification of tyrosine residues. The fluorescence emission spectrum of MCO insulin containing TETA almost completely overlapped with that of non oxidized insulin, confirming the protective effect of TETA against MCO. GSH formulated MCO insulin showed a spectrum comparable to that of excipient free MCO insulin, while MCO of insulin in presence of EDTA appeared to result in partial loss of its structural features.

Extrinsic Bis-ANS fluorescence was used as a sensitive probe for the formation of new hydrophobic surfaces in insulin exposed to MCO. A moderate increase in Bis-ANS fluorescence of the MCO (excipient free) sample was observed, as previously reported [5], while all other formulations tested showed Bis-ANS fluorescence spectra comparable to that of the negative control (data not shown). This indicates that all the excipients used inhibit MCO-induced formation of new hydrophobic surfaces.

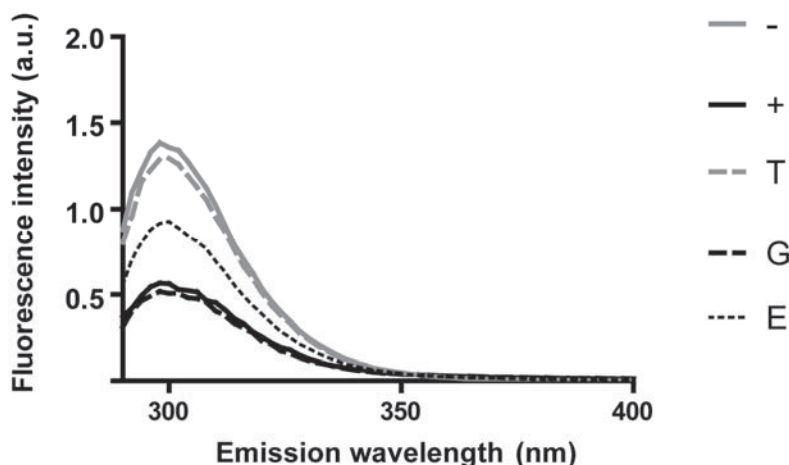


Figure 3B. Intrinsic steady-state fluorescence of insulin samples incubated for 72 h at 4 °C. Negative control (-) was insulin incubated in PB, other samples were incubated with 40 μM Cu^{2+} and 4 mM ascorbate in absence (+, positive control) or presence of 100 μM TETA (T), GSH (G), or EDTA (E), as indicated in the graph. Intrinsic steady-state fluorescence data were obtained averaging the spectra of two batches.

Inhibition by TETA of aggregation and fragmentation of a monoclonal antibody during MCO

To confirm the protective properties of TETA using another therapeutic protein, MCO was applied to IgG and the products were analyzed by SEC and extrinsic Bis-ANS fluorescence, which were previously shown to be suitable techniques to pick up oligomers, fragments and structural modification of this IgG exposed to MCO [10]. Figure 4A shows the SEC profiles of untreated IgG and MCO IgG in presence and absence of 100 μM TETA and Figure 4B the monomer, aggregate and fragment contents derived from the SEC analysis.

The results clearly illustrate the protection by TETA against aggregation and fragmentation of MCO IgG.

Moreover, the fluorescence of Bis-ANS, a dye sensitive to hydrophobic regions in proteins, indicated that TETA prevents the generation of aggregates containing new hydrophobic regions during MCO of IgG (Figure 5).

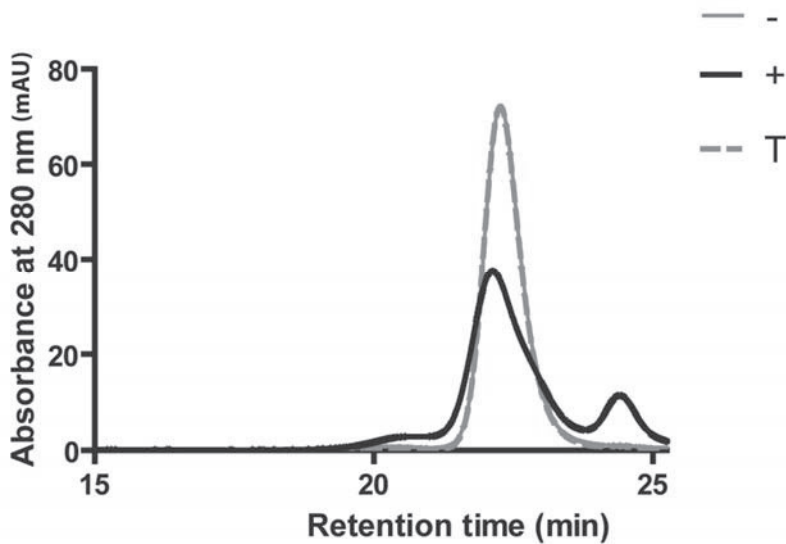


Figure 4A. SEC profiles of IgG samples. Negative control (-) was IgG incubated in CSB, other samples were incubated with $40 \mu\text{M Cu}^{2+}$ and 4 mM ascorbate in absence (+, positive control) or presence of $100 \mu\text{M TETA}$ (T), as indicated in the graph.

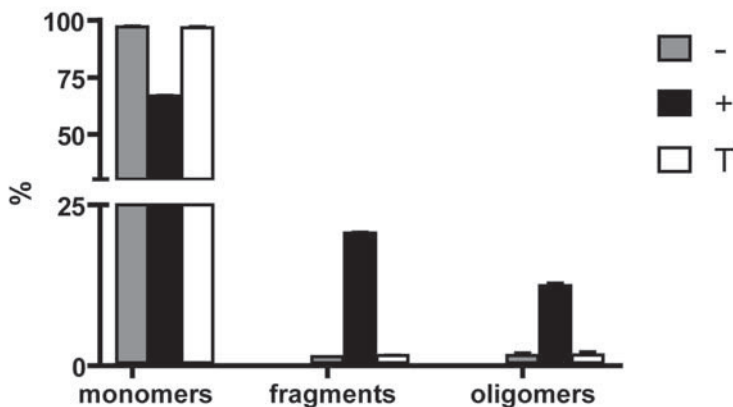


Figure 4B. Percentages of aggregated and fragmented IgG calculated from SEC profiles after 3 h of incubation time at room temperature. Negative control (-) was IgG incubated in CSB, other samples were incubated with $40 \mu\text{M Cu}^{2+}$ and 4 mM ascorbate in absence (+, positive control) or presence of $100 \mu\text{M TETA}$ (T), as indicated in the graph. Error bars represent the deviation from the average of two batches.

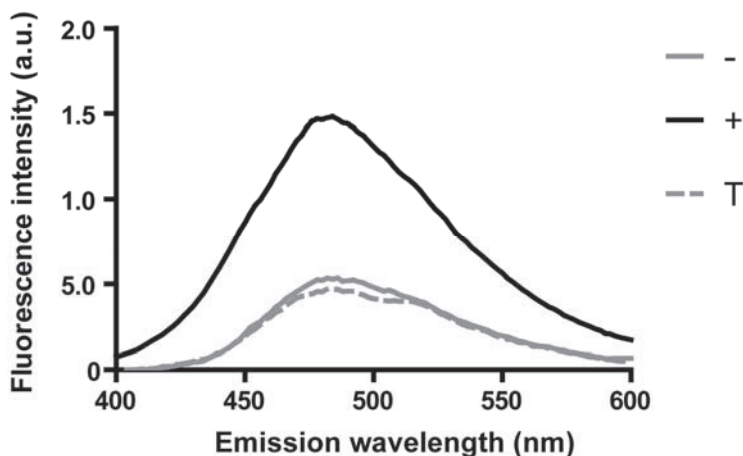


Figure 5. Extrinsic Bis-ANS fluorescence of IgG samples after 3 h incubation at room temperature. Negative control (-) was IgG incubated in CSB, other samples were incubated with 40 μM Cu^{2+} and 4 mM ascorbate in absence (+, positive control) or presence of 100 μM TETA (T), as indicated in the graph. Spectra represent the average obtained from two batches.

Discussion

MCO represents a common degradation pathway of protein and peptide [47] therapeutics and justifies the search for formulation strategies for its inhibition. Classic inhibitors of MCO are chelating agents such as EDTA. Depending on the stability constant of the coordination complex that each chelating agent can form with different metals, the choice of the chelator can depend on the metal involved in the catalyzed oxidation. Excess of EDTA, relative to Cu^{2+} , is often used to quench MCO involving Cu^{2+} but several studies involving Fe^{2+} have suggested its pro-oxidant activity [20, 48], thus favoring protein degradation.

In this work it is shown that the chelating agent TETA protects insulin and IgG from aggregation and fragmentation during MCO via Cu^{2+} /ascorbate. TETA is an FDA approved drug [21] and it has been recently widely investigated in the treatment of diabetes mellitus for its selective copper ion-chelating properties [23], therefore it was selected as antioxidant in the present studies. GSH was included in our study for its radical scavenging activity [49] and because it was reported to inhibit copper catalyzed oxidation in presence of a reducing agent such as ascorbic acid [16], besides being an excellent antioxidant in the human body [17]. EDTA is broadly used as chelating agent in pharmaceutical

formulations [20] and has been previously used to quench metal catalyzed oxidation involving copper ions [2, 4, 7, 8].

In this work we showed that TETA, among the excipients employed (100 μM , in a molar excipient: Cu^{2+} ratio of 2.5:1) almost totally prevented insulin aggregation and fragmentation, as monitored by SEC, NTA and LOPC analysis. TETA still prevented insulin aggregation at 50 μM , but to a lesser extent than at 100 μM (data not shown).

Other structural features of insulin were shown to be largely preserved in presence of 100 μM TETA, as demonstrated by far-UV CD and fluorescence studies. Chemical modifications responsible for insulin aggregation (during MCO under our applied conditions), namely DOPA and DOCH [11], appeared to be inhibited by TETA, based on a chemical derivatization assay with benzylamine. These observations, together with TETA's observed protective effect against MCO-induced aggregation of a monoclonal antibody, suggest that it is a promising candidate to be considered for oxidation-sensitive protein formulations. However, follow-up studies are needed to elucidate whether TETA also inhibits oxidation of amino acid residues like methionine and tryptophan (which are not present in insulin), the oxidation of which can have undesirable pharmacological consequences [50].

The beneficial properties of TETA are probably due the high affinity constant for the complex TETA: Cu^{2+} ($\log K \approx 15.0$ at pH 7.0) and the square-planar geometry in which Cu^{2+} is most stable [19]. GSH instead does not inhibit MCO, probably because at the concentration used, the amount of reduced glutathione (GSH) responsible for the antioxidant activity [16] is not enough to sequester copper ions, as part of GSH reduces Cu^{2+} into Cu^+ , yielding GSSG which is unable to prevent MCO [16].

Increasing the concentration of GSH might better chelate copper ions, however due to its reducing properties, GSH is deleterious for the integrity of disulfide bridges, as indicated by the reduction of insulin's disulfide bridge at 5 and 1 mM within 3 hours at room temperature (data not shown).

Interestingly, EDTA can form a stable complex with Cu^{2+} , with a slightly higher stability constant than TETA ($\log K = 15.9$ at pH 7.4) [51], but the geometry of this stable complex can be lost after interactions with buffer salts [52-53], rendering the metal ion available for catalyzing protein oxidation. Higher concentrations of EDTA might however present beneficial effects for

proteins where metal coordination is not crucial for maintaining native structural features.

Conclusion

We described that micromolar concentrations of TETA, in comparison with other potential anti-oxidants, effectively inhibits copper catalyzed protein oxidation, aggregation and fragmentation. Since metal ions are ubiquitous and often contaminate therapeutic protein formulations inducing oxidative chemical modifications, which eventually can produce inactive and immunogenic products, TETA should be taken into serious consideration as a protein formulation excipient. Follow-up studies are warranted to fine-tune the optimal protective concentration of TETA, according the protein under investigation.

Acknowledgements

The authors thank Schering-Plough for financial support and providing insulin for this project.

References

- [1] S. Li, C. Schöneich, R. T. Borchardt. Chemical instability of protein pharmaceuticals: Mechanisms of oxidation and strategies for stabilization. *Biotechnol. Bioeng.* **1995**, *48*, 490-500.
- [2] Q. Z. Luo, M. K. Joubert, R. Stevenson, R. R. Ketchem, L. O. Narhi, J. Wypych. Chemical Modifications in Therapeutic Protein Aggregates Generated under Different Stress Conditions. *J. Biol. Chem.* **2011**, *286*, 25134-25144.
- [3] X. Huang, C. S. Atwood, R. D. Moir, M. A. Hartshorn, R. E. Tanzi, A. I. Bush. Trace metal contamination initiates the apparent auto-aggregation, amyloidosis, and oligomerization of Alzheimer's A β peptides. *J. Biol. Inorg. Chem.* **2004**, *9*, 954-960.
- [4] S. Li, T. H. Nguyen, C. Schöneich, R. T. Borchardt. Aggregation and precipitation of human relaxin induced by metal-catalyzed oxidation. *Biochemistry* **1995**, *34*, 5762-5772.
- [5] R. Torosantucci, B. Kükrer, A. Mero, M. Van Winsen, R. Tantipolphan, W. Jiskoot. Plain and mono-pegylated recombinant human insulin exhibit similar stress-induced aggregation profiles. *J. Pharm. Sci.* **2011**, *100*, 2574-2585.
- [6] C. Schöneich. Mechanisms of metal-catalyzed oxidation of histidine to 2-oxo-histidine in peptides and proteins. *J. Pharm. Biomed. Anal.* **2000**, *21*, 1093-1097.
- [7] M. M. van Beers, M. Sauerborn, F. Gilli, V. Brinks, H. Schellekens, W. Jiskoot. Oxidized and aggregated recombinant human interferon beta is immunogenic in human interferon beta transgenic mice. *Pharm. Res.* **2011**, *28*, 2393-2402.
- [8] S. Hermeling, L. Aranha, J. M. A. Damen, M. Slijper, H. Schellekens, D. J. A. Crommelin, W. Jiskoot. Structural characterization and immunogenicity in wild-type and immune tolerant mice of degraded recombinant human interferon alpha2b. *Pharm. Res.* **2005**, *22*, 1997-2006.
- [9] S. Hermeling, H. Schellekens, C. Maas, M. F. Gebbink, D. J. Crommelin, W. Jiskoot. Antibody response to aggregated human interferon alpha2b in wild-type and transgenic immune tolerant mice depends on type and level of aggregation. *J. Pharm. Sci.* **2006**, *95*, 1084-1096.
- [10] V. Filipe, W. Jiskoot, A. H. Basmeleh, A. Halim, H. Schellekens. Immunogenicity of different stressed IgG monoclonal antibody formulations in immune tolerant transgenic mice. *MAbs* **2012**, *4*, 740-752.
- [11] R. Torosantucci, O. Mozziconacci, V. Sharov, C. Schöneich, W. Jiskoot. Chemical Modifications in Aggregates of Recombinant Human Insulin Induced by Metal-Catalyzed Oxidation: Covalent Cross-Linking via Michael Addition to Tyrosine Oxidation Products. *Pharm. Res.* **2012**, *29*, 2276-2293.
- [12] S. J. Encyclopedia of Pharmaceutical Technology. *3rd ed.* New York: Informa HealthCare. **2007**.

- [13] R. Amorati, L. Valgimigli. Modulation of the antioxidant activity of phenols by non-covalent interactions. *Org. Biomol. Chem.* **2012**, *10*, 4147-4158.
- [14] H. Faraji, R. C. Lindsay. Characterization of the antioxidant activity of sugars and polyhydric alcohols in fish oil emulsions. *J. Agric. Food. Chem.* **2004**, *52*, 7164-7171.
- [15] R. J. Elias, D. J. McClements, E. A. Decker. Antioxidant activity of cysteine, tryptophan, and methionine residues in continuous phase beta-lactoglobulin in oil-in-water emulsions. *J. Agric. Food. Chem.* **2005**, *53*, 10248-10253.
- [16] Y. Ohta, N. Shiraishi, T. Nishikawa, M. Nishikimi. Copper-catalyzed autoxidations of GSH and L-ascorbic acid: mutual inhibition of the respective oxidations by their coexistence. *Biochim. Biophys. Acta.* **2000**, *1474*, 378-382.
- [17] C. Kerksick, D. Willoughby. The antioxidant role of glutathione and N-acetyl-cysteine supplements and exercise-induced oxidative stress. *J. Int. Soc. Sports Nutr.* **2005**, *2*, 38-44.
- [18] J. D. Breccia, M. M. Andersson, R. Hatti-Kaul. The role of poly(ethyleneimine) in stabilization against metal-catalyzed oxidation of proteins: a case study with lactate dehydrogenase. *Biochim. Biophys. Acta.* **2002**, *1570*, 165-173.
- [19] J. Lu. Triethylenetetramine pharmacology and its clinical applications. *Mol. Cancer. Ther.* **2010**, *9*, 2458-2467.
- [20] S. Zhou, B. Zhang, E. Sturm, D. L. Teagarden, C. Schöneich, P. Kolhe, L. M. Lewis, B. K. Muralidhara, S. K. Singh. Comparative evaluation of disodium edetate and diethylenetriaminepentaacetic acid as iron chelators to prevent metal-catalyzed destabilization of a therapeutic monoclonal antibody. *J. Pharm. Sci.* **2010**, *99*, 4239-4250.
- [21] G. J. Cooper. Therapeutic potential of copper chelation with triethylenetetramine in managing diabetes mellitus and Alzheimer's disease. *Drugs* **2011**, *71*, 1281-1320.
- [22] H. Y. Cho, R. A. Blum, T. Sunderland, G. J. S. Cooper, W. J. Jusko. Pharmacokinetic and Pharmacodynamic Modeling of a Copper-Selective Chelator (TETA) in Healthy Adults. *J. Clin. Pharmacol.* **2009**, *49*, 916-928.
- [23] G. J. Cooper. Selective divalent copper chelation for the treatment of diabetes mellitus. *Curr. Med. Chem.* **2012**, *19*, 2828-2860.
- [24] D. Gong, X. Chen, M. Middleditch, L. Huang, G. Vazhoor Amarsingh, S. Reddy, J. Lu, S. Zhang, K. Ruggiero, A. R. Phillips, G. J. Cooper. Quantitative proteomic profiling identifies new renal targets of copper(II)-selective chelation in the reversal of diabetic nephropathy in rats. *Proteomics* **2009**, *9*, 4309-4320.
- [25] D. Gong, J. Lu, X. Chen, S. Y. Choong, S. Zhang, Y. K. Chan, S. Glyn-Jones, G. D. Gamble, A. R. Phillips, G. J. Cooper. Molecular changes evoked by triethylenetetramine treatment in the extracellular matrix of the heart and aorta in diabetic rats. *Mol. Pharmacol.* **2006**, *70*, 2045-2051.
- [26] D. Gong, J. Lu, X. Chen, S. Reddy, D. J. Crossman, S. Glyn-Jones, Y. S. Choong, J. Kennedy, B. Barry, S. Zhang, Y. K. Chan, K. Ruggiero, A. R. Phillips, G. J. Cooper. A copper(II)-

- selective chelator ameliorates diabetes-evoked renal fibrosis and albuminuria, and suppresses pathogenic TGF-beta activation in the kidneys of rats used as a model of diabetes. *Diabetologia* **2008**, *51*, 1741-1751.
- [27] M. Jullig, X. Chen, A. J. Hickey, D. J. Crossman, A. Xu, Y. Wang, D. R. Greenwood, Y. S. Choong, S. J. Schonberger, M. J. Middleditch, A. R. Phillips, G. J. Cooper. Reversal of diabetes-evoked changes in mitochondrial protein expression of cardiac left ventricle by treatment with a copper(II)-selective chelator. *Proteomics Clin. Appl.* **2007**, *1*, 387-399.
- [28] J. Lu, Y. K. Chan, G. D. Gamble, S. D. Poppitt, A. A. Othman, G. J. Cooper. Triethylenetetramine and metabolites: levels in relation to copper and zinc excretion in urine of healthy volunteers and type 2 diabetic patients. *Drug Metab. Dispos.* **2007**, *35*, 221-227.
- [29] J. Lu, Y. K. Chan, S. D. Poppitt, G. J. Cooper. Determination of triethylenetetramine (TETA) and its metabolites in human plasma and urine by liquid chromatography-mass spectrometry (LC-MS). *J. Chromatogr. B. Analyt. Technol. Biomed. Life Sci.* **2007**, *859*, 62-68.
- [30] J. Lu, D. Gong, S. Y. Choong, H. Xu, Y. K. Chan, X. Chen, S. Fitzpatrick, S. Glyn-Jones, S. Zhang, T. Nakamura, K. Ruggiero, V. Obolonkin, S. D. Poppitt, A. R. Phillips, G. J. Cooper. Copper(II)-selective chelation improves function and antioxidant defences in cardiovascular tissues of rats as a model of diabetes: comparisons between triethylenetetramine and three less copper-selective transition-metal-targeted treatments. *Diabetologia* **2010**, *53*, 1217-1226.
- [31] J. Lu, S. D. Poppitt, A. A. Othman, T. Sunderland, K. Ruggiero, M. S. Willett, L. E. Diamond, W. D. Garcia, B. G. Roesch, G. J. Cooper. Pharmacokinetics, pharmacodynamics, and metabolism of triethylenetetramine in healthy human participants: an open-label trial. *J. Clin. Pharmacol.* **2010**, *50*, 647-658.
- [32] M. Ugarte, M. Brown, K. A. Hollywood, G. J. Cooper, P. N. Bishop, W. B. Dunn. Metabolomic analysis of rat serum in streptozotocin-induced diabetes and after treatment with oral triethylenetetramine (TETA). *Genome Med.* **2012**, *4*, 35.
- [33] V. Filipe, B. Kükreer, A. Hawe, W. Jiskoot. Transient molten globules and metastable aggregates induced by brief exposure of a monoclonal IgG to low pH. *J. Pharm. Sci.* **2012**, *101*, 2327-2339.
- [34] J. Brange, L. Langkjaer, S. Havelund, A. Volund. Chemical stability of insulin. 1. Hydrolytic degradation during storage of pharmaceutical preparations. *Pharm. Res.* **1992**, *9*, 715-726.
- [35] J. P. Pennington, C. Schöneich, J. F. Stobaugh. Selective fluorogenic derivatization with isotopic coding of catechols and 2-amino phenols with benzylamine: A chemical basis for the relative determination of 3-hydroxy-tyrosine and 3-nitro-tyrosine peptides. *Chromatographia* **2007**, *66*, 649-659.

- [36] H. Buss, T. P. Chan, K. B. Sluis, N. M. Domigan, C. C. Winterbourn. Protein carbonyl measurement by a sensitive ELISA method. *Free Radic. Biol. Med.* **1997**, *23*, 361-366.
- [37] R. L. Levine, D. Garland, C. N. Oliver, A. Amici, I. Climent, A. G. Lenz, B. W. Ahn, S. Shaltiel, E. R. Stadtman. Determination of Carbonyl Content in Oxidatively Modified Proteins. *Methods in Enzymol.* **1990**, *186*, 464-478.
- [38] A. Z. Reznick, L. Packer. Oxidative Damage to Proteins - Spectrophotometric Method for Carbonyl Assay. *Methods in Enzymol* **1994**, *233*, 357-363.
- [39] Y. Pocker, S. B. Biswas. Conformational dynamics of insulin in solution. Circular dichroic studies. *Biochemistry* **1980**, *19*, 5043-5049.
- [40] V. S. Sharov, E. S. Dremina, N. A. Galeva, G. S. Gerstenecker, X. Li, R. T. Dobrowsky, J. F. Stobaugh, C. Schöneich. Fluorogenic Tagging of Peptide and Protein 3-Nitrotyrosine with 4-(Aminomethyl)-benzenesulfonic Acid for Quantitative Analysis of Protein Tyrosine Nitration. *Chromatographia* **2010**, *71*, 37-53.
- [41] V. S. Sharov, E. S. Dremina, J. Pennington, J. Killmer, C. Asmus, M. Thorson, S. J. Hong, X. Li, J. F. Stobaugh, C. Schöneich. Selective fluorogenic derivatization of 3-nitrotyrosine and 3,4-dihydroxyphenylalanine in peptides: a method designed for quantitative proteomic analysis. *Methods Enzymol.* **2008**, *441*, 19-32.
- [42] D. H. Montes-Cortes, J. J. Hicks, G. M. Ceballos-Reyes, J. R. Garcia-Sanchez, R. Medina-Navarro, I. M. Olivares-Corichi. Chemical and functional changes of human insulin by in vitro incubation with blood from diabetic patients in oxidative stress. *Metabolism* **2010**, *59*, 935-942.
- [43] I. M. Olivares-Corichi, G. Ceballos, R. Medina-Santillan, R. Medina-Navarro, A. M. Guzman-Grenfell, J. J. Hicks. Oxidation by reactive oxygen species (ROS) alters the structure of human insulin and decreases the insulin-dependent D-glucose-C14 utilization by human adipose tissue. *Front. Biosci.* **2005**, *10*, 3127-3131.
- [44] R. Tantipolphan, S. Romeijn, J. den Engelsman, R. Torosantucci, T. Rasmussen, W. Jiskoot. Elution behavior of insulin on high-performance size exclusion chromatography at neutral pH. *J. Pharm. Biomed. Anal.* **2010**, *52*, 195-202.
- [45] T. Rasmussen, M. R. Kasimova, W. Jiskoot, M. van de Weert. The chaperone-like protein alpha-crystallin dissociates insulin dimers and hexamers. *Biochemistry* **2009**, *48*, 9313-9320.
- [46] M. Amidi, H. C. Pellikaan, A. H. de Boer, D. J. Crommelin, W. E. Hennink, W. Jiskoot. Preparation and physicochemical characterization of supercritically dried insulin-loaded microparticles for pulmonary delivery. *Eur. J. Pharm. Biopharm.* **2008**, *68*, 191-200.
- [47] S. W. Hovorka, J. Y. Hong, J. L. Cleland, C. Schöneich. Metal-catalyzed oxidation of human growth hormone: Modulation by solvent-induced changes of protein conformation. *J. Pharm. Sci.* **2001**, *90*, 58-69.
- [48] E. R. Stadtman. Metal ion-catalyzed oxidation of proteins: biochemical mechanism and biological consequences. *Free Radic. Biol. Med.* **1990**, *9*, 315-325.

- [49] D. Butterfield, A. Castegna, C. Pocernich, J. Drake, G. Scapagnini, V. Calabrese. Nutritional approaches to combat oxidative stress in Alzheimer's disease. *J. Nutr. Biochem.* **2002**, *13*, 444.
- [50] D. Liu, D. Ren, H. Huang, J. Dankberg, R. Rosenfeld, M.J. Cocco, L. Li, D.N. Brems, R.L. Remmele. Structure and stability changes of human IgG1 Fc as a consequence of methionine oxidation. *Biochemistry* **2008**, *47*, 5088–5100.
- [51] M.K. Moi, S.J. Denardo, C.F. Meares, Stable bifunctional chelates of metals used in radiotherapy. *Cancer Res.* **1990**, *50*, 789–793.
- [52] Y. Tampo, S. Onodera, M. Yonaha. Mechanism of the biphasic effect of ethylenediaminetetraacetate on lipid-peroxidation in iron-supported and reconstituted enzymatic system. *Free. Radic. Biol. Med* **1994**, *17*, 27–34.
- [53] L. Burai, V. Hietapelto, R. Kiraly, E. Toth, E. Brucher. Stability constants and ¹H relaxation effects of ternary complexes formed between Gd-DTPA, Gd-DTPA- BMA, Gd-DOTA, and Gd-EDTA and citrate, phosphate, and carbonate ions. *Magn. Reson. Med* **1997**, *38*, 146–150.

Chapter 6

Identification of oxidation sites and covalent cross-links in metal catalyzed oxidized interferon beta-1a: potential implications for protein aggregation and immunogenicity

Riccardo Torosantucci^{1,2}, Victor S. Sharov², Miranda van Beers³, Vera Brinks⁴, Christian Schöneich² and Wim Jiskoot¹

¹Division of Drug Delivery Technology, Leiden Academic Centre for Drug Research (LACDR), Leiden University, Leiden, the Netherlands.

²Department of Pharmaceutical Chemistry of Kansas University, Lawrence, Kansas, USA.

³Bioprocessing Technology Institute, Agency for Science Technology and Research (A*STAR), Singapore.

⁴Department of Pharmaceutics, Utrecht Institute for Pharmaceutical Sciences (UIPS), Utrecht University, Utrecht, the Netherlands.

Molecular Pharmaceutics **2013**, *10*, 2311-2322.

Abstract

Oxidation via Cu^{2+} /ascorbate of recombinant human interferon beta-1a (IFN β -1a) leads to highly immunogenic aggregates, however it is unknown which amino acids are modified and how covalent aggregates are formed. In the present work we mapped oxidized and cross-linked amino acid residues in aggregated IFN β -1a, formed via Cu^{2+} /ascorbate catalyzed oxidation. Size exclusion chromatography (SEC) was used to confirm extensive aggregation of oxidized IFN β -1a. Circular dichroism and intrinsic fluorescence spectroscopy indicated substantial loss of secondary and tertiary structure, respectively. Derivatization with 4-(aminomethyl) benzenesulfonic acid was used to demonstrate, by fluorescence in combination with SEC, the presence of tyrosine (Tyr) oxidation products. High performance liquid chromatography coupled to electrospray ionization mass spectrometry of reduced, alkylated and digested protein was employed to localize chemical degradation products. Oxidation products of methionine, histidine, phenylalanine (Phe), tryptophan and Tyr residues were identified throughout the primary sequence. Covalent cross-links via 1,4- or 1,6-type addition between primary amines and DOCH (2-amino-3-(3,4-dioxocyclohexa-1,5-dien-1-yl) propanoic acid, an oxidation product of Phe and Tyr) were detected. There was no evidence of disulfide bridge, Schiff base, or dityrosine formation. The chemical cross-links identified in this work are most likely responsible for the formation of covalent aggregates of IFN β -1a induced by oxidation, which have previously been shown to be highly immunogenic.

Introduction

Recombinant human interferon beta (IFN β), a cytokine with anti-inflammatory and tumor-suppressor functions [1] is considered as the first choice treatment of multiple sclerosis, a severe neurodegenerative autoimmune disease [2]. Interferon beta-1a (IFN β -1a), in contrast to interferon beta-1b (IFN β -1b) [3], is glycosylated at asparagine 80 [4] carrying mainly biantennary and triantennary glycan structures [5-6]. IFN β -1a has an average molecular weight of about 22.5 kDa, contains 166 amino acid residues and is produced in Chinese hamster ovarian (CHO) cells [6]. As described by Karpusas et al. [7], the protein contains five alpha helices, an intramolecular disulfide bridge between cysteines in positions 31 and 141, and a free cysteine (Cys) in position 17.

Like many other protein therapeutics, IFN β is prone to aggregation, which has been correlated with enhanced immunogenicity [8]. Furthermore, it has been demonstrated that the removal of protein aggregates reduces the immunogenicity of IFN β formulations [9-11]. In addition, IFN β -1b (Betaferon[®]), which contains more aggregates than IFN β -1a products (Avonex[®], Rebif[®]), has been found to be the most immunogenic IFN β product in several preclinical and clinical studies [12-13].

Protein aggregates induced by metal-catalyzed oxidation (MCO) have been found to be particularly immunogenic in preclinical models. For instance, Hermeling et al. showed that recombinant human interferon alpha-2b (IFN α -2b) forms immunogenic aggregates upon oxidative stress induced by Cu²⁺/ascorbate catalyzed oxidation, using a transgenic mouse model immune tolerant to the human protein [14-15]. Similarly, IFN β -1a aggregates and monoclonal antibody aggregates, both produced via the same oxidative system, were shown to be highly immunogenic in transgenic immune tolerant mouse models [8, 16]. We therefore believe that characterization of chemical modifications and cross-links caused by Cu²⁺/ascorbate catalyzed oxidation is of high importance, since these data may shed light on structure-immunogenicity relationships for IFN β -1a and potentially other therapeutic proteins.

The scope of the present work was to identify the chemical modifications in Cu²⁺/ascorbate oxidized IFN β -1a, including covalent cross-links that may be involved in aggregation. Here we report a comprehensive characterization of

oxidative modifications in IFN β -1a following MCO and discuss putative mechanisms of MCO-induced IFN β -1a aggregation. Our data strongly support the formation of electrophilic oxidation products, which can be further involved in aggregate formation via 1,4- or 1,6-type addition to pre-existing protein nucleophiles, such as primary amine groups, in agreement with our recent mechanistic studies on insulin as a model protein [17].

Materials and Methods

Materials

IFN β -1a (0.26 mg/mL protein in 20 mM sodium acetate buffer, pH 4.8, containing 154 mM arginine) was kindly provided by Biogen Idec Inc. (Cambridge, MA, USA). PNGase F, L-ascorbic acid, ethylenediamine tetraacetic acid (EDTA), copper dichloride, arginine, monobasic and dibasic sodium hydrogen phosphate, ammonium bicarbonate (ABI), sodium chloride, sodium azide, SDS, dithiothreitol (DTT), iodoacetamide, glacial acetic acid, and acetonitrile were purchased from Sigma–Aldrich (St.Louis, MO, USA). Milli-Q water was used for the preparation of all the formulations. All chemicals were of analytical grade and used without further purification. 4-(aminomethyl) benzenesulfonic acid (ABS) was synthesized according to a published procedure [18]. Endoproteinases Glu-C and trypsin were purchased from Promega (Madison, WI, USA).

Preparation of untreated and oxidized IFN β 1-a formulations

IFN β -1a was prepared and treated as reported by van Beers et al [8]. Briefly, the protein solution was dialyzed against 100 mM sodium phosphate buffer and 200 mM sodium chloride, pH 7.2 (PBS). This dialyzed solution is referred to as untreated IFN β -1a. To obtain oxidized IFN β -1a, untreated IFN β -1a, diluted to 200 μ g/mL with PBS, was incubated with 4 mM ascorbate and 40 μ M CuCl₂ for 3 hours at room temperature. The oxidation reaction was stopped by adding 100 mM EDTA to a final concentration of 1 mM as previously reported [17].

ABS derivatization

Untreated and oxidized protein (0.2 mg/mL) were dialyzed against 50 mM ABI, pH 8.0, using a 3.5-kDa MWCO Slide-A-Lyzer Cassette (Asheville, NC, USA), before derivatization with ABS. To 250 μ L of dialyzed samples 7.5 μ L of 0.1 M sodium hydroxide were added to adjust the pH to 9.5. Then 100 mM ABS stock solution was added to a final concentration of 10 mM. Subsequently, 5 mM K₃Fe(CN)₆ stock solution in Milli-Q water was added to a final concentration of 0.5 mM. The reaction was conducted for 1 hour at room temperature, before performing SEC analysis or fluorescence measurement (as reported below in the section Size exclusion chromatography and Fluorescence spectroscopy, respectively). Controls for non-specific fluorescence included (i) oxidized and non-oxidized protein prior to derivatization and (ii) reagents alone (i.e. ABS/K₃Fe(CN)₆) incubated under the same conditions.

Size exclusion chromatography

To determine the aggregate content and to investigate the effect of reducing agents on oxidized and untreated IFN β -1a, SEC was performed by using a TSKgel Super SW2000 column protected by a Super SW guard column (Sigma Aldrich, St. Louis, MO, USA). An SPD-6AV UV and fluorescence detector (Shimadzu, Columbia, MD, USA) was used to record the chromatograms at a wavelength of 280 nm and at excitation/emission wavelength combination of 295/350nm, respectively. A flow rate of 0.35 mL/min was applied using a 515 HPLC pump and 717 Plus autosampler (Waters, Milford, MA, USA). The mobile phase consisted of 200 mM sodium chloride, 0.05% (w/v) sodium azide and 0.1% (w/v) SDS in 100 mM sodium phosphate, pH 7.2, which was filtered through a 0.2- μ m filter prior to use.

To detect fluorescent benzoxazole products in the ABS-derivatized samples, we used an Insulin HMWP Column, 7.8 \times 300 mm (Waters) connected to a HPLC system (Shimadzu, Columbia, MD, USA) coupled with a Shimadzu RF-20A fluorescence detector. Excitation and emission wavelengths were set at 360 and 490 nm, respectively. The mobile phase composition and flow rate were as previously reported [19].

Fluorescence spectroscopy

The emission spectra of the ABS-derivatized samples, diluted two fold in ABI, were measured in a 0.5-mL quartz fluorescence cuvette with an RF-5000U fluorescence spectrophotometer (Shimadzu) with excitation and emission wavelengths range set at 360 and 400-600 nm, respectively, and bandwidths set at 5 nm.

To test the potential presence of dityrosine, fluorescence of the oxidized IFN β -1a was measured in triplicate, using excitation and emission wavelengths set at 315 and 420 nm, respectively, as described previously [20]. Tryptophan (Trp) intrinsic fluorescence was measured with a Tecan infinite M1000 fluorometer (Tecan group Ltd., Männedorf, Switzerland) upon excitation at 295 nm and emission recorded from 310-500 nm with a step size of 2 nm, 50 flashes (frequency 400 Hz), a gain of 150 and a Z-position of 20.0 mm. Duplicates of 200 μ L of each sample were analyzed in black polystyrene 96-well plates (Greiner Bio-One, Frickenhausen, Germany).

Circular dichroism spectroscopy

Circular dichroism (CD) spectra of untreated and oxidized IFN β -1a (0.1 mg/mL) were recorded from 190 to 250 nm, using a Jasco J-815 CD spectrometer (Jasco International, Tokyo, Japan). Analyses were performed in a 1-mm (far-UV CD) path length quartz cuvette at 25 °C using a scan rate of 100 nm/min, a response time of 2 s, and a bandwidth of 1 nm. Each spectrum was the result of an averaging of six repeated scans and background was corrected with the corresponding buffer spectrum. The CD signals were converted to mean residue ellipticity $[\theta]_{\text{mrw}, \lambda}$, using a mean residue weight (MRW, calculated as $\text{MRW} = \text{M}/(\text{N}-1)$, where M is the average molecular weight of the untreated (glycan-free) protein (i.e. 20027 Da, based on the protein's chemical formula $\text{C}_{908}\text{H}_{1408}\text{N}_{246}\text{O}_{252}\text{S}_7$) and N is the number of amino acid residues in the chain).

Reduction, alkylation and digestion

Untreated and oxidized protein (0.2 mg/mL) were dialyzed against 50 mM ABI, pH 8.0, using a 3.5-kDa MWCO Slide-A-Lyzer Cassette (Asheville, NC, USA), and reduced by addition of 50 mM DTT, freshly prepared in 50 mM ABI,

pH 8.0, to a final concentration of 5 mM. The samples were incubated for 45 minutes at 45 °C using a Thermo NES heating bath (Thermo Scientific, NC, USA). Subsequently, 200 mM iodoacetamide, freshly prepared in 50 mM ABI, pH 8.0, was added to a final concentration of 20 mM. The digestion was performed as follows: IFN β -1a was incubated with Glu-C endoproteinase at a IFN β -1a/Glu-C ratio of 10:1 (w/w), for 1 hour at 37 °C. Next, trypsin was added (IFN β -1a/trypsin ratio 20:1 (w/w)) and the mixture was incubated for an additional hour at the same temperature. Finally, 4 μ L of a solution of PNGase F, dissolved according to the manufacturer's protocol, was added to 76 μ L of the protein mixture, which was then incubated overnight at 37 °C.

MS/MS analysis

Digested and non-digested samples were analyzed by means of an LTQ-FT hybrid linear quadrupole ion trap Fourier transform ion cyclotron resonance (FT-ICR) mass spectrometer (Thermo-Finnigan, Bremen, Germany) [21]. The MS/MS spectra were analyzed with the web-based software MassMatrix [22-25], which was used to simulate mass spectra and the theoretical fragment tables of the b- and y-ions [26] for the native, oxidized and cross-linked peptide products. The simulated spectra were compared to the experimental MS/MS spectra in order to validate the proposed product and cross-link structures. A mass accuracy sensitive probability-based scoring algorithm for database searching of tandem mass spectrometry data by MassMatrix software was employed for peptide identification; the manual filter was set at mass/charge ratio (m/z) accuracy <0.1 amu for both parent peptide and fragment ions.

Results

Comparison of untreated and oxidized IFN β -1a by SEC and spectroscopic methods

SEC analysis was used to verify whether the aggregation profile of oxidized IFN β -1a was similar to that observed earlier [8] and to study a potential involvement of disulfide bridging in aggregate formation. Comparison of the chromatograms of untreated and oxidized IFN β -1a (Figure 1A) shows extensive aggregation of the oxidized product and both chromatograms are in close agreement with the results published by van Beers et al [8].

Furthermore, the treatment of oxidized IFN β -1a with DDT did not have a major impact on the elution behavior, indicating that the majority of the aggregates were formed by non-reducible covalent bonds. In contrast, we observed that for untreated IFN β -1a, the reduction with DDT resulted in a decrease in dimer content by approximately 60% (Figure 1A), indicating that most of the dimers in the untreated IFN β -1a were formed through disulfide bridging.

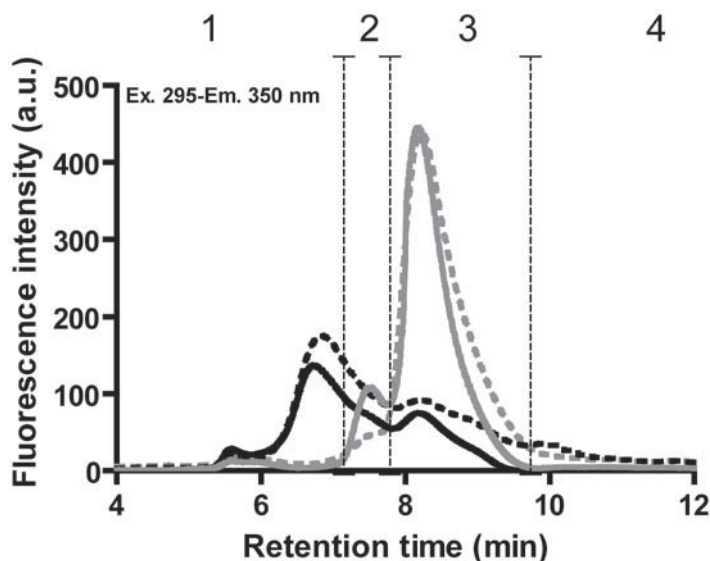


Figure 1A. SEC (TSKgel Super SW2000 column) with intrinsic tryptophan fluorescence detection of untreated IFN β -1a before (solid grey chromatogram) and after reduction and alkylation (dashed grey) and oxidized IFN β -1a before (solid black) and after reduction and alkylation (dashed black). The vertical dashed lines show the range of each peak: (1) mainly representing oligomers, (2) dimers, (3) monomers, (4) fragments.

SEC with fluorescence detection of ABS-tagged proteins was used to study whether the monomers or aggregates contain DOPA (3,4-dihydroxyphenylalanine) and/or DOCH (2-amino-3-(3,4-dioxocyclohexa-1,5-dien-1-yl) propanoic acid), produced by oxidation of tyrosine (Tyr) and/or phenylalanine (Phe) residues and subject to fluorogenic derivatization with ABS^[17] and/or 5-hydroxytryptophan, a Trp oxidation product which can also form fluorescent benzoxazole products upon ABS derivatization^[27-28]. Our data show that after derivatization of the oxidized and dialyzed protein with

ABS, the total SEC fluorescence peak area (i.e. the sum of all the peak areas under the curve) for the ABS-derivatized oxidized IFN β -1a is about six fold higher than that of the ABS-derivatized untreated protein (Figure 1B), indicating that MCO of IFN β -1a leads to formation of DOPA/DOCH and/or 5-hydroxytryptophan residues in the oxidized protein.

ABS derivatization of non-oxidized IFN β -1a also produces a weak fluorescent signal mainly associated with protein monomer (Figure 1B), suggesting a background oxidation in the untreated protein.

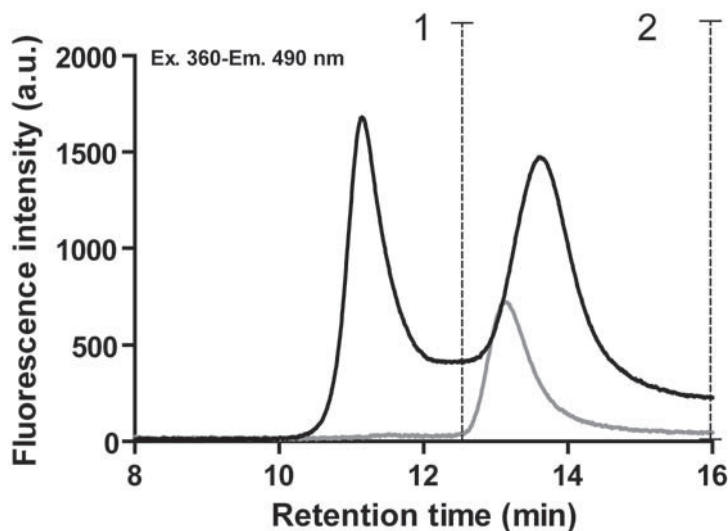


Figure 1B. SEC (Insulin HMWP Column) with ABS fluorescence detection of ABS-derivatized untreated IFN β -1a (grey) and ABS-derivatized oxidized IFN β -1a (black). The vertical dashed lines show the range of each peak: (1) mainly representing oligomers, (2) dimers and monomers (with this column it is not possible to discriminate dimer from monomer).

The ABS fluorescence of ABS derivatized oxidized and untreated IFN β -1a was also measured by steady-state fluorescence. The results show a seven fold increase in fluorescence intensity for the oxidized protein (Figure 2), which is consistent with the SEC data.

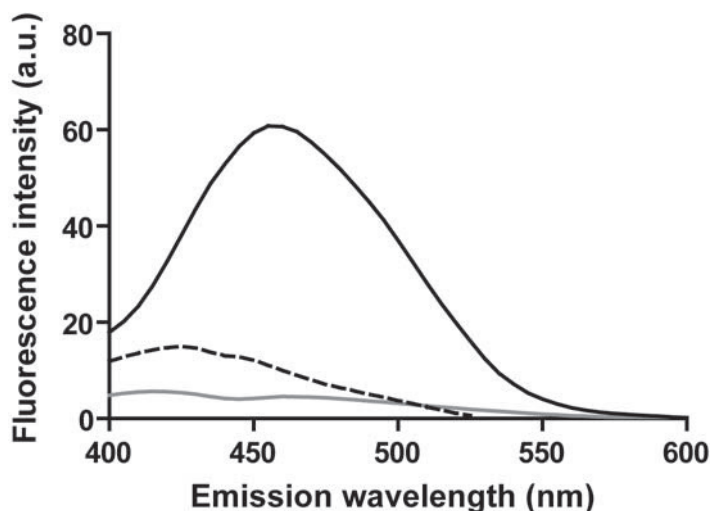


Figure 2. Extrinsic fluorescence emission spectra of ABS-derivatized untreated IFN β -1a (grey), ABS-derivatized oxidized IFN β -1a (black), and oxidized IFN β -1a (dashed black). Spectra represent the average of two batches.

Further structural characterization was performed by CD (Figure 3) and intrinsic steady-state fluorescence measurements (Figure 4). Likely as a result of oxidation and cross-link formation, it was found that the content of alpha helix in oxidized IFN β -1a had decreased, as indicated by the drop in negative CD signal, with a concomitant increase in random coil structure, as indicated by the higher 208/222 nm ratio measured for the oxidized protein (1.041 ± 0.024) as compared with its native counterpart (0.729 ± 0.004) [29-30].

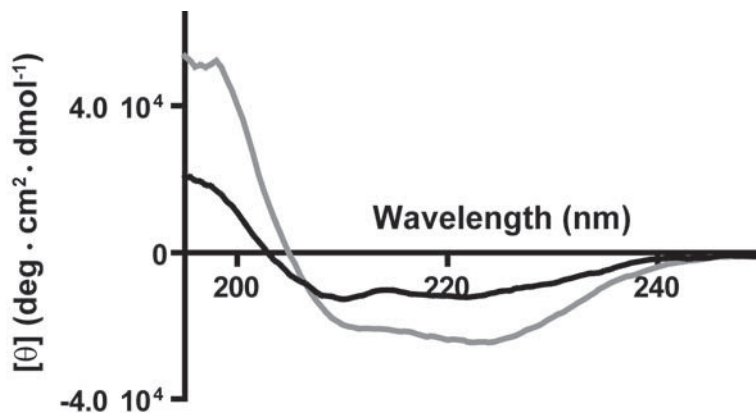


Figure 3. Far-UV CD spectra of untreated IFN β -1a (grey) and oxidized IFN β -1a (black). Spectra represent the average of two batches.

Moreover, a substantial decrease of Trp fluorescence was observed, pointing to chemical modification of Trp residues and/or loss of tertiary structure in general. No shift in the emission maximum was however observed.

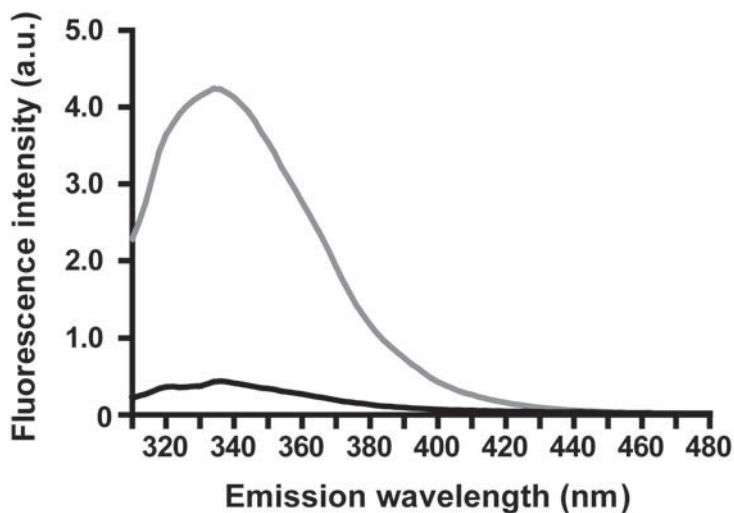


Figure 4. Intrinsic steady-state fluorescence of untreated IFN β -1a (grey) and oxidized IFN β -1a (black). Spectra represent the average of two batches.

Mass spectrometry analysis

Undigested IFN β -1a

The data of liquid chromatography coupled to electrospray ionization mass spectrometry (LC-ESI-MS) analysis of undigested untreated IFN β -1a (Figure 5A) are in agreement with previously reported results [31]: the spectrum of the protein represents a mixture of multiple glycoforms (mainly fucosylated and sialylated protein) where the most abundant isoform contains one mono-fucosylated, biantennary structure carrying two sialic acid residues, featuring a total molecular weight of 22376 Da. The spectrum of the oxidized protein represents a single broad peak with a maximum at 22460.5 Da resulting from an overlay of multiple heterogeneously oxidized protein isoforms (Figure 5B), similar to results published for another oxidized protein [32].

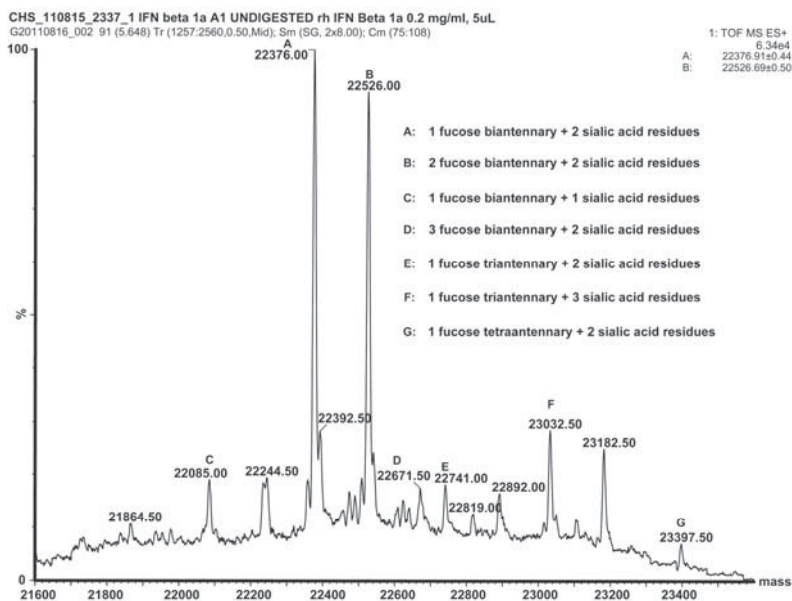


Figure 5A. Deconvoluted mass spectrum of undigested untreated IFN β -1a

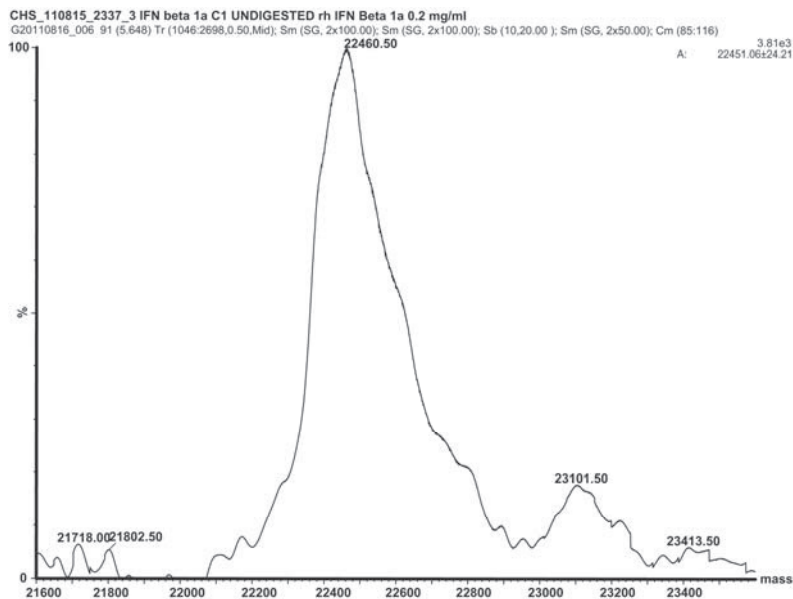


Figure 5B. Deconvoluted mass spectrum of undigested oxidized IFN β -1a

Sequence-specific analysis of IFN β -1a oxidative modifications

This section focuses on the identification of amino acid sequence-specific oxidative protein modifications through MS/MS analysis of IFN β -1a digests and the results will be presented in the following order: Methionine (Met), Phe, Histidine (His), Tyr and Trp oxidation. It is noteworthy that some peptide sequences potentially contain more than one modification, and that some MS/MS spectra may represent a mixture of peptide isoforms with the same m/z but different locations of oxidative modifications within the sequence. Table I lists all the chemically modified peptides detected. Although a few modifications were observed also in peptides derived from the untreated protein (Table I, last column), most modifications were observed in peptides from oxidized IFN β -1a and involved Met, Phe, His, Tyr and Trp residues.

Table II shows all the potential targets for MCO, including the ones found oxidized in the present study.

Table I. Chemical modifications measured by LC-ESI-MS/MS in peptides from oxidized and untreated IFN β 1a obtained after reduction, alkylation and enzymic digestion.

Chemical modifications and reference to corresponding mass spectrum	Peptide	Experimental m/z	Charge	Theoretical mass	Δ m	Oxidized IFN β 1a*	Un-treated IFN β 1a*
M ₁ (O) Figure S1	M ₄ SYNLLGFLQR ₁₁	679.35	2	1356.70	0.00	+	+
M ₁ (O), Y ₃ (O) Figure S2	M ₄ SYNLLGFLQR ₁₁	687.35	2	1372.69	+0.01	+	-
Y ₃ (DOCH) Figure S3	M ₄ SYNLLGFLQR ₁₁	678.34	2	1354.68	0.00	+	-
M ₁ (loss CH ₃ S) Figure S4	M ₄ SY NLLGFLQR ₁₁	647.35	2	1292.68	+0.02	+	+
F ₃₈ (O) Figure S5 (a-c)	M ₃₆ NFDIPEIK ₄₅	626.30	2	1250.59	+0.01	+	-

M ₃₆ (O) Figure S6(a-c)	M ₃₆ NFDIPEEIK ₄₅	626.30	2	1250.59	+0.01	+	+
M ₆₂ (O) Figure S7	M ₆₂ LQNIFAIFR ₇₁	634.84	2	1267.68	0.00	+	-
M ₆₂ (loss CH ₃ S) Figure S8	M ₆₂ LQNIFAIFR ₇₁	402.23	3	1203.68	+0.01	+	-
M ₁₁₇ (O), H ₁₂₁ (O) Figure S9	L ₁₁₆ MSSLHLK ₁₂₃	480.76	2	959.52	0.00	+	-
F ₅₀ (O), Q(deamidation in several positions) Figure S10	Q ₄₆ LQQFK ₅₂	468.76	2	935.48	+0.04	+	-
H ₉₃ (O) Figure S11	N ₈₆ LLANVYHQINHLK ₉₉	846.96	2	1691.92	0.00	+	-
H ₉₇ (O) Figure S12	N ₈₆ LLANVYHQINHLK ₉₉	846.96	2	1691.92	0.00	+	-
H ₉₃ (O), H ₉₇ (O) Figure S13	N ₈₆ LLANVYHQINHLK ₉₉	854.96	2	1707.91	+0.01	+	-

H ₉₃ (asn) Figure S14(a-b)	N ₈₆ LLANVYHQINHLK ₉₉	827.46	2	1652.91	+0.01	+	-
H ₉₇ (asn) Figure S15(a-b)	N ₈₆ LLANVYHQINHLK ₉₉	827.46	2	1652.91	+0.01	+	-
H ₁₃₁ (O), Y ₁₃₂ (O) Figure S16(a-c)	I ₁₂₉ LHLYLK ₁₃₄	401.74	2	801.48	0.00	+	-
Y ₁₃₈ (DOCH), H ₁₄₀ (O) Figure S17	E ₁₃₇ YSHCAWTIVR ₁₄₇	697.81	2	1393.62	0.00	+	-
H ₁₄₀ (O), C141(IAM)# Figure S18	Y ₁₃₈ SHCAWTIVR ₁₄₇	654.81	2	1307.62	0.00	+	-
W ₂₂ (O), N ₂₅ (deamidation) Figure S19	L ₂₀ LWQLNGR ₂₇	508.78	2	1015.55	+0.01	+	+
W ₂₂ (N-fkyn), N ₂₅ (deamidation) Figure S20	L ₂₀ LWQLNGR ₂₇	516.78	2	1031.55	+0.01	+	+

* + detected; - not detected

#(IAM): alkylation with iodoacetamide

Table II. Oxidation prone amino acid residues and oxidized amino acids detected in peptides derived from oxidized IFN β -1a.¹

Methionine	Phenylalanine	Tyrosine	Tryptophan	Histidine
1	<i>8</i>	3	22	93*
36	<i>15</i>	<i>30</i>	<i>79#</i>	97*
62	<u>38</u>	<i>60</i>	<i>143#</i>	<u>121*</u>
117	50	<i>92</i>		131
	<i>67</i>	<u>125</u>		140
	<i>70#</i>	<u>126</u>		
	<i>111</i>	<u>132</u>		
	<i>154#</i>	138		
	<i>156</i>	<i>155</i>		
		<i>163</i>		

¹ Bold numbers: oxidized residues; bold underlined numbers: oxidized residues involved in H-bond critical for the correct folding of IFN β -1a; underlined numbers: residues involved in H-bond critical for the correct folding of IFN β -1a (Karpusas et al. [7]); plain italic numbers: non-oxidized residues.

Hydrophobic residues that stabilize the core of the molecule.

* Residues that coordinate a zinc ion, responsible for dimer formation.

A supplementary Table S1 (available online on Molecular Pharmaceutics) shows all the potential amino acid modifications included in the settings of a database search for oxidized, reduced, alkylated and digested IFN β -1a samples. All annotated MS/MS spectra for oxidative protein modifications along with suggested peptide structures presented as inserts are shown in the supplementary Figures S1-S20 (available on line on Molecular Pharmaceutics). Note that in the supplementary figures, the peptide structures of the non-modified amino acid residues are displayed in a one-letter code, while the respective full structures are drawn for the suggested oxidatively modified and alkylated/deamidated residues.

Methionine oxidation

Met1 has been found susceptible to oxidation already by other authors [7, 31]. The b2⁺ ion in Figure S1, where the peptide M₁SYNLLGFLQR₁₁ is displayed, shows the incorporation of one oxygen atom (+16 Da) into the sequence

Met1Ser2: here, Ser is less prone to oxidation than Met, hence the target of oxidation is likely Met1. Figure S2 shows the same peptide with two oxygen atoms incorporated (+32 Da), which may represent a mixture of two sequences where either Met1 is oxidized to its sulfone, or DOPA (formed from Tyr3) and Met sulfoxide are present together. This is illustrated in the inserts to Figure S2, showing two potential b_2^+ ions, one with a mass increase of +16 Da (mono oxidized, indicated as Met ox) and another with the mass increase of +32 Da (di-oxidized, indicated as Met (ox)₂). The second insert shows two fragments with m/z 1123.57 and 1139.25, which may represent the y_9^+ ions for the unmodified and oxidized form of Tyr3; the ratio of these peaks suggests that the peptide containing oxidized Met1 and DOPA in position 3 is far less abundant than the unmodified peptide (a fraction of less than 10%).

However, this value does not necessarily reflect a lower rate of DOPA formation compared to Met sulfone; rather, it may indicate a higher reactivity of DOPA, resulting in DOCH and further cross-linked products. A spectrum of the doubly charged peptide ion with m/z 678.34 in Figure S3 shows such an example where Tyr is oxidized to DOCH based on a mass increase of 14 Da, which corresponds to the incorporation of one oxygen atom and loss of two hydrogen atoms, albeit at very low abundance of both y_9^+ and $b_3^+-H_2O$ sequence-indicating ions.

We were also able to detect a characteristic loss of methane sulfenic acid (CH_3SOH , -64 Da, compared with the mono oxidized sequence) from the N-terminus oxidized Met (Figure S4), which was suggested earlier as diagnostic for identifying peptides containing oxidized Met [26, 33].

Met36 is located in a solvent exposed domain of IFN β -1a [7, 31]. Figure S5a and S5b represent the MS/MS spectra matching the sequence M₃₆NFDIPEEIK₄₅, in which either Met36 or Phe38 is oxidized. These two products are not resolved by our HPLC method and the respective spectra overlay, as evidenced by the presence of two potential fragment ions for y_8^+ at m/z 990.48 and 1006.44 (Figure S5b) for oxidized Met36 and oxidized Phe38, respectively. As additional evidence for oxidized Phe38, the ion at m/z 228.18 can be considered, which most likely represents the $b_2^+-H_2O$ ion (indicated as F ox) from the parent peptide with oxidized Phe38 (Figure S5c). Though the fraction of the peptide with oxidized Phe38 is rather small (ca. 3-5% based on the relative abundance of fragment ion y_8^+ in Figure S5b, indicated as F ox), it

is noteworthy that in the control spectra (non-oxidized IFN β -1a) both fragments at 1006.44 and at 228.18 were not observed (Figure S6a-S6c). Altogether, these data suggest that untreated IFN β -1a already contains some oxidized Met36 residues, whereas oxidized Phe38 is only present in oxidized IFN β -1a.

Met62 is a buried residue [7, 31]. It was resistant to oxidation by hydrogen peroxide [31], however, in conditions of MCO, we detected MS/MS spectra for the sequence M₆₂LQNIFAIFR₇₁ containing the oxidized Met62 (Figure S7). Again, the spectrum for the loss of methane sulfenic acid in position 62, indicative of Met62 oxidation, was observed (Figure S8).

Met117 is a solvent exposed residue [7, 31] and is most susceptible to oxidation (under mild oxidative conditions via hydrogen peroxide), as compared to Met1, Met36 and Met62 [31]. Figure S9 represents a spectrum for the sequence L₁₁₆MSSLHLK₁₂₃, where besides Met117, His121 is oxidized to 2-oxo-His. The distinct b₂⁺ and y₃⁺ ions indicate oxidation of Met117 and His121, respectively.

Phenylalanine oxidation

The fragment containing oxidized Phe38 (M₃₆NF₃₈DIPEEIK₄₅) has been described above in the section Methionine oxidation.

Phe50 is adjacent to several Gln residues, which may undergo deamidation, during digestion or MCO. Figure S10 presents a typical MS/MS spectrum indicating the oxidation of Phe50, in addition to deamidation of one of the Gln residues. Formation of pyroglutamic acid, which should be attributed only to the cyclization of N-terminal Gln in the peptide (-18 Da) during the LC-MS analysis, was also detected.

Histidine and tyrosine oxidation

His oxidation to 2-oxo-His is well documented and has been measured in proteins such as insulin [34-36]. Stadtman et al. showed that His oxidation also can yield asparagine as a potential product [37].

The sequence N₈₆LLANVYHQINHLK₉₉ obtained after digestion with a combination of trypsin and endoproteinase Glu-C, contains two His residues in positions 93 and 97 and one Tyr residue in position 92. Several observed

combinations of His93 or His97 mono oxidation (+16 Da on His), oxidation of both His residues (+32 Da), and formation of Asn in positions 93 and 97 are shown in Figures S11, S12, S13, S14(a-b), S15(a-b), where the respective modifications are proven by $b7^+$, $b8^+$, and $b12^+$ ions, as well as $y3^+$, $y7^+$, $y8^+$, and $y12^{++}$ ions. In Figure S15 are shown only the ions which differ from Figure S14.

His121 and Tyr3 oxidation was already demonstrated for the fragments $L_{116}MSSLHLK_{123}$ and $M_1SYNLLGFLQR_{11}$, respectively, as discussed above.

Sequence $I_{129}LHYLK_{134}$ contains two potential sites for oxidation: His131 and Tyr132. The ions highlighted in Figure S16a fit to oxidation of either His131 or

Tyr132, whereas in Figure S16b, based on multiple fragments for the $y4^+$ ion, oxidation of both amino acid residues is suggested. The ions $y4^+-H_2O$ and $b4^+$ in Figure S16b, at m/z 574.26 and m/z 559.29, respectively, support the simultaneous oxidation of His and Tyr. Also, the region of the spectrum between 200 and 400 m/z contains two peaks identified as $b3^+$ in which His (Figure S16b, H ox, m/z 380.28) or Tyr (Figure S16c, Y ox, m/z 364.11) are oxidized. Furthermore, in Figure S16c is depicted the ion $y3^{++}$ supporting Tyr oxidation. Altogether, it seems that three different peptides containing either oxidized His131, oxidized Tyr132, or both amino acids oxidized, were detected simultaneously.

In the sequence $E_{137}YSHCAWTIVR_{147}$, containing a missed cleavage site and 2 additional oxygen atoms, there are 3 potential oxidation sites: Tyr138, His140, and Trp143. In the spectrum shown in Figure S17 the $y5^+-H_2O$ ion at m/z 656.96 rules out Trp oxidation, $y8^{++}$ at m/z 501.36, in the insert, supports His oxidation, and $b3^+$ and $b4^{++}$ are in accordance with Tyr oxidation to DOCH. Further evidence for His140 oxidation is shown in Figure S18, where Cys is derivatized with iodoacetamide, and N-terminal Glu (E) is cleaved-off by Glu-C.

Tryptophan oxidation



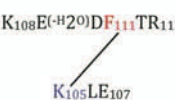
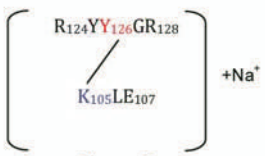
Trp22 oxidation was detected in both the oxidized and the control samples, suggesting a spontaneous oxidation of this residue during protein storage or handling. Spectra presented in Figures S19 and S20 show the formation of the major oxidative products, hydroxyl Trp (probably hydroxylated at position 5), and N-formyl kynurenine [38-39], respectively, as evidenced through the

presence of the sequence-indicative ions $y3^+$ - $y7^+$ and some b^+ ions, particularly $b3^+$. In addition to Trp oxidation, Asn25 deamidation was detected in peptide L₂₀LWQLNGR₂₇ from both oxidized and control IFN β -1a, which could be expected given the highly deamidation prone N₂₅G sequence [40].

Cross-links

This section focuses on MS/MS identification of covalent cross-links formed through 1,4- and/or 1,6-type addition to the electrophilic product of Tyr oxidation, i.e. DOCH, resulting from MCO of IFN β -1a. As we have only MS/MS but no NMR data of our reaction products, we have to assume that both reactions are possible. Table III lists all the cross-linked peptides detected by MS/MS and Figures 6a, 7a, 8a and 9a represent the corresponding MS/MS spectra along with the peptide cross-links. The structures displayed in Figures 6b, 7b, 8b and 9b representatively show only the products of 1,4-addition. Data will be presented starting from the first chemically modified electrophilic amino acid measured, i.e. DOCH in the first observed position (Tyr3) of IFN β -1a. Data reported were obtained from IFN β -1a that was oxidized, reduced, alkylated and digested.

Table III. Cross-links measured by LC-ESI-MS/MS in peptides derived from oxidized IFN β -1a after reduction, alkylation and enzymatic digestion (in blue nucleophilic amino acids, in red amino acids oxidized to DOCH).

Cross-link*	Experimental m/z	Charge	Theoretical mass	Δm
 <p>Figure 6</p>	756.02	3	2265.11	-0.05
 <p>Figure 7</p>	756.03	3	2265.11	-0.02
 <p>Figure 8</p>	598.3	2	1194.60	+0.00
 <p>Figure 9</p>	569.79	2	1137.56	+0.02

* (IAM): alkylation with iodoacetamide; (-H₂O): loss of 1 water molecule.

Met1 – Tyr30

The free N-terminus of Met1 is a good nucleophile for 1,4- or 1,6-type addition under our applied conditions (pH 7.2), where the N-terminal amino group is in part deprotonated. Figure 6a shows the MS/MS spectrum corresponding with the cross-link between Met1 and Tyr30 in the respective tryptic peptides, as illustrated by the scheme in Figure 6b. The series of y-ions in the peptide A (where the prefix A indicates the ions that belong to the peptide M₁SYNLLGFLQR₁₁) of the cross-link (Ay²⁺ to Ay⁹⁺) together with Ab¹⁺ in the lower insert (zoomed region m/z 1046 -1060) demonstrate that the

peptide A is linked to peptide B through the Met1 amino group, whereas Bb1⁺-H₂O and Bb1⁺-NH₃ ions (zoomed m/z region 1498-1514) indicate the involvement of Tyr30 of the peptide B in the cross-link formation. Note that in the sequence Y₃₀CLKDR₃₅ both Cys and Lysine (Lys) residues are in alkylated form (displayed by the mass of the parent peptide and fragment ion Bb5⁺⁺). Furthermore, we noticed that both Met1 and Tyr3 in the cross-linked peptide are not oxidized, suggesting that the cross-link may protect these residues from oxidation.

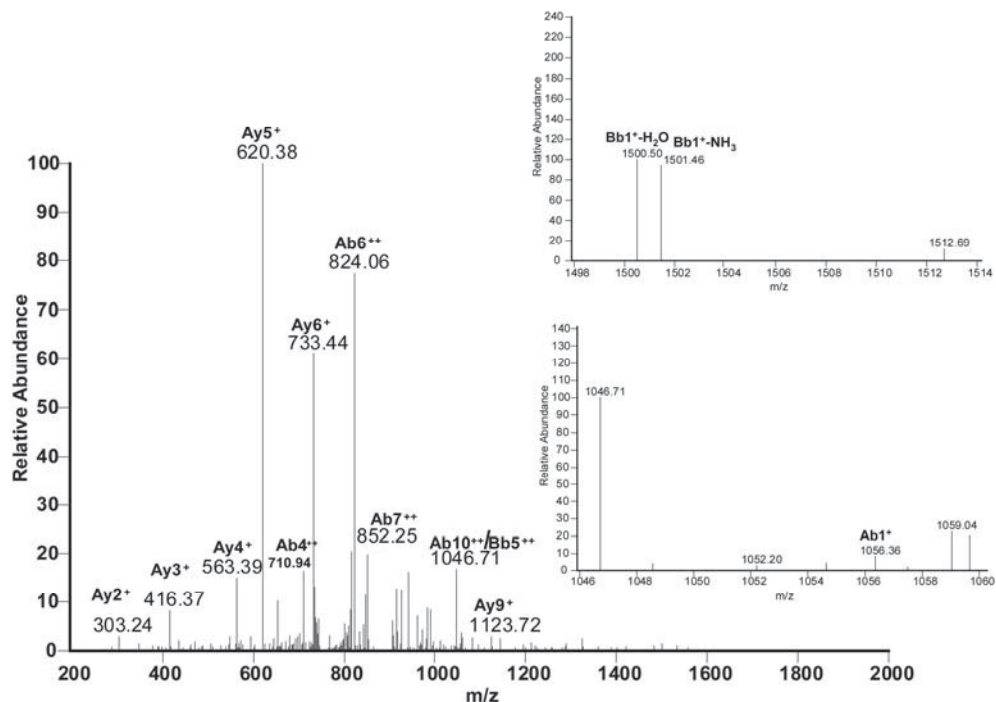


Figure 6a. MS/MS spectrum for the sequence M₁SYNLLGFLQR₁₁ cross-linked through Met1 to the sequence Y₃₀C^(IAM)LK^(IAM)DR₃₅.

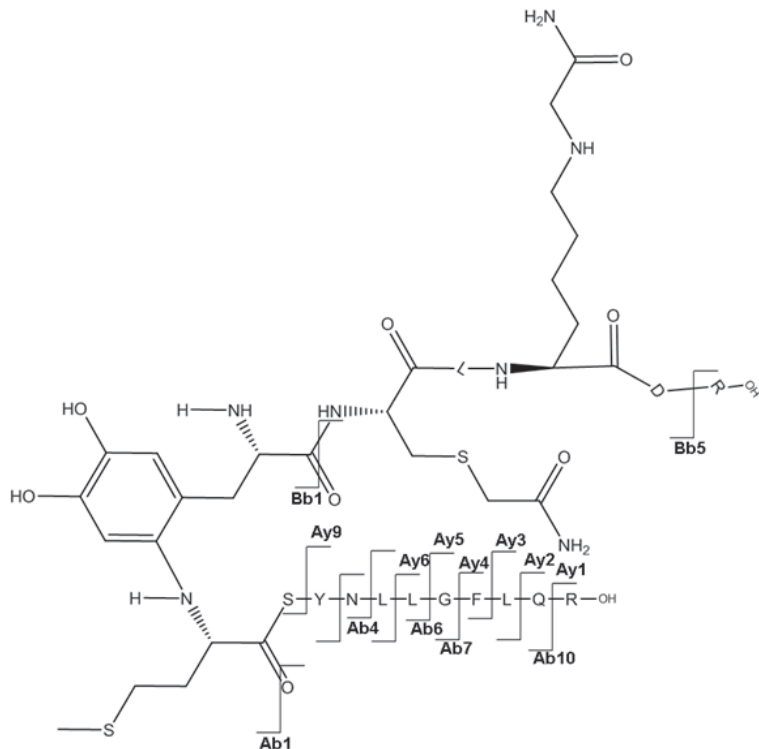


Figure 6b. Suggested chemical structure of the cross-linked sequence (theoretical *mass* 2265.11, experimental *m/z* 756.02, $[M+H]^{3+}$, Δm from parent peptide -0.05).

Met1 – Tyr60

Figure 7a, reports the MS/MS spectrum for the cross-link involving Met1 and Tyr60. The structure provided in Figure 7b, where Met1 is covalently bound to Tyr60, was drawn for the position 6 of the aromatic ring of DOPA (or DOCH), which is sterically less hindered than the positions 1 and 2. In the peptide $M_1SYNLLGFLQR_{11}$, an additional mass shift of +16 should be attributed to Tyr3 oxidation to DOPA, as suggested by the presence of ion $Ab3^{2+}$, ruling out the oxidation of another sensitive residue, Phe8. The ion $Ab2^+$ supports the structure shown in Figure 7b. In addition, fragments matching ions $Ay9^+$ and $Bb3^+$ disprove the involvement of sequences $Y_3NLLGFLQR_{11}$ and $D_{54}AA_{56}$ in the cross-link formation.

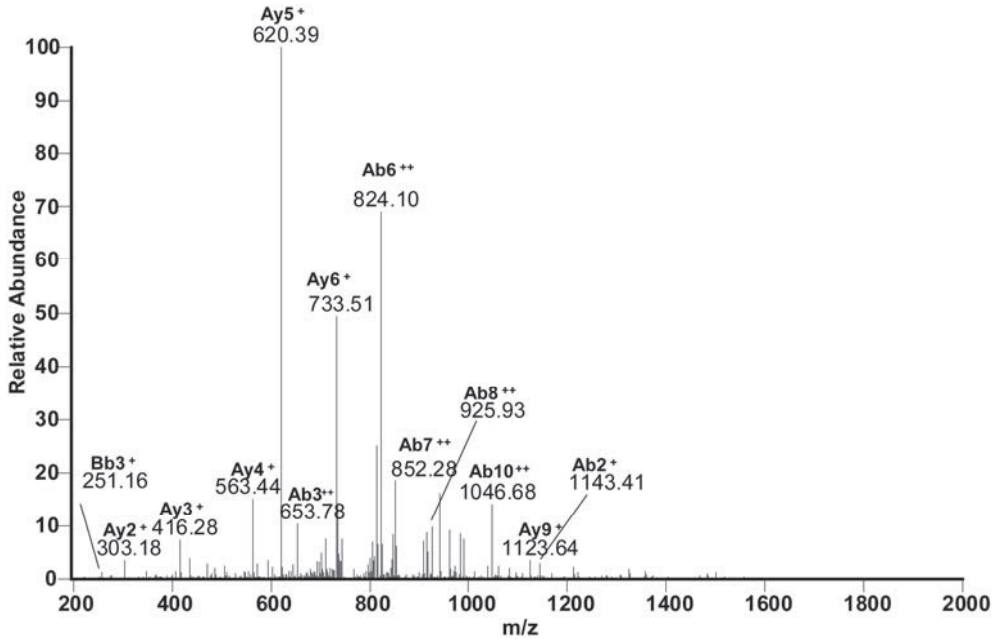


Figure 7a. MS/MS spectrum of sequence M₁SYNLLGFLQR₁₁ cross-linked through Met1 to the sequence D₅₄AALTIY₆₀E₆₁.

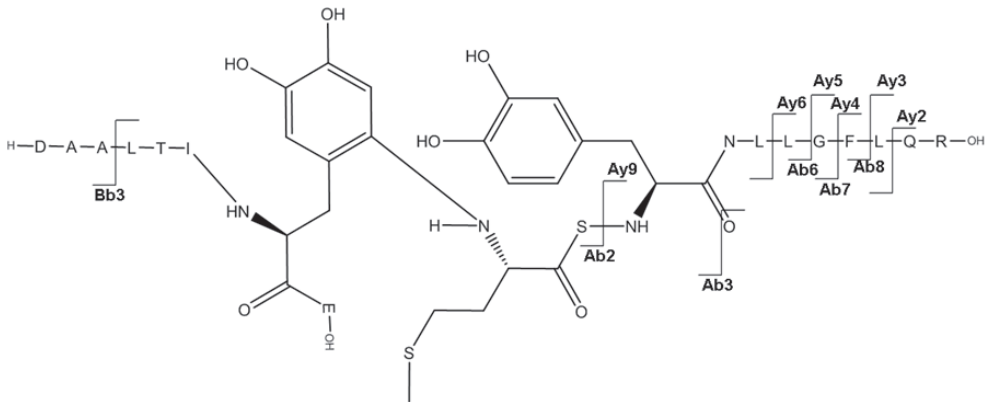


Figure 7b. Suggested chemical structure of the cross-linked sequence (theoretical mass 2265.11, experimental m/z 756.03, $[M+H]^3+$, Δm from parent peptide -0.02).

Lys105 - Phe111

Figure 8a displays the MS/MS spectrum consistent with a cross-link between Lys105 and Phe111. It must be noticed that the mass for this cross-link is 18 Da lower than the mass that would be expected. This is due to loss of water on Glu109 in the sequence $K_{108}EDFTR_{113}$, which can arise from the cyclization with its N-terminal amino group or with the more nucleophilic amino group of Lys108, which would lead to the formation of a 1,4 diazocine-like structure as shown by Koriatopoulou et al [41]. The presence of an intense fragment ion $Bb1^{++}$ in particular shows that the sequence $K_{108}EDFTR_{113}$ is covalently attached to Lys105, as illustrated in Figure 8b. Furthermore, the fragment ion $By2^+$ proves that neither Leu106 nor Glu107 of the sequence $K_{105}LE_{107}$ are involved in the cross-linked structure.

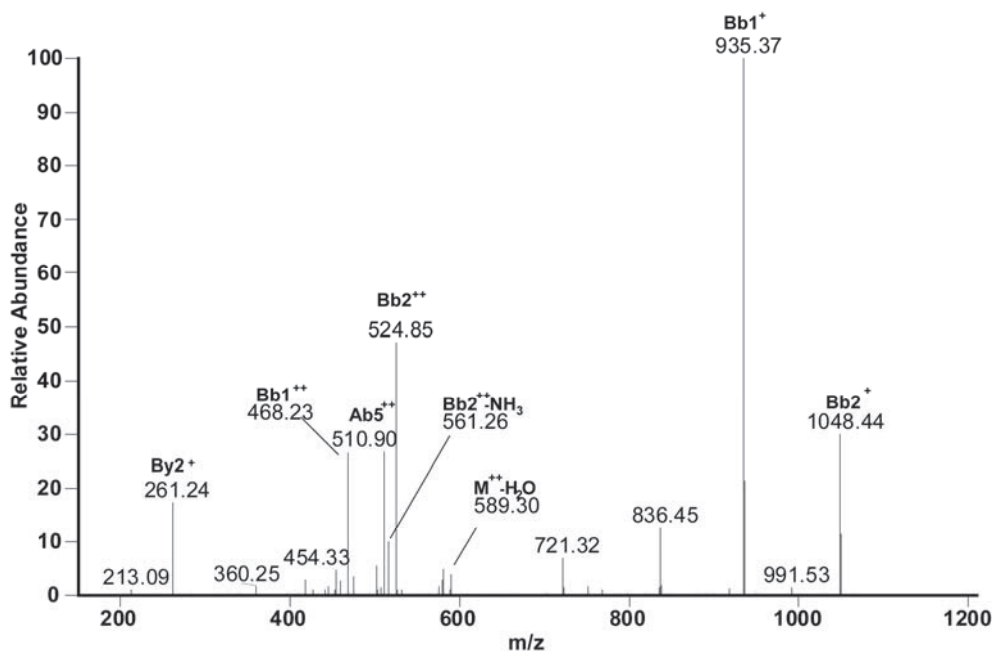


Figure 8a. MS/MS spectrum of sequence $K_{105}LE_{107}$ cross-linked through Lys105 to the sequence $K_{108}E^{(-H_2O)}DF_{111}TR_{113}$.

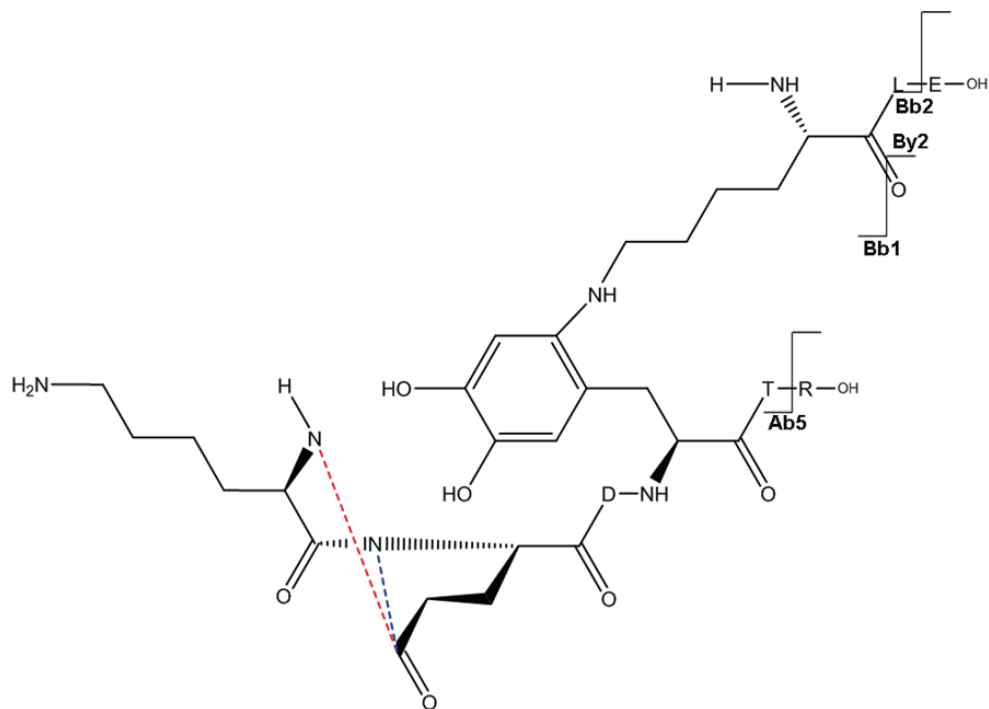


Figure 8b. Suggested chemical structure of the cross-linked sequence (theoretical *mass* 1194.60, experimental *m/z* 598.30, $[M+H]^{2+}$, Δm from parent peptide +0.00).

Lys105 – Tyr126

The cross-linked sequence $R_{124}YYGR_{128}$ with $K_{105}LE_{107}$ through Lys105 and Tyr126 is presented in Figure 9. Here there are two adjacent Tyr residues (in $R_{124}YYGR_{128}$) which can be involved in the cross-link. The $Ay3^{++}$ and $Ay4^{++}$ related ions however suggest that Tyr126 (and not Tyr125) serves as electron acceptor in the cross-link. $[Bb1 + Na]^+$ and $[Bb2 + Na]^+$ fragments prove the involvement of Lys105 in the peptide cross-linking. The sodiation of the respective fragment ions (except for $By2^+$) is due to complex formation between the C-terminal carboxyl of Arg128 and residual sodium ions present in samples, likely due to incomplete removal of sodium phosphate buffer during protein dialysis after MCO.

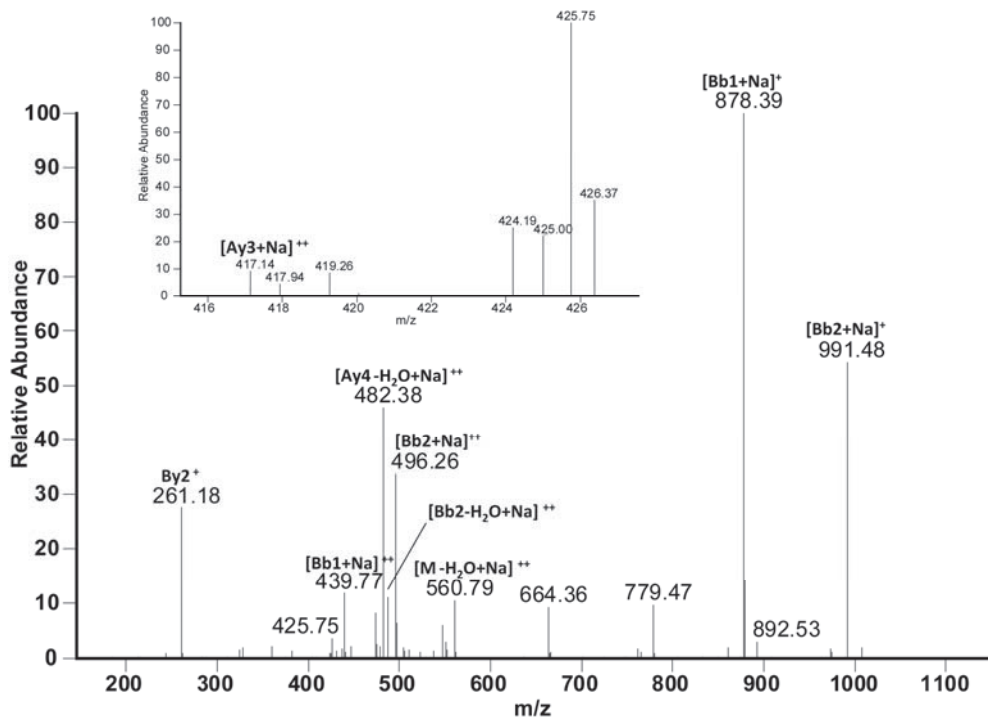


Figure 9a. MS/MS spectrum of sodiated sequence $K_{105}LE_{107}$ linked through Lys105 to the sequence $R_{124}YY_{126}GR_{128}$ (the inset show the MS/MS spectrum zoomed in the m/z range 415-428).

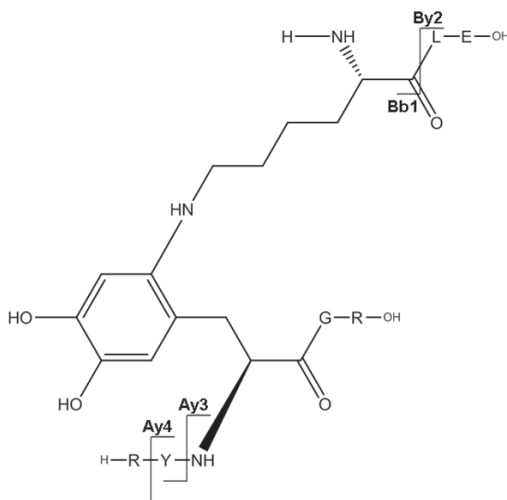


Figure 9b. Suggested chemical structure of the cross-linked sequence (theoretical $mass$ 1137.56, experimental m/z 569.79, $[M+H]^{2+}$, Δm from native parent peptide +0.02).

Discussion

Oxidative chemical modification of amino acid residues may alter the secondary and tertiary protein structure, favoring interaction between protein surfaces and subsequently leading to non-covalent aggregation. Indeed, MCO (using the oxidative system presented in this paper) of proteins, such as growth hormone [42], IFN α -2b [14], IFN β -1a [8], IgG1 [16], IgG2 [43], insulin and PEGylated insulin [19], relaxin [44], recombinant SHa (29–231) prion protein [45], and superoxide dismutase [46], have been shown to lead to extensive aggregation. Moreover, protein aggregates generated by MCO have been shown to be particularly immunogenic.

For instance, Hermeling et al. [14–15], using a transgenic immune tolerant mouse model, discovered that aggregated IFN α -2b, oxidized via metal catalysis was more immunogenic than IFN α -2b aggregates that were produced otherwise.

More recently, van Beers and colleagues hypothesized that a particular combination of oxidation and covalent aggregation could be responsible for the immune response against IFN β -1a exposed to MCO, though no particular mechanisms for chemical cross-linking were demonstrated [8]. Similarly, MCO of an IgG1 was found to produce immunogenic aggregates [16].

Here, performing an extensive mass spectrometric characterization of IFN β -1a oxidized under conditions identical to those in the above examples (i.e., Cu²⁺/ascorbate catalysis), we describe chemical modifications of multiple residues that can affect the structure of IFN β -1a. Results of the current study, in particular, reveal that the oxidative modification of Phe and Tyr results in an electron acceptor structure, namely DOCH, which may be involved in IFN β -1a cross-linking through a 1,4- or 1,6-type addition mechanism of primary amines to DOCH. The results reported in this work are in agreement with the data we recently published using insulin as a model protein [17]. However, since Met and Trp are not present in insulin, we did not know whether these are involved in covalent cross-linking of other proteins such as IFN β -1a. Although we detected oxidation of 4 Met residues and 1 Trp residue in oxidized IFN β -1a, we found no evidence of Met or Trp being involved in covalent cross-links. These data are in contrast with the common opinion that Trp oxidation could lead to new carbonyl groups and subsequent cross-linking via Schiff base formation [47]. However, the imine structure generated through

Schiff base formation is reversible unless it is reduced with sodium borohydride or cyanoborohydride to form a secondary amine group [48], which may explain why Trp oxidation did not seem to be involved in aggregation of IFN β -1a.

Our data on ABS derivatization of the control samples (Figure 1B) support the hypothesis that DOCH is an intermediate in the covalent cross-links of IFN β -1a aggregates induced by MCO. SEC analysis under reducing conditions did not point to disulfide-mediated covalent cross-links. Furthermore, fluorescence spectroscopy data and MS/MS analysis helped to exclude other potential mechanisms of aggregation, such as dityrosine formation. This suggests that the reaction between two tyrosyl radicals is not favorable under our experimental conditions [49].

In addition to the putative cross-links via a 1,4- or 1,6-type addition mechanism, extensive oxidative modifications of numerous amino acid residues were induced during MCO: Met in positions 1, 36, 62 and 117 were found to be oxidized to sulfoxides. Met1 was also oxidized to a higher oxidation state to form Met sulfone. His oxidation to 2-oxo-His, as observed before in insulin and other proteins exposed to similar oxidative conditions [50], targeted IFN β -1a residues in positions 93, 97, 121, 131 and 140. Moreover, oxidative modification to Asn was detected for His93 and His97.

Unfortunately, we failed to detect reliable spectra for ABS-derivatized peptides derived from oxidized IFN β -1a (unpublished data). This could be attributed to either relatively low abundance of such modifications or further chemical reactions, which may occur during the analysis, thus interfering with the detection based on a mass increase of 179, 196 and 366 Da [27].

Table II demonstrates that not all of the potential targets for MCO were found oxidized. Most of the unmodified amino acids, such as Phe70, Trp79 and Tyr125, are in fact residues which are responsible for stabilizing the hydrophobic core of the molecule through a broad network of hydrogen bonds [7]. This could protect them from MCO and chemical cross-linking. A similar explanation could be given for the relatively low number of detected cross-linked peptides, which is far below the theoretically possible number of cross-links.

Besides the chemical modifications discussed above, based on far-UV CD measurements we noticed that MCO leads to changes in IFN β -1a's secondary

structure resulting in the conversion of alpha helices to disordered structures [29, 51]. Interestingly, this was also seen upon MCO of IFN α -2b [14], but not of IgG1, which has only minor alpha helical content and for which its beta-sheet content seemed to be largely maintained after MCO [16]. Nevertheless, MCO of IgG1 did result in immunogenic aggregates [16], comparable to the observations with IFN α -2b and IFN β -1a. This suggests that the change in secondary structure in oxidized IFN α -2b and IFN β -1a is not a major factor contributing to the immunogenicity of these products. Rather, the combination of covalent aggregation and chemical modifications, which are probably very similar across the different proteins, likely contribute to the immunogenicity of proteins exposed to MCO. The structural changes observed in the present study, i.e. oxidation, conformational changes and aggregation, are comparable to the ones previously measured in IFN α -2b, although at that time a detailed MS/MS analysis was not performed and only Met oxidation was investigated [14]. However, recently DOPA formation in IFN α -2b was measured by our group (unpublished data), and, considering that both interferons share similar structural features, we suggest that the same type of chemical modifications and cross-links could be expected in IFN α -2b.

Conclusion

In this work we mapped the modifications of the primary structure in oxidized and immunogenic aggregates of IFN β -1a, focusing on the amino acids potentially involved in covalent cross-linking. Several oxidative modifications were identified, especially in oxidation prone solvent-exposed amino acids. The primary role of DOPA and DOCH, i.e. Tyr and Phe oxidation products, as electron acceptors for 1,4- or 1,6-type addition, has been confirmed. These results are in agreement with the mechanistic studies previously performed on insulin, and potentially might be extended to other proteins exposed to similar oxidative conditions.

Acknowledgements

The authors thank Dr. Nadya Galeva for performing MS measurements, The University of Kansas and the National Institutes of Health (PO1AG12993) for financial support, and Leiden University Fund/Slingelands (LUF, 1111/19-4-

11\O, SI) and Nederlandse Stichting voor Farmacologische Wetenschappen (NSFW) for travel grants to Riccardo Torosantucci.

References

- [1] C. Kaynor, M. Xin, J. Wakefield, J. Barsoum, X. Q. Qin. Direct evidence that IFN-beta functions as a tumor-suppressor protein. *J. Interferon Cytokine Res.* **2002**, *22*, 1089-1098.
- [2] P. A. Calabresi. Diagnosis and management of multiple sclerosis. *Am. Fam. Physician* **2004**, *70*, 1935-1944.
- [3] L. Runkel, W. Meier, R. B. Pepinsky, M. Karpusas, A. Whitty, K. Kimball, M. Brickelmaier, C. Muldowney, W. Jones, S. E. Goelz. Structural and functional differences between glycosylated and non-glycosylated forms of human interferon-beta (IFN-beta). *Pharm. Res.* **1998**, *15*, 641-649.
- [4] I. Nelissen, E. Martens, P. E. Van Den Steen, P. Proost, I. Ronsse, G. Opdenakker. Gelatinase B/matrix metalloproteinase-9 cleaves interferon-beta and is a target for immunotherapy. *Brain* **2003**, *126*, 1371-1381.
- [5] Y. Kagawa, S. Takasaki, J. Utsumi, K. Hosoi, H. Shimizu, N. Kochibe, A. Kobata. Comparative-Study of the Asparagine-Linked Sugar Chains of Natural Human Interferon-Beta-1 and Recombinant Human Interferon-Beta-1 Produced by 3 Different Mammalian-Cells. *J. Biol. Chem.* **1988**, *263*, 17508-17515.
- [6] H. S. Conradt, H. Egge, J. Peter-Katalinic, W. Reiser, T. Siklosi, K. Schaper. Structure of the carbohydrate moiety of human interferon-beta secreted by a recombinant Chinese hamster ovary cell line. *J. Biol. Chem.* **1987**, *262*, 14600-14605.
- [7] M. Karpusas, M. Nolte, C. B. Benton, W. Meier, W. N. Lipscomb, S. Goelz. The crystal structure of human interferon beta at 2.2-angstrom resolution. *Proc. Natl. Acad. Sci. U.S.A.* **1997**, *94*, 11813-11818.
- [8] M. M. van Beers, M. Sauerborn, F. Gilli, V. Brinks, H. Schellekens, W. Jiskoot. Oxidized and aggregated recombinant human interferon beta is immunogenic in human interferon beta transgenic mice. *Pharm. Res.* **2011**, *28*, 2393-2402.
- [9] M. M. van Beers, M. Sauerborn, F. Gilli, V. Brinks, H. Schellekens, W. Jiskoot. Aggregated recombinant human interferon Beta induces antibodies but no memory in immune-tolerant transgenic mice. *Pharm. Res.* **2010**, *27*, 1812-1824.
- [10] R. A. Rifkin, E. T. Maggio, S. Dike, D. A. Kerr, M. Levy. n-Dodecyl-beta-d-Maltoside Inhibits Aggregation of Human Interferon-beta-1b and Reduces Its Immunogenicity. *J. Neuroimmune Pharmacol.* **2011**, *6*, 158-162.
- [11] M. B. Seefeldt, M. S. Rosendahl, J. L. Cleland, L. K. Hesterberg. Application of high hydrostatic pressure to dissociate aggregates and refold proteins. *Curr. Pharm. Biotechnol.* **2009**, *10*, 447-455.

- [12] A. Bertolotto, S. Malucchi, A. Sala, G. Orefice, P. B. Carrieri, M. Capobianco, E. Milano, F. Melis, M. T. Giordana. Differential effects of three interferon betas on neutralising antibodies in patients with multiple sclerosis: a follow up study in an independent laboratory. *J. Neurol. Neurosurg. Psychiatry* **2002**, *73*, 148-153.
- [13] C. Scagnolari, F. Bellomi, O. Turriziani, F. Bagnato, V. Tomassini, V. Lavalpe, M. Ruggieri, F. Bruschi, G. Meucci, G. Dicunzio, G. Antonelli. Neutralizing and binding antibodies to IFN-beta: relative frequency in relapsing-remitting multiple sclerosis patients treated with different IFN-beta preparations. *J. Interferon Cytokine Res.* **2002**, *22*, 207-213.
- [14] S. Hermeling, L. Aranha, J. M. A. Damen, M. Slijper, H. Schellekens, D. J. A. Crommelin, W. Jiskoot. Structural characterization and immunogenicity in wild-type and immune tolerant mice of degraded recombinant human interferon alpha2b. *Pharm. Res.* **2005**, *22*, 1997-2006.
- [15] S. Hermeling, H. Schellekens, C. Maas, M. F. Gebbink, D. J. Crommelin, W. Jiskoot. Antibody response to aggregated human interferon alpha2b in wild-type and transgenic immune tolerant mice depends on type and level of aggregation. *J. Pharm. Sci.* **2006**, *95*, 1084-1096.
- [16] V. Filipe, W. Jiskoot, A. H. Basmeleh, A. Halim, H. Schellekens. Immunogenicity of different stressed IgG monoclonal antibody formulations in immune tolerant transgenic mice. *MAbs* **2012**, *4*, 740-752.
- [17] R. Torosantucci, O. Mozziconacci, V. Sharov, C. Schöneich, W. Jiskoot. Chemical Modifications in Aggregates of Recombinant Human Insulin Induced by Metal-Catalyzed Oxidation: Covalent Cross-Linking via Michael Addition to Tyrosine Oxidation Products. *Pharm. Res.* **2012**, *29*, 2276-2293.
- [18] C. Gallo-Rodriguez, X. D. Ji, N. Melman, B. D. Siegman, L. H. Sanders, J. Orlina, B. Fischer, Q. Pu, M. E. Olah, P. J. van Galen, et al. Structure-activity relationships of N6-benzyladenosine-5'-uronamides as A3-selective adenosine agonists. *J. Med. Chem.* **1994**, *37*, 636-646.
- [19] R. Torosantucci, B. Kükroer, A. Mero, M. Van Winsen, R. Tantipolphan, W. Jiskoot. Plain and mono-pegylated recombinant human insulin exhibit similar stress-induced aggregation profiles. *J. Pharm. Sci.* **2011**, *100*, 2574-2585.
- [20] C. Giulivi, K. J. Davies. Dityrosine: a marker for oxidatively modified proteins and selective proteolysis. *Methods Enzymol.* **1994**, *233*, 363-371.
- [21] K. Ikehata, T. G. Duzhak, N. A. Galeva, T. Ji, Y. M. Koen, R. P. Hanzlik. Protein targets of reactive metabolites of thiobenzamide in rat liver in vivo. *Chem. Res. Toxicol.* **2008**, *21*, 1432-1442.
- [22] H. Xu, M. A. Freitas. A mass accuracy sensitive probability based scoring algorithm for database searching of tandem mass spectrometry data. *BMC Bioinformatics* **2007**, *8*, 133.

- [23] H. Xu, M. A. Freitas. MassMatrix: a database search program for rapid characterization of proteins and peptides from tandem mass spectrometry data. *Proteomics* **2009**, *9*, 1548-1555.
- [24] H. Xu, L. Yang, M. A. Freitas. A robust linear regression based algorithm for automated evaluation of peptide identifications from shotgun proteomics by use of reversed-phase liquid chromatography retention time. *BMC Bioinformatics* **2008**, *9*, 347.
- [25] H. Xu, L. Zhang, M. A. Freitas. Identification and characterization of disulfide bonds in proteins and peptides from tandem MS data by use of the MassMatrix MS/MS search engine. *J. Proteome Res.* **2008**, *7*, 138-144.
- [26] B. Paizs, S. Suhai. Fragmentation pathways of protonated peptides. *Mass Spectrom. Rev.* **2005**, *24*, 508-548.
- [27] V. S. Sharov, E. S. Dremina, N. A. Galeva, G. S. Gerstenecker, X. Li, R. T. Dobrowsky, J. F. Stobaugh, C. Schöneich. Fluorogenic Tagging of Peptide and Protein 3-Nitrotyrosine with 4-(Aminomethyl)-benzenesulfonic Acid for Quantitative Analysis of Protein Tyrosine Nitration. *Chromatographia* **2010**, *71*, 37-53.
- [28] V. S. Sharov, E. S. Dremina, J. Pennington, J. Killmer, C. Asmus, M. Thorson, S. J. Hong, X. Li, J. F. Stobaugh, C. Schöneich. Selective fluorogenic derivatization of 3-nitrotyrosine and 3,4-dihydroxyphenylalanine in peptides: a method designed for quantitative proteomic analysis. *Methods Enzymol.* **2008**, *441*, 19-32.
- [29] C. E. Bobst, R. R. Abzalimov, D. Houde, M. Kloczewiak, R. Mhatre, S. A. Berkowitz, I. A. Kaltashov. Detection and characterization of altered conformations of protein pharmaceuticals using complementary mass spectrometry-based approaches. *Anal. Chem.* **2008**, *80*, 7473-7481.
- [30] S. M. Kelly, T. J. Jess, N. C. Price. How to study proteins by circular dichroism. *Biochim. Biophys. Acta* **2005**, *1751*, 119-139.
- [31] S. Orru, A. Amoresano, R. Siciliano, R. Napoleoni, O. Finocchiaro, A. Datola, E. De Luca, A. Sirna, P. Pucci. Structural analysis of modified forms of recombinant IFN-beta produced under stress-simulating conditions. *Biol. Chem.* **2000**, *381*, 7-17.
- [32] V. S. Sharov, N. A. Galeva, E. S. Dremina, T. D. Williams, C. Schöneich. Inactivation of rabbit muscle glycogen phosphorylase b by peroxynitrite revisited: does the nitration of Tyr613 in the allosteric inhibition site control enzymatic function? *Arch. Biochem. Biophys.* **2009**, *484*, 155-166.
- [33] R. A. J. O'Hair, G. E. Reid. Neighboring group versus cis-elimination mechanisms for side chain loss from protonated methionine, methionine sulfoxide and their peptides. *Eur. J. Mass Spectrom.* **1999**, *5*, 325-334.
- [34] R. Z. Cheng, S. Kawakishi. Site-specific oxidation of histidine residues in glycosylated insulin mediated by Cu²⁺. *Eur. J. Biochem.* **1994**, *223*, 759-764.
- [35] V. Sadineni, C. Schöneich. Selective oxidation of Zn²⁺ - Insulin catalyzed by Cu²⁺. *J. Pharm. Sci.* **2007**, *96*, 1844-1847.

- [36] S. W. Hovorka, H. Biesiada, T. D. Williams, A. Huhmer, C. Schöneich. High sensitivity of Zn-2+ insulin to metal-catalyzed oxidation: Detection of 2-oxo-histidine by tandem mass spectrometry. *Pharm. Res.* **2002**, *19*, 530-537.
- [37] E. R. Stadtman. Oxidation of free amino acids and amino acid residues in proteins by radiolysis and by metal-catalyzed reactions. *Annu. Rev. Biochem.* **1993**, *62*, 797-821.
- [38] L. B. Anderson, M. Maderia, A. J. Ouellette, C. Putnam-Evans, L. Higgins, T. Krick, M. J. MacCoss, H. Lim, J. R. Yates, 3rd, B. A. Barry. Posttranslational modifications in the CP43 subunit of photosystem II. *Proc. Natl. Acad. Sci. U. S. A.* **2002**, *99*, 14676-14681.
- [39] S. W. Taylor, E. Fahy, J. Murray, R. A. Capaldi, S. S. Ghosh. Oxidative post-translational modification of tryptophan residues in cardiac mitochondrial proteins. *J. Biol. Chem.* **2003**, *278*, 19587-19590.
- [40] G. Palmisano, M. N. Melo-Braga, K. Engholm-Keller, B. L. Parker, M. R. Larsen. Chemical Deamidation: A Common Pitfall in Large-Scale N-Linked Glycoproteomic Mass Spectrometry-Based Analyses. *J. Proteome Res.* **2012**, *11*, 1949-1957.
- [41] K. Koriatopoulou, N. Karousis, G. Varvounis. Novel synthesis of the pyrrolo[2,1-c][1,4]benzodiazocine ring system via a Dieckmann condensation. *Tetrahedron* **2008**, *64*, 10009-10013.
- [42] S. W. Hovorka, J. Y. Hong, J. L. Cleland, C. Schöneich. Metal-catalyzed oxidation of human growth hormone: Modulation by solvent-induced changes of protein conformation. *J. Pharm. Sci.* **2001**, *90*, 58-69.
- [43] Q. Z. Luo, M. K. Joubert, R. Stevenson, R. R. Ketchem, L. O. Narhi, J. Wypych. Chemical Modifications in Therapeutic Protein Aggregates Generated under Different Stress Conditions. *J. Biol. Chem.* **2011**, *286*, 25134-25144.
- [44] S. Li, T. H. Nguyen, C. Schöneich, R. T. Borchardt. Aggregation and precipitation of human relaxin induced by metal-catalyzed oxidation. *Biochemistry* **1995**, *34*, 5762-5772.
- [45] J. R. Requena, D. Groth, G. Legname, E. R. Stadtman, S. B. Prusiner, R. L. Levine. Copper-catalyzed oxidation of the recombinant SHa(29-231) prion protein. *Proc. Natl. Acad. Sci. U. S. A.* **2001**, *98*, 7170-7175.
- [46] R. Rakhit, P. Cunningham, A. Furtos-Matei, S. Dahan, X. F. Qi, J. P. Crow, N. R. Cashman, L. H. Kondejewski, A. Chakrabartty. Oxidation-induced misfolding and aggregation of superoxide dismutase and its implications for amyotrophic lateral sclerosis. *J. Biol. Chem.* **2002**, *277*, 47551-47556.
- [47] N. Rauniyar, L. Prokai. Detection and identification of 4-hydroxy-2-nonenal Schiff-base adducts along with products of Michael addition using data-dependent neutral loss-driven MS3 acquisition: method evaluation through an in vitro study on cytochrome c oxidase modifications. *Proteomics* **2009**, *9*, 5188-5193.
- [48] C. Dohno, A. Okamoto, I. Saito. Stable, specific, and reversible base pairing via Schiff base. *J. Am. Chem. Soc.* **2005**, *127*, 16681-16684.

- [49] Y. Kato, N. Kitamoto, Y. Kawai, T. Osawa. The hydrogen peroxide/copper ion system, but not other metal-catalyzed oxidation systems, produces protein-bound dityrosine. *Free Radic. Biol. Med.* **2001**, *31*, 624-632.
- [50] C. Schöneich. Mechanisms of metal-catalyzed oxidation of histidine to 2-oxo-histidine in peptides and proteins. *J. Pharm. Biomed. Anal.* **2000**, *21*, 1093-1097.
- [51] N. Greenfield, G. D. Fasman. Computed circular dichroism spectra for the evaluation of protein conformation. *Biochemistry* **1969**, *8*, 4108-4116.

Chapter 7

Immune mechanisms underlying immunogenicity of aggregated recombinant human interferon alpha-2a in immune tolerant mice

Melody Sauerborn^{1#}, Riccardo Torosantucci^{2#}, Louis Boon³, Wim Jiskoot², Huub Schellekens^{1,4}, Vera Brinks¹

authors contributed equally

¹Department of Pharmaceutics, Utrecht Institute for Pharmaceutical Sciences (UIPS), Utrecht University, Utrecht, the Netherlands

²Division of Drug Delivery Technology, Leiden Academic Centre for Drug Research (LACDR), Leiden University, Leiden, the Netherlands

³Bioceros, Utrecht, the Netherlands

⁴Department of Innovation and Environmental Sciences, Utrecht University, Utrecht, the Netherlands

Submitted for publication

Abstract

Purpose. To investigate the immune mechanism responsible for the immunogenicity of aggregated recombinant human interferon alpha-2a (rhIFN α) and to study if the presence of aggregated rhIFN β increases rhIFN α 's immunogenicity.

Methods. Transgenic mice immune tolerant for human interferon alpha were treated with native or aggregated rhIFN α . After a washout, the mice were rechallenged with aggregated or native rhIFN α to study immunological memory. Mice depleted from CD4⁺ T-cells were used to test for CD4⁺ T-cell involvement in immunogenicity. Furthermore, the mice were treated with a formulation containing aggregated rhIFN β and native rhIFN α to test whether aggregated rhIFN β acts as an adjuvant for rhIFN α .

Results. Native rhIFN α did not elicit antibodies, demonstrating the immune tolerant status of the transgenic mice. Aggregated rhIFN α was immunogenic in immune tolerant mice but did not induce immunological memory. Blocking CD4⁺ T-cells abolished the antibody response against aggregated rhIFN α . Aggregated rhIFN β did not increase immunogenicity of native rhIFN α .

Conclusions. An atypical immune response with T-cell dependent and T-cell independent characteristics appears to be involved in the formation of antibodies elicited by aggregated rhIFN α , in line with previous results obtained with rhIFN β . Moreover, highly aggregated rhIFN β does not act as adjuvant for native rhIFN α .

Introduction

The number of recombinant human protein drugs entering the market is expanding greatly. Due to their intrinsic low toxicity and high versatility they are excellent drugs to treat various diseases [1]. Nonetheless, protein drugs do have a major disadvantage, namely immunogenicity [2], i.e., during treatment some patients will form anti-drug antibodies (ADAs). Those ADAs can interfere with kinetics, compromise efficacy, lead to infusion reactions and even cause life-threatening side-effects [3-5]. So, immunogenicity poses a serious health risk and increases costs of therapy.

In order to lower immunogenicity, either by developing products with minimal immunogenicity, by adjusting treatment regimen, or by identifying patients at risk, more insight into the underlying immune mechanisms is needed. Immune tolerant mouse models have proven to be very suitable to assess which product-related characteristics, such as aggregates, lead to ADA formation and to study the immune processes responsible for this [6-9]. We have previously shown that for highly aggregated recombinant human interferon beta-1b (rhIFN β , Betaferon®) the immune response leading to ADA formation shares characteristics of both a T-cell independent response, i.e., involvement of marginal zone B-cells and no apparent immunological memory formation, and characteristics of a T-cell dependent immune response, i.e., involvement of CD4⁺ T-cells [10].

The primary aim of this study was to determine if such an atypical immune response would also be responsible for the ADA formation against another highly aggregated and immunogenic protein, metal catalyzed oxidized recombinant human interferon alpha-2a (rhIFN α). We therefore performed a set of experiments in an immune tolerant mouse model for human interferon alpha-2a, in which we studied the presence of an immunological memory response upon rechallenge with either native or aggregated rhIFN α and the involvement of CD4⁺ T-cells in the formation of ADAs. In addition, we studied whether immunogenic, highly aggregated rhIFN β , when mixed with native rhIFN α , would induce or enhance an ADA response against native rhIFN α .

Materials and Methods

Materials

RhIFN α was provided as liquid formulation (1.5 mg/mL in 25 mM ammonium acetate, 120 mM NaCl, acetic acid, pH 5) by Hoffmann-La Roche (Basel, Switzerland). Betaferon[®] (Bayer Schering Pharma AG, Berlin, Germany) was reconstituted with 0.54% NaCl, according to the instructions in the package insert.

Tris, glycine, SDS, L-ascorbic acid, copper (II) chloride, disodium hydrogen phosphate, hydrogen peroxide and EDTA were purchased from Sigma-Aldrich, Schnelldorf, Germany. Slide-A-Lyzer dialysis cassettes, molecular weight cut-off 10 kDa, were purchased from Thermo Fisher Scientific, Breda, the Netherlands. All chemicals were of analytical grade and used without further purification. Deionized water was purified through a Purelab Ultra System (ELGA LabWater Global Operations, Marlow, UK) prior to use. Lithium heparin gel tubes were obtained from Greiner Bio-One B.V. (Alphen aan den Rijn, the Netherlands).

Preparation of native and aggregated rhIFN α formulations

RhIFN α , as received from the provider, was dialyzed against 10 mM sodium phosphate buffer, pH 7.4 (PB). Aggregation of rhIFN α was induced by metal catalyzed oxidation (hereafter refer to as aggregated rhIFN α) [11], performed after dilution of rhIFN α to 0.3 mg/mL, and by subsequent incubation with 40 μ M CuCl₂ (previously prepared in 400 μ M stock solution in PB) for 10 minutes. Subsequently, ascorbate (previously prepared in 400 mM stock solution in PB) was added to a final concentration of 4 mM. After three hours the reaction was quenched by adding 100 mM EDTA (previously dissolved in PB) to a final concentration of 1 mM, as previously reported [12-13]. The aggregated samples were dialyzed using 10 kDa cut-off dialysis cassettes against PB for 24 hours. Both formulations were subsequently characterized for protein concentration and structure (see below).

Mixture of rhIFN α and Betaferon[®]

The mixture of native rhIFN α with Betaferon[®] was obtained by mixing 0.66 mL of rhIFN α (0.15 mg/mL in PB) with 0.33 mL of Betaferon[®] 0.15 mg/mL, yielding final concentrations of 0.1 mg/mL of rhIFN α and 0.05 mg/mL rhIFN β , pH 7.0. The formulation was subsequently analyzed by SEC (size exclusion chromatography) and SDS-PAGE (sodium dodecyl sulfate epolyacrylamide) to verify the non-aggregated state of rhIFN α in the mixture.

Analytical characterization of the formulations

UV/VIS absorption spectroscopy

UV/VIS absorption measurements were performed with an Agilent 8453 UV/VIS spectrophotometer (Waldbronn, Germany), which included a Peltier element for temperature control and a magnetic stirrer. The Peltier element was stirred by an Agilent 89090A controller. Quartz cells with a path length of 1 cm were used for all measurements. Scans were taken from 200-900 nm with 1 nm intervals. The protein concentration was determined by measuring the absorbance at 278.5 nm, using an extinction coefficient (0.1 %; 1 cm; 278.5 nm) of 1.06 [14].

Far-UV circular dichroism (far-UV CD) spectroscopy

Far-UV CD spectra were recorded from 190 to 250 nm using a Jasco J-815 CD spectrometer (Jasco International, Tokyo, Japan). Analyses were performed in a 1-mm path length quartz cuvette at 20 °C using a scan rate of 100 nm/min, a response time of 2 s, and a bandwidth of 1 nm. Each spectrum was the result of an averaging of 6 repeated scans, background corrected with the corresponding buffer spectrum. The CD signals were converted to molar differential extinction coefficient, $\Delta\epsilon$.

Intrinsic steady state fluorescence

Intrinsic fluorescence was measured in 96-well plates using the plate reader unit of the FS920 fluorescence spectrometer (Edinburgh Instruments, Livingston, UK). All the formulations were diluted to a protein concentration of 0.1 mg/ml to avoid inner filter effects. The concentration after dilution was

confirmed with a BCA assay. Tryptophan residues were selectively excited at 295 nm. Emission spectra were recorded from 305 to 500 nm using a step size of 2 nm, gain of 115, Z-position of 20 mm, number of flashes 100 with a frequency of 400 Hz. Triplicates for each sample were analyzed.

Sodium dodecyl sulfate polyacrylamide gel electrophoresis (SDS-PAGE)

Acrylamide gradient gels (4-20%, tris-HCl), were run under reducing (sample buffer containing 5% (v/v) β -mercaptoethanol) and non-reducing (sample buffer without β -mercaptoethanol) conditions at room temperature. The electrophoresis buffer was 25 mM tris(hydroxymethyl)aminomethane, 192 mM glycine, and 0.1% (w/v) SDS. Gel electrophoresis was performed with a Biorad Protean III system (Biorad, Veenendaal, the Netherlands). Samples analyzed under reducing conditions were boiled for 2 min before application to the gel to favor the reduction of disulfide bonds. A low-range molecular weight standard (Biorad) was included on the gel for determination of molecular weight.

Western blotting

Protein bands in SDS-PAGE gels were blotted onto a polyvinylidene difluoride immuno blotting membrane with a mini trans-blot electrophoretic transfer cell (Biorad, Veenendaal, the Netherlands). Blots were blocked for 2 hours at room temperature with 0.1% (w/v) nonfat milk powder in 0.1% (v/v) Tween 20 in phosphate-buffered saline (PBS) with constant orbital shaking. After washing with 0.1% (v/v) Tween 20 in PBS and with water, the blots were incubated with polyclonal rabbit anti-hIFN α (PBL Biomedical Laboratories, Piscataway, NJ, US) in 0.1% (w/v) nonfat milk powder in 0.1% (v/v) Tween 20 in PBS overnight at 4 °C with constant orbital shaking. Blots were washed with 0.1% (v/v) Tween 20 in PBS and with water and further incubated with peroxidase goat anti-rabbit IgG (Sigma-Aldrich) in 0.1% (w/v) nonfat milk powder in 0.1% (v/v) Tween 20 in PBS overnight at 4 °C with constant orbital shaking. Afterwards blots were again washed with 0.1% (v/v) Tween 20 in PBS and with water, and then incubated in a solution of 4-chloro-1-naphtol (Sigma- Aldrich) in methanol (20% (v/v)), water, and H₂O₂ (0.015%

(v/v)). After color development the blots were stored overnight to increase the intensity of the bands.

Size-exclusion chromatography (SEC)

Samples (100 μ g protein/mL) were analyzed by SEC with a TSK-GEL 3000 column (TOSOH BIOSCIENCE GmbH, Stuttgart, Germany), using a mobile phase of 50 mM sodium phosphate and 200 mM sodium chloride, pH 7.2, filtered through a 0.2- μ m filter prior to use, at a flow rate of 0.50 mL/min by a Waters 2695 controller equipped with an autosampler and a Waters 2996 photodiode array detector (Waters, Milford, MA, USA). The column was calibrated by analyzing protein molecular weight standards obtained from Sigma-Aldrich (i.e., thyroglobulin, BSA, ovalbumin, α -chymotrypsin, and myoglobin).

Mouse studies

Breeding

Heterozygous FVB/N transgenic (TG) mice immune tolerant for hIFN α and their non-transgenic (NTG) littermates were bred at the Central Laboratory Animal Institute (Utrecht University, the Netherlands). The genotype of the offspring was determined by PCR showing the presence or absence of the hIFN α gene in chromosomal DNA isolated from ear tissue. Food (Hope Farms, Woerden, the Netherlands) and water (acidified) were available *ad libitum*, and all animal experiments were performed according to Institutional Ethical Committee Regulations of Utrecht University, the Netherlands.

Immunogenicity and immunological memory response

TG and NTG mice were injected intraperitoneally (i.p.) with 10 μ g of native rhIFN α or aggregated rhIFN α (n= 24 per group) for 5 days per week during 3 consecutive weeks (days 0-4, days 7-11 and days 14-18). After an injection-free period of 6 weeks, half of the TG and NTG mice (n=12) were rechallenged with 10 μ g native rhIFN α and the other half (n=12) were rechallenged with 10 μ g aggregated rhIFN α on 2 consecutive days (days 63 and 64). Blood was collected via cheek puncture before the start of the experiment, on different

days during the 3 treatment weeks (days 7, 11, 14 and 18), during washout (days 21, 28 and 42) and before rechallenge (days 56, 58 and 60). At each blood sampling time point, blood was collected before injection to prevent interference of ADA-drug complexes in antibody determination, and was taken from 7 out of 24 mice per group per time point to prevent oversampling. At 13 days after rechallenge (day 77) all mice were sacrificed and blood was isolated. Plasma was obtained from blood after centrifugation in lithium heparin tubes (3000 g, 10 min) and stored at -20 °C until further analysis.

Involvement of CD4⁺ T-cells in the formation of ADAs

TG and NTG mice (n=18 per group) were treated with 10 µg aggregated rhIFN α or 5 µg ovalbumin adsorbed to aluminum hydroxide gel (Sigma-Aldrich BV, Zwijndrecht, the Netherlands) in 100 µl PBS (ova) for 5 days per week during 3 consecutive weeks (days 0-4, days 7-11 and days 14-18). Ova is a T-cell dependent antigen and served as control for a CD4⁺ T-cell immune response. As control for a T-cell independent immune response, TG and NTG mice were treated with Pneumovax[®] (n=18 per group), according to Scheikl and colleagues [15]. Primary i.p. immunization was performed with 1 µg of Pneumovax[®] in 100 µl PBS on day 0, followed by a second i.p. injection with another 1 µg of Pneumovax[®] on day 11.

To study involvement of the CD4⁺ T-cells, half of the mice (n=9 per group) received 3 i.p. injections of rat anti-CD4 antibody GK 1.5 (150 µg in 100 µl PBS) (Bioceros, Utrecht, the Netherlands) before the start of treatment. Depletion was maintained by administration of 150 µg GK 1.5 every 3 to 4 days during the 3 treatment weeks. Blood was collected via cheek puncture before the start of the experiment and during treatment (days 9 and 16) from 3 or 6 mice out of 9. On day 23 all mice were sacrificed and blood was isolated. During the experiment, 2 TG and 2 NTG mice died due to fighting. Numbers of remaining mice can be found in Figure 5.

To confirm depletion of CD4⁺ T cells, additional groups of mice (n=22) were treated with GK 1.5 or PBS following the same procedure as described before. During every treatment week, some of these mice were sacrificed and single-cell suspensions of spleens were tested by flow cytometry for depletion by a non-competing anti-CD4 monoclonal RM4-4 antibody (BD Bioscience, the Netherlands). Measurements were taken using a FACSCanto II[®] (BD

Bioscience) and analysis was performed with the FACSDiva software v6.1.1 (BD Bioscience). Depletion efficiency was on average >95% throughout the experiment (data not shown).

Immunogenicity of rhIFN α when co-administered with Betaferon[®]

TG and NTG mice were injected i.p. with 10 μ g of (i) native rhIFN α , (ii) aggregated rhIFN α , or (iii) the mixture of native rhIFN α and Betaferon[®] (n=6 per group) for 3 weeks, 5 days per week (days 0-4, days 7-11 and days 14-18). Blood was drawn via cheek puncture from 3 out of 6 mice per time point to prevent oversampling, before the start of the experiment and on days 9 and 14. On day 21, all mice were sacrificed and blood was isolated. Plasma was obtained after centrifugation in lithium heparin tubes (3000 g, 10 min) and stored at -20°C until further analysis.

Determination of antibody titers by enzyme-linked immunosorbent assay (ELISA)

Plasma was analyzed for anti-rhIFN α antibodies, anti-rhIFN β antibodies (Betaferon[®]) and anti-ova antibodies by ELISA, as described in detail by Hermeling et al [7, 16]. In the case of Pneumovax[®], anti-pneumococcal polysaccharide antibodies were detected by the following method. Mouse plasma was preadsorbed to pneumococcal cell wall polysaccharide (CWPS) antigens to capture non-specific antibodies against CWPS, a known impurity of the Pneumovax[®] vaccine [15]. In brief, mouse plasma was diluted 1:100 in PBS, mixed with 2 μ g of CWPS and the mixture was incubated for 30 min at room temperature. Adsorbed samples (100 μ l) were added to 0.05 μ g/well Pneumovax[®] coated microtiter plates, which were then incubated for two hours followed by incubation with primary antibody and secondary antibody. After each step plates were washed 3 times with washing buffer (0.05 % (w/v) Tween 20 in PBS). After adding the secondary antibody a color reaction was initiated by adding 3,3',5,5'-tetramethylbenzidine (Roche, Almere, the Netherlands) and stopped after 10 minute incubation time by adding 0.18 M sulfuric acid. Optical density values for all ELISAs were measured at 450 nm wavelength with a microplate reader (Novopath; Biorad, the Netherlands) and data analysis was performed with GraphPad Prism 4.03 software (San Diego,

CA, USA). Samples were defined positive if their mean absorbance values were at least three times higher than the 95th percentile value of negative control plasma. OD450-log dilution plots were fitted to a sigmoidal dose-response curve and the reciprocal of the dilution corresponding to 50% of the maximal signal (EC50 value) was defined as the titer. Negative samples were assigned a titer of 0, and were taken along in data-analyses.

Statistics

For the immunological memory experiment, differences in anti-rhIFN α antibody titers between initial treatments were assessed using a nonparametric Kruskal-Wallis test. The same test was used to assess difference in ADAs before and after rechallenge. First an overall effect of time (before and after rechallenge) was assessed. If this overall effect was significant, further tests were performed to specify which groups differed. For the CD4⁺ T-cell depletion study and co-administration of native rhIFN α and Betaferon[®] experiment also a nonparametric Kruskal-Wallis test was used to assess statistical difference in antibody titers between groups. For all comparisons an overall effect of treatment (all time points combined) was determined; if statistically different, further statistical testing was performed to determine differences in titers per time point. A p value ≤ 0.05 was considered significant.

Results and Discussion

Physicochemical characterization of native rhIFN α , aggregated rhIFN α and the rhIFN α and Betaferon[®] mixture

Two batches of native rhIFN α and aggregated rhIFN α were prepared. Reported analytical data represent the average \pm lower/upper value for the two batches and are summarized in Table I. Our results are in fair agreement with those reported for rhIFN alpha-2b (which contains Arg in position 23 instead of Lys, as in rhIFN alpha-2a used in the present study) by Hermeling et al. [16] and are briefly discussed below.

The mixture of native rhIFN α with Betaferon[®] was prepared in duplicate and analyzed by SEC and SDS-PAGE to verify the monomeric nature of rhIFN α .

Characteristics of native and aggregated rhIFN α

The chromatographic behavior of the aggregated protein indicated a substantial reduction in the monomer content, next to a large fraction of higher molecular weight species, when compared to native rhIFN α , which contained 99% of monomeric protein besides a small amount of dimer according to SEC (Table I). SDS-PAGE showed an apparent molecular weight of about 17 kDa under reducing and non-reducing conditions for native rhIFN α , whereas aggregated rhIFN α was characterized by the presence of higher molecular weight species, which appeared to be mainly mediated by non-reducible covalent bonds (Figure 1, panel a and b). Western blotting indicated that that the aggregated protein still contained native epitopes (Figure 1, panel c).

Table 1. Summary of SEC results and spectroscopic features of rhIFN α and its aggregated form.

Sample	SEC	UV	Far-UV CD	Fluorescence maximum				
	Monomer ¹ (soluble fraction)	OD ratio 280/260 nm	OD at 350 nm	208 nm ($\Delta\epsilon$)	222 nm ($\Delta\epsilon$)	$\Delta\epsilon$ ratio 208/222 nm	λ nm	Intensity (a.u.)
Native rhIFN α	1.1 \pm 0.6	0	1.85 \pm 0.03	0.006 \pm 0.002	-5.34 \pm 0.97	-5.03 \pm 0.96	326 \pm 1	19.7 \pm 0.7
Aggregated rhIFN α	55.3 \pm 8.5	0	1.10 \pm 0.15	0.22 \pm 0.07	-3.12 \pm 1.28	-2.89 \pm 1.16	330 \pm 1	7.9 \pm 1.3

¹ Percentages were calculated based on SEC peak areas relative to the total peak area of native rhIFN α : $AUC_{peak}/AUC_{native, total} \times 100$.

² For the aggregated protein due to the broad overlapping peaks, an exact estimation of the molecular weight of the multimers was not achievable.

³ The insoluble fraction was defined as the fraction that was not recovered by SEC; percentages were calculated from the total peak area in SEC and the total peak area of native rhIFN α : $(AUC_{native, total} - AUC_{sample, total})/AUC_{native, total} \times 100$.

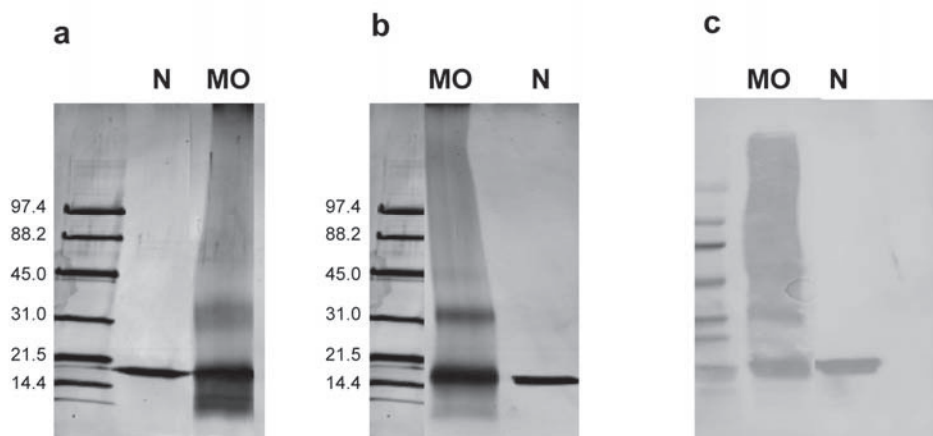


Figure 1. SDS-PAGE of native (N) and aggregated by metal catalyzed oxidation (MO) rhIFN α -2a under (a) reducing conditions and (b) non-reducing conditions, and (c) Western Blotting obtained from a gel run under non-reducing conditions. Numbers on the left indicate molecular weight (kDa) of the markers.

UV spectra of aggregated rhIFN α showed a decrease in the A280/A260 ratio, besides an increase in the optical density at 350 nm, providing further evidence of the presence of aggregates in the stressed formulation via metal catalysis [17]. Intrinsic steady state fluorescence suggested a more hydrophilic environment of the tryptophan residues in the stressed sample, where a lower intensity and a red-shifted spectrum (emission maximum 330 ± 1 nm), was recorded in comparison to the native protein (emission maximum 326 ± 1 nm). Far-UV CD measurements pointed to a decrease in α -helical content for aggregated rhIFN α but no major changes towards other secondary structures, since no statistical difference between the 208/222 nm intensity ratio of native and stressed rhIFN α was measured (Table I).

Characteristics of the rhIFN α and Betaferon[®] mixture

The association state of rhIFN α in the formulation containing rhIFN α and Betaferon[®] was investigated by SEC. The chromatograms show that rhIFN α was maintained in its monomeric state (Figure 2). Furthermore, no changes in the soluble fraction of Betaferon[®] were observed before and after the addition of rhIFN α (Figure 2), highlighting that mixing of rhIFN α with rhIFN β did not lead to major changes in the aggregation status of either of the two proteins.

Using SDS-PAGE, it was confirmed that rhIFN α recovered from the rhIFN α and Betaferon[®] mixture, was indeed in its monomeric non-aggregated state, as demonstrated by the detection of a single band with the same molecular weight of native rhIFN α (data not shown). Similarly, Betaferon[®] alone and in combination with rhIFN α showed similar bands. Based on Western blotting, native rhIFN α and rhIFN α recovered from the combined rhIFN α and Betaferon[®] solution (not shown) contained intact epitopes.

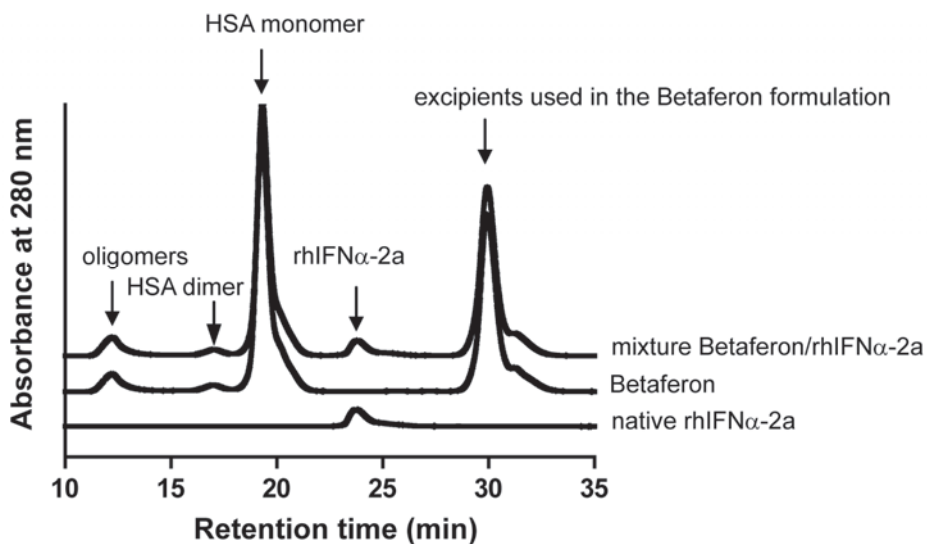


Figure 2. SEC of native rhIFN α , Betaferon and the mixture Betaferon/rhIFN α . The identity of the peaks from left to right is: oligomers, HSA dimer, HSA monomer, rhIFN α -2a, excipients used in the Betaferon formulation. Note that no rhIFN β peak could be identified, probably because the protein is highly aggregated [18].

Mouse studies

Immunogenicity of native and aggregated rhIFN α

TG and NTG mice were treated with either native rhIFN α or aggregated rhIFN α for 3 weeks followed by a treatment-free period of 6 weeks (washout). Native rhIFN α caused an ADA response in all NTG mice (Figure 3a), while it was very poorly immunogenic in the TG mice (2 out of 24 mice had detectable antibody levels, each at only 2 time points (t= 18 and t=42 days), illustrating the immune tolerant status of these mice towards rhIFN α . Since the two TG mice with detectable antibody levels displayed similar antibody responses as the NTG mice at only two time points, the antibody titers were considered statistical outliers and these two mice were excluded from further analyses.

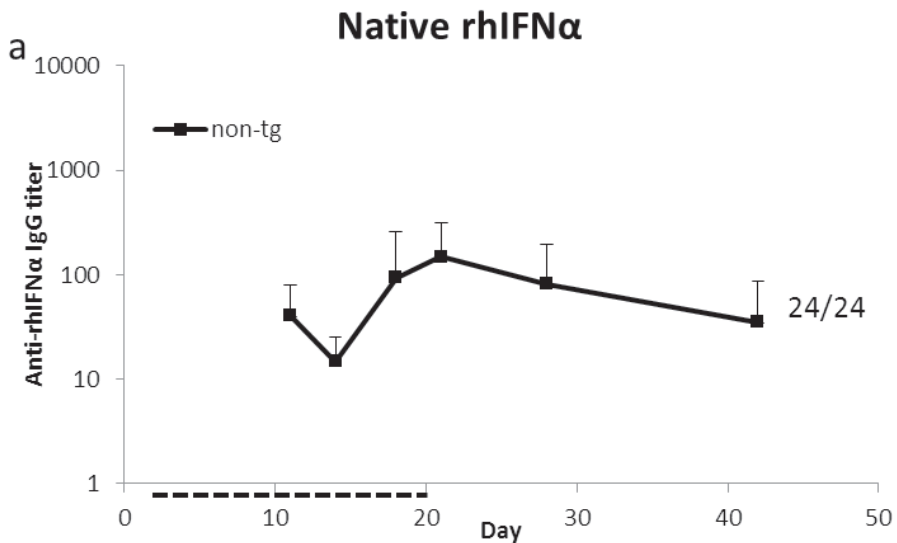


Figure 3a. Anti-rhIFN α IgG titers of NTG (non-tg, black lines) mice treated with native rhIFN α during the initial three treatment weeks (dashed line below x-axis) and washout period. Two out of 24 TG mice treated with native rhIFN α showed detectable antibody titers on days 18 and 42, these mice were considered outliers and are not presented. The number of antibody positive mice out of the total number of mice per group is given. Data represent mean + standard deviation per time point (n= 24).

In contrast, aggregated rhIFN α caused an antibody response in both the NTG (22 out of 24 responders) and TG mice (21 out of 24 responders) (Figure 3b). For the NTG mice, treatment with aggregated rhIFN α gave higher titers than treatment with native rhIFN α ($p=0.002$, Figure 3).

These results show that native rhIFN α is poorly immunogenic in the TG mice and that by aggregation immunogenicity is strongly enhanced. This corresponds to our previous findings with recombinant human interferon alpha-2b [16, 19], and to our recent results with human monoclonal IgG [8], showing that metal catalyzed oxidation of therapeutic proteins results in aggregation and enhanced immunogenicity.

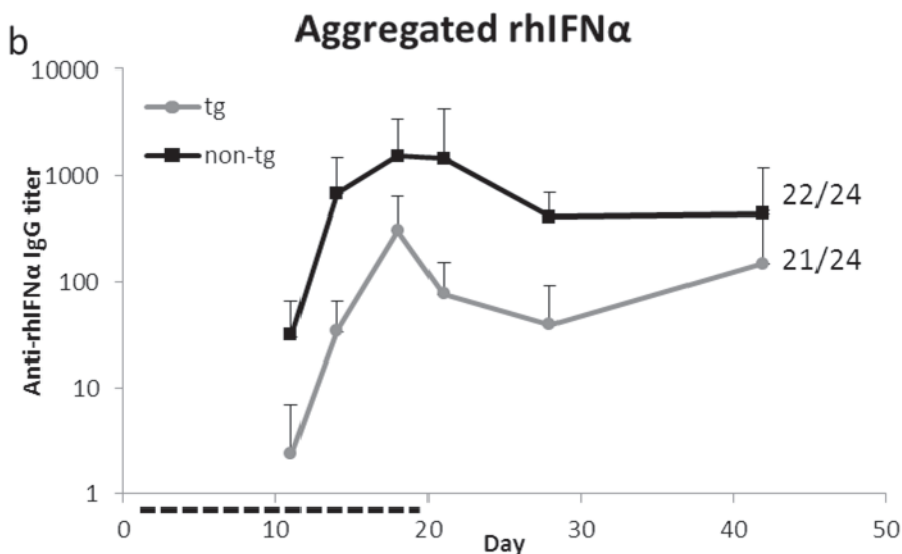


Figure 3b. Anti-rhIFN α IgG titers of TG (tg, grey lines) and NTG (non-tg, black lines) mice treated with aggregated rhIFN α during the initial three treatment weeks (dashed line below x-axis) and washout period. The number of antibody positive mice out of the total number of mice per group is given. Data represent mean + standard deviation per time point ($n=24$).

Immunological memory response

NTG mice displayed low antibody titers before rechallenge independent of the initial treatment, while TG mice had detectable titers before rechallenge only when initially treated with aggregated rhIFN α (Figure 4). NTG mice initially treated with native rhIFN α showed increased antibody levels after rechallenge with native and aggregated rhIFN α (overall effect, $p=0.038$, Figure 4, panel a). This was most apparent in NTG mice initially treated and rechallenged with native rhIFN α , ($p<0.001$). NTG mice initially treated with aggregated rhIFN α had higher antibody titers after rechallenge with both rhIFN α products (overall effect $p<0.001$, Figure 4, panel b); this effect was most pronounced in mice rechallenged with aggregated rhIFN α ($p=0.004$). In TG mice initially treated with aggregated rhIFN α , no statistically significant increase in antibody titers was present upon rechallenge with native or aggregated rhIFN α (overall effect, $p=0.077$, Figure 4, panel b).

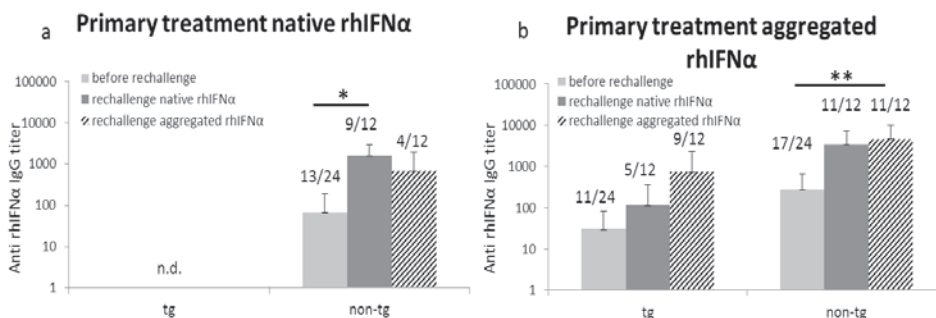


Figure 4. Anti-rhIFN α IgG titers of TG (tg) and NTG (non-tg) mice receiving primary treatment with native rhIFN α (a) and aggregated rhIFN α (b). Bars show titers before rechallenge (light grey) and after rechallenge with native rhIFN α (dark grey) or with aggregated rhIFN α (striped). Data represent mean + standard deviation. Above each bar the number of antibody positive mice out of the total number of mice per group is given. * indicates $p<0.05$. ** indicates $p<0.01$. n.d.=not detectable.

These results suggest that for NTG mice a memory response is present when either native or aggregated rhIFN α is given as primary treatment, and when either of the two products is given during rechallenge. Interestingly, antibody titers after rechallenge appear to be higher when the same product is given during initial treatment and rechallenge. This indicates that there is some

level of specificity in the immunological memory response and that there are distinct features in native or aggregated rhIFN α responsible for this specificity. This could be due to differences in exposed epitopes between aggregated and native rhIFN α and/or to the formation of new epitopes in aggregated rhIFN α as a result of the oxidation; it was recently shown for insulin that the same oxidation mechanism used to create rhIFN α aggregates leads to numerous chemical changes and cross-links in insulin [13].

For the TG mice there was no statistically significant immunological memory response observed, although there is a trend towards increased antibody levels after rechallenge (Figure 4, panel b). This apparent lack of immunological memory is similar to our previous observations with rhIFN β in immune tolerant mice for hIFN β [10]. However, studies assessing the presence of memory T- and B-cells should be performed to provide more definite proof on the presence or absence of immunological memory formation.

Involvement of CD4⁺ T-cells in the formation of ADAs

To study whether CD4⁺ T-cells are involved in the antibody response against aggregated rhIFN α , TG and NTG mice depleted from their CD4⁺ T-cells were treated with aggregated rhIFN α (Figure 5, panel a). Control groups of TG and NTG mice were treated with ova (a T-cell dependent antigen, Figure 5, panel b) or Pneumovax[®] (a T-cell independent antigen, Figure 5, panel c). CD4⁺ T-cell depletion in both TG and NTG mice treated with aggregated rhIFN α resulted in an almost abolished antibody response (overall effect, p=0.009 for TG and p=0.003 for NTG) with most apparent effects at the end of testing. Only 1 out of 8 NTG mice showed detectable antibody levels after depletion. As expected, CD4⁺ T-cell depletion also diminished antibody titers against the T-cell dependent antigen ova in both TG and NTG mice (overall effect p<0.001 for both), while the antibody response against the T-cell independent antigen Pneumovax[®] remained unaffected (overall effect p=0.408 for TG and p=0.741 for NTG).

These results indicate that the antibody response against aggregated rhIFN α is dependent on CD4⁺ T-cells. Together with the previous observation of an apparent lack of immunological memory, it appears that the immune mechanisms underlying immunogenicity of aggregated rhIFN α resemble the mechanisms underlying immunogenicity of Betaferon[®] [10]; both appear to lack

immunological memory and both involve CD4⁺ T-cells. However, it has to be noted that for the antibody response against Betaferon[®], early involvement of marginal zone B-cell in particular led to the hypothesis of a T-cell independent trigger of immunogenicity, and of ancillary T-cell involvement in actual antibody production [10].

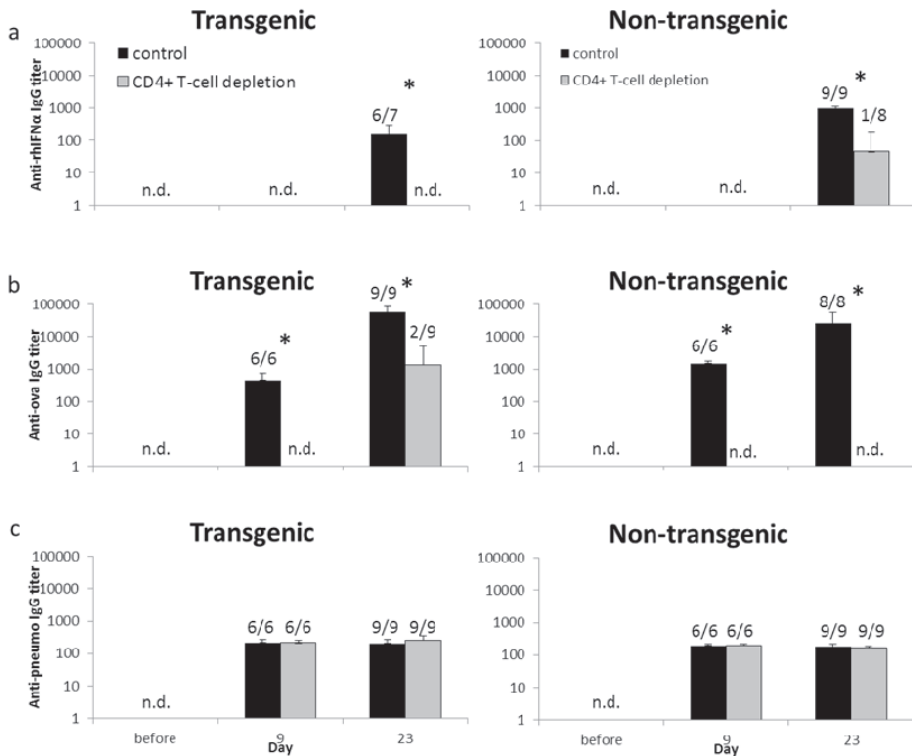


Figure 5. Total anti-rhIFN β IgG titers (a), total anti-ova IgG titers (b) and total anti-pneumo IgG titers (c) of TG and NTG mice treated with aggregated rhIFN α , ovalbumin or Pneumovax[®], respectively. Data represent mean + standard deviation per time point. Above each bar the number of antibody positive mice out of the total number of sampled mice per group is given. Black bars represent control mice with CD4⁺ T-cells, grey bars indicate mice depleted from CD4⁺ T-cells. * shows statistical difference in antibody titers between control mice and mice without CD4⁺ T-cells ($p < 0.05$). n.d.= not detectable.

Nonetheless, this is the first study showing that the immune mechanisms underlying immunogenicity of two highly aggregated proteins might be comparable. Moreover, this and the previous study [10] indicate the importance of clinical studies looking into the immune mechanisms in humans involved in immunogenicity of therapeutic proteins. Sparse patient data on re-induction of treatment with interferon beta and monoclonal antibodies indicate that immunological memory might also be absent in patients [20], but this needs to be confirmed in larger patient cohorts.

Immunogenicity of rhIFN α when co-administered with Betaferon[®]

TG and NTG mice were treated with either native rhIFN α , aggregated rhIFN α or the combined rhIFN α and Betaferon[®] solution. Figure 6 shows the corresponding anti-rhIFN α IgG titers of the TG and NTG mice. For the TG mice, only aggregated rhIFN α was capable of inducing ADAs (overall effect $p < 0.0001$, Figure 6a), which was most apparent on day 21. Native rhIFN α and the combined rhIFN α and Betaferon[®] solution did not cause detectable ADA formation in these mice.

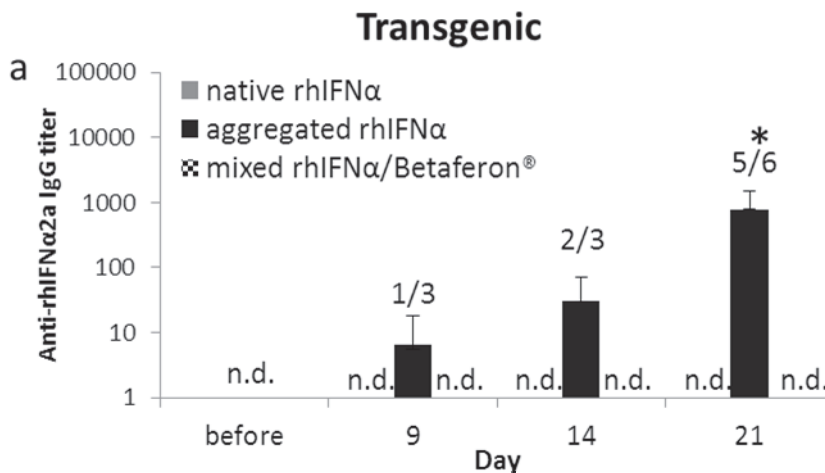


Figure 6a. Anti-rhIFN α IgG titers of TG mice treated with either native rhIFN α (grey bars), aggregated rhIFN α (black bars) or the mixture of rhIFN α /Betaferon[®] (black and white pattern). Above each bar the number of antibody positive mice out of the total number of sampled mice per group is given. Data represent mean + standard deviation per time point. * indicates $p < 0.05$ between the three treatment groups. n.d = not detectable.

For the NTG mice (Figure 6b) ADAs were formed for all 3 treatments, however no differences in ADA titers between treatments were found ($p=0.122$). This confirms some of our previous studies [19] in which NTG mice, in contrast to TG mice, could not discriminate between poorly and highly immunogenic formulations.

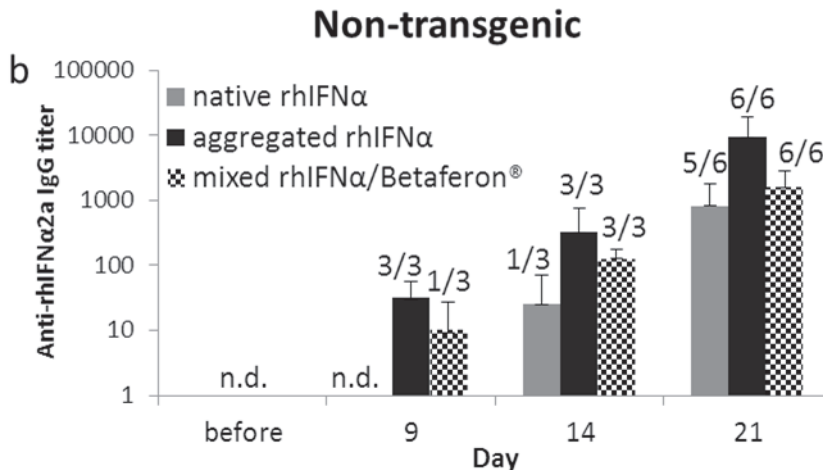


Figure 6b. Anti-rhIFN α IgG titers of NTG mice treated with either native rhIFN α (grey bars), aggregated rhIFN α (black bars) or the mixture of rhIFN α /Betaferon $^{\circledR}$ (black and white pattern). Above each bar the number of antibody positive mice out of the total number of sampled mice per group is given. Data represent mean + standard deviation per time point. n.d. = not detectable.

Both TG and NTG mice treated with combined rhIFN α and Betaferon $^{\circledR}$ solution formed antibodies against rhIFN β (data not shown), confirming that immune tolerance was specific for rhIFN α .

These findings show that Betaferon $^{\circledR}$ does not trigger immunogenicity of rhIFN α , although it causes the formation of anti- rhIFN β antibodies. It can therefore be concluded that activation of the immune pathways involved in immunogenicity of Betaferon $^{\circledR}$ does not lower the threshold for immunogenicity of native rhIFN α . Betaferon $^{\circledR}$ is therefore not functioning as adjuvant. It would be interesting to study if the lack of stimulatory effect by Betaferon $^{\circledR}$ is also applicable to other therapeutic proteins, and if well-known

adjuvants are actually capable of enhancing immunogenicity of native rhIFN α and other non-immunogenic proteins in the immune tolerant mouse model.

In the current experiment we co-administered the two protein species in one formulation, however they were not chemically linked, as was confirmed by SEC (Figure 2). Several studies have shown that depending on the immunostimulatory molecules, linkage might be important in exerting their effect [21-22]. It might therefore be worth studying immunogenicity of rhIFN α when covalently bound to immunogenic rhIFN β aggregates.

Conclusion

The immune mechanisms underlying immunogenicity of aggregated rhIFN α resemble the immune mechanisms underlying immunogenicity of Betaferon[®]; an apparent lack of immunological memory and involvement of CD4⁺ T-cells. Immunogenic and highly aggregated Betaferon[®] does not act as adjuvant for non-immunogenic rhIFN α .

References

- [1] B. Leader, Q. J. Baca, D. E. Golan. Protein therapeutics: a summary and pharmacological classification. *Nat. Rev. Dru. Discov.* **2008**, *7*, 21-39.
- [2] M. D. Barbosa, E. Celis. Immunogenicity of protein therapeutics and the interplay between tolerance and antibody responses. *Drug Discov. Today* **2007**, *12*, 674-681.
- [3] G. M. Bartelds, C. A. Wijbrandts, M. T. Nurmohamed, S. Stapel, W. F. Lems, L. Aarden, B. A. Dijkmans, P. P. Tak, G. J. Wolbink. Anti-infliximab and anti-adalimumab antibodies in relation to response to adalimumab in infliximab switchers and anti-tumour necrosis factor naive patients: a cohort study. *Ann. Rheum. Dis.* **2010**, *69*, 817-821.
- [4] M. K. de Vries, E. Brouwer, I. E. van der Horst-Bruinsma, A. Spoorenberg, J. C. van Denderen, A. Jamnitski, M. T. Nurmohamed, B. A. Dijkmans, L. A. Aarden, G. J. Wolbink. Decreased clinical response to adalimumab in ankylosing spondylitis is associated with antibody formation. *Ann. Rheum. Dis.* **2009**, *68*, 1787-1788.
- [5] H. Schellekens. Immunologic mechanisms of EPO-associated pure red cell aplasia. *Best Pract. Res. Clin. Haematol.* **2005**, *18*, 473-480.
- [6] M. M. van Beers, M. Sauerborn, F. Gilli, S. Hermeling, V. Brinks, H. Schellekens, W. Jiskoot. Hybrid transgenic immune tolerant mouse model for assessing the breaking of B cell tolerance by human interferon beta. *J. Immunol. Methods* **2010**, *352*, 32-37.

- [7] S. Hermeling, W. Jiskoot, D. Crommelin, C. Bornaes, H. Schellekens. Development of a transgenic mouse model immune tolerant for human interferon Beta. *Pharm. Res.* **2005**, *22*, 847-851.
- [8] V. Filipe, W. Jiskoot, A. H. Basmeh, A. Halim, H. Schellekens. Immunogenicity of different stressed IgG monoclonal antibody formulations in immune tolerant transgenic mice. *MAbs.* **2012**, *4*, 740-752
- [9] V. Brinks, W. Jiskoot, H. Schellekens. Immunogenicity of Therapeutic Proteins: The Use of Animal Models. *Pharm. Res.* **2011**, *28*, 2379-2385.
- [10] M. Sauerborn, M. M. van Beers, W. Jiskoot, G. M. Kijanka, L. Boon, H. Schellekens, V. Brinks. Antibody Response Against Betaferon(R) in Immune Tolerant Mice: Involvement of Marginal Zone B-cells and CD4⁺ T-cells and Apparent Lack of Immunological Memory. *J. Clin. Immunol* **2013**, *33*, 255-263.
- [11] E. R. Stadtman. Metal ion-catalyzed oxidation of proteins: biochemical mechanism and biological consequences. *Free Radic. Biol. Med.* **1990**, *9*, 315-325.
- [12] R. Torosantucci, B. Kükler, A. Mero, M. Van Winsen, R. Tantipolphan, W. Jiskoot. Plain and mono-pegylated recombinant human insulin exhibit similar stress-induced aggregation profiles. *J. Pharm. Sci.* **2011** *100*, 2574-2585.
- [13] R. Torosantucci, O. Mozziconacci, V. Sharov, C. Schöneich, W. Jiskoot. Chemical Modifications in Aggregates of Recombinant Human Insulin Induced by Metal-Catalyzed Oxidation: Covalent Cross-Linking via Michael Addition to Tyrosine Oxidation Products. *Pharm. Res.* **2012**, *29*, 2276-93 .
- [14] T. A. Bewley, H. L. Levine, R. Wetzel. Structural Features of Human-Leukocyte Interferon-a as Determined by Circular-Dichroism Spectroscopy. *Int. J. Pept. Prot. Res.* **1982**, *20*, 93-96.
- [15] T. Scheikl, B. Reis, K. Pfeffer, B. Holzmann, S. Beer. Reduced notch activity is associated with an impaired marginal zone B cell development and function in Sly1 mutant mice. *Mol. Immunol.* **2009**, *46*, 969-977.
- [16] S. Hermeling, L. Aranha, J. M. Damen, M. Slijper, H. Schellekens, D. J. Crommelin, W. Jiskoot. Structural characterization and immunogenicity in wild-type and immune tolerant mice of degraded recombinant human interferon alpha2b. *Pharm. Res.* **2005**, *22*, 1997-2006.
- [17] C. R. M. L. A. Kuelzto, in *Methods for Structural Analysis of Protein Pharmaceuticals, Vol. 3* (Ed.: D. J. A. C. W. Jiskoot), AAPS, **2005**.
- [18] M. M. van Beers, W. Jiskoot, H. Schellekens. On the role of aggregates in the immunogenicity of recombinant human interferon beta in patients with multiple sclerosis. *J. Interferon Cytokine Res.* **2010**, *30*, 767-775.
- [19] S. Hermeling, H. Schellekens, C. Maas, M. F. Gebbink, D. J. Crommelin, W. Jiskoot. Antibody response to aggregated human interferon alpha2b in wild-type and transgenic immune tolerant mice depends on type and level of aggregation. *J. Pharm. Sci.* **2006**, *95*, 1084-1096.

- [20] S. Ben-Horin, Y. Mazor, H. Yanai, Y. Ron, U. Kopylov, M. Yavzori, O. Picard, E. Fudim, Y. Maor, A. Lahat, D. Coscas, R. Eliakim, I. Dotan, Y. Chowers. The decline of anti-drug antibody titres after discontinuation of anti-TNFs: implications for predicting re-induction outcome in IBD. *Aliment. Pharmacol. Ther.* **2012**, *35*, 714-722.
- [21] A. M. Cuesta, E. Suarez, M. Larsen, K. B. Jensen, L. Sanz, M. Compte, P. Kristensen, L. Alvarez-Vallina. Enhancement of DNA vaccine potency through linkage of antigen to filamentous bacteriophage coat protein III domain I. *Immunology* **2006**, *117*, 502-506.
- [22] B. Slutter, P. C. Soema, Z. Ding, R. Verheul, W. Hennink, W. Jiskoot. Conjugation of ovalbumin to trimethyl chitosan improves immunogenicity of the antigen. *J. Control Release* **2010**, *143*, 207-214.

Chapter 8

Development of a transgenic mouse model to study the immunogenicity of recombinant human insulin

Riccardo Torosantucci¹, Vera Brinks², Grzegorz Kijanka², Liem Andhyk Halim², Melody Sauerborn², Huub Schellekens² and Wim Jiskoot¹

¹Division of Drug Delivery Technology, Leiden Academic Centre for Drug Research (LACDR), Leiden University, Leiden, the Netherlands.

²Department of Pharmaceutics, Utrecht Institute for Pharmaceutical Sciences (UIPS), Utrecht University, Utrecht, the Netherlands.

Submitted for publication

Abstract

Mouse models are increasingly used to assess the immunogenicity of recombinant human (rh) therapeutic proteins and to investigate the immunological processes leading to anti-drug antibodies (ADAs). In 1994 a transgenic (TG) mouse model for studying the immunogenicity of insulin variants was described (Ottesen et al., *Diabetologia* 37:1178-1185). However, this model requires the use of complete Freund's adjuvant (CFA), which changes the formulation and thus limits its applicability for studying the effect of formulation-related factors on immunogenicity. The aim of this work was to develop an adjuvant-free TG mouse model for evaluating the immunogenicity of rh insulin (insulin) formulations. Intraperitoneal administration of insulin (20 µg/dose, 12 doses over a period of 4 weeks) did not break the immune tolerance of the TG mice, whereas it did elicit antibodies in non transgenic (NTG) mice. This tolerance in TG mice could be circumvented by insulin covalently bound to 50 nm polystyrene nanoparticles as well as by oxidized and aggregated insulin and to a lesser extent by commercially available insulin products.

Introduction

With the development of recombinant DNA technology it has become possible to produce well-defined recombinant human (rh) therapeutic proteins [1-2]. Despite the fact that these proteins are structurally very similar to their endogenous counterparts, almost all rh proteins for therapeutic use are immunogenic [3-4].

Many factors influence the immunogenicity of a protein drug, which can be categorized into patient-dependent (e.g., type of disease, genetic background), treatment-dependent (e.g., dose, dosing schedule, route of administration, co-medication) and product-dependent factors [5-6]. An increasing number of publications support aggregation of therapeutic proteins as one of the major product-related factors influencing immunogenicity [7-8].

For rh interferon alpha (IFN α) and rh interferon beta (IFN β), transgenic immune tolerant mouse models have been shown to be a valuable tool to study the product-related factors contributing to the immunogenicity and the underlying mechanisms [9-11]. For human insulin, the first transgenic (TG) mouse model was described in 1994 by Ottensen et al. [12] to study the impact of the modifications of the insulin sequence on the formation of new epitopes.

However, while they used complete Freund's adjuvant (CFA) to trigger the immune system, we prefer CFA free models to study formulation-related factors because the addition of CFA alters the formulation, CFA may affect protein's structure (unpublished observation from our lab) and likely affects the biodistribution of the protein.

The primary aim of this work was to create a CFA free TG mouse model to study the immunogenicity of rh insulin (insulin) formulations. Next, to study the applicability of the mouse model, we compared the immunogenicity of oxidized and aggregated insulin, oxidized non-aggregated insulin, and three different commercially available formulations of insulin variants (i.e. Levemir[®], Insulatard[®], Actrapid[®]).

Materials and Methods

Materials

Insulin containing 0.4% (w/w) zinc ions was provided by Merck (Oss, the Netherlands). Three commercially available insulin formulations, i.e.

Insulatard® (long acting insulin suspension obtained with zinc and protamine), Levemir® (long acting insulin modified on Lys B 29 with a fatty acid) and Actrapid® (neutral unmodified insulin solution) were a gift from the Leiden University Medical Center. Copper(II) chloride, ascorbic acid, ethylenediamine tetraacetic acid (EDTA), ammonium bicarbonate (ABI), sodium citrate, citric acid, arginine, disodium hydrogen phosphate, n-hydroxysulfosuccinimide sodium salt (NHS-sulfo), 1-(3-dimethylaminopropyl)-3-ethylcarbodiimide HCl (EDAC), 2-N-morpholinoethanesulfonic acid (MES), were bought from Sigma-Aldrich (Schnelldorf, Germany). Glacial acetic acid and acetonitrile were purchased from Boom (Meppel, the Netherlands). 3.5 kDa Slide-A-Lyzer dialysis cassettes were purchased from Thermo Fisher Scientific (Etten-Leur, the Netherlands). Polystyrene nanoparticles (NP), (diameter 50 nm) that contain surface carboxyl groups, were purchased from Polysciences GmbH (Eppelheim, Germany). All chemicals were of analytical grade and used without further purification. Deionized water was purified through a Purelab Ultra System (ELGA LabWater Global Operations, Marlow, UK) prior to use.

Preparation of unmodified insulin solutions

Insulin solutions of 1 mg/mL were prepared by dissolving insulin in 0.1 M HCl. Subsequently, 50 mM sodium phosphate buffer (PB), pH 7.4, was added up to 1 mL and the pH adjusted to 7.4. The concentration was calculated by UV spectroscopy, using a molecular weight of 5.8 kDa and an extinction coefficient of $6200 \text{ M}^{-1} \text{ cm}^{-1}$ at 276 nm [13]. Insulatard®, Levemir® and Actrapid® were diluted to 0.2 mg/mL with PB, prior to injection.

Preparation of oxidized aggregated and oxidized non-aggregated insulin

Oxidized and aggregated insulin (PB-MCO) was prepared as previously reported [14]. To obtain oxidized non-aggregated insulin, metal catalyzed oxidation (MCO, via the oxidative system Cu^{2+} /ascorbate) was performed in 50 mM sodium citrate buffer, pH 3.0 (CB) for 3 hours at room temperature. To this end, insulin solution of 1 mg/mL was prepared by dissolving insulin directly in CB. MCO was performed by addition to 1 mL of 1 mg/mL insulin, 100 μL of 0.4 mM CuCl_2 in CB to a final concentration of 40 μM . The reaction

was performed in 2-mL Eppendorf tubes covered with aluminum foil to protect the reaction mixture from light. After 10 min of incubation of insulin with Cu^{2+} , to allow copper to bind to insulin, the oxidation reaction was started by the addition of 11 μL of 400 mM ascorbic acid in CB to a final concentration of 4 mM. The reaction was quenched after 3 h of incubation at room temperature by adding 11.2 μL of a 100 mM EDTA in CB, pH 3 to a final concentration of 1mM. The oxidized sample was extensively dialyzed at 4 °C against CB. Next, a second dialysis against 250 mM ammonium bicarbonate (ABI) buffer, pH 8.0, for 24 h, was performed. These procedures, as previously reported [14], prevented insulin aggregation. Further we will refer to this oxidized non-aggregated insulin as ABI-MCO.

Preparation of insulin covalently bound to 50 nm polystyrene nanoparticles

Insulin was covalently bound onto 50-nm polystyrene nanoparticles (NP) following the procedure described by Kalkanidis et al [15]. Briefly, to prepare 9.00 mL of 1 mg/mL covalently bound insulin, 3.6 mL of NP (2.5 % w/v, aqueous suspension) were suspended in 2.25 mL of 0.2 M MES. Then 1.125 mL of 28.80 mg/mL EDAC in water, were added dropwise over a period of 10 minutes. After that, 1.125 mL of 360 mM NHS-sulfo in water, were added and the reaction mixture was left to equilibrate for 2 hours at room temperature on a rotating plate (final pH was 6.0). After 2 hours, the pH was brought to 6.9-7.0 with 1 M NaOH and 900 μL of 10 mg/mL insulin in PB pH 7.0 were dissolved in the mixture (final insulin concentration was 1 mg/mL, pH 7.0). Coupling was carried out overnight at room temperature before 24 hours dialysis against 50 mM PB, pH 7.4 (further we will refer to this suspension as NP-ins). In order to verify whether insulin was covalently bound to the NP or only adsorbed, an insulin control (hereafter called insulin adsorbed on NP (ADS-ins)) was prepared following a similar procedure but without NHS-sulfo and without EDAC. Because of the nature of the reagents (NHS-sulfo and EDAC), carboxylic groups in insulin can be potentially activated during coupling with NP. Hence, a second control (hereafter called cross-linked insulin (CR-ins)) was prepared in the same way as described above for the preparation of NP-ins, but without the addition of NP.

SDS-PAGE

Acrylamide gradient gels (10-20% tris-tricine, Bio-Rad, Veenendaal, the Netherlands) were run under reducing and non-reducing condition as described before [16]. The cathode electrophoresis buffer was 0.1 M tris(hydroxymethyl) aminomethane, 0.1 M tricine, and 3 mM SDS, pH 8.3. The anode electrophoresis buffer was 0.1 M Tris pH 8.9. Gel electrophoresis was performed with a Biorad Protean III system (Biorad). Samples were boiled for 2 min before application to the gel. A polypeptide marker solution (Biorad) was included for determination of the molecular weight.

Centrifugation

Centrifugation in presence of SDS was performed prior to size exclusion chromatography (SEC) analysis for NP-ins and ADS-ins (not CR-ins, which was centrifuged as described below), to investigate the amount of insulin adsorbed and covalently bound, calculated by comparison with native insulin. 2 mL of NP-ins and ADS-ins (final insulin concentration 1 mg/mL), were loaded into Ultra-Clear centrifuge tubes (1/2 x 2 in., 13 x 51 mm, Beckman Coulter, Inc, Brea, CA), in presence of 20 mg SDS (i.e., 1% w/v SDS). Native insulin, 2 mL of 1 mg/mL, was loaded in another tube without SDS. Next, the tubes were centrifuged with a BECKMAN Titanium Centrifuge Type 70 Ti (Ultra Fixed Angle Rotor) for 30 minutes at 50000 rpm, (250000 g). (Beckman Coulter, Fullerton, CA). Supernatant was diluted two-fold in 50 mM PB, pH 7.4, prior to SEC analysis. CR-ins was centrifuged for 10 minutes, 4 °C at 16162 g with a bench centrifuge (Sigma 1-15 bench centrifuge, Shropshire, UK), without SDS, to remove insoluble aggregates that might block the SEC column.

Size exclusion chromatography (SEC)

SEC experiments were performed using an Agilent 1200 HPLC system (Agilent Technologies, Palo Alto, CA, USA), consisting of a 1200 series HPLC pump, degasser, autosampler G1329A, and a variable wavelength detector G1316A. The SEC eluent was composed of a mixture of 1 g/L arginine in water:acetonitrile:glacial acetic acid 65:20:15 (v/v/v), as described in the United States and European Pharmacopoeias [17-18], and chromatograms were acquired using UV absorption at 276 nm.

Dynamic light scattering (DLS)

DLS measurements were performed with a Malvern Zetasizer Nano ZS (Malvern, Herrenberg, Germany) equipped with a 633-nm He-Ne laser and operating at an angle of 173°. The software used to collect and analyze the data was the Dispersion Technology Software version 6.01 from Malvern. Each sample, containing 5 µl of NP, NP-ins or ADS-ins, diluted with 495 µl water, was measured in single-use polystyrene half-micro cuvettes (Fisher Emurgo, Landsmeer, The Netherlands). Water as a dispersant (viscosity 0.8872 cP and RI 1.330) was used to measure different formulations of nanoparticles, mentioned above. To measure plain insulin, 500 µl of 10 mg/mL human insulin in 50 mM PB, pH 7.4, and PB as a solvent (viscosity 1.0200 cP and RI 1.335) was used. The measurements were made at a position of 4.65 mm from the cuvette wall with an automatic attenuator and at a controlled temperature of 25°C. For each sample, 15 runs of 10 s were performed, with three repetitions. The intensity size distribution, the Z-average diameter (Z-ave) and the polydispersity index (PDI) were obtained from the autocorrelation function using the “general purpose mode”. The default filter factor of 50% and the default lower threshold of 0.05 and upper threshold of 0.01 were used.

Circular dichroism spectroscopy (CD)

Far-UV CD measurements were performed as previously described [16].

Mouse studies

Breeding

Balb/c mice, transgenic for the human insulin gene, were obtained from Dr. J. Kapp. TG animals were bred with non-transgenic (NTG) Balb/c mice to obtain heterozygous TG offspring and NTG littermates, used in the *in vivo* studies presented here. Animals were bred at the Central Laboratory Animal Institute (Utrecht University, the Netherlands). NTG Balb/c mice were purchased (since breeding did not result in sufficient NTG littermates) at the Centre d'Élevage Janvier (Le Genest-Saint-Isle, France). Food (Hope Farms, Woerden, the Netherlands) and water (acidified) were available *ad libitum*. The presence or absence of the human insulin gene was determined by real

time PCR (rtPCR) in chromosomal DNA isolated from ear tissue. All animal experiments described were approved by the Animal Ethical Committee of the Utrecht University.

Functional immune system: response to foreign protein

To test whether the transgene interfered with the general capacity to produce antibodies we immunized both TG (n=4) and NTG (n=4) animals with 5 µg of human serum albumin (HSA, i.p.) on five consecutive days for three weeks, according to Hermeling et al. Blood was taken before the start of the immunization and on days 9 and 18 by cheek puncture. On day 28 mice blood was collected via heart puncture under isoflurane anesthesia followed by cervical dislocation. The obtained plasma was stored at -80°C until further analysis.

Validation of the insulin mouse model: Immunogenicity of insulin and NP-ins

TG and NTG mice were treated for 4 weeks with 3 i.p. injections per week (Monday/Wednesday/Friday) of 20 µg of unmodified insulin (19 mice per group). The same schedule and number of animals was used to study if insulin bound to nanospheres (NP-ins) would be able to induce antibody formation. Blood was drawn from all mice per group by cheek puncture before the injection schedule started and additionally on day 14. On day 28, blood was collected via heart puncture under isoflurane anesthesia followed by cervical dislocation for all mice. Plasma was stored at -80°C until further analysis.

Application of the insulin mouse model: Immunogenicity of insulin formulations

98 animals, 49 TG and 49 NTG, were used to compare the potential immunogenicity of PB-MCO, ABI-MCO, Levemir®, Insulatard® and Actrapid®, with insulin and NP-ins. To this end, 7 mice per group were used and the same injection schedule was used as described above. Blood was drawn before the injection schedule started and on day 28 via heart puncture under isoflurane anesthesia followed by cervical dislocation for all mice. Storage was performed at -80 °C until further analysis.

Binding antibody assay

Plasma was analyzed for binding antibodies against insulin or HSA by direct ELISA, as described in detail by Hermeling et al [10]. Microtiter plates were coated with 100 μ l of 5 μ g/ml native insulin or 5 μ g/ml HSA, depending on the assay, overnight at 4°C. Samples were considered positive when the OD at 450 nm of the 20 or 10 fold diluted plasma was higher than the cut-off value, calculated according to Mire-Sluis et al [19]. Positive and negative control samples were included in each ELISA plate. The plots of OD 450 versus dilution were fitted to a sigmoidal curve and the reciprocal of the dilution at the midpoint was considered the titer of the plasma. Sigmoidal curves were calculated using a fourth order polynomial degree regression curve, elaborated with GraphPad version 4.03. Each plate contained negative plasma from NTG animals (i.e., before injection of any formulation) and positive plasma from NP-ins treated NTG and TG animals. To confirm the specificity of the antibodies for insulin, and their cross-reactivity, selected antibody-positive plasma samples of TG and NTG mice (2 samples per group) were spiked for 1 hr with increasing amounts of insulin (100 μ g max), bovine serum albumin (BSA, 100 μ g max), bovine insulin, bovine insulin's chain A or Chain B, before adding the samples to the plate and performing the ELISA as described before. Samples from NTG mice treated with NP-ins were diluted 200-fold while samples from TG mice treated with NP-ins and from NTG and TG treated with insulin, were 20-fold diluted.

Statistical analysis

Antibody titers were first checked for normal distribution. After determining they were not normally distributed a non-parametric Mann-Whitney U test was used to compare antibody titers between groups. Significant differences between groups in the number of responders were determined with a Fisher's test. A calculated probability (p) value equal than or below 0.05 was considered to be statistically significant.

Results and Discussion

Physicochemical characterization of NP-INS, PB-MCO and ABI-MCO

Conjugation of human insulin to carboxylated polystyrene nanoparticles: evaluation of covalent binding, conjugation efficiency and characterization of particle size

Chemical covalent linkage between insulin and polystyrene nanoparticles (NP) was achieved following a previously described procedure [15]. To investigate the nature of the coupling, the amount of insulin covalently coupled versus the adsorbed one, and to exclude the presence of protein aggregates, we used SDS-PAGE, SEC and DLS analysis. Results suggest that mainly particles coated with covalently bound human insulin, with a Z-average of 55.21 ± 0.11 were present. No substantial increase in particle size was observed when insulin was mixed with non-activated particles (50.37 ± 0.21) indicating little or noncovalent binding of insulin to the NP.

Furthermore, the presence of free insulin in the mixture of ADS-ins likely explains the slightly lower average diameter. The low PDI measured with DLS (<0.1 for all NP formulations studied) points to the absence of NP aggregates.

The absence of aggregates in NP-ins and the successful conjugation of insulin to NP was further confirmed with SDS-PAGE (Figure 1, panel A, B and C). In particular panel A indicates the covalent nature of the bond between insulin and NP, since free insulin was barely detected. Panel B shows that the broad band at the top of Figure 1, panel A is solely due to NP and provides evidence that the coupling procedure with NHS-sulfo and EDAC does not induce aggregates formation as for these reagents used with insulin but without NP (Figure 1, panel C).

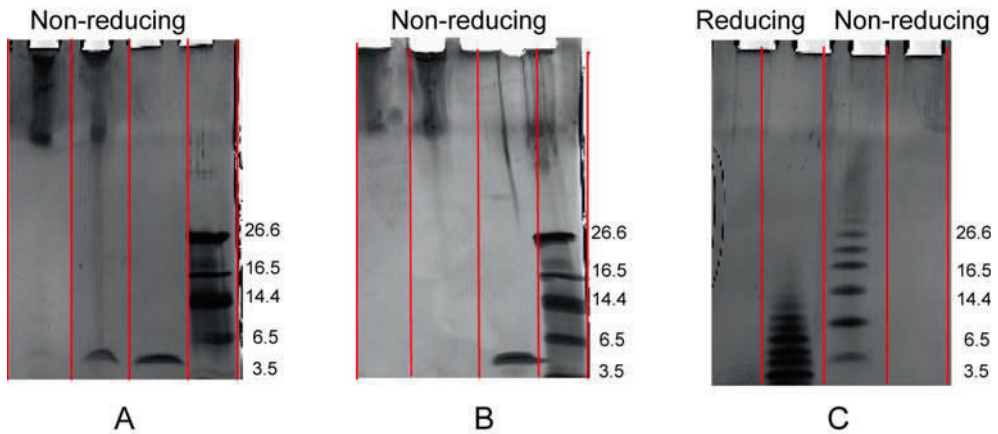


Figure 1. SDS-PAGE results: A, from left to right: nanoparticles-insulin (NP-ins), insulin adsorbed on nanoparticles (ADS-ins), rh insulin (insulin), polypeptide standard (M.W. indicated in kDa); B, from left to right: NP-ins, polystyrene nanoparticles (NP), insulin, polypeptide standard; C, from left to right: buffer, reducing SDS-PAGE of cross-linked insulin (CR-ins), non-reducing SDS PAGE of CR-ins, buffer.

Aggregate content and structural changes in PB-MCO and ABI-MCO

PB-MCO has been extensively characterized before [14, 16]. SEC and CD analysis were used to confirm our previous results: PB-MCO insulin contained $23.1 \pm 3.6\%$ aggregates and its secondary structure was substantially perturbed, as demonstrated by the reduction of the intensity of the entire spectrum and an increased 208/223 nm ratio, relative to insulin (PB-MCO 1.30 ± 0.03 ; insulin 1.19 ± 0.01), consistent with our previous data. ABI-MCO showed an amount of aggregates comparable to that of insulin, based on SEC analysis (ABI-MCO $0.7 \pm 0.2\%$; insulin $0.4 \pm 0.2\%$). CD analysis instead suggested that the content of alpha helix in ABI-MCO had decreased, parallel to an increase in random coil structure [20], based on the higher 208/223 ratio, which was 1.40 ± 0.02 . This is likely due to oxidation of amino acid residues on insulin chain A and B which are normally involved in forming an alpha-helix structure, namely Tyr A14 and A19 and, His B10 and Tyr B16 [21].

Furthermore, the introduction of new oxygen atoms on His, Phe and Tyr residues, may alter the native hydrogen bond network of insulin, inducing insulin to assume a non-native like secondary structure [22].

Validation of the insulin mouse model and immunogenicity of insulin formulations

Immunization of transgenic and non-transgenic mice with human serum albumin

Mice were injected with 5 μg HSA daily for five consecutive days for three consecutive weeks. Anti-HSA IgG titers at days 11 and 18 were determined. TG animals showed an antibody response against HSA which was comparable to that in NTG animals, showing that the transgene did not interfere with the general capacity of the TG animals to produce antibodies. This is in line with previous TG mouse models for IFN α -2b [9, 23], IFN β -1a [10-11] and insulin [12], which were also shown to be similarly responsive to the administration of a foreign protein as their NTG counterpart.

Immunogenicity of insulin and NP-ins

NTG and TG mice were injected with 20 μg of native insulin for 4 weeks (3 i.p. inj./week). Figure 2 shows the total IgG titers at day 28.

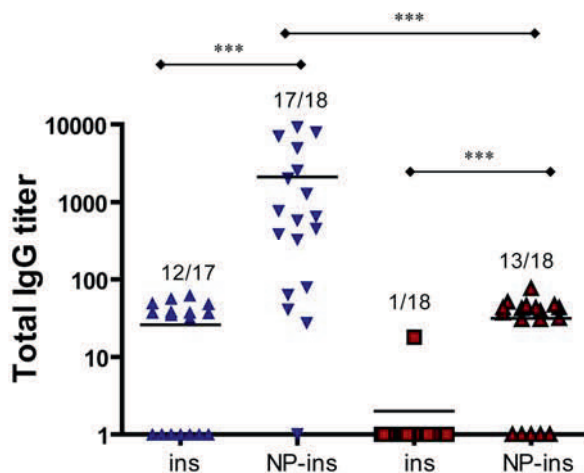


Figure 2. Total anti-insulin IgG titers after 28 days in NTG (blue) and TG (red) animals treated with rh insulin (ins) and nanoparticles-ins (NP-ins). Non-responders were assigned an arbitrary titer of 1 and they have been included in the calculation of the average titers depicted in this figure. Values above the bars represent the number of positive out of total mice. *** indicates $p < 0.001$. Five animals died during the studies for unknown reasons.

Of the TG mice injected with insulin only 1 out of 18 develop antibodies against human insulin. In contrast, nearly 50% of the NTG mice treated with insulin developed measurable antibody titers after two weeks of treatment (data not shown) which increased to about 70% after 4 weeks of treatment.

This shows that the TG mice are tolerant for human insulin, while NTG mice are not. To validate that TG mice (and the NTG controls) can form anti-human insulin antibodies they were treated with NP-ins. This formulation contains a particulate form of insulin which is likely to expose repetitive epitopes.

Several studies have demonstrated that presentation of such structures to the immune system, can result in antibody formation [7, 24].

Indeed, both NTG and TG animals do develop antibody against human insulin by the administration of NP-ins. For the TG mice 50% and 72% showed antibodies after 14 (data not shown) and 28 days, respectively. 94.4 % of NTG mice were antibody positive after 14 (data not shown) and 28 days. Based on Fisher's test, the number of responders (both TG and NTG) was higher for NP-ins treated mice compared to mice treated with insulin ($p=0.022$).

In addition to the differences in number of responders, we also found differences in antibody titers. When combining all treatment data, NTG mice displayed significantly higher antibody titers than TG mice. In more detail, NTG mice treated with NP-ins had higher antibody titers compared to (i) NTG mice treated with insulin ($p<0.001$, at days 14 and 28) and to (ii) NP-ins treatment in TG mice ($p<0.001$) (Figure 2). Similarly, TG mice treated with insulin show significantly lower antibody titers as with NP-ins ($p<0.001$). The immunogenicity of NP-ins, where insulin is covalently bound on the surface of the particles is likely due to the particulate character [25] and to the exposure of repetitive native-like epitopes [7, 24].

As observed before in other mouse models [10, 26], the same formulation induced a higher antibody titer in NTG mice than in TG mice, likely due to the absence of the human insulin gene in NTG mice. Furthermore, human and murine insulin feature high homology (i.e., > 92%, because of 4 different amino acid residues). Hence, there might be cross reactivity between insulin (either mouse or human, which are in theory both produced in TG animals) and ADAs. This could compromise detection of anti-insulin antibodies by ELISA due to binding between the circulating insulin and anti-human insulin antibodies, as observed by Thomas et al [27].

In addition, murine and human insulin contain an identical A-chain loop, which is a well known antigenic determinant on insulin [28-29]. Furthermore, due to the high sequence homology between human and murine insulin and a comparable rigid structure of the A-chain loop, human insulin might not be as immunogenic for NTG animals as we see for other foreign proteins with lower degree of homology. Perhaps this is why not all NTG mice immunized with human insulin were seropositive and the antibody titers in the seropositive ones were low. Concluding, differences in titers among TG mice may arise from differences in their transgene number (for human insulin).

Specificity of the antibodies for human insulin

Spiking plasma with increasing amounts of insulin and BSA confirmed the specificity of the antibodies measured: whereas spiking with insulin significantly diminished the OD at 450 nm for all positive mice ($p < 0.05$), BSA did not inhibit the OD 450 signal ($p > 0.05$), confirming the specificity of the antibodies for native insulin (Figure 3).

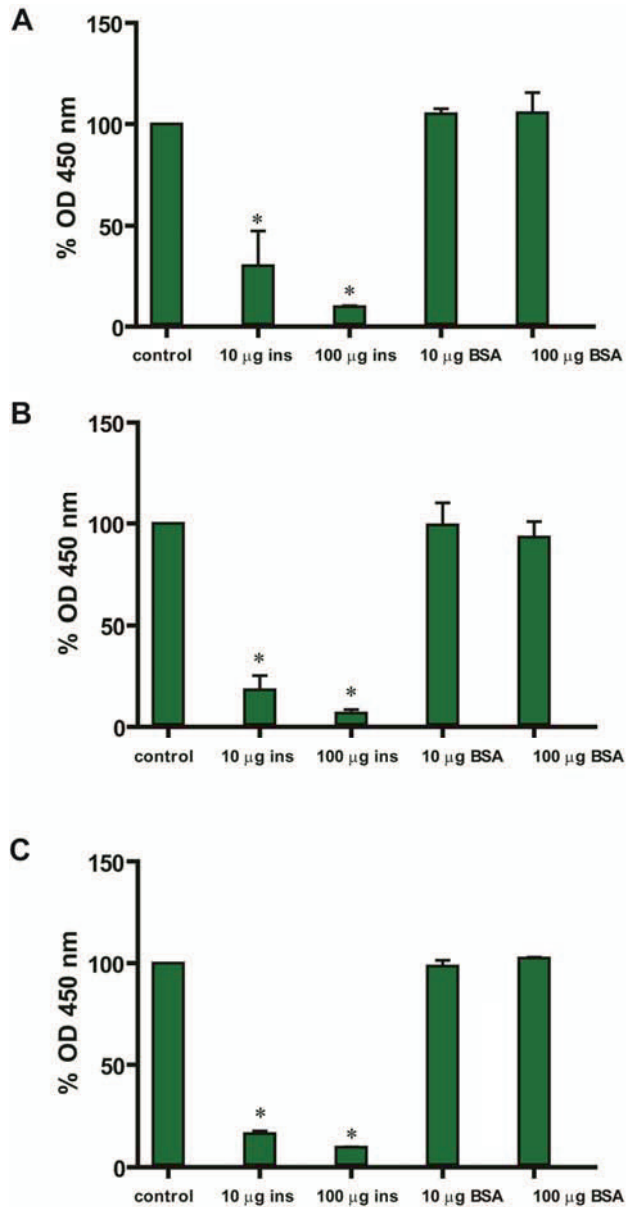
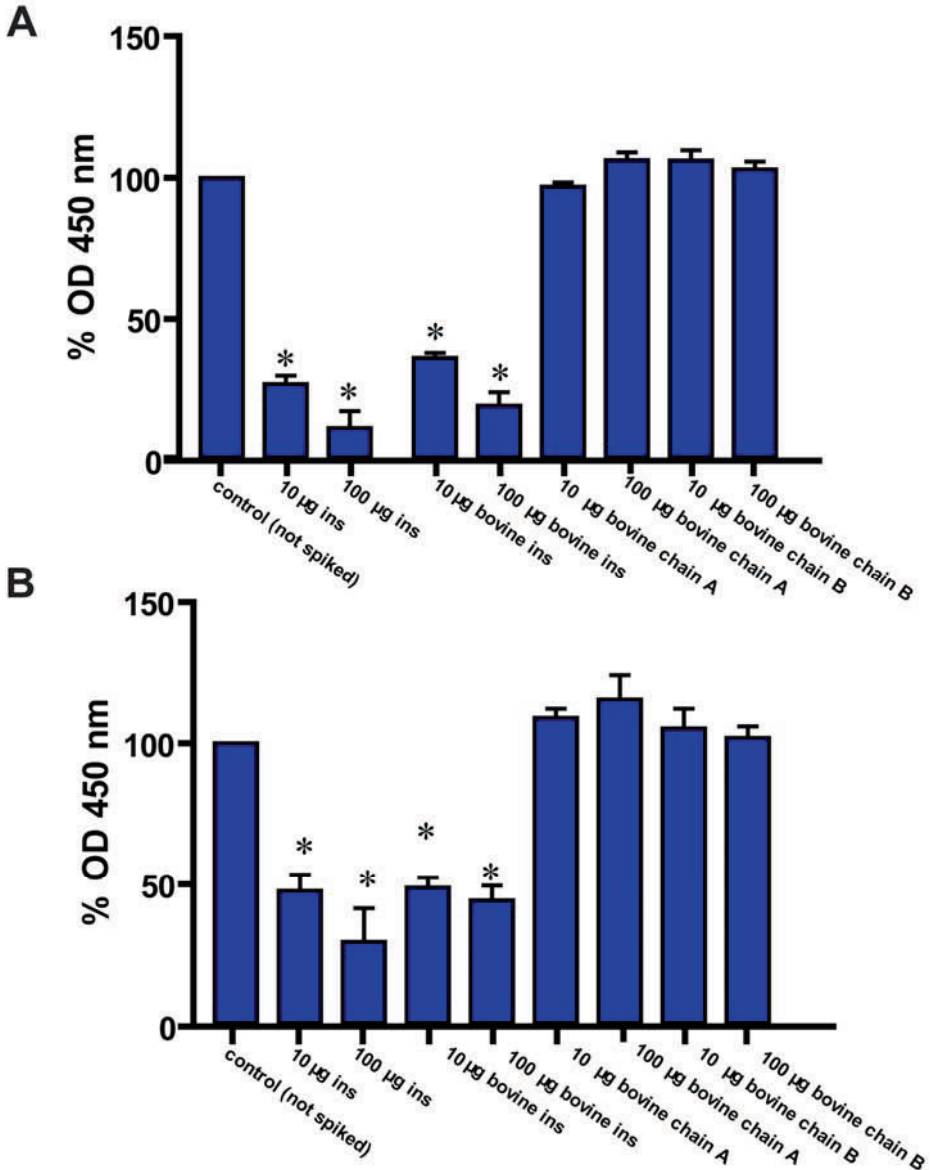


Figure 3. Spiking of plasma of NTG mice treated with nanoparticles-ins (NP-ins) (panel A), TG mice treated with NP-ins (panel B), NTG mice treated with rh insulin (ins) (panel C). Plasma was incubated with 10 or 100 µg ins or bovine serum albumin (BSA), as indicated at the x-axis. In the control sample no protein was added. Two antibody positive mice were used for each group. Data were normalized against the control and represented as mean + upper value. * indicates that the OD % was significantly lower than the control ($p < 0.05$).

Cross-reactivity of the antibodies

In order to check whether the antibodies raised against human insulin cross-react with bovine insulin or its separate chains A and B, positive plasma samples were spiked with increasing amounts of human insulin, bovine insulin, bovine insulin's chain A and bovine insulin's chain B (Figure 4).



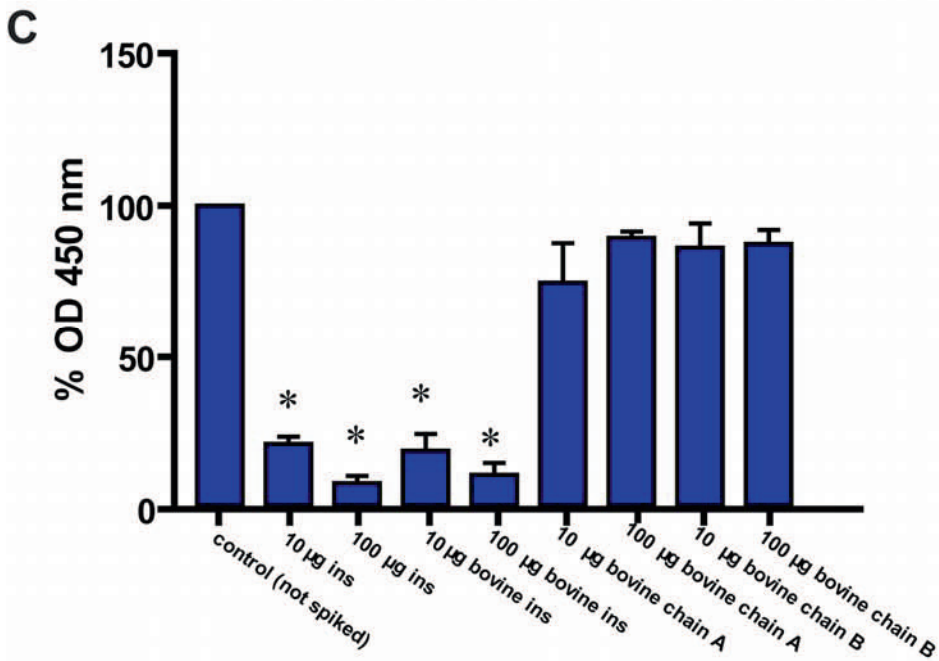


Figure 4. Spiking of plasma of NTG mice treated with nanoparticles-ins (NP-ins) (panel A), TG mice treated with NP-ins (panel B), NTG mice treated with rh insulin (ins) (panel C). Plasma was incubated, separately with ins, bovine insulin, bovine insulin's chain A and bovine insulin's chain B (i.e. 10 and 100 µg). In the control sample no protein was added (not spiked). Two antibody positive mice were used for each group. Data were normalized against the control and represented as mean + upper value. * indicates that the OD % was significantly lower than the control ($p < 0.05$).

While bovine insulin, which shares with human insulin ~ 94% of the primary structure (i.e. 48 over 51 amino acids are identical) (Figure 5) as well as higher order structural features (i.e. secondary and tertiary structure), was recognized by the anti-human insulin antibodies, separated insulin's chains from bovine source were not. These findings suggest that the antibodies cross-react with bovine insulin and recognize conformational epitopes rather than linear epitopes.

A-CHAIN

	1	11	21
Human	GIVEQCCTSI	CSLYQLENYC	N
Bovine	GIVEQCCASV	CSLYQLENYC	N
Mouse/Rat	GIVDQCCTSI	CSLYQLENYC	N

B-CHAIN

	1	11	21	30
Human	FVNQHLCGSH	LVEALYLVCG	ERGFFYTPKT	
Bovine	FVNQHLCGSH	LVEALYLVCG	ERGFFYTPKA	
Mouse/Rat	FVKQHLCGPH	LVEALYLVCG	ERGFFYTPKS	
I				
Mouse/Rat	FVKQHLCGSH	LVEALYLVCG	ERGFFYTPMS	
II				

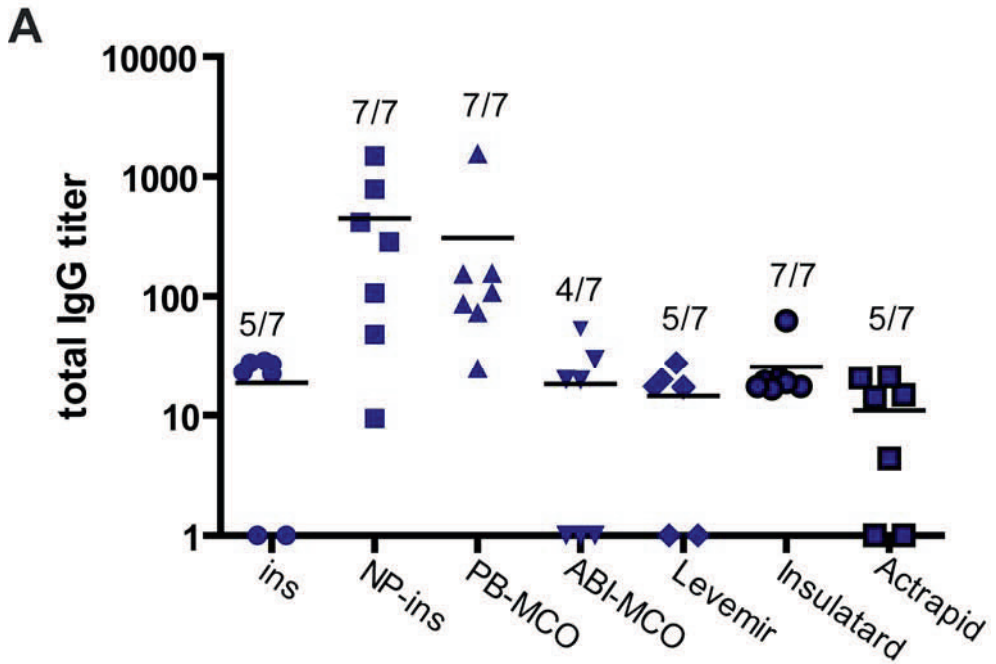
Figure 5. The amino acid sequences of human, bovine, mouse and rat insulin. Differences with human insulin are highlighted in red.

Immunogenicity of insulin formulations

In panel A and B of Figure 6 are shown the total anti insulin IgG titer in NTG and TG animals respectively. As expected, TG mice did not develop antibodies against native insulin, while 50% of the mice treated with NP-ins were antibody positive, in agreement with what was observed during our validation experiment. Similarly, half of the TG animals treated with PB-MCO were antibody positive and had comparable titers to those treated with NP-ins. This is in agreement with earlier results where IFN α -2a (unpublished results from our group), IFN α -2b [23], IFN β -1a [26] and IgG1 [30], oxidized and aggregated with the oxidative system Cu²⁺/ascorbate, induced ADAs. Although ABI-MCO formulations lacked aggregates, 33% of the animals were found to be positive.

This suggests that the chemical modifications induced during oxidation and/or the perturbation of the secondary structure contributed to the slightly enhanced immunogenicity of this formulation. Levemir[®] and Insulatard[®] were poorly immunogenic in TG animals (1 mouse over 7 was positive for both formulations), while Actrapid[®] did not elicit any immune response.

Significantly lower titers ($p < 0.05$) were detected in TG animals treated with NP-ins, PB-MCO and Insulatard® compared to NTG (Figure 6, panel B) mice treated with these formulations. In ABI-MCO and Levemir® treated animals, the titers of TG and NTG mice were comparable.



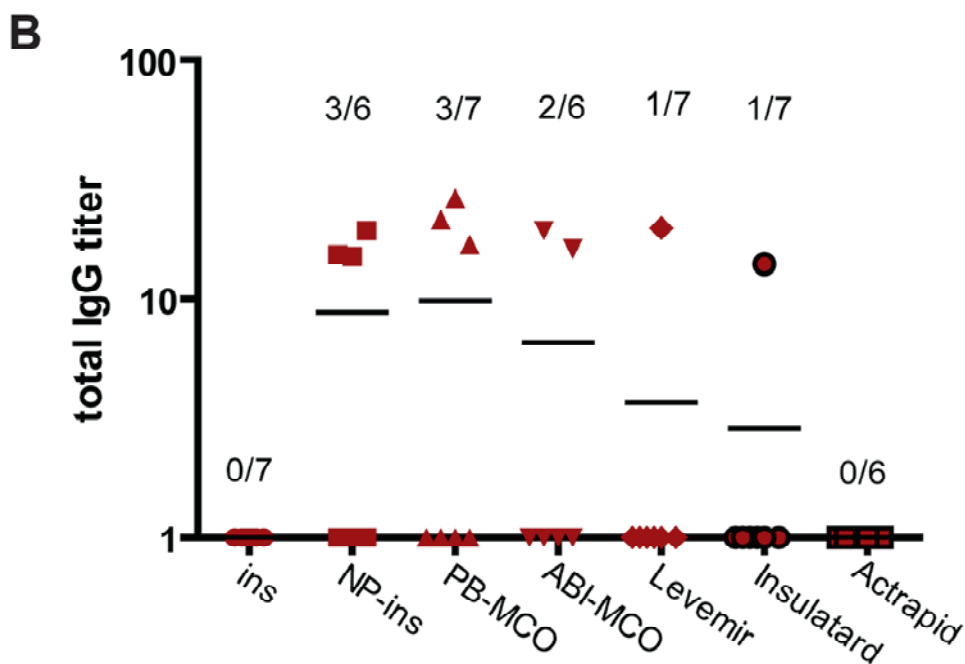


Figure 6. Total anti-insulin IgG titer after 28 days in NTG animals (panel A). Non-responders were assigned an arbitrary titer of 1 and they have been included in the calculation of the titers depicted in this figure. Values above the bars represent the number of positive out of total mice. Samples: rh insulin (ins), nanoparticles-insulin (NP-ins), oxidized and aggregated insulin (PB-MCO), oxidized non aggregated insulin (ABI-MCO), long acting insulin modified on Lys B 29 with fatty acid (Levemir®), long acting insulin obtained as a zinc suspension (Insulatard®), fast acting insulin (Actrapid®). Total anti-insulin IgG titer after 28 days in TG animals (panel B). Animal treatment and graph layout are the same of panel A. Please note that since TG mice treated with ins and Actrapid® had no detectable antibody and no responders (variance of the group=0), statistical testing involving this two groups was not allowed. Titers among groups with detectable antibody and responders were comparable. Three animals died during the studies for unknown reasons.

Conclusion

Here we reported the validation and application of a TG mouse model, immune tolerant for human insulin, for the study of product-related factors influencing the immunogenicity of insulin. In these studies it was confirmed that the combination of covalent aggregation and chemical modifications, induced via the oxidative system Cu^{2+} /ascorbate, likely contributes to the immunogenicity of therapeutic proteins. This mouse model represents a

promising tool to study in more detail the immune mechanisms of antibody formation against therapeutic proteins, using insulin as a model protein.

References

- [1] T. U. Gerngross. Advances in the production of human therapeutic proteins in yeasts and filamentous fungi *Nat. Biotechnol.* **2004**, *22*, 1409-1414.
- [2] I. S. Johnson. Human Insulin from Recombinant DNA Technology. *Science* **1983**, *219*, 632-637.
- [3] H. Schellekens. How to predict and prevent the immunogenicity of therapeutic proteins. *Biotechnol. Annu. Rev.* **2008**, *14*, 191-202.
- [4] H. Schellekens. The immunogenicity of therapeutic proteins and the Fabry antibody standardization initiative. *Clin. Ther.* **2008**, *30 Suppl B*, S50-51.
- [5] M. Sauerborn, V. Brinks, W. Jiskoot, H. Schellekens. Immunological mechanism underlying the immune response to recombinant human protein therapeutics. *Trends Pharmacol. Sci.* **2010**, *31*, 53-59.
- [6] H. Schellekens. Factors influencing the immunogenicity of therapeutic proteins. *Nephrol. Dial. Transplant.* **2005**, *20 Suppl 6*, vi3-9.
- [7] S. Kumar, S. K. Singh, X. L. Wang, B. Rup, D. Gill. Coupling of Aggregation and Immunogenicity in Biotherapeutics: T- and B-Cell Immune Epitopes May Contain Aggregation-Prone Regions. *Pharm. Res.* **2011**, *28*, 949-961.
- [8] A. S. Rosenberg. Effects of protein aggregates: an immunologic perspective. *AAPS J* **2006**, *8*, E501-507.
- [9] S. Hermeling, L. Aranha, J. M. Damen, M. Slijper, H. Schellekens, D. J. Crommelin, W. Jiskoot. Structural characterization and immunogenicity in wild-type and immune tolerant mice of degraded recombinant human interferon alpha2b. *Pharm. Res.* **2005**, *22*, 1997-2006.
- [10] S. Hermeling, W. Jiskoot, D. Crommelin, C. Bornaes, H. Schellekens. Development of a transgenic mouse model immune tolerant for human interferon Beta. *Pharm. Res.* **2005**, *22*, 847-851.
- [11] M. M. van Beers, M. Sauerborn, F. Gilli, S. Hermeling, V. Brinks, H. Schellekens, W. Jiskoot. Hybrid transgenic immune tolerant mouse model for assessing the breaking of B cell tolerance by human interferon beta. *J. Immunol. Methods* **2010**, *352*, 32-37.
- [12] J. L. Ottesen, P. Nilsson, J. Jami, D. Weilguny, M. Duhrkop, D. Bucchini, S. Havelund, J. M. Fogh. The potential immunogenicity of human insulin and insulin analogues evaluated in a transgenic mouse model. *Diabetologia* **1994**, *37*, 1178-1185.
- [13] J. Brange, L. Langkjaer, S. Havelund, A. Volund. Chemical stability of insulin. 1. Hydrolytic degradation during storage of pharmaceutical preparations. *Pharm. Res.* **1992**, *9*, 715-726.

- [14] R. Torosantucci, O. Mozziconacci, V. Sharov, C. Schöneich, W. Jiskoot. Chemical Modifications in Aggregates of Recombinant Human Insulin Induced by Metal-Catalyzed Oxidation: Covalent Cross-Linking via Michael Addition to Tyrosine Oxidation Products. *Pharm. Res.* **2012**, *29*, 2276-2293.
- [15] M. Kalkanidis, G. A. Pietersz, S. D. Xiang, P. L. Mottram, B. Crimeen-Irwin, K. Ardipradja, M. Plebanski. Methods for nano-particle based vaccine formulation and evaluation of their immunogenicity. *Methods* **2006**, *40*, 20-29.
- [16] R. Torosantucci, B. Kükreer, A. Mero, M. Van Winsen, R. Tantipolphan, W. Jiskoot. Plain and mono-pegylated recombinant human insulin exhibit similar stress-induced aggregation profiles. *J. Pharm. Sci.* **2011**, *100*, 2574-2585.
- [17] Insulin, Human, European Directorate for the Quality of Medicines (EDQM), **2001**.
- [18] Insulin, The United States Pharmacopeia Convention, Inc., Rockville, MD, **2002**.
- [19] A. R. Mire-Sluis, Y. C. Barrett, V. Devanarayan, E. Koren, H. Liu, M. Maia, T. Parish, G. Scott, G. Shankar, E. Shores, S. J. Swanson, G. Taniguchi, D. Wierda, L. A. Zuckerman. Recommendations for the design and optimization of immunoassays used in the detection of host antibodies against biotechnology products. *J. Immunol. Methods* **2004**, *289*, 1-16.
- [20] C. E. Bobst, R. R. Abzalimov, D. Houde, M. Kloczewiak, R. Mhatre, S. A. Berkowitz, I. A. Kaltashov. Detection and characterization of altered conformations of protein pharmaceuticals using complementary mass spectrometry-based approaches. *Anal Chem* **2008**, *80*, 7473-7481.
- [21] L. Xie, C. L. Tsou. Comparison of secondary structures of insulin and proinsulin by FTIR. *J. Protein Chem.* **1993**, *12*, 483-487.
- [22] F. Mulinacci, E. Poirier, M. A. Capelle, R. Gurny, T. Arvinte. Enhanced physical stability of human calcitonin after methionine oxidation. *Eur. J. Pharm. Biopharm.* **2011**, *78*, 229-238.
- [23] S. Hermeling, H. Schellekens, C. Maas, M. F. Gebbink, D. J. Crommelin, W. Jiskoot. Antibody response to aggregated human interferon alpha2b in wild-type and transgenic immune tolerant mice depends on type and level of aggregation. *J. Pharm. Sci.* **2006**, *95*, 1084-1096.
- [24] W. Wang, S. K. Singh, N. Li, M. R. Toler, K. R. King, S. Nema. Immunogenicity of protein aggregates—Concerns and realities. *Int. J. Pharm.* **2012**, *431*, 1-11.
- [25] B. S. Zolnik, A. Gonzalez-Fernandez, N. Sadrieh, M. A. Dobrovolskaia. Nanoparticles and the immune system. *Endocrinology* **2010**, *151*, 458-465.
- [26] M. M. van Beers, M. Sauerborn, F. Gilli, V. Brinks, H. Schellekens, W. Jiskoot. Oxidized and aggregated recombinant human interferon beta is immunogenic in human interferon beta transgenic mice. *Pharm. Res.* **2011**, *28*, 2393-2402.
- [27] J. W. Thomas, V. J. Virta, L. J. Nell. Heterogeneity and specificity of human anti-insulin antibodies determined by isoelectric focusing. *J. Immunol.* **1985**, *134*, 1048-1052.

- [28] S. Allauzen, S. Joly, C. Granier, F. Molina, O. Bouix, B. Pau, M. Bouanani. Immunoanalysis of Human Insulin Using Monoclonal-Antibodies Reveals Antigenicity of Evolutionarily Conserved Residues. *Mol. Immunol.* **1995**, *32*, 27-36.
- [29] K. Keck. Ir-gene control of immunogenicity of insulin and A-chain loop as a carrier determinant. *Nature* **1975**, *254*, 78-79.
- [30] V. Filipe, W. Jiskoot, A. H. Basmeh, A. Halim, H. Schellekens. Immunogenicity of different stressed IgG monoclonal antibody formulations in immune tolerant transgenic mice. *MAbs* **2012**, *4*, 740-752.

Chapter 9

Summary and perspectives

Summary

Recombinant human protein therapeutics have unique structural and biological features which make them useful to treat several diseases [1].

However, a drawback of this class of drugs is that they are immunogenic, i.e. a proportion of patients develop anti-drug antibodies (ADAs) during treatment [2]. Among the many factors involved in protein immunogenicity, protein aggregation has been identified as an important risk factor [3]. Aggregates that are generated through oxidative stress have been found to be particularly immunogenic [4-7]. The aim of this thesis was to investigate the mechanisms behind protein aggregation as a result of metal catalyzed oxidation (MCO) [8], and to study the relationship between oxidation, aggregation and immunogenicity of therapeutic proteins.

Chapter 2 is a literature review of the structural and pharmaceutical consequences of oxidation observed in protein and peptide therapeutics, focusing on antibodies, calcitonin, granulocyte colony-stimulating factor, growth hormone, interferon alpha and beta, insulin, oxytocin and parathyroid hormone.

Chapter 3 deals with the aggregation behavior under stress conditions of PEGylated insulin compared with its unpegylated counterpart. Recombinant human insulin was conjugated on lysine B29 with 5-kDa PEG and subjected to heating at 75 °C, metal-catalyzed oxidation, and glutaraldehyde cross-linking. Under each of the applied stress conditions, insulin and PEGylated insulin showed comparable degradation profiles. All the stressed samples were shown to contain submicron aggregates in the size range between 50 and 500 nm. Several stressed samples also contained micron sized particles. Mainly covalent aggregates composed of protein molecules with different degrees of modification in the secondary and tertiary structure were measured, depending on the stress method applied. PEGylation, however, was shown not to affect the sensitivity of insulin towards aggregation [9].

Therapeutic proteins such as recombinant human interferon alfa, recombinant human interferon beta and monoclonal antibodies form highly immunogenic

aggregates induced via copper catalyzed oxidation. In **Chapter 4** the chemical mechanism responsible for insulin aggregation induced by MCO with Cu^{2+} /ascorbate, is described. Oxidized insulin was shown to contain DOPA (3,4-dihydroxyphenylalanine) and DOCH (2-amino-3-(3,4-dioxocyclohexa-1,5-dien-1-yl) propanoic acid), originated from Phe and Tyr residues. DOCH, being an electron acceptor for 1,4- or 1,6-type addition (i.e. Michael addition), was found responsible for new cross-links resulting in covalent aggregation of insulin during MCO. Specifically, 1,4- or 1,6-type addition products were detected between DOCH at positions B16, B26, A14, and A19, and free amino groups of the N-terminal amino acids Phe B1 and Gly A1, and side chains of Lys B29, His B5 and His B10. Fragments originating from peptide bond hydrolysis were also measured ^[10].

Chapter 5 describes studies on the anti-oxidant properties of several excipients during Cu^{2+} /ascorbate catalyzed oxidation of human insulin. Among the excipients studied, 100 μM triethylenetetramine (TETA) was the only one to inhibit almost completely oxidation-induced insulin aggregation, fragmentation and structural changes. TETA also prevented aggregation and fragmentation of a monoclonal IgG1 under identical oxidative conditions, indicating its general applicability as anti-oxidant for copper-sensitive proteins. In conclusion, TETA is a promising candidate excipient for formulations of oxidation-sensitive proteins.

Oxidation via Cu^{2+} /ascorbate of recombinant human interferon beta-1a (IFN β) leads to highly immunogenic aggregates. In **Chapter 6** a study is presented on the identification of the oxidation sites and covalent cross-links in IFN β exposed to MCO. Oxidation products of Met, His, Phe, Trp and Tyr residues were identified throughout the primary sequence. Similar to insulin (**Chapter 4**), covalent cross-links via 1,4- or 1,6-type addition between primary amines and DOCH were detected, while there was no evidence of disulfide bridge, Schiff base, or dityrosine formation. The chemical cross-links identified are most likely responsible for the formation of immunogenic covalent aggregates of IFN β induced by oxidation.

In **Chapter 7** the immune mechanism responsible for the immunogenicity of aggregated recombinant human interferon alpha-2a (IFN α -2a) and the influence of aggregated IFN β on IFN α 's immunogenicity is studied. Transgenic mice immune tolerant for IFN α were treated with native or aggregated IFN α . After a washout period, the mice were rechallenged with aggregated or native IFN α to test for CD4⁺ T-cell involvement in immunogenicity. Furthermore, the mice were treated with a formulation containing aggregated IFN β and native IFN α to test whether aggregated IFN β acts as an adjuvant for IFN α . After a washout period and a rechallenge with either aggregated or native IFN α an apparent lack of immunological memory was observed. When we blocked CD4⁺ T-cell function in immune tolerant mice, aggregated rhIFN α failed to induce ADAs. Finally, immune tolerant mice treated with a mixture of aggregated IFN β and native IFN α did not develop an antibody response against IFN α . These results are in line with previous results obtained with IFN β [11].

Chapter 8 reports the validation of an adjuvant-free mouse model, which is intended as a tool to evaluate the immunogenicity of insulin formulations. Administration of human insulin (20 μ g/dose, 12 doses over a period of 4 weeks) resulted in an immune response in non-transgenic animals, whereas the transgenic mice proved to be immune tolerant. This tolerance in transgenic mice could be circumvented when they were treated with insulin that was covalently bound to 50 nm polystyrene nanoparticles. This transgenic mouse model for human insulin was applied for comparing the immunogenicity of insulin formulations and may be of use to further investigate the mechanism behind the immunogenicity of therapeutic proteins, using insulin as a model protein.

Perspectives

The scientific work presented in this thesis aimed to contribute to the development of safer, less immunogenic biopharmaceuticals, by describing the mechanisms behind MCO-induced aggregation of therapeutic proteins and its relationship with immunogenicity. Further research is however needed to better prevent degradation of therapeutic proteins and better understand the factors contributing to their immunogenicity. This section provides some

perspectives for future research, focusing on: strategies to prevent protein degradation and analytical tools for protein characterization.

Strategies to prevent protein degradation

During the last two decades, industry became increasingly aware of the risk of degraded products, particularly aggregates, in protein formulations, justifying the search for solutions to prevent or reduce aggregation [3].

In general, two approaches can be employed to prevent protein degradation. The first is to improve protein stability by modifying the protein molecule, either by genetic engineering [12] or by chemical modification [13] (i.e. bio-conjugation like PEGylation). The second option is to improve stability by proper formulation [14]. An example of the first approach is the production of a human interleukin-1 where Asn36 is mutated into Ser36 [15]. The three-dimensional structure of this genetically engineered protein was shown to be identical to that of the native protein with dichroic studies and proton NMR. The mutant was resistant against base-catalyzed and temperature-induced deamidation [15].

Chemical modification, like conjugation of proteins with polymers (i.e. PEG), in some cases can be a solution as demonstrated for instance by the higher stability of PEGylated IFN proteins relative to their unmodified counterparts [16]. PEGylation has been used to increase the half life, resistance to enzymatic degradation and to prevent formation of fibrillar aggregates [17-19]. However, as shown in chapter 3, PEGylation did not prevent degradation of insulin in a liquid formulation. In our studies however we used a 5 kDa PEG, therefore we cannot exclude that other forms of PEGylation may improve the stability.

Excipients are widely employed to protect proteins from aggregation and oxidation [14]. In chapter 5, several anti-oxidant molecules were screened for their potential protective effect towards MCO-induced aggregation and fragmentation of insulin and a monoclonal antibody. Among the molecules screened triethylenetetramine [20] (TETA) turned out to be the most promising one in preventing MCO. However, it is currently unknown if TETA can prevent oxidation of amino acid residues not involved in aggregation, such as methionine and tryptophan, which are not present in insulin. Future studies, with the aid of tandem mass spectrometry, should verify the protective effect of TETA against oxidation of such amino acid residues.

Surfactant excipients, like polysorbate 80, are widely employed in protein formulation and useful for preventing aggregation [21]. One of the major drawbacks of polysorbates is that they contain alkyl chains that could auto-oxidize, generating protein-damaging peroxides. Given that peroxide formation is enhanced in aerobic environment and further promoted by light [21], a first strategy to reduce the amount of these reactive molecules in polysorbates would be preventing any contact with air/oxygen during storage.

Next, the addition of anti-oxidant excipients can be beneficial for inhibiting or minimizing generation of radicals. In this case chelating agents like TETA should not be used since these anti-oxidants are not able to scavenge radicals. Instead, molecules like methionine, vitamin E or glutathione could be considered, as shown by Ha et al [22]. Concluding, to prevent degradation a thorough understanding of the mechanisms involved is required. In chapter 4, for instance, by using high sensitive tandem mass spectrometry analysis and selective fluorogenic tagging [23-24], we showed that insulin aggregation under our oxidative system was due to tyrosine oxidation products that can react with amino groups in the insulin molecule. Based on these findings we further proposed two strategies to inhibit or reduce aggregation (chapter 4).

Similarly, mechanisms involved in several other pathways of degradation should be analyzed with the final goal of preventing any type of protein degradation.

Analytical tools for protein characterization

When a protein degrades, generally a heterogeneous mixture of degradation products with different physico-chemical features are formed, such as aggregates with different size, shape, protein conformation and chemical modifications, as well as structurally modified monomers and fragments [9]. Potentially any of these species can contribute to unwanted side reactions.

The availability of robust and reliable analytical tools capable of characterizing all of these species is required in research as well as for quality control (QC) purposes. For aggregate characterization, most of the routine analytical techniques approved for QC analysis, focus on the size range $>1 \mu\text{m}$ and $<100 \text{ nm}$, which obviously leave a big gap in the subvisible size range [25]. Techniques like nanoparticle tracking analysis [26] (NTA, used in several of the studies presented in this thesis) and flow imaging, allow visualization and

quantification of particulate aggregates and provide size information. These methods are increasingly used as characterization tools to fill the size gap previously mentioned [27]. Furthermore, an accurate mapping of chemical modifications of protein drugs can be achieved with high sensitive MS/MS analysis. Nonetheless, some chemical modifications like Trp oxidation can be artifact generated during sample preparation [28]. To prevent misinterpretation of the results, selective chemical derivatization (like the fluorogenic derivatization shown in chapter 4 that can be performed on oxidized Trp as well) before MS analysis, can be considered.

References

- [1] B. Leader, Q. J. Baca, D. E. Golan. Protein therapeutics: a summary and pharmacological classification. *Nat. Rev. Drug. Discov.* **2008**, *7*, 21-39.
- [2] Y. Vugmeyster, X. Xu, F. P. Theil, L. A. Khawli, M. W. Leach. Pharmacokinetics and toxicology of therapeutic proteins: Advances and challenges. *World J. Biol. Chem.* **2012**, *3*, 73-92.
- [3] W. Wang, S. K. Singh, N. Li, M. R. Toler, K. R. King, S. Nema. Immunogenicity of protein aggregates-concerns and realities. *Int. J. Pharm.* **2012**, *431*, 1-11.
- [4] V. Filipe, W. Jiskoot, A. H. Basmeh, A. Halim, H. Schellekens. Immunogenicity of different stressed IgG monoclonal antibody formulations in immune tolerant transgenic mice. *MAbs* **2012**, *4*, 740-752.
- [5] S. Hermeling, L. Aranha, J. M. A. Damen, M. Slijper, H. Schellekens, D. J. A. Crommelin, W. Jiskoot. Structural characterization and immunogenicity in wild-type and immune tolerant mice of degraded recombinant human interferon alpha2b. *Pharm. Res.* **2005**, *22*, 1997-2006.
- [6] S. Hermeling, H. Schellekens, C. Maas, M. F. Gebbink, D. J. Crommelin, W. Jiskoot. Antibody response to aggregated human interferon alpha2b in wild-type and transgenic immune tolerant mice depends on type and level of aggregation. *J. Pharm. Sci.* **2006**, *95*, 1084-1096.
- [7] M. M. van Beers, M. Sauerborn, F. Gilli, V. Brinks, H. Schellekens, W. Jiskoot. Oxidized and aggregated recombinant human interferon beta is immunogenic in human interferon beta transgenic mice. *Pharm. Res.* **2012**, *28*, 2393-2402.
- [8] E. R. Stadtman. Metal ion-catalyzed oxidation of proteins: biochemical mechanism and biological consequences. *Free. Radic. Biol. Med.* **1990**, *9*, 315-325.
- [9] R. Torosantucci, B. Kukrer, A. Mero, M. Van Winsen, R. Tantipolphan, W. Jiskoot. Plain and mono-pegylated recombinant human insulin exhibit similar stress-induced aggregation profiles. *J. Pharm. Sci.* **2011**, *100*, 2574-2585.

- [10] R. Torosantucci, O. Mozziconacci, V. Sharov, C. Schöneich, W. Jiskoot. Chemical Modifications in Aggregates of Recombinant Human Insulin Induced by Metal-Catalyzed Oxidation: Covalent Cross-Linking via Michael Addition to Tyrosine Oxidation Products. *Pharm. Res.* **2012**, *29*, 2276-2293
- [11] M. M. van Beers, M. Sauerborn, F. Gilli, V. Brinks, H. Schellekens, W. Jiskoot. Aggregated recombinant human interferon Beta induces antibodies but no memory in immunetolerant transgenic mice. *Pharm. Res.* **2010**, *27*, 1812-1824.
- [12] M. Kamionka. Engineering of therapeutic proteins production in Escherichia coli. *Curr. Pharm. Biotechnol.* **2011**, *12*, 268-274.
- [13] S. Jevsevar, M. Kunstelj, V. G. Porekar. PEGylation of therapeutic proteins. *Biotechnol. J.* **2010**, *5*, 113-128.
- [14] W. Wang. Instability, stabilization, and formulation of liquid protein pharmaceuticals. *Int. J. Pharm.* **1999**, *185*, 129-188.
- [15] P. T. Wingfield, R. J. Mattaliano, H. R. MacDonald, S. Craig, G. M. Clore, A. M. Gronenborn, U. Schmeissner. Recombinant-derived interleukin-1 alpha stabilized against specific deamidation. *Protein. Eng.* **1987**, *1*, 413-417.
- [16] A. Basu, K. Yang, M. Wang, S. Liu, R. Chintala, T. Palm, H. Zhao, P. Peng, D. Wu, Z. Zhang, J. Hua, M. C. Hsieh, J. Zhou, G. Petti, X. Li, A. Janjua, M. Mendez, J. Liu, C. Longley, M. Mehlig, V. Borowski, M. Viswanathan, D. Filpula. Structure-function engineering of interferon-beta-1b for improving stability, solubility, potency, immunogenicity, and pharmacokinetic properties by site-selective mono-PEGylation. *Bioconjug. Chem.* **2006**, *17*, 618-630.
- [17] K. Hinds, J. J. Koh, L. Joss, F. Liu, M. Baudys, S. W. Kim. Synthesis and characterization of poly(ethylene glycol)-insulin conjugates. *Bioconjug. Chem.* **2000**, *11*, 195-201.
- [18] K. D. Hinds, S. W. Kim. Effects of PEG conjugation on insulin properties. *Adv. Drug. Deliv. Rev.* **2002**, *54*, 505-530.
- [19] T. Uchio, M. Baudys, F. Liu, S. C. Song, S. W. Kim. Site-specific insulin conjugates with enhanced stability and extended action profile. *Adv. Drug. Deliv. Rev.* **1999**, *35*, 289-306.
- [20] G. J. Cooper. Therapeutic potential of copper chelation with triethylenetetramine in managing diabetes mellitus and Alzheimer's disease. *Drugs* **2011**, *71*, 1281-1320.
- [21] B. A. Kerwin. Polysorbates 20 and 80 used in the formulation of protein biotherapeutics: Structure and degradation pathways. *J. Pharm. Sci.* **2008**, *97*, 2924-2935.
- [22] E. Ha, W. Wang, Y. J. Wang. Peroxide formation in polysorbate 80 and protein stability. *J. Pharm. Sci.* **2002**, *91*, 2252-2264.
- [23] V. S. Sharov, E. S. Dremina, N. A. Galeva, G. S. Gerstenecker, X. Li, R. T. Dobrowsky, J. F. Stobaugh, C. Schöneich. Fluorogenic Tagging of Peptide and Protein 3-Nitrotyrosine with 4-(Aminomethyl)-benzenesulfonic Acid for Quantitative Analysis of Protein Tyrosine Nitration. *Chromatographia* **2010**, *71*, 37-53.
- [24] V. S. Sharov, E. S. Dremina, J. Pennington, J. Killmer, C. Asmus, M. Thorson, S. J. Hong, X. Li, J. F. Stobaugh, C. Schöneich. Selective fluorogenic derivatization of 3-nitrotyrosine and

- 3,4-dihydroxyphenylalanine in peptides: a method designed for quantitative proteomic analysis. *Methods Enzymol.* **2008**, *441*, 19-32.
- [25] J. F. Carpenter, T. W. Randolph, W. Jiskoot, D. J. Crommelin, C. R. Middaugh, G. Winter, Y. X. Fan, S. Kirshner, D. Verthelyi, S. Kozlowski, K. A. Clouse, P. G. Swann, A. Rosenberg, B. Cherney. Overlooking subvisible particles in therapeutic protein products: gaps that may compromise product quality. *J. Pharm. Sci.* **2009**, *98*, 1201-1205.
- [26] V. Filipe, A. Hawe, W. Jiskoot. Critical evaluation of Nanoparticle Tracking Analysis (NTA) by NanoSight for the measurement of nanoparticles and protein aggregates. *Pharm. Res.* **2010**, *27*, 796-810.
- [27] J. den Engelsman, P. Garidel, R. Smulders, H. Koll, B. Smith, S. Bassarab, A. Seidl, O. Hainzl, W. Jiskoot. Strategies for the assessment of protein aggregates in pharmaceutical biotech product development. *Pharm. Res.* **2011**, *28*, 920-933.
- [28] I. Perdivara, L. J. Deterding, M. Przybylski, K. B. Tomer. Mass spectrometric identification of oxidative modifications of tryptophan residues in proteins: chemical artifact or post-translational modification? *J. Am. Soc. Mass. Spectrom.* **2010**, *21*, 1114-1117.

Appendix 1

Nederlandse samenvatting (Dutch summary)

Samenvatting

Recombinante humane therapeutische eiwitten hebben unieke structurele en biologische eigenschappen waardoor ze bruikbaar zijn voor de behandeling van verschillende aandoeningen. Een nadeel van deze klasse geneesmiddelen is dat ze immunogeen zijn, wat wil zeggen dat sommige patiënten anti-geneesmiddel antilichamen (ADAs) tijdens de behandeling ontwikkelen. Van de vele factoren die betrokken zijn bij eiwit-immunogeniciteit is aggregatie van eiwitten een belangrijke risicofactor.

Aggregaten die door oxidatieve stress worden gevormd zijn bijzonder immunogeen gebleken. Het doel van dit proefschrift was om de mechanismen achter eiwitaggregatie ten gevolge van gekatalyseerde oxidatie te onderzoeken (MCO), en daarnaast om de relatie tussen oxidatie, aggregatie en immunogeniciteit van therapeutische eiwitten te bestuderen.

Hoofdstuk 2 beschrijft een literatuuronderzoek van de structurele en biologische gevolgen van oxidatie waargenomen in therapeutische eiwitten en peptiden, met name gericht op antilichamen, calcitonine, granulocyt koloniestimulerende factor, groeihormoon, interferon alfa en bèta, insuline, oxytocine en bijschildklierhormoon.

Hoofdstuk 3 vergelijkt het aggregatiegedrag van gepegyleerde en niet-gepegyleerde insuline onder stresscondities. Recombinant humaan insuline werd aan lysine B29 geconjugeerd met 5-kDa PEG en onderworpen aan verhitting bij 75 °C, metaal gekatalyseerde oxidatie en glutaaraldehyde cross-linking. Onder elke stressconditie toonden insuline en gepegyleerd insuline vergelijkbare degradatieprofielen. Alle gestreste monsters bleken aggregaten te bevatten in de ordegrootte tussen 50 en 500 nm. Ook microneeltjes werden in diverse gestreste monsters gevonden. Afhankelijk van de toegepaste stress werden voornamelijk covalente aggregaten samengesteld uit eiwitmoleculen met verschillende mate van modificatie in de secundaire en tertiaire structuur gemeten. Pegylatie bleek echter de gevoeligheid van insuline voor aggregatie niet te beïnvloeden.

Therapeutische eiwitten zoals recombinant humaan interferon alfa, recombinant humaan interferon bèta en monoklonale antilichamen vormen

zeer immunogene aggregaten geïnduceerd onder invloed van koper gekatalyseerde oxidatie. In **Hoofdstuk 4** wordt het chemische mechanisme beschreven van insulineaggregatie door MCO, geïnduceerd door middel van Cu^{2+} /ascorbinezuur. Geoxideerde insuline bleek DOPA (3,4-dihydroxyfenylalanine) en DOCH (of propionzuur) te bevatten, afkomstig van Phe en Tyr residuen. DOCH, dat een elektronenacceptor is voor 1,4 - of 1,6-type toevoeging (d.w.z. Michael-additie), bleek verantwoordelijk te zijn voor nieuwe cross-links die resulteerden in covalente aggregatie van insuline tijdens MCO. Specifiek werden 1,4 - of 1,6-type additie producten gedetecteerd tussen DOCH op posities B16, B26, A14 en A19, en de vrije aminogroepen van de N-terminale aminozuren Phe B1 en Gly A1 en de zijketens van Lys B29, His B5 en His B10. Fragmenten afkomstig van gehydrolyseerde peptidebindingen werden ook gemeten.

Hoofdstuk 5 beschrijft het onderzoek naar de anti-oxiderende eigenschappen van verschillende hulpstoffen tijdens Cu^{2+} /ascorbaat gekatalyseerde oxidatie van humaan insuline. Van de onderzochte hulpstoffen bleek 100 μM triethyleentetramine (TETA) de enige stof die vrijwel volledig door oxidatie-geïnduceerde insulineaggregatie, -fragmentatie en structurele veranderingen van insuline verminderde. TETA voorkwam ook aggregatie en fragmentatie van een monokonaal IgG1 onder identieke oxidatieve omstandigheden, wat de algemene toepasbaarheid van TETA aangeeft als anti-oxidant voor kopergevoelige eiwitten. Concluderend is TETA een veelbelovende kandidaat als hulpstof in formuleringen van oxidatie-gevoelige eiwitten.

Oxidatie via Cu^{2+} /ascorbaat van recombinant humaan interferon bèta-1a ($\text{IFN}\beta$) leidt tot zeer immunogene aggregaten. In **Hoofdstuk 6** wordt een studie gepresenteerd naar de identificatie van de oxidatieplaatsen en covalente cross-links in $\text{IFN}\beta$, blootgesteld aan MCO. Oxidatieproducten van Met, His, Phe, Trp en Tyr restgroepen werden geïdentificeerd in de primaire structuur van het eiwit. Vergelijkbaar met insuline (**Hoofdstuk 4**) werden covalente crosslinks via 1,4 - of 1,6-type addities tussen primaire amines en DOCH gevonden, terwijl er geen bewijs was voor de vorming van een disulfide brug, Schiff base, of dityrosine. De geïdentificeerde chemische cross-links,

veroorzaakt door oxidatie, zijn hoogstwaarschijnlijk verantwoordelijk voor de vorming van immunogene covalente aggregaten van IFN β .

In **Hoofdstuk 7** is het immunologische mechanisme bestudeerd dat verantwoordelijk is voor de immunogeniciteit van geaggregeerd recombinant humaan interferon alfa-2a (IFN α -2a) en de invloed van geaggregeerd IFN β op IFN α 's immunogeniciteit. Transgene muizen die immunotolerant zijn voor IFN α werden behandeld met natief (in oorspronkelijke staat verkerend) of geaggregeerd IFN α . Na een uitwasperiode werden de muizen opnieuw blootgesteld aan natief of geaggregeerd IFN α om de betrokkenheid van CD4⁺ T-cellen in de immunogeniciteit te testen. Voorts werden de muizen behandeld met een formulering die geaggregeerd IFN β en oorspronkelijk IFN α bevatte om te testen of IFN β werkt als een adjuvans voor IFN α . Na een uitwasperiode en een hernieuwde blootstelling met geaggregeerd of natief IFN α werd een schijnbaar gebrek aan immunologisch geheugen waargenomen. Wanneer we de CD4⁺ T-cell functie blokkeerden in immunotolerante muizen werden geen ADAs geïnduceerd door geaggregeerd rhIFN α . Tenslotte ontwikkelden immunotolerante muizen, behandeld met een mengsel van geaggregeerd IFN β en natief IFN α , geen antilichaamreactie tegen IFN α . Deze resultaten komen overeen met eerdere resultaten verkregen met IFN β .

Hoofdstuk 8 rapporteert de validatie van een adjuvans-vrij muismodel, dat is bedoeld als hulpmiddel om de immunogeniciteit van insulineformuleringen te evalueren. Toediening van humaan insuline (20 μ g/dosis, 12 doseringen over een periode van 4 weken) resulteerde in een immuunrespons in niet-transgene dieren, daar waar de transgene muizen immuuntolerant bleken te zijn. Deze tolerantie in transgene muizen kon worden omzeild indien ze werden behandeld met insuline dat covalent is gebonden aan polystyrene nanodeeltjes met een diameter van 50 nm. Dit transgene muismodel voor humane insuline werd toegepast om de immunogeniciteit van insulineformuleringen te vergelijken en kan van nut zijn voor verder onderzoek naar het mechanisme achter de immunogeniciteit van therapeutische eiwitten, met insuline als model eiwit.

Perspectieven

Het wetenschappelijk werk dat in dit proefschrift is gepresenteerd heeft als doel een bijdrage te leveren aan de ontwikkeling van veiligere, minder immunogene biofarmaca, door het beschrijven van de mechanismen achter MCO-geïnduceerde aggregatie van therapeutische eiwitten en de relatie met immunogeniciteit. Verder onderzoek is echter nodig om de degradatie van therapeutische eiwitten beter te verhinderen en een beter inzicht te krijgen in de factoren die bijdragen aan hun immunogeniciteit.

Dit gedeelte biedt een aantal perspectieven voor toekomstig onderzoek, gericht op strategieën om eiwitafbraak te verhinderen en analytische methoden ontwikkelen voor eiwitkarakterisering.

Strategieën om eiwitaggregatie te verhinderen

In de laatste twee decennia is de farmaceutische industrie zich meer bewust geworden van de risico's van afbraakproducten in eiwitformuleringen, voornamelijk aggregaten, wat de zoektocht naar oplossingen voor het voorkomen en verminderen van aggregatie rechtvaardigt. Doorgaans kunnen twee strategieën ingezet worden om eiwitdegradatie te voorkomen. De eerste strategie richt zich op het verbeteren van de eiwitstabiliteit door het eiwitmolecuul te modificeren, door genetische of chemische modificatie (bijvoorbeeld door bio-conjugatie zoals pegylatie). De tweede optie is het formuleren van een eiwitmolecuul. Een voorbeeld van de eerste strategie is de productie van een humaan interleukin-1 eiwit waar Asn36 gemuteerd is tot Ser36. De driedimensionale structuur van dit genetisch gemanipuleerde eiwit bleek identiek te zijn aan die van het oorspronkelijke eiwit, zoals aangetoond met circulair dichroïsme en proton NMR. De eiwitmutant was resistent tegen base-gekatalyseerde en hitte-geïnduceerde deamidatie.

Chemische modificatie, zoals conjugatie van eiwitten met polymeren (bijvoorbeeld PEG), kan in sommige gevallen een oplossing zijn, zoals dat bijvoorbeeld is aangetoond door de relatief hogere stabiliteit van gepegyleerde IFN eiwitten ten opzichte van hun ongemodificeerde varianten. Pegylatie is ingezet om de halfwaardetijd te verhogen om resistentie tegen enzymatische degradatie te vergroten en om de vorming van fibrillaire aggregaten tegen te gaan. Maar zoals is aangetoond in hoofdstuk 3 werd de

degradatie van insuline in een vloeibare formulering niet verhinderd door pegylatie. In onze studies hebben wij echter een 5-kDa PEG gebruikt, waardoor wij niet kunnen uitsluiten dat andere vormen van pegylatie de stabiliteit ten goede kunnen komen. Hulpstoffen worden veelal ingezet om eiwitten te beschermen tegen aggregatie en oxidatie. In hoofdstuk 5 zijn verschillende anti-oxiderende moleculen getest op hun potentieel beschermende effect tegen MCO-geïnduceerde aggregatie en fragmentatie van insuline en een monoclonaal antilichaam. Eén van de geteste moleculen, triethyleentetra-amine (TETA), bleek het meest veelbelovend te zijn om MCO te verhinderen. Het is op dit moment echter niet bekend of TETA oxidatie kan verhinderen van aminozuurresiduen die niet betrokken zijn bij aggregatie, zoals methionine en tryptofaan, welke niet aanwezig zijn in insuline.

Toekomstige studies zouden het beschermende effect van TETA moeten verifiëren tegen oxidatie van zulke aminozuurresiduen met hulp van tandem-massaspectrometrie. Oppervlakte-actieve hulpstoffen zoals polysorbaat 80 worden veel ingezet in eiwitformuleringen en zijn tevens nuttig om eiwit aggregatie te verhinderen. Eén van de grote nadelen van polysorbaten is dat zij alkyl ketens bezitten die kunnen auto-oxideren, waardoor eiwit beschadigende peroxides ontstaan. Aangezien peroxidevorming sterker is in een aërobe omgeving en verder versterkt wordt door licht, zou een eerste strategie om de hoeveelheid van deze reactieve moleculen in polysorbaten terug te dringen zijn om elk contact met lucht/zuurstof tijdens opslag te vermijden. Vervolgens kan de toevoeging van anti-oxiderende hulpstoffen behulpzaam zijn om de vorming van radicalen te verminderen of te minimaliseren. In dit geval zouden chelatoren zoals TETA niet gebruikt moeten worden, omdat deze anti-oxidantia niet in staat zijn om radicalen weg te vangen. Daarentegen kunnen moleculen zoals methionine, vitamine E of glutathion overwogen worden.

Concluderend, om degradatie te verhinderen is een sterk inzicht nodig in de achterliggende mechanismen. In hoofdstuk 4 bijvoorbeeld, door het gebruik van hoog gevoelige tandem-massaspectrometrische analyse en selectieve fluorogene labels, toonden wij aan dat insulineaggregatie in ons oxidatieve systeem plaatsvond door oxidatieproducten van tyrosine die kunnen reageren met aminogroepen in het insulinemolecuul. Gebaseerd op deze bevindingen stelden wij twee strategieën voor om aggregatie te verhinderen of te

reduceren (hoofdstuk 4). De mechanismen die betrokken zijn bij verscheidene andere degradatieprocessen zouden op gelijke manier geanalyseerd moeten worden om elke andere manier van eiwitdegradatie tegen te gaan.

Analytische hulpmiddelen voor eiwitkarakterisatie

Wanneer een eiwit degradeert, vormt zich over het algemeen een heterogene mix van degradatieproducten met verschillende fysisch-chemische eigenschappen, zoals aggregaten met verschillen in grootte, vorm, eiwitconformatie en chemische modificaties, alsmede qua structuur gemodificeerde monomeren en fragmenten. Elk van deze soorten kan mogelijk bijdragen aan ongewilde nevenreacties.

Voor een adequate karakterisatie van elk van deze soorten degradatieproducten moet men de beschikking hebben over betrouwbare, robuuste analysemethoden. De meeste van de routineuze analytische technieken voor de karakterisatie van aggregaten bij kwaliteitscontrole, richten zich op een deeltjesgrootte van $>1 \mu\text{m}$ en $<100 \text{ nm}$, welke duidelijk een groot gat laten in het subvisuele deeltjesgroottebereik. Technieken zoals nanoparticle tracking analyse (NTA, welke gebruikt is in verscheidene studies gepresenteerd in dit proefschrift) en flow imaging microscopie maken het mogelijk om deeltjesaggregatie te visualiseren en kwantificeren, en geven informatie over de deeltjesgrootte. Deze methoden worden in toenemende mate gebruikt als karakterisatiehulpmiddelen om het eerder genoemde gat in het deeltjesgroottebereik te dichten.

Daarnaast kan een nauwkeurig beeld worden gevormd van chemische modificaties van eiwitgeneesmiddelen met hoog gevoelige MS/MS-analyse. Sommige gedetecteerde chemische modificaties zoals Trp-oxidatie kunnen echter artefacten zijn die ontstaan tijdens de monstervoorbereiding. Selectieve chemische derivatisering voorafgaand aan de MS-analyse kan overwogen worden om misinterpretatie van de resultaten te voorkomen. Bijvoorbeeld, een vergelijkbare fluorogene derivatisatie zoals in hoofdstuk 4 wordt getoond kan op geoxideerde Trp-residuen toegepast worden.

Appendix 2

Abbreviations

Abbreviations

ABI	ammonium bicarbonate
ABS	4-(aminomethyl) benzenesulfonic acid
ADAs	anti-drug antibodies
Ag	antigen
ANOVA	analysis of variance
Asn	asparagine
AUC	area under the curve
BABs	binding antibodies
BAM	benzylamine
CB	sodium citrate buffer
CD	circular dichroism
CDRs	complementarity determining regions
CFA	complete Freund's adjuvant
CHO	Chinese hamster ovary
CSB	sodium citrate sucrose buffer
CT	calcitonin
Cu ²⁺	bivalent copper ion
Cys	cysteine
DHB	dihydroxybenzoic acid
DLS	dynamic light scattering
DNA	deoxyribonucleic acid
DNPH	2,4-dinitrophenylhydrazine
DO	dissolved oxygen
DOCH	2-amino-3-(3,4-dioxocyclohexa-1,5-dien-1-yl) propanoic acid
DOPA	3,4-dihydroxyphenylalanine
DTT	DL-dithiothreitol
E. coli	Escherichia coli
EDAC	1-(3-dimethylaminopropyl)-3-ethylcarbodiimide
EDTA	ethylenediaminetetraacetic acid
ELISA	enzyme-linked immunosorbent assay
ESI-MS	electrospray ionization mass spectrometry
ESI-ToF	electrospray ionization time of flight
Fab	fragment antigen-binding
Fc	fragment crystallisable
FcRn	neonatal Fc receptor
FDA	Food and Drug Administration

FT-ICR MS	Fourier transform ion cyclotron resonance mass spectrometry
G-CSF	granulocyte colony stimulating factor
GH	growth hormone
GM-CSF	granulocyte macrophage colony stimulating factor
GnHCl	guanidine hydrochloride
GPC	gel permeation chromatography
GSH	reduced glutathione
His	histidine
HMWO	high-molecular-weight oligomers
HSA	human serum albumin
IAM	iodoacetamide
IFN α -2a	interferon alpha-2a
IFN α -2b	interferon alpha-2b
IFN β -1a	interferon beta-1a
IgG	immunoglobulin G
i.m.	intramuscular
i.p.	intraperitoneal
i.v.	intravenous
LOPC	light obscuration particle counting
Lys	lysine
mAbs	monoclonal antibodies
MCO	metal catalyzed oxidation
MeO-PEG-NHS	Alpha-methoxy omega-carboxylic acid succinimidyl ester poly(ethylene glycol)
MES	2-N-morpholino-ethanesulfonic acid
Met	methionine
Nab	neutralizing antibody
NHS-sulfo	N-hydroxysulfosuccinimide sodium salt
NP	polystyrene nanoparticles
NTA	nanoparticle tracking analysis
NTG	non transgenic
OD	optical density
PAGE	polyacrylamide gel electrophoresis
PB	sodium phosphate buffer
PBS	phosphate buffered saline
PCR	polymerase chain reaction
PDI	polydispersity index
PEG	polyethylene glycol

Phe	phenylalanine
PTH	parathyroid hormone
PVDF	polyvinylidene difluoride
ROS	reactive oxygen species
RP-HPLC	reversed-phase high pressure liquid chromatography
rtPCR	real time PCR
SA	sinapinic acid
s.c.	subcutaneous
SDS	sodium dodecyl sulfate
SEC	size-exclusion chromatography
SEM	standard error of the mean
Td	T-cell dependent
TETA	triethylenetetramine
TFA	trifluoroacetic acid
TG	transgenic
Ti	T-cell independent
TMB	3,3',5,5'-tetramethylbenzidine
Trp	tryptophan
Tyr	tyrosine
USP	United States Pharmacopeia
UV	ultraviolet
v/v	volume/volume
w/w	weight/weight
Z-ave	Z-average diameter

Appendix 3

List of publications

List of publications

2013

R. Torosantucci, V. S. Sharov, M. van Beers, V. Brinks, C. Schöneich, W. Jiskoot. Identification of oxidation sites and covalent cross-links in metal catalyzed oxidized interferon beta-1a: potential implications for protein aggregation and immunogenicity. *Molecular Pharmaceutics* **2013**, *10*, 2311-2322.

R. Torosantucci, D. Weinbuch, R. Klem, W. Jiskoot. Triethylenetetramine prevents insulin aggregation and fragmentation during copper catalyzed oxidation. *European Journal of Pharmaceutics and Biopharmaceutics* **2013**, *84*, 464-471.

R. Torosantucci, V. Brinks, G. Kijanka, L. Andhyk Halim, M. Sauerborn, H. Schellekens and W. Jiskoot. Development of a transgenic mouse model to study the immunogenicity of recombinant human insulin. *Submitted for publication*.

R. Torosantucci, C. Schöneich, W. Jiskoot. Oxidation of therapeutic proteins and peptides: structural and biological consequences. *Submitted for publication*.

M. Sauerborn[#], **R. Torosantucci**[#], L. Boon, W. Jiskoot, H. Schellekens, V. Brinks. Immune mechanisms underlying immunogenicity of aggregated recombinant human interferon alpha 2a in immune tolerant mice. *Submitted for publication*.

[#] authors contributed equally

2012

R. Torosantucci, O. Mozziconacci, V. Sharov, C. Schöneich, W. Jiskoot. Chemical modifications in aggregates of recombinant human insulin induced by metal-catalyzed oxidation: covalent cross-linking via Michael addition to tyrosine oxidation products. *Pharmaceutical Research* **2012**, *29*, 2276-2293.

2011

R. Torosantucci, B. Kükreer, A. Mero, M. Van Winsen, R. Tantipolphan, W. Jiskoot. Plain and mono-pegylated recombinant human insulin exhibit similar stress-induced aggregation profiles. *Journal of Pharmaceutical Sciences* **2011**, *100*, 2574-2585.

2010

R. Tantipolphan, S. Romeijn, J. Engelsman, **R. Torosantucci**, T. Rasmussen, W. Jiskoot. Elution behavior of insulin on high-performance size exclusion chromatography at neutral pH. *Journal of Pharmaceutics and Biomedical Analysis*, **2010**, *52*, 195-202.

2009

F. De Simone, J. Andres, **R. Torosantucci**, J. Waser. Catalytic formal homo-Nazarov cyclization. *Organic Letters* **2009**, *11*, 1023-1026.

2008

M. Faccini, M. Balakrishnan, M. B. J. Diemeer, **R. Torosantucci**, A. Driessen, D. N. Reinhoudt, W. Verboom. Photostable nonlinear optical polycarbonates. *Journal of Materials Chemistry* **2008**, *18*, 5293-5300.

M. Faccini, M. Balakrishnan, **R. Torosantucci**, A. Driessen, D. N. Reinhoudt, W. Verboom. Facile attachment of nonlinear optical chromophores to polycarbonates. *Macromolecules* **2008**, *41*, 8320-8323.

Appendix 4

Curriculum Vitae

Curriculum Vitae



Riccardo Torosantucci was born in Rome, Italy, 22nd September 1980. In July 2008 he received his master degree in Chemistry and Pharmaceutical Technologies from the University of Rome “La Sapienza”. He completed the first internship of his master studies working for six months in supramolecular chemistry, in particular on the synthesis of calixarenes at the Department of

Biologically Active Substances of University of Rome “La Sapienza” under the supervision of Prof. Dr. Bruno Botta. Next, in July 2007, Riccardo was awarded the “Master’s thesis abroad travel grant” and he joined for six months the group of Supramolecular Chemistry and Technology (SMCT) directed by Prof. Dr. David Nicholas Reinhoudt at Twente University, The Netherlands. During this period he worked on the synthesis of new polymers for second-order nonlinear optics. After his master thesis defence in July 2008, from October until December 2008, Riccardo worked at the Laboratory of Catalysis and Organic Synthesis (LCSO) of the École Polytechnique Fédérale de Lausanne (EPFL), Switzerland, under the supervision of Prof. Dr. Jérôme Waser, focusing mainly on the synthesis of heterocyclic compounds. In March 2009 Riccardo started his PhD at the Division of Drug Delivery Technology at Leiden University, The Netherlands, under the supervision of Prof. Dr. Wim Jiskoot, Prof. Dr. Huub Schellekens and Dr. Vera Brinks, on a project entitled “Unwanted immunogenicity of therapeutic proteins”. In May 2011, as a part of his PhD project, he spent 5 months at the Department of Pharmaceutical Chemistry of Kansas University, Lawrence, USA, in the group directed by Prof. Dr. Christian Schöneich, where he worked on mass spectrometric characterization of therapeutic protein aggregates induced via metal catalyzed oxidation. Since May 2013 Riccardo is working as a project manager at Coriolis-Pharma in Munich, Germany.

Grants & Awards

2012

- First prize for oral presentation at the ninth biennial meeting of the Globalization of Pharmaceutics Education Network, Monash University, Melbourne, Australia.
- GlaxoSmithKline Housing Grant
- Merck & Co. Travel Grant
- Nederlandse Stichting voor Farmacologische Wetenschappen (NSFW) travel grant *2012*

2011

- CASSS Separation Science Society travel grant
- Leids Universiteits Fonds travel grant (Leiden University, NL)
- Nederlandse Stichting voor Farmacologische Wetenschappen (NSFW) travel grant *2011*

2007

- "Master's thesis abroad travel grant", University of Rome "La Sapienza"

2006

- Scholarship at the Department of Pharmaceutical Chemistry, University of Rome "La Sapienza"

Appendix 5

Acknowledgements

Completing this thesis would not have been possible without the support, aid and unconditioned love from my family: my wife Olga Ekin, my sister Gaetana, my mother Antonella and my father Alberto who continuously share my joys and sorrows.

I want to express my gratitude to ALL friends and colleagues at Leiden University and especially the ones at the Division of Drug Delivery Technology, for their kindness, helpfulness and constant availability. You all made my daily life -inside and outside Leiden University- great!

I also would like to thank Prof. Dr. Joke Bouwstra for her availability in discussing scientific topics.

Many thanks to my office mates: Christophe Barnier Quer and Vasco Filipe in the early days and Pim Schipper and Onanong Nuchuchua (Pu) in the last period for bringing good mood in the office every day.

Special thanks to Dr. Jeroen van Smeden and Ahmad Sediq for being my paranymphs; to Stefan Romeijn, Pim Schipper and Ahmad Sediq for translating the summary of this thesis to Dutch; to Connie van Gent, Remôn Heeneman and Dr. Michelle Janssens for their endless help and availability with administrative issues.

I want to acknowledge and mention my sincere gratitude to Dr. Başak Kükreer, Dr. Ruedeeporn Tantipolphan (Sun), Dr. Miranda Maria Christina van Beers, Dr. Melody Sauerborn, Dr. Anna Mero, Grzegorz Kijanka and Halim, L.A. (Andhyk), all friends and scientists, for their great contributions to the scientific work presented in this thesis.

Thanks to Dr. John den Engelsman for providing me with the insulin used in these studies and for inviting me to present our results to his scientific group at Organon NV/Merck.

I also benefited from outstanding work of graduate and undergraduate students whose efforts contributed to this thesis: Daniel Weinbuch, Margot van Winsen, Robin Klem and Anna Hoekstra.

Sincere thanks to Prof. Dr. Christian Schöneich for hosting me in his laboratories and together with Dr. Victor Sharov, Dr. Dremina Yelena, Dr. Nadya Galeva, Dr. Olivier Mozziconacci, Dr. Daniel Steinmann, Christopher Asmus, Dr Maria Feeney and Jessica Haywood for making amazing all the five months spent at the Department of Pharmaceutical Chemistry of Kansas University, Lawrence, for the daily scientific discussion in the chemistry of protein aggregates, for introducing me in “hardcore” mass spectrometry, and for being my family in the USA.

Furthermore, I want to thank all of those who contributed to shape the trajectory towards the start of my PhD project:

Prof. Dr. Jérôme Waser and Dr. Filippo De Simone from the Laboratory of Catalysis and Organic Synthesis (LCSO) at the École Polytechnique Fédérale de Lausanne (EPFL).

All members of the Department of Supramolecular Chemistry and Technology (SMCT) of Twente University: Prof. Dr. D.N Reinhoudt, Dr. Wim Verboom, Dr. Mirko Faccini, Dr. Albert Ruggi, Dr. Riccardo Salvio, Dr. Francesca Costantini, Dr. Kim Wimbush, Dr. Ignacio Pérez-Victoria, Dr. Henk Dam, Dr. Elisabetta Fanizza, Dr. Jealemy Galindo.

Prof. Dr. Bruno Botta, master of chemistry and life who allowed me to join his laboratories at the department of Biologically Active Substance of the University of Rome “La Sapienza” and Twente University, where my experience abroad began.

My amazing university mates with whom I shared success, joys and frustrations during my master studies in Rome: Daniele Vernaroli, Stefania Saccoccio, Lavinia Mareschi, Massimo Pizzichelli, Angela Molinaro, Marco Petitti, Daniela

Bruni, Marco Mollicelli, Luca De Martino, Stefano Stirpe, Stefano Di Girolamo, Paolo Lazzeroni, Denis Cera.

Last but indeed not least, I want to thank my great friends: I “Gemelli” Luca e Matteo Romanelli, Massimiliano Piccioni e i mitici Edoardo Cortese e Sandro Pasquini, for sharing since our childhood unforgettable moments.

Riccardo